

AD-A070 254

FORD AEROSPACE AND COMMUNICATIONS CORP NEWPORT BEACH --ETC F/G 20/4
PRESSURE GRADIENT EFFECTS ON SUPERSONIC BOUNDARY LAYER TURBULEN--ETC(U)
FEB 79 A J LADERMAN F33615-77-C-3016

UNCLASSIFIED

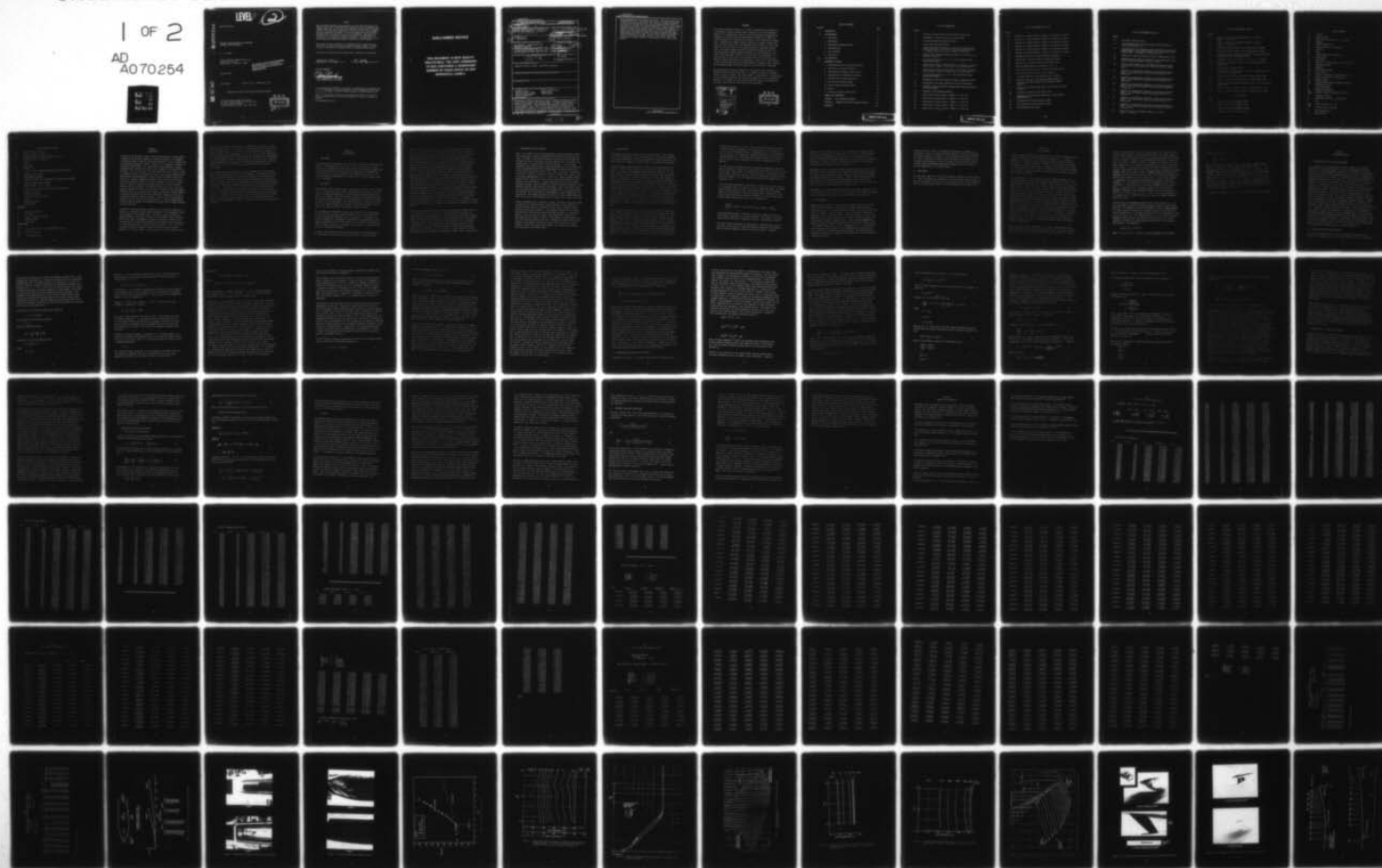
U-6467

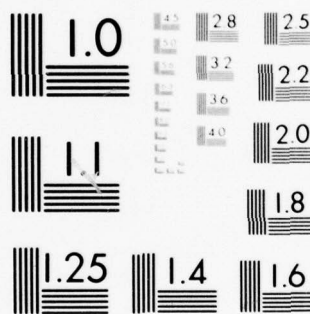
AFFDL-TR-79-3005

NL

1 OF 2

AD
A070254





MICROCOPY RESOLUTION TEST CHART
NATIONAL BUREAU OF STANDARDS-1963-A

LEVEL

2

AD A070254

AFFDL-TR-79-3005

PRESSURE GRADIENT EFFECTS ON SUPERSONIC
BOUNDARY LAYER TURBULENCE

A. J. Laderman

Ford Aerospace & Communications Corp
Aeronutronic Division
Newport Beach, California 92660

THIS DOCUMENT IS BEST QUALITY PRACTICABLE.
THE COPY FURNISHED TO DDC CONTAINED A
SIGNIFICANT NUMBER OF PAGES WHICH DO NOT
REPRODUCE LEGIBLY.

February 1979

Final Report

March 30, 1977 - December 30, 1978

Approved for public release; distribution unlimited.

Air Force Flight Dynamics Laboratory
Air Force Wright Aeronautical Laboratories
Air Force Systems Command
Wright-Patterson Air Force Base, Ohio 45433



DDC FILE COPY

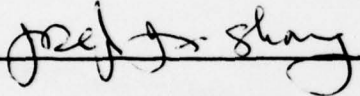
79 06 20 014

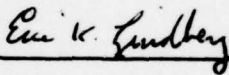
NOTICE

When Government drawings, specifications, or other data are used for any purpose other than in connection with a definitely related Government procurement operation, the United States Government thereby incurs no responsibility nor any obligation whatsoever; and the fact that the Government may have formulated, furnished, or in any way supplied the said drawings, specifications, or other data, is not to be regarded by implication or otherwise as in any manner licensing the holder or any other person or corporation, or conveying any rights or permission to manufacture, use, or sell any patented invention that may in any way be related thereto.


This report has been reviewed by the Information Office (OI) and is releasable to the National Technical Information Service (NTIS). At NTIS, it will be available to the general public, including foreign nations.

This technical report has been reviewed and is approved for publication.





FOR THE COMMANDER


PETER J. BUTKEWICZ, Col, USAF
Chief, Aeromechanics Division

If your address has changed, if you wish to be removed from our mailing list, or if the addressee is no longer employed by your organization please notify _____ W-PAFB, OH 45433 to help us maintain a current mailing list.

Copies of this report should not be returned unless return is required by security considerations, contractual obligations, or notice on a specific document.

DISCLAIMER NOTICE

**THIS DOCUMENT IS BEST QUALITY
PRACTICABLE. THE COPY FURNISHED
TO DDC CONTAINED A SIGNIFICANT
NUMBER OF PAGES WHICH DO NOT
REPRODUCE LEGIBLY.**

UNCLASSIFIED

SECURITY CLASSIFICATION OF THIS PAGE (When Data Entered)

19 REPORT DOCUMENTATION PAGE		READ INSTRUCTIONS BEFORE COMPLETING FORM	
1. REPORT NUMBER AFFDL-TR-79-3005	2. GOVT ACCESSION NO.	3. RECIPIENT'S CATALOG NUMBER	
4. TITLE PRESSURE GRADIENT EFFECTS ON SUPERSONIC BOUNDARY LAYER TURBULENCE	5. TYPE OF REPORT & PERIOD COVERED Final Technical Report. 30 Mar 77-		
7. AUTHOR(s) A. J. Laderman	6. PERFORMING ORGANIZATION NUMBER U-6467		
9. PERFORMING ORGANIZATION NAME AND ADDRESS FORD AEROSPACE & COMMUNICATIONS CORP AERONUTRONIC DIVISION FORD ROAD, NEWPORT BEACH, CALIFORNIA 92660	10. PROGRAM ELEMENT, PROJECT, TASK AREA & WORK UNIT NUMBERS 2307-N4-05		
11. CONTROLLING OFFICE NAME AND ADDRESS AIR FORCE FLIGHT DYNAMICS LABORATORY (FXM) WRIGHT-PATTERSON AIR FORCE BASE, OH 45433	12. REPORT DATE Feb 1979		
14. MONITORING AGENCY NAME & ADDRESS (if different from Controlling Office) 180p	13. NUMBER OF PAGES 167		
16. DISTRIBUTION STATEMENT (of this Report) Approved for public release; distribution unlimited.		15. SECURITY CLASS. (of this report) UNCLASSIFIED	
17. DISTRIBUTION STATEMENT (of the abstract entered in Block 20, if different from Report)			
18. SUPPLEMENTARY NOTES			
19. KEY WORDS (Continue on reverse side if necessary and identify by block number) Supersonic flow Turbulent shear stress Turbulent boundary layer Mixing length Adverse pressure gradient Eddy viscosity Velocity correlation Skin friction			
20. ABSTRACT (Continue on reverse side if necessary and identify by block number) Measurements of mean flow profiles at several streamwise locations in a supersonic turbulent boundary layer growing under a continuous adverse pressure gradient are reported. Tests were performed at a freestream Mach number of 3, for an adiabatic wall, using two curved ramps designed to produce constant pressure gradient flows. The velocity profile data, when transformed to incompressible coordinates, are in good agreement with Coles universal "wall-wake" velocity profile and they indicate that the boundary layer is in local equilibrium and essentially independent of upstream history. In addition, the			

DD FORM 1 JAN 73 1473 EDITION OF 1 NOV 65 IS OBSOLETE

UNCLASSIFIED

SECURITY CLASSIFICATION OF THIS PAGE (When Data Entered)

391 853

Jm

UNCLASSIFIED

SECURITY CLASSIFICATION OF THIS PAGE(When Data Entered)

→ Coles wake parameters and Clauser shape factors, characterizing the transformed profiles, are in accord with the results of low speed correlations of adverse pressure gradient flows. The turbulent transport terms were extracted from the mean flow field data and indicate that for a given ramp, the profile of turbulent shear stress normalized by the wall shear, versus distance from the surface, normalized by the local boundary thickness, is severely distorted by the pressure gradient although it is apparently insensitive to local conditions. The peak value of the normalized shear stress profile was found to correlate the pressure gradient normalized by conditions upstream of the ramp. Both the mixing length and the eddy viscosity distributions across the boundary layer reflect similar distortions due to pressure gradient as those observed in the shear stress profile.

UNCLASSIFIED

SECURITY CLASSIFICATION OF THIS PAGE(When Data Entered)

FOREWORD

This report describes the latest in a series of experimental investigations of high-speed turbulent boundary layers carried out by the Fluid Mechanics Section of the Aeronutronic Division of the Ford Aerospace & Communications Corporation. Previous work has been devoted to studies of the effect of various parameters on transition and turbulence in the compressible boundary layer, including Mach number, Reynolds number, heat transfer and mass addition. The most recent effort was concerned with the influence of wall temperature on the structure of a zero pressure gradient, supersonic boundary layer. The present program was directed toward examining the effects of a continuous adverse pressure gradient produced by a curved adiabatic, isentropic compression ramp. Results of detailed mean flow measurements are described and turbulent shear stress distributions extracted from the time averaged conservation equations are presented. Because of the large quantity of data involved, the results are shown primarily in graphical form. However, the interested reader may request copies of the detailed data tabulations.

The work described herein was supported by the Flight Dynamic Laboratory at Wright-Patterson Air Force Base, Ohio. Dr. Joseph J.S. Shang of AFFDL/FXM served as project engineer. The author wishes to acknowledge Dr. A. Demetriades for his collaboration during the planning and preparation of the experimental program; L. Von Seggern for his assistance during various critical phases of the tests, and G. Hart for fabrication of the ramp models.

Accession For	
NTIS GRA&I	<input checked="" type="checkbox"/>
DDC TAB	<input type="checkbox"/>
Unannounced	<input type="checkbox"/>
Justification	
By	
Distribution/	
Availability Codes	
Dist.	Avail and/or special
A	23/24

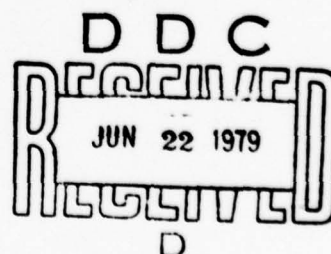


TABLE OF CONTENTS

SECTION		PAGE
I	INTRODUCTION	1
II	THE EXPERIMENT	3
	1. Wind Tunnel	3
	2. Ramp Design	3
	3. Preliminary Flowfield Surveys	5
	4. Instrumentation	6
	5. Test Procedure	8
	6. Test Matrix	9
III	DATA REDUCTION	10
IV	EXPERIMENTAL RESULTS	13
	1. Characterization of the Pressure Gradient	13
	2. Correlation of Velocity Profiles	13
	3. Non-dimensional Boundary Layer Profiles	20
	4. Determination of Streamwise Derivatives	27
	5. Turbulent Shear Stress Distribution	29
	a) Zero Pressure Gradient Region	29
	b) Adverse Pressure Gradient Region	30
	c) Results	31
	6. Turbulent Transport Coefficients	34
V	SUMMARY AND CONCLUSIONS	37
	APPENDIX A DATA REDUCTION PROGRAMS	139
	APPENDIX B COMMENTS ON THE MIXING LENGTH CONSTANT	159
	REFERENCES	165

LIST OF ILLUSTRATIONS

FIGURE

- 1 Schematic of Ramp Contours and Wind Tunnel Installation
- 2 Photographs of Ramps Installed in the Wind Tunnel
- 3 Schlieren Photograph of Ramp Flow Field
- 4 Surface Pressure Distributions
- 5 Lateral Pitot Pressure Surveys at Selected y' Locations Above Surface for Ramp 1. X Station is 5 cm Upstream of Ramp T.E.
(- Denotes Location of p_t vs y' Profiles in Figure 6)
- 6 Vertical Pitot Pressure Profiles for Ramp 1 at x Station 12.7 cm Upstream of Ramp T.E.
- 7 Pitot Pressure Surveys p_t vs y' at .635 cm Intervals Along Centerline of Ramp 1
- 8 Typical Lateral Static Pressure Surveys at Selected y' Locations Above Surface of Ramp 3. X Station is 5.7 cm from Ramp L.E.
- 9 Typical Lateral Pitot Pressure Surveys at Selected y' Locations Above Surface of Ramp 3. X Station is 4.4 cm from Ramp L.E.
- 10 Pitot Pressure Surveys p_t vs y' at .635 cm Intervals Along Centerline of Ramp 3
- 11 Photographs of the Pitot Pressure and Total Temperature Probes
- 12 Photographs of the Static Pressure and Preston Tube Probes
- 13 Schematic of Adverse Pressure Gradient Ramps Indicating Location of Survey Stations
- 14 Schematic of Data Reduction Routine
- 15 Typical Plot of p_t/p_o versus y' (Ramp 3, $x = 3.81$ cm)
- 16 Typical Plot of p_s/p_o versus y' (Ramp 3, $x = 3.81$ cm)
- 17 Typical Plot of T_t/T_{oe} versus y' (Ramp 3, $x = 3.81$ cm)
- 18 Typical Plot of U_{meas} versus y' (Ramp 3, $x = 3.81$ cm)
- 19 Typical Plot of $T_{o_{meas}}$ versus y' (Ramp 3, $x = 3.81$ cm)

LIST OF ILLUSTRATIONS (cont'd)

FIGURE

- 20 Profiles of u versus Distance y Normal to the Surface for Ramp 1
- 21 Profiles of ϕ versus Distance y Normal to the Surface for Ramp 1
- 22 Profiles of p versus Distance y Normal to the Surface for Ramp 1
- 23 Profiles of u versus Distance y Normal to the Surface for Ramp 3
- 24 Profiles of ϕ versus Distance y Normal to the Surface for Ramp 3
- 25 Profiles of p versus Distance y Normal to the Surface for Ramp 3
- 26 Streamwise Variation of Pressure Gradient Parameter β_k
- 27 Typical Law of the Wake Velocity Correlations, Ramp 1
- 28 Typical Law of the Wake Velocity Correlations, Ramp 3
- 29 Velocity Correlations in the Vicinity of $y^+ = 10$
- 30 Distribution of Wake Function W Across the Boundary Layer
- 31 Velocity Deficit Form of the Velocity Profiles
- 32 Streamwise Variation of the Boundary Layer Thickness
- 33 Streamwise Variation of the "Wake Strength Parameter" $\tilde{\pi}$
- 34 Correlation of Wake Parameter $\tilde{\pi}$ with Pressure Gradient Parameter β_k
- 35 Correlation of Clauser Shape Factor G with Pressure Gradient Parameter β_k
- 36 Streamwise Variation of Wall Shear Stress
- 37 Comparison of Skin Friction Coefficient to Zero Pressure Gradient Results
- 38 Non-dimensional Velocity Profiles, Ramp 1
- 39 Non-dimensional Velocity Profiles, Ramp 3
- 40 Mach Number Profiles, Ramp 1

LIST OF ILLUSTRATIONS (cont'd)

FIGURE

- 41 Mach Number Profiles, Ramp 3
- 42 Whitfield-High Model of Turbulent Shear Stress Distribution
Across the Boundary Layer
- 43 Non-dimensional Total Temperature-Velocity Profiles for Non-Unity
Prandtl Number, Zero Pressure Gradient Flow with Adiabatic Walls
Showing Effect of Exponent in Velocity Power Law
- 44 Comparison of Power Law Velocity Profile to Experimental Profile
- 45 Experimental Non-dimensional Profiles of Total Temperature versus
Velocity Showing Influence of Pressure Gradient
- 46 Effect of Heat Transfer on Total Temperature-Velocity Profiles
for Non-unity Prandtl Number, Zero Pressure Gradient Boundary
Layer
- 47 Comparison of Experimental Flowfield to Curve-Fitted Flowfield,
Ramp 1. Plot of Velocity versus Curvilinear Distance S at
Selected y 's
- 48 Comparison of Experimental Flowfield to Curve-Fitted Flowfield,
Ramp 1. Plot of Mass Flux versus Curvilinear Distance S at
Selected y 's
- 49 Comparison of Experimental Flowfield to Curve-Fitted Flowfield,
Ramp 1. Plot of Static Pressure versus Curvilinear Distance S
at Selected y 's
- 50 Comparison of Experimental Flowfield to Curve-Fitted Flowfield,
Ramp 3. Plot of Velocity versus Curvilinear Distance S at
Selected y 's
- 51 Comparison of Experimental Flowfield to Curve-Fitted Flowfield,
Ramp 3. Plot of Mass Flux versus Curvilinear Distance S at
Selected y 's
- 52 Comparison of Experimental Flowfield to Curve-Fitted Flowfield,
Ramp 3. Plot of Static Pressure versus Curvilinear Distance S
at Selected y 's
- 53 Typical Variation of Streamwise Gradient of ρu with y ,
Ramp 3, $x = 7.62$ cm)

LIST OF ILLUSTRATIONS (cont'd)

FIGURE

- 54 Typical Variation of Streamwise Gradient of ou^2 with y ,
(Ramp 3, $x = 7.62$ cm)
- 55 Typical Variation of Streamwise Gradient of p with y ,
(Ramp 3, $x = 7.62$ cm)
- 56 Normalized Turbulent Shear Stress Distributions for Ramp 1
- 57 Normalized Turbulent Shear Stress Distributions for Ramp 3
- 58 Effect of Pressure Gradient on Normalized Turbulent Shear Stress
Distribution Across the Boundary Layer
- 59 Streamwise Variation of Turbulent Shear Stress τ for Ramp 3
- 60 Variation of Peak Shear Stress τ/τ_w with Pressure Gradient
Parameter β_{ko}
- 61 Typical Profile of du/dy versus y
- 62 Distribution of Mixing Length ℓ/δ Across the Boundary Layer for
Zero Pressure Gradient Flow
- 63 Effect of Adverse Pressure Gradient on Mixing Length, Ramp 1
- 64 Effect of Adverse Pressure Gradient on Mixing Length, Ramp 3
- 65 Variation of Normalized Eddy Viscosity with y/δ for Zero Pressure
Gradient Flow
- 66 Effect of Adverse Pressure Gradient on Eddy Viscosity, Ramp 1
- 67 Effect of Adverse Pressure Gradient on Eddy Viscosity, Ramp 3

LIST OF TABLES

TABLE

- 1 Typical Printout from PROGRAM BLSURV2
- 2 Typical Printout from PROGRAM VCOLES
- 3 Typical Printout from PROGRAM TBLJNDIM
- 4 Summary of Boundary Layer Parameters

LIST OF SYMBOLS

A	$(\gamma-1)M_\infty^2$
a	speed of sound
c_f	skin friction coefficient $\equiv \tau_w / (\frac{1}{2} \rho_e u_e^2)$
d	diameter
G	Clauser shape factor
H	Crocco parameter $\equiv T_o - T_w / T_{oe} - T_w$
h	enthalpy
\bar{h}	h/h_e
k	inverse radius of curvature, $1/R$
ℓ	mixing length
M	Mach number
m	exponent in velocity power law $u/u_e = (y/\delta)^{1/m}$
p_o	stagnation pressure
p	pressure
P_{rm}	mixed Prandtl number
p_t	pitot pressure
Δp	Preston tube reading = $p_t(\text{Preston tube}) - p_s$
R	radius of curvature of ramp surface
Re	Reynolds number
Re_θ	Reynolds number based on momentum thickness
s	streamwise distance
T	static temperature
T_o	stagnation temperature
T_{meas}	measured stagnation temperature, also T_t
u	streamwise velocity
u^+	transformed velocity $\equiv \int (\rho/\rho_w)(du/u_\tau)$
\bar{u}	u/u_e
u_{DEF}	velocity deficit = $u^+ - u_e^+$
u_τ	friction velocity $(\tau_w/\rho_w)^{1/2}$
W	Coles wake function
x	axial distance

LIST OF SYMBOLS (cont'd)

y	distance normal to surface
y'	distance normal to tunnel axis
y ⁺	normalized distance normal to surface $\equiv yu_\tau/\nu_w$
z	distance lateral to tunnel axis
λ	$(5/2)m$
β	$1/(1 + ky)$
β_k	$(dp/dx)(\delta^*/\tau_w)$
β_{ko}	β_k with (δ^*/τ_w) evaluated immediately upstream of ramp
δ	boundary layer thickness
δ^*	displacement thickness
δ_k^*	velocity thickness (or incompressible displacement thickness)
Δ	Clauser's displacement thickness
ϵ	eddy viscosity; also $(1 - P_{rm})$
κ	Prandtl mixing length constant defined in Equation 4.2
μ	molecular viscosity
ν	kinematic viscosity.
\tilde{w}	Coles wake strength parameter
ρ	density
θ	momentum thickness
τ	shear stress

Subscripts

∞	freestream condition
w	wall value
e	value at boundary layer edge
o	stagnation value
s	static value

Superscripts

$()^*$	value based on local p_s and freestream P_o and T_o
$()'$	fluctuating value
$\overline{()}$	time averaged value

SECTION I

INTRODUCTION

Solution of the supersonic boundary layer equations requires accurate models to describe the turbulent transport of energy and momentum. The transport coefficients cannot be derived from first principles, but must be deduced from well-designed experimental studies. Ideally, it is preferred to measure the turbulence terms directly, e.g., using the hot wire anemometer, although documentation of the mean flow field is still necessary to interpret the hot wire data. Even in the absence of direct information, the so-called "inverse" or "indirect" method can be applied to extract the transport properties from detailed mean flow measurements by means of the time averaged conservation equations. Although considerable progress in this direction has been made for the zero pressure gradient, flat plate boundary layer, there is still a dearth of specific information concerning flows with a finite continuous variation in static pressure. This problem arises from the fact that while numerous experimental studies have been made of boundary layers with pressure gradients (see, e.g., the exhaustive catalog of experimental results compiled by Fernholz and Finley¹) few have been sufficiently complete and reliable to successfully apply the "indirect" method. In fact, for continuous pressure gradient flows, no direct hot wire measurements of transport properties are available and only Sturek² has reported on turbulent shear stresses calculated from mean flow data.

The present study was undertaken, therefore, to systematically study the influence of a continuous adverse pressure gradient on a two-dimensional, supersonic, adiabatic wall boundary layer. The adverse pressure gradient was generated using a curved ramp, located on the test section floor of the FACC Mach 3 wind tunnel, and designed to produce an isentropic compression with constant dp/dx . Two ramps were designed for this purpose, one corresponding to a weak and the other to a moderate pressure gradient. While it may have been more desirable to design the ramps for constant pressure gradient parameter $\beta_k \equiv (\delta_k^*/\tau_w) (dp/dx)$, and thus maintain a constant influence of the

pressure gradient on the boundary layer, the local values of δ_k^* and τ_w could not be predicted prior to the experiment. On the other hand, it is shown later that the boundary layer is in a state of local equilibrium and, therefore, is controlled only by local conditions, i.e., c_f , M_e , β_k , etc. Thus, maintaining the pressure gradient constant allows the overall flow field to be characterized by a single parameter dp/dx (or, more exactly, by β_{k0} where δ^*/τ_w is evaluated immediately upstream of the ramp) while providing the opportunity to study the effect of the local β_k , and in this sense the experiment yields greater information.

The ultimate goal of this program is the direct measurement of the turbulent shear stresses using the x-array hot wire anemometer. In preparation for this task, detailed measurements of the mean flow field over the curved ramps have been carried out. This report describes these measurements and the results of the data analysis. Details of the experiment are presented in Section 2, while the method of analysis is summarized in Section 3 and the results are discussed in Section 4. In particular, it is shown that the mean flow profiles, when suitably transformed, agree with the universal "wall-wake" velocity profile and that the pressure gradient parameter β_k correlates the data with low speed results. In addition, the distribution across the boundary layer of turbulent shear stress, mixing length, and eddy viscosity were determined using the "indirect" method modified by Sturek² to account for the effects of longitudinal curvature.

SECTION II

THE EXPERIMENT

1. WIND TUNNEL

The experiment was carried out in the FACC Mach 3 supersonic wind tunnel (SWT). This is a continuous flow facility with a 7.87 cm by 8.64 cm test section located 40.6 cm downstream of the throat section. The turbulent boundary layer at the entrance to the test section is fully developed and is approximately 0.7 cm thick. All tests were conducted for stagnation conditions of $.973 \times 10^5 \text{ N/M}^2$ and 317°K corresponding to a nominal $M_\infty = 3$ and unit Reynolds number $= 6.57 \times 10^6/\text{meter}$.

2. RAMP DESIGN

Using Method of Characteristics theory, and ignoring the effect of the boundary layer, two continuously curved ramps, designated Ramp 1 and Ramp 3, were designed to produce two-dimensional, constant pressure gradient (dp/dx) flows. Based on the boundary layer characteristics upstream of the ramp leading edge, the pressure gradient parameter $\delta_{ko} \equiv (\delta_k^*/\tau_w)(dp/dx)$ was nominally 0.4 and 1.85 for Ramps 1 and 3, respectively. The ramp contours and a sketch of the ramp installed in the wind tunnel test section are indicated in Figure 1. Photograph of the ramps installed in the tunnel is shown in Figure 2.

The ramp models were designed to replace the floor plate of the wind tunnel test section and to provide a smooth continuation of the lower nozzle block. In order to avoid flow breakdown in the test section, as a consequence of blockage introduced by the presence of the models, the maximum height of the ramps was restricted to 1.8 cm (see Figure 1). As a result, this limited the length of Ramp 3 to about 9 cm, although this was found to be adequate for the purposes of the present experiment.

For Ramp 1, the curvature of the surface was started at the leading edge of the model which, in turn, mated to the trailing edge of the nozzle block.

Although a filler material was used to smooth the transition, the combined effects of curvature and joint misalignment resulted in the generation of a weak shock disturbance at the leading edge of the ramp. This is apparent in the Spark-Schlieren photograph of Figure 3a, which otherwise indicates a disturbance-free flow. Since static pressure measurements indicated that the shock induced pressure rise was less than 10% of the total pressure increase along the ramp, the effect of the leading edge shock on the subsequent development of the flow was considered negligible, and the ramp was judged adequate for use. A different strategy was adopted in the fabrication of Ramp 3. For this model, surface curvature was not initiated until 2.54 cm downstream of the leading edge with the portion in between machined flat. This separated the curved section of the ramp from the junction with the nozzle block trailing edge. With a filler material again used to smooth the transition from the nozzle to the ramp model, it was possible to produce a shock-free flow over the initial portion of the ramp. This is illustrated in the Schlieren photograph of Figure 3b. The density disturbances which are apparent in the photograph were demonstrated by pressure measurements to represent a continuous compression fan. Furthermore, the pressure measurements show that the oblique shock observed in the downstream flow originates 2.5-3 cm downstream of the beginning of the curved ramp. The shock is a consequence of coalescence of pressure waves generated by the ramp, and its existence, location and origin are predicted by the Method of Characteristics solution to the flow field.

Each ramp was provided with 0.084 cm diameter pressure ports aligned along the ramp centerline at 1.27 cm intervals. The measured surface pressure distributions for the two ramp models are shown in Figure 4, which also includes data obtained from the static pressure surveys discussed later. The observed scatter in the data can be attributed to small inaccuracies in the pressure measurements and to slight imperfections in the surface contour. In both cases, however, the measured pressure increase is sufficiently linear that the flow can be considered as characterized by a constant pressure gradient with dp/dx equal to 1.2 mmHg/cm and 5 mmHg/cm for Ramps 1 and 3, respectively.

3. PRELIMINARY FLOW FIELD SURVEYS

Prior to the conduct of the final measurements, qualitative pressure surveys were carried out to insure two dimensional, disturbance-free flow over the ramps. For Ramp 1, pitot pressure surveys to examine the flow volume over the ramp were made at seven axial stations ranging from 1.2 cm ahead of the leading edge to 2.5 cm upstream of the trailing edge. At each station, continuous pitot pressure surveys extending laterally (z) to 1 cm either side of the ramp centerline were made at approximately one dozen vertical (y') locations from the surface to about 1.8 cm above the surface. In addition, at the same x stations, continuous p_t versus y' profiles were traced at five z locations (approximately ± 1.0 , $\pm .4$ and 0 cm). Typical records, shown in Figures 5 and 6, indicate the flow is free of gross disturbances with only marginal cross flow effects. A graphic representation of the flow field is presented in Figure 7 where continuous p_t versus y' profiles obtained at .63 cm intervals along the ramp centerline are plotted. Flow is from right to left with the right hand profile located .63 cm downstream of the leading edge of the ramp and the left hand profile corresponding to 14.6 cm downstream of the leading edge. The leading edge shock (actually two closely spaced weak shock waves also visible in the Schlieren record of Figure 3a) is clearly indicated.

Similar measurements were carried out for Ramp 3 and typical results are shown in Figures 8-10. Figure 8 presents lateral surveys of static pressure at several positions above the ramp surface, while lateral traverses of pitot pressure are indicated in Figure 9. Both figures indicate that the flow is two-dimensional and relatively disturbance-free and Figure 8, in particular, implies no cross flow near the center of the ramp model. Figure 10 is a pitot pressure map, similar to Figure 7, which depicts the development of the flow field along the length of the ramp. Although the crossing of the pitot pressure traces slightly obscures the clarity of the figure, it is still possible to detect the oblique shock formed by the coalescence of pressure waves generated by the curved surface.

4 . INSTRUMENTATION

Measurements were made of mean profiles of pitot pressure, static pressure, and recovery temperature across the boundary layer. Each probe was mounted in the tunnel separately to avoid any possibility of mutual interference between probes and to minimize blockage caused by the presence of the probes.

The pitot pressure probe consisted of a .0152 cm O.D. tube which was acid etched to provide a gradual taper along its tip to its .0076 cm I.D. The probe was attached to an aerodynamic strut which was soldered to a conical body, housing a miniaturized Kulite pressure transducer (Model VQH-250-10), located at the front of a remotely driven actuator. The close coupling between the transducer and the probe tip afforded a significant improvement in the response time of the measurement. The transducer sensitivity of approximately 10 mmHg/mv was checked by calibration prior to each run. The estimated maximum error in the pitot pressure measurements was 4% when the probe was located adjacent to the wall near the front of the ramp and diminished to 0.25% in the freestream over the rear of the ramp. Various probe corrections due to rarefaction and viscous effects were found to be negligible although slight interference effects, caused by proximity of the surface, were observed for positions very close to the wall. These effects, however, were very small and restricted to, at most, a few positions and, therefore, no corrections were made.

Static pressure measurements were made using an ogive-cylinder shaped probe with a 0.051 cm diameter. Four static pressure ports located equally spaced around the probe periphery were located at 0.63 cm from the probe tip. The probe connected to a Dynisco Model TC APT 85-2 pressure transducer located outside the wind tunnel. The estimated maximum error in the static pressure measurement varied from 2% with the probe positioned at the beginning of the ramp to 0.6% at the rear of Ramp 3. Viscous interaction corrections for the static probe were found to be negligible for the Mach number-Reynolds number conditions of the present tests. However, the static pressure profiles indicated a small (10%) interference effect near the surface of the ramp which

extended out to about $y' = .12$ cm. Since the static pressure varied nearly linearly through the remainder of the boundary layer, it was possible to correct for the interference effect by extrapolating the static pressure profile to the wall. This permitted a redundant determination of the surface pressure distribution. These results are shown in Figure 4 where they are seen to provide excellent agreement with the direct measurements of wall pressure.

For both the static pressure and the pitot pressure measurements, particular care was exercised to insure that the probe axis was parallel to the local ramp surface prior to the survey. Both probes were found to be insensitive to yaw for yaw angles less than 5 degrees. Since this condition was easily satisfied across the boundary layer, the boundary layer pressure measurements were unaffected by yaw.

A bare wire Ch-Al thermocouple, installed in a ceramic tube and also attached to an aerodynamic strut, was used for the total temperature probe. The thermocouple wires were welded to form a disc 0.013 cm thick, thereby providing almost the same resolution as the pitot pressure probe. The probe was calibrated in the wind tunnel freestream to determine its recovery factor versus Reynolds number characteristic, which can be expressed as:

$$\frac{T_{\text{meas}} - T}{T_0 - T} = 0.9151 + .4799 \times 10^{-3} (Re_{o,D})^{.5} - .02302 \times 10^{-3} Re_{o,D}$$

The probe Reynolds number is evaluated at the total temperature T_0 using a characteristic length equal to the disc thickness. The output of the thermocouple could be read with a resolution of 0.01 mv, corresponding to 0.25°K.

The tunnel stagnation pressure was measured with a 0-800 mmHg Heise pressure gauge with a least count of 1 mmHg and stagnation temperature was sensed by a Precision Digital Temperature Indicator which read directly in degrees

Fahrenheit with a resolution of 1°F ($.6^{\circ}\text{K}$). Although the ramps were not instrumented to measure surface temperature, on the basis of a similar boundary layer study (3) performed in the same facility, it was assumed that $T_w = .945 T_{o_e} = 300^{\circ}\text{K}$ which corresponds essentially to the adiabatic wall condition. Measurement of surface pressure was made with the model TC APT 85-2 Dynisco transducer used for the static pressure surveys.

Measurement of wall shear stress was made using Preston tubes with 0.1, 0.163, and 0.236 cm O.D.s. The smallest and largest tubes were sized using criteria available in the literature for adverse pressure gradient flows to determine the minimum and maximum probe diameters. Again, the Dynisco pressure transducer used for the static pressure measurements was used to acquire the Preston tube data. Since the results were found to agree within 5%, only the data for the 0.1 cm diameter probe are discussed later.

Photographs of the several probes described above are shown in Figures 11 and 12. In each case, flow is from left to right and the probe support is designed so that aerodynamic disturbances are swept downstream of the probe tip.

5. TEST PROCEDURE

Profile data was acquired by first locating the probe adjacent to the ramp surface where the surface was located using a 10-power microscope with a calibrated graticle. For the pitot pressure profile, the probe was then moved vertically upward at selected intervals until the transducer response was sufficiently rapid to move the probe at a constant slow rate. For the other parameters, the variations were sufficiently small to permit continuous traversing across the entire boundary layer. A voltage signal proportional to probe position and the sensor signal were fed to an A/D system whose output was recorded on tape cassette to form a permanent data file. Probe position intervals ranging from 0.5 mils to 5 mil (depending on the sensor and the rate of change of the measured variable) were used. The recorded data was subsequently stored in the Company's main computer where it was processed via a time share terminal.

Although the probe actuator is provided with two degrees of freedom, it is constrained to move in a vertical direction (normal to the tunnel centerline) as opposed to normal to the surface. While the probe could be moved in both the x and y' directions in order to track the normal to the surface, it was considered more convenient to obtain the surveys along the vertical and use a simple computer programmed interpolation routine to convert the data to profiles perpendicular to the model surface.

6. TEST MATRIX

All tests were conducted at the tunnel stagnation conditions listed in Section 2. Mean flow surveys were conducted at the axial stations shown in Figure 13, which also includes the location of the wall pressure ports and illustrates the start of the ramp surface relative to the trailing edge of the nozzle block.

SECTION III

DATA REDUCTION

The data reduction procedure was programmed for the Company's Honeywell 66/40 digital computer and all data processing was carried out via a time share terminal. A schematic of the data reduction routine is shown in Figure 14. The routine is actually comprised of a number of sub-routines, each designed to complete a specific calculation. The output of each sub-routine is stored in a DATA FILE which is used as input to subsequent sub-routines and which can be accessed via a graphics terminal to provide a hard copy graphical representation of the file contents.

The pitot pressure, static pressure and recovery temperature profile data are recorded separately on tape cassette during the boundary layer survey. The tape cassettes are then fed to the computer creating three data files for each survey station. These files serve as input to Program BLSURV2 which performs three functions. First, the data is converted from "as read" units to physical units. Second, since the y' positions for the static pressure and recovery temperature profiles differs from those for the pitot pressure survey, the data for the former is interpolated to provide static pressure and recovery temperature data at the same y' locations as the pitot pressure. Finally, mean flow properties were calculated by means of standard gasdynamic equations using an iterative procedure to account for the calibrated recovery temperature characteristics of the T_o probe. The resulting boundary layer profiles were stored in DATA File ZMFLXXXX, where Z denotes the ramp and XXXX represents the x station. A typical printout from BLSURV2 is shown in Table 1. Similarly, to demonstrate the density of the data points and the quality of the measurements, plots of P_t/P_o , P_s/P_o and T_t/T_{oe} versus y' are shown in Figures 15-17, respectively. Profiles of U_{meas} and $T_{o,meas}$ for the same x station are presented in Figures 18 and 19, respectively.

For a given ramp, the Files ZMFLXXXX serve as input to PROGRAM NEWFLOW which uses a simple four point interpolation scheme to convert the profiles measured along the vertical to profiles along the normal to the surface. At a given x

station the interpolation is carried out using profile data along the vertical at that station together with vertical profile data at the nearest upstream station. The interpolated flow field, which includes profiles along the normal at all x stations, is stored in a single DATAFILE NEWFLOWZ where Z denotes the ramp. The content of NEWFLOW is shown, for example, in Figures 20, 21 and 22 where, respectively, u , ρ and p_s have been plotted against the distance normal to the surface, y . Similar plots for Ramp 3 are shown in Figures 23-25. In addition, normal profile data at each x station is stored in separate DATA FILES ZNFLXXXX. The latter is used as input to PROGRAM VCOLES which correlates the experimental data with Coles "Law of the Wake." This calculation provides the boundary layer thickness δ , the wall shear stress τ_w , and the wake parameter \tilde{w} . Furthermore, the transformed velocity profile is stored in DATA FILE ZVCOXXXX in u^+ , y^+ coordinates and in DATA FILE ZVDEFXXXX in velocity deficit coordinates. A sample printout of the output of PROGRAM VCOLES is shown in Table 2. Using the value of δ provided by VCOLES and either DATA FILE ZNFLXXXX or NEWFLOWZ as input, PROGRAM TBLJNDIM calculates non-dimensional profiles of y/δ versus u/u_e , ρ/ρ_e , etc., as well as the integral properties of the boundary layer. A sample printout of the results of PROGRAM TBLJNDIM is presented in Table 3.

As shown later, the streamwise derivatives of the flow variables u , ρu , ρu^2 , and p are needed to extract the turbulent transport properties from the mean flow data. To accomplish this DATA FILE NEWFLOWZ is input to PROGRAM RAMSHER. An x survey station is selected as a reference location and the associated y values are denoted as y_0 . The remaining profiles are then interpolated to find $u(s, y_0)$, $\rho u(s, y_0)$, etc. The streamwise distance s at y_0 is easily determined knowing the axial location x of the survey station and the local surface curvature. For each y_0 the flow properties are curve-fit by the method of least squares to the expression:

$$F(s, y_0) = F_1 + F_2 s + F_3 s^2$$

where $F = u$, ρu , ρu^2 , or p . With F_1 , F_2 and F_3 determined, the streamwise

derivatives are given by:

$$\frac{\partial F}{\partial s} = F_2 + 2 F_3 s$$

Once the derivatives are determined for a given profile, PROGRAM RAMSHER computes τ/τ_w versus y_0 and creates DATA FILES ZSHERXXX, storing y , τ/τ_w , and the streamwise derivatives, and ZEDYXXX, storing y , τ , σ and $\partial u/\partial y$. File ZEDYXXX is input finally to PROGRAM EDDY which calculates the mixing length and eddy viscosity as a function of y . PROGRAM RAMSHER can also be easily modified to create a data file storing either u_{data} , ∂u_{data} , etc., vs s for selected y_0 or $u_{curvefit}$, $\partial u_{curvefit}$, etc., versus s . Accessing these files via the graphics terminal provides a plot of either the experimental or curve fitted flow field which is convenient for visually assessing the quality of the data or the adequacy of the curve fit.

A listing of the programs used in the data reduction can be found in Appendix A.

SECTION IV

EXPERIMENTAL RESULTS

1. CHARACTERIZATION OF THE PRESSURE GRADIENT

In his treatise on the incompressible turbulent boundary layer, Clauser⁴ concluded that the proper parameter to use for characterizing equilibrium profiles in a flow with pressure gradient is $\delta \equiv (\delta^*/\tau_w)dp/dx$. For compressible flows, Alber and Coats⁵ suggested replacing δ with $\delta_k \equiv (\delta_k^*/\tau_w)dp/dx$ and in their study at $M_\infty = 4$, Lewis, et al⁶ found indeed that using δ_k provides an improved correlation with the low speed data. For the present experiment, the variation of δ_k with axial position x is plotted in Figure 26. It is shown later that τ_w increases with x much faster than δ_k^* and, since dp/dx is a constant, then, as indicated in Figure 26, δ_k decreases in the axial direction, particularly for RAMP 3. Figure 26 includes the data of Sturek and Danberg⁷ which also obtained for constant dp/dx using a curved ramp similar to that involved in the present tests. While a direct comparison cannot be made since the axial coordinate x has not been properly normalized, their data also show that δ_k decreases with increasing x confirming the present findings. Furthermore, the magnitude of δ_k in their experiments indicates that the relative influence of their pressure gradient should be much larger than in the present case. This point is addressed later in this report. The data of Lewis, et al,⁶ is also shown in Figure 26 to demonstrate the similarity in the magnitude of the pressure gradient parameter δ_k with the present results. Since their test was carried out for an increasing pressure gradient, dp/dx , their values of δ_k increase in the streamwise direction. However, for equilibrium boundary layers, this should be immaterial and only the local value of δ_k is significant. Reference to the results of Lewis, et al,⁶ will be made in the next section when the present data is compared with the low speed correlations.

2. CORRELATION OF THE VELOCITY PROFILES

It has become common practice to compare experimentally measured velocity profiles to a well-defined law (e.g., Coles composite "wall-wake" correlation)⁸

that describes the behavior of an equilibrium turbulent boundary layer. Using an appropriate transformation to convert the compressible data to an equivalent incompressible form, this comparison permits an assessment of the quality of the data, represents a means for evaluating the characteristic boundary layer parameters (e.g., δ , c_f , etc.), and, in the non-constant pressure case, assists in isolating the effects of pressure gradient on the development of the boundary layer and provides a basis for comparison with other experiments. The comparison of the experimental data to the classical boundary layer profile involves curve-fitting the transformed data to the classical profile, while iterating the values of the unknown parameters until the rms deviation of the curve-fit is minimized. Details of the curve-fitting procedure and a discussion of the results are presented below.

Starting with the conventional mixing length expression:

$$\tau = \tau_w = \rho \ell^2 (du/dy)^2 \quad 1$$

and combining with the Prandtl hypothesis:

$$\ell = \kappa y \quad 2$$

yields the following relation:

$$du^+ \equiv \left(\frac{\rho}{\rho_w} \right)^{\frac{1}{2}} \frac{du}{u_\tau} = \frac{1}{\kappa} \frac{dy}{y} \quad 3$$

Integration of the above expression gives

$$u^+ = \frac{1}{\kappa} \ln y^+ + C \quad 4$$

where:

$$y^+ \equiv y u_\tau / \nu_w$$

Equation 4 is the conventional "Law-of-the-Wall" which, following Coles, has been replaced by the more general "Law-of-the-Wake" formulation of the mean velocity profile, i.e., by:

$$u^+ = \frac{1}{\kappa} \ln y^+ + C + \frac{\tilde{\pi}}{\kappa} W(y/\delta) \quad 5$$

In Equation 5 $\tilde{\pi}$ is a parameter representing the strength of the wake component of the boundary layer, W is Coles tabulated wake function which can be approximated by $2 \sin^2(\pi y/2\delta)$ and the constants κ and C are given their incompressible values 0.41 and 5.0, respectively.

Equation 5 contains three unknowns: δ , u_τ and $\tilde{\pi}$. Substituting the edge conditions into Equation 5 yields:

$$u_e^+ = \frac{1}{\kappa} \ln \frac{\delta u_\tau}{v_w} + C + \frac{2\tilde{\pi}}{\kappa} \quad 6$$

which can be used to express $\tilde{\pi}$ in terms of u_τ and δ . This reduces the number of unknowns in Equation 5 to two, whose values are adjusted until the data fit the equation such that the rms error is a minimum. Data near the wall and near the edge of the boundary layer are excluded from the curve-fit and only data for which $y^+ \geq 50$ and $y/\delta \leq 0.9$ are used to determine the boundary layer parameters.

Although the curve-fit procedure is restricted to the wall-wake region, it is instructive to compare the experimental data to the "universal" velocity profile across the entire boundary layer. In the sub-layer region, the velocity profile is commonly expressed as:

$$u^+ = y^+ \quad 7$$

The transition between the sublayer and wall regions of the boundary layer has been examined by Spalding⁹ (and later by Kleinstein¹⁰ using a more formal approach) who suggests that the velocity profile in this zone can be

described by:

$$y^+ = u^+ + \exp(-\kappa C) [\exp(\kappa u^+) - f(u^+)]$$

where

8

$$f(u^+) = 1 + \kappa u^+ + \frac{1}{2} (\kappa u^+)^2 + \frac{1}{6} (\kappa u^+)^3 + \frac{1}{24} (\kappa u^+)^4$$

Note that Equation 8 reduces to Equation 7 as $\kappa u^+ \rightarrow 0$ and that Equation 4 is recovered when $\kappa u^+ \gg 1.0$. Equations 8 and 5 are used to represent the universal velocity profile across the boundary layer.

Typical plots of the experimental velocity profiles in transformed coordinates are shown in Figures 27 and 28 for Ramp 1 and Ramp 3, respectively. The values of u^+ have been determined directly from Equation 4.3 using the measured density profiles to carry out the integration. This avoids reliance on analytical transformations and their approximations. The Van Driest Transformation, for example, which has been successfully used for flat plate boundary layers, assume constant pressure and relates the density to the velocity via the Crocco relation. Equation 8 has been represented by dashed lines. For clarity, a plot of Equation 5 has been omitted since the differences between the experimental values of u^+ and the theoretical values cannot be resolved within the scale used in the figure. In the region $y^+ < 50$, the data tend to lie above the theoretical curve (a feature common to a considerable body of experimental data) with the discrepancy reaching a maximum in the range $10 < y^+ < 20$. This portion of the velocity profile has been replotted to a larger scale in Figure 29 where for each ramp data from the $dp/dx = 0$ survey station and the most farther downstream station on the ramp have been included, together with the theoretical profiles given by Equations 4, 7, and 8. The $dp/dx = 0$ data for Ramp 1 is seen to be in excellent agreement with Equation 8 while for Ramp 3, the data lies slightly above Equation 8. In addition, it is observed that when $dp/dx > 0$, then for both ramps there is a small but definite increase in the discrepancy between the experimental u^+ and Equation 8 in the streamwise direction. The reason for this is not immediately

obvious, but it reflects in the mixing length calculations in Section IV-6, and is discussed further in Appendix B.

For both ramps, a plot of the wake function W , for the same survey stations shown in Figures 27-29, is presented in Figure 30, where it is compared to Coles' approximation $2 \sin^2 (\pi y/2\delta)$. Although the agreement between the experimental and theoretical wake function is considered reasonable, there is a systematic increase in the difference $W - 2 \sin^2 (\pi y/2\delta)$ in the streamwise direction, with the sign of this difference changing from - to + as the outer edge of the boundary layer is approached. Furthermore, in contrast to the sine function which vanishes as $y/\delta \rightarrow 0$, W remains finite as the wall is approached.

In Reference 8, Coles discusses the effect of pitot probe errors on velocity measurements near the wall. These errors, which arise from a variety of sources and include probe interference effects, uncertainty in probe position, and the influence of locally high turbulence levels, are difficult to diagnose and to correct. This, in fact, is the main reason why the curve-fitting procedure is restricted to data for which $y^+ > 50$. For the present tests, the discrepancies between the data and the universal correlation as illustrated in Figure 29 and for particularly $y/\delta < 0.2$ in Figure 30, are similar in trend and magnitude to those associated with the numerous experiments examined by Coles⁸ and are not considered unusual. Consequently, the curve-fitting procedure is assumed to provide an accurate determination of the parameters δ , u_τ and $\tilde{\pi}$. A summary of the boundary layer parameters obtained from the curve-fitting process is presented in Table 2.

Clauser⁴ defines an effective displacement thickness of the turbulent boundary layer in terms of the transformed velocities as:

$$\Delta = -\delta \int_0^\infty (u^+ - u_e^+) d(y/\delta) \quad 9a$$

and the corresponding shape factor as:

$$G = \int_0^{\infty} (u^+ - u_e^+)^2 d(y/\Delta) \quad 9b$$

where for constant pressure layers G and Δ/δ have the values 6.8 and 3.6, respectively. Written in the velocity defect form used in Equation 9, Equation 8 becomes:

$$u^+ - u_e^+ = \frac{1}{\kappa} \ln y/\delta - \frac{\tilde{\kappa}}{\kappa} (W-2) \quad 10$$

Typical plots of $u^+ - u_e^+$ versus y/Δ for survey stations located just upstream of, at the midpoint, and at the rear of the ramp, are shown in Figure 31 for Ramp 1 and Ramp 3 in order to illustrate the effect of the pressure gradient on the shape of the velocity profile. For Ramp 1, the pressure gradient is relatively weak and δ_k is nearly constant and the velocity profiles are independent of streamwise location. The pressure gradient for Ramp 3 is stronger and initially the velocity profile is distorted (compare $x = 5.08$ cm station to $x = 0$ cm station). However, since δ_k decreases with x , the effect of the pressure gradient diminishes and the shape of the velocity profile at the rear of the ramp is almost identical to that where $dp/dx = 0$.

A plot of the boundary layer thickness δ versus axial position x is shown in Figure 32 which includes values of δ obtained from the curve-fit to the Law-of-the-Wake correlation and those determined directly from the measured velocity profile. The latter were evaluated from visual inspection of the profile by selecting the y location where the boundary layer data merged with the data in the external stream and denoting this position and the associated velocity as the edge conditions. The thickness δ was defined then as the y position where $u = 0.995 u_e$. With the exception of the forward portion of Ramp 3, the results derived from the correlation are in excellent agreement with those obtained from the profile data. The values of δ used subsequently in this report are those determined from the curve-fit of the velocity profile.

Figure 33 presents a plot of the wake parameter $\tilde{\omega}$ versus axial station x . For both ramps, $\tilde{\omega}$ jumps to a peak value then similar to δ_k , decreases as the rear of the ramp is approached. However, while δ_k is a maximum at the leading edge of the ramp, the variation of $\tilde{\omega}$ with x in this region is much slower, with $\tilde{\omega}$ not reaching its maximum value until $x = 3$ or 4 cm. Since the pressure waves generated by the curved ramp surface are swept downstream, then just behind the leading edge of the ramp the outer portion of the boundary layer retains a memory of its upstream history (i.e., the flow here is still characteristic of $dp/dx = 0$). This is also the wake portion of the boundary layer which contributes largely to the value of $\tilde{\omega}$. Therefore, just downstream of the leading edge, the boundary layer is not in equilibrium with the local value of δ_k . (Strictly speaking, the procedure for curve-fitting the data to the "Law-of-the-Wake" is not valid for these first few survey stations since the velocity correlation is restricted to equilibrium flows). This is indicated in Figure 34 where $\tilde{\omega}$ is plotted versus δ_k . The lack of correlation between $\tilde{\omega}$ and δ_k at the first two ramp survey stations for Ramp 3 is quite apparent. Figure 34 also includes the data of Sturek & Danberg⁷ and Lewis, et al⁶, and the results of a number of low speed experiments examined by Coles & Hirst¹¹ and correlated by Lewis, et al⁶. Interestingly enough, the data of Sturek and Danberg⁷ lie near the upper bound to the spread of the low speed data while those of the present tests fall near the lower bound of the low speed data. For Ramp 1, the values of δ_k are too small to identify any specific trend of $\tilde{\omega}$ with δ_k . Finally, a plot of Clauser's⁴ shape factor G versus δ_k is shown in Figure 35. Again, the present data for Ramp 3 lie near the lower bound of the spread of the low speed data, although the general trend of increasing G with increasing δ_k is apparent. The results for Ramp 1 lie within the low speed data spread while, for comparison, the results of Lewis, et al⁶ are near the upper bound of the low speed data and in slightly better agreement with the theoretical results of Mellor and Gibson¹². Excluding the flow just downstream of the ramp leading edge, the results shown in Figures 34 and 35 are in agreement with the earlier findings of Lewis, et al⁶; namely, that the boundary layer is in approximate local equilibrium throughout the adverse pressure gradient region. Thus, the boundary layer profiles are characterized by local conditions only and unaffected by the fact that δ_k is not constant.

A plot of the wall shear stress τ_w , determined from the curve-fit to the "Law-of-the-Wake," versus axial station is shown in Figure 36 which includes wall shear measurements made with the 0.1 cm diameter Preston tube. The Preston tube data was reduced using the Bradshaw-Unsworth¹³ correlation:

$$\frac{\Delta p}{\tau_w} = 96 + 60 \log_{10}(u_d/50v_w) + 23.7 \left[\log_{10}(u_d/50v_w) \right]^2 + 10^4 M_\infty^2 \left[(u_d/v_w)^{0.26} - 2.0 \right]$$

where Δp is the Preston tube reading, d is the tube diameter and $M_\infty = u_\infty/a_\infty$. The two sets of results are in very good agreement although the Preston tube measurements are generally lower than the data obtained from the velocity correlation with a maximum difference of 9% at the rear of Ramp 3. Both results, however, show a continuous increase in τ_w in the downstream direction. To be consistent with the selection of the boundary layer thickness δ , the wall shear stress determined from the curve-fit to Equation 5 is used subsequently in this report. A plot of the local skin friction coefficient c_f versus Re_δ is presented in Figure 37 which includes, for comparison, the skin friction coefficient for $dp/dx = 0$ calculated from the Karman-Schoenberg equation together with the Van Driest transformation as outlined in Hopkins and Inouye¹⁴. For a given M_∞ and Re_δ , the maximum deviation between the measured c_f and that calculated for $dp/dx = 0$ is about 10% with the measured values somewhat larger. This contrasts with earlier findings which indicate that c_f decreases as δ_k is increased. Nevertheless, it appears that the increase in the local wall shear stress is the consequence of increases in the local dynamic pressure brought about by the pressure gradient.

3. NON-DIMENSIONAL BOUNDARY LAYER PROFILES

As indicated in Section 3, the boundary layer profiles measured along the

vertical to the surface of the ramp (i.e., perpendicular to the tunnel axis) were interpolated to provide profiles normal to the surface. With the boundary layer thickness δ now determined as described in Section IV-2, the boundary layer profiles along the normal can be non-dimensionalized. At each survey station, the velocity u at the position $y = \delta$ was arbitrarily assumed equal to $0.995 u_e$, providing a means for specifying u_e . The profile data was searched to find $y = y_e$ at $u = u_e$, and the edge values of the remaining properties were defined as their values at y_e . The edge conditions u_e , ρ_e , and M_e and the integral properties δ^* and θ and listed in Table 2. Because of the variation of static pressure across the boundary layer and the lack of a freestream region of uniform flow, it was necessary to modify the conventional expressions for the integral properties. The definitions used here were suggested by McLafferty and Barber¹⁵, and recommended by Sturek and Danberg⁷, and take into account the flux deficit appearing within the boundary layer referenced to "ideal" properties calculated with the experimental static pressure profile. The integral thicknesses are referenced to the ideal properties at the wall and in the case of constant static pressure reduce to the classical definitions. According to this interpretation, the integral profiles are given by:

$$u_w^\# \delta_k^* = \int_0^\infty (u^\# - u) dy$$

$$\rho_w^\# u_w^\# \delta^* = \int_0^\infty (\rho^\# u^\# - \rho u) dy$$

$$\rho_w^\# u_w^{\#2} \theta = \int_0^\infty \rho u (u^\# - u) dy$$

where the ideal properties $\rho^\#$ and $u^\#$ are calculated using the measured static pressure profile assuming constant total temperature equal to the freestream T_{oe} value and constant stagnation pressure equal to the test section total pressure p_o .

Profiles of u/u_e versus y/δ at each survey station along the curved surface are shown in Figures 38 and 39, for Ramps 1 and 3, respectively. Similarly,

profiles of Mach number, M , versus y/δ for Ramps 1 and 3 are shown, respectively, in Figures 40 and 41. These figures indicate that for each ramp, the development of the boundary layer is gradual and continuous and free of discontinuities. For Ramp 3 in particular, the profile plots reveal gradual changes in the sublayer thickness which occur along the length of the ramp.

In a recent paper, Whitfield and High¹⁶ examined the effect of non-unity Prandtl number on the total temperature-velocity relationship for zero pressure gradient flows. The classical Crocco relation $H = u/u_e$ is restricted to unity Prandtl number, an assumption made to eliminate the turbulent shear stress terms from the combined energy-momentum equation. As a consequence, the Crocco relations fail to predict the well-known total temperature overshoot observed in non-unity Prandtl number, adiabatic boundary layers. To overcome this problem, Whitfield and High¹⁶ introduced an approximate model for the turbulent shear stress distribution and derived an analytical solution which provides a reasonable agreement with experimental observations (e.g., see Reference 3). For the present experiments, it was found that the H versus u/u_e relation is insensitive to the pressure gradient although, as shown later, the shear stress distribution apparently is strongly dependent on τ_k . It is of interest, therefore, to examine more closely the Whitfield and High¹⁶ solution. The combined energy momentum equation can be expressed as:

$$\frac{d^2 \bar{h}}{d\bar{u}^2} + (1 - P_{rm}) \frac{1}{\tau} \frac{d\tau}{d\bar{u}} \frac{d\bar{h}}{d\bar{u}} + P_{rm} (\gamma - 1) M_\infty^2 = 0 \quad 11$$

where, using the Whitfield-High notation, the overbars represent normalization with respect to the freestream values (i.e., $\bar{h} = h/h_\infty$, $\bar{u} = u/u_\infty$). Whitfield and High assume that the Reynolds shear stress is proportional to the turbulent kinetic energy which, on the basis of an earlier study¹⁷, leads to the following approximation:

$$\tau = u_\tau^2 \exp(-4(y/\delta)^{5/2}) \quad 12$$

Using the definition of u_τ , Equation 12 can be rewritten as:

$$\frac{\tau}{\tau_w} = \frac{c}{c_w} \exp (- 4(y/\delta)^{5/2}) \quad 13$$

With the further assumption that the velocity profile can be expressed as a power law:

$$\bar{u} = (y/\delta)^{1/m} \quad 14$$

Equation 11 can be written in the form:

$$\bar{h} \frac{d^2 \bar{h}}{d \bar{u}^2} - \epsilon (4 - \gamma \bar{u}^{\gamma-1} \bar{h} + \frac{d \bar{h}}{d \bar{u}}) \frac{d \bar{h}}{d \bar{u}} + (1 - \epsilon) A \bar{h} = 0 \quad 15$$

where:

$$\epsilon = 1 - \text{Pr}_m$$

$$\gamma = 5/2 \text{ m}$$

$$A = (\gamma-1) M_\infty^2$$

Equation 15 is a second order, non-linear ordinary differential equation for $\bar{h}(\bar{u})$ which was solved by Whitfield and High¹⁶ assuming a solution of the form:

$$\bar{h}(u) = \bar{h}_0(\bar{u}) + \epsilon \bar{h}_1(\bar{u}) + \dots \quad 16$$

subject to the boundary conditions for the adiabatic case:

$$\frac{d\bar{h}_0(0)}{d\bar{u}} = \frac{d\bar{h}_1(0)}{d\bar{u}} = 0 \quad 17$$

$$\bar{h}_0(1) = 1$$

$$\bar{h}_1(1) = 0$$

Returning to Equation 13 the density ratio (using a typical measured adiabatic wall profile for $M_\infty = 3$ and $dp/dx = 0$), the exponential term and the ratio τ/τ_w have been plotted in Figure 42. It is seen that the density change across the sublayer is much larger than the change in exponential term so that τ/τ_w reaches a peak value of almost 1.5 at $y/\delta \sim 0.15$. As shown later, the shear stress distribution in Figure 42 is similar to that for $\delta_k \sim 0.4$. In a recent study, Sandborn¹⁸ concluded that for $dp/dx = 0$, the shear stress distribution τ/τ_w versus y/δ is essentially independent of Mach number and insensitive to wall temperature. In fact, his "best estimate" of τ/τ_w versus y/δ is closely approximated by the exponential term in Equation 13 and Figure 42. Consequently, the Whitfield-High¹⁶ analysis is repeated below using the following expression for the turbulent shear stress:

$$\tau = u_\tau^2 \rho_w \exp(-4(y/\delta)^{5/2}) \quad 18$$

Note that at $y/\delta = 0$ Equation 18 is equivalent to Equation 4.12. Again, using the definition of u_τ , Equation 18 becomes:

$$\frac{\tau}{\tau_w} = \exp(-4(y/\delta)^{5/2}) \quad 19$$

Assuming $u = (y/\delta)^{1/m}$, Equation 11 can be expressed as:

$$\frac{d^2 \bar{h}}{d^2 \bar{u}} - \epsilon 4\gamma \bar{u}^{\gamma-1} \frac{d\bar{h}}{d\bar{u}} + (1-\epsilon)A = 0 \quad 20$$

where Equation 20 is now a second order, linear differential equation for $\bar{h}(u)$ subject to the boundary conditions given by Equation 17. It is again assumed that the solution has the form expressed by Equation 16 leading to:

$$\bar{h} = 1 + \frac{A}{2} [1-\bar{u}^2] - \epsilon \left\{ \frac{A}{2} [1-\bar{u}^2] + \frac{4A\gamma}{(\gamma+1)(\gamma+2)} [1-\bar{u}^{\gamma+2}] \right\} \quad 21$$

where at the wall:

$$\bar{h}_w = 1 + \frac{A}{2} - \epsilon \left(\frac{A}{2} - \frac{4A\gamma}{(\gamma+1)(\gamma+2)} \right) \quad 22$$

Note that Equation 21 reduces to the Crocco relation when $\epsilon = 0$.

In the present nomenclature, the Crocco parameter H can be expressed as:

$$H = \frac{\bar{h} + \frac{A}{2} \bar{u}^2 - \bar{h}_w}{1 + \frac{A}{2} - \bar{h}_w} \quad 23$$

so that, substituting Equations 21 and 22 into Equation 23, we have for the adiabatic case:

$$H = \bar{u}^2 \frac{\left[1 - \frac{8 \gamma \bar{u}^2}{(\gamma+1)(\gamma+2)} \right]}{\left[1 - \frac{8 \gamma}{(\gamma+1)(\gamma+2)} \right]} \quad 24$$

Thus, to first order, the $H - \bar{u}$ relationship is independent of both M_∞ and Pr_m although it does depend on the velocity power law exponent m . It is interesting to note that the correction introduced by retaining the shear stress term in Equation 11 represents a departure from the Walz¹⁹ quadratic law rather than the linear Crocco relation.

To verify that the power series solution for $\bar{h}(\bar{u})$ converges rapidly, Equation 20 was solved retaining terms of the order of ϵ^2 . While the resulting solution for H now shows a dependence on ϵ , it differs from the first order solution by less than 1%.

For the case of constant wall temperature, Equation 11 was solved subject to the boundary conditions:

$$\begin{aligned} \bar{h}_0(0) &= \bar{h}_w \\ \bar{h}_1(0) &= 0 \\ \bar{h}_0(1) &= 1 \\ \bar{h}_1(1) &= 0 \end{aligned} \quad 25$$

Following the same procedure used for the adiabatic case, we obtain for the $H - \bar{u}$ relation:

$$H = \bar{u} \left\{ 1 + \frac{\epsilon}{1 + \frac{A}{2} - \bar{h}_w} \left[\frac{4A\gamma}{(\gamma+1)(\gamma+2)} (1 - \bar{u}^{\gamma+1}) - \frac{4}{\gamma+1} \left(1 + \frac{A}{2} - \bar{h}_w \right) (1 - \bar{u}^\gamma) - \frac{A}{2} (1 - \bar{u}) \right] \right\}.$$

26

In this case again, the Crocco relation $H = \bar{u}$ is recovered when $\epsilon = 0$.

The consequences of the present solutions for H versus \bar{u} will now be considered. For the adiabatic case, Equation 24 is plotted in Figure 43 for several values of m and is compared to the Whitfield-High¹⁶ solution (for $M_\infty = 3$, $Pr_m = .88$, $m = 7$) and typical experimental data (for the same Mach number). It is seen that shape of the H versus \bar{u} curve given by Equation 24 is quite similar to the solution of Whitfield and High¹⁶ (and to the data) and that both predict the T_o overshoot. However, for a given y/δ , Equation 24 predicts larger values of H than the Whitfield-High¹⁶ solution. In addition, increasing the value of m shifts Equation 24 closer to the data. A comparison of the power law velocity profile for several values of m to a typical experimental zero pressure gradient, adiabatic wall velocity profile is shown in Figure 44. This plot demonstrates that the power law profile does not provide a good representation of the data inasmuch as the value of m which fits the experimental profile increases with y/δ . In Figure 43, this implies that $H - \bar{u}$ relation shifts toward curves with increasing values of m as \bar{u} increases. In view of the sensitivity of Equation 24 to the exponent m it would be of interest to solve the basic equation using a more realistic velocity profile. This, however, would probably require a numerical solution.

It should be pointed out that for the adiabatic case, the temperature difference $T_{oe} - T_w$ is not large and for the present case where $M_\infty = 3$, is only

about 18 - 20°C. The parameter H is quite sensitive and for example, an increment of 0.1 in H represents only a 2° change in the local total temperature. Hence, the apparently large differences in Figure 43 correspond to only a few degrees in absolute temperature. With this in mind, it is suggested that the T_o distribution across the boundary layer is insensitive to the model assumed for the turbulent shear stresses. This may explain why the present tests, where the pressure gradient produces large changes in the shear stress distribution, indicate similar results for the variation of H versus \bar{u} . This is shown in Figure 45 when H versus \bar{u} has been plotted for $dp/dx = 0$ and for forward and aft position on both ramps. The similarity in the H profiles is quite obvious and in general, differences from the $dp/dx = 0$ case cannot be distinguished.

Before closing this discussion, it is instructive to examine the solution for the constant wall temperature case. A plot of Equation 26 for $M_\infty = 3$, $Pr_m = .88$, $m = 7$ and several values of wall temperature is presented in Figure 46 where it is compared to the Crocco relation, the Whitfield-High¹⁶ solution and typical experimental data³. The differences between Equation 26 and the solution of Whitfield and High are quite small, both are in good agreement with the data, and it is apparent that even for modest heat transfer rates (i.e., the $T_w/T_{oe} = .714$ case) the classical Crocco relation is a good approximation to the data.

4 DETERMINATION OF STREAMWISE DERIVATIVES

In order to calculate the turbulent shear stress distribution at survey stations located along the curved ramp surface, it is necessary to first calculate the y profile of the streamwise gradient of ou , ou^2 and p . At this stage, the flow field data is specified in terms of profiles of u , ρ , ou , etc., along the normal to the surface at several streamwise locations. The set of y locations generally differ at each survey station. Therefore, a reference station, generally located near the midpoint of the ramp, is selected and the y locations at this station are denoted y_o . At each remaining station, the profile data is

interpolated to determine the flow properties at y_0 . For each y_0 then, the properties u , ∂u , ∂u^2 and p are curve-fit to a second order polynomial in terms of the streamwise distance s and the resulting expression can be differentiated analytically to determine $d \partial u(y_0, s)/ds$, etc.

An illustration of the newly interpolated flow field and the resulting curve-fitted flow field is shown for Ramp 1 in Figures 47-49 where, respectively, u , ∂u and p have been plotted versus s for selected y positions. Similar plots of u , ∂u and p versus s for Ramp 3 are shown in Figures 50-52, respectively. In carrying out the curve-fit, particular caution must be exercised concerning the data from the first few survey stations on the ramp. The pressure waves generated by the ramp are swept downstream and the leading pressure wave penetrates the outer edge of the boundary layer several centimeters downstream of the ramp leading edge. In this region, the inner portion of the boundary layer feels the influence of the pressure gradient while the outer portion is characteristic of $dp/dx = 0$. Moving downstream from the leading edge, the inner portion influenced by $dp/dx > 0$ grows thicker while the outer portion, where the effect of $dp/dx = 0$ persists, tends to vanish. Data from survey stations within this region should be excluded from the curve-fit since the profiles here are not characteristic of the equilibrated boundary layer in an adverse pressure gradient. This effect is illustrated in Figure 51 where the data at x stations 0, .63, and 1.9, particularly at the outer edge of the layer, does not blend smoothly with the downstream flow field.

A partial test of the validity of the curve-fit is provided by examining the changes introduced by arbitrarily eliminating data from some of the survey stations. For Ramp 1, for example, the results obtained by retaining the rear survey stations and eliminating one or more of the forward survey stations (starting with $x = 2.74$ cm) differed to an unacceptable degree. Only a slight improvement was observed by reversing the procedure. However, a significant improvement was obtained by including the $x = -1.27$ station in the curve-fit. In this case, eliminating downstream stations produces only small changes in the curve-fit parameters and provided acceptable shear stress distributions over most of the ramp. Including this station, although it is located upstream

of the ramp, was justified by the relatively small pressure gradient associated with Ramp 1 and the fact that the edge properties do not vary significantly in the streamwise direction (see Figures 47-49). For Ramp 3, however, it was considered necessary to exclude the data from the first three ramp stations from the curve-fit.

Illustrations of the y variation of the streamwise derivatives $\partial \rho u / \partial s$, $\partial \rho u^2 / \partial s$, and $\partial p / \partial s$ for Ramp 3, $x = 7.62$ cm are shown in Figures 54-56, respectively. These curves are not considered typical since the magnitude of the derivatives and the shape of the curves depend on s and dp/dx , but they demonstrate that the curve-fitting procedure yields continuous results with relatively little scatter in the derivatives.

5. TURBULENT SHEAR STRESS DISTRIBUTION

a. Zero Pressure Gradient Region

Combining the continuity and streamwise momentum equations for a zero pressure gradient, adiabatic boundary layer yields:

$$\tau - \tau_w = \int_0^y \frac{\partial}{\partial x} (\rho u^2) dy - u \int_0^y \frac{\partial}{\partial x} (\rho u) dy \quad 27$$

Following Sturek² we assume that the flow is locally similar (i.e., that u/u_e , ρ/ρ_e , etc., are functions only of y/δ) so that Equation 4.27 can be rewritten as:

$$\frac{\tau - \tau_w}{\rho_\infty u_\infty^2} = \frac{1}{\delta} \frac{d\delta}{dx} \left[\int_0^y \frac{\rho u^2}{\rho_\infty u_\infty^2} dy - \frac{u}{u_\infty} \int_0^y \frac{\rho u}{\rho_\infty u_\infty} dy \right] \quad 28$$

The assumption of local similarity is a convenient approximation and is not valid near the wall. However, in this region the contribution of the convective terms is quite small and the use of the approximation across the entire boundary layer is justified. With this assumption, we can also write:

$$\frac{1}{\delta} \frac{d\delta}{dx} = \frac{1}{\theta} \frac{d\theta}{dx} = \frac{1}{\theta} \frac{c_f}{2} \quad 29$$

Substituting this relation into Equation 28, we have:

$$\frac{\tau}{\tau_w} = 1 + \frac{1}{\theta \rho_\infty u_\infty^2} \left(\int_0^y \rho u^2 dy - u \int_0^y \rho u dy \right) \quad 30$$

which can be evaluated numerically using the measured profile data.

b. Adverse Pressure Gradient Region

According to Sturek², the equations of continuity and momentum conservation for a two dimensional boundary layer over a surface with longitudinal curvature are:

Continuity

$$\frac{\partial}{\partial s} (\rho u) + \frac{\partial}{\partial y} [(1 + ky)(\rho v + \overline{\rho'v'})] = 0 \quad 31$$

Momentum

$$\begin{aligned} \frac{1}{1+ky} \rho u \frac{du}{ds} + (\rho v + \overline{\rho'v'}) \frac{du}{dy} + (\rho v + \overline{\rho'v'}) u \frac{k}{1+k} \\ = - \frac{1}{1+ky} \frac{\partial p}{\partial s} + \frac{\partial \tau}{\partial y} \end{aligned} \quad 32$$

Integrating Equations 31 and 32 in the direction y normal to the surface and combining the resulting equations yields the following relation for the shear stress distribution:

$$\begin{aligned} \frac{\tau}{\tau_w} = 1 + \frac{1}{\tau_w} \left\{ \int_0^y \theta \frac{\partial}{\partial s} (\rho u^2) dy - u \theta \int_0^y \frac{\partial}{\partial s} (\rho u) dy \right. \\ \left. - 2 \int_0^y \left[\int_0^y \frac{\partial}{\partial s} (\rho u) dy \right] u \theta^2 k dy + \int_0^y \theta \frac{\partial p}{\partial s} dy \right\} \quad 33 \end{aligned}$$

The streamwise derivatives $\frac{\partial}{\partial s}$ appearing in the above equation were determined using the curve-fit procedure described in the previous section. The values of the wall stress τ_w were taken from the correlation of the measured profile data with Coles "Law-of-the-Wake."

c. Results

The computed normalized shear stress distributions for Ramp 1 are shown in Figure 56 and include the stress distribution in the zero pressure gradient region 1.27 cm upstream of the ramp leading edge and those obtained in the adverse pressure gradient region at stations ranging from $x = 5.27$ to 12.79 cm. The scatter in the data points is nil and for clarity, the shear stress distributions have been represented by continuous lines drawn through the data points. In the zero pressure gradient case, the computed shear stress distribution is in good agreement with expectations based on Sandborn's "best estimate" for flat plate boundary layers.¹⁸ For the adverse pressure gradient region, the stress distributions indicate a peak at $y \approx 0.2$ to 0.3 cm ($y/\delta \approx .3$ to .45), with the location of the peak value shifting away from the wall at the downstream locations. In addition, the shear stress remains finite at the edge of the layer although there is a systematic shift in the sign of the residual τ from negative to slightly positive in the downstream direction.

If the data input to Equation 33 were completely accurate, the shear stress should tend to zero in the external flow. (Actually, the flow in the external stream is not uniform, so that the streamwise derivatives there do not identically vanish and τ remains finite, albeit small). Even if the measured profiles were highly accurate, each of the subsequent manipulations to which the data is subjected introduces an uncertainty which reflects in the final result. Thus, the non-vanishing stress at the boundary layer edge in Figure 56 is believed to be primarily a consequence of the data processing. It is

possible to "correct" the data so that the shear stress does vanish at the edge of the boundary layer. For example, Sturek² altered his profile of $\partial u / \partial s$ versus y to eliminate a large negative residual stress at $y/\delta = 1.0$. However, there is no rationale for changing only one of the derivative terms to the exclusion of the others. It is also possible to alter the curve-fit described in Section IV-4 by excluding some of the profile stations. Here again, there is no basis for culling the data used in the curve-fit except for data just behind the leading edge as discussed in the previous section. Consequently, the data has been left unaltered and the shear stress distributions at x stations 8.98, 10.25 and 11.52 cm, where τ/τ_w becomes negligible at the edge of the boundary layer, are considered representative of Ramp 1.

Since the flow properties from $y = 0$ to $y = y$ all contribute to the magnitude of τ at $y = y$, any correction which would cause $\tau \rightarrow 0$ at $y = \delta$ would also introduce a change of the same sign and a proportional magnitude to the peak shear stress. In Figure 56, it appears that if τ was adjusted to vanish at the edge of the layer, then the stress distributions τ/τ_w versus y/δ tend to approach each other. This implies that the normalized shear stress distribution is insensitive to x location, i.e., to ξ_k , and is, instead, dependent on dp/dx . The results show further that even a weak pressure gradient $\xi_k \approx 0.4$ produces a peak shear stress 60% greater than the wall shear.

The shear stress distributions for Ramp 3 are shown in Figure 57 which includes again the zero pressure gradient result and the results for surveys stations in the adverse pressure region ranging from $x = 3.18$ to 7.62 cm. While the peak shear stress in this case is 3 to 3.5 times the wall value, the behavior of the stress distribution as a function of x is similar to that observed for Ramp 1 and most of the comments made concerning the Ramp 1 results apply to Ramp 3 as well. In particular, the shear stress does not completely vanish at the edge of the boundary layer (although $\tau \rightarrow 0$ in the external stream). The residual shear stress at $y \sim \delta$ is generally positive with a maximum absolute value of $0.4 \tau_w$, which is probably the maximum uncertainty introduced by the data processing procedure, and is now only 10% of the maximum shear stress

in the boundary layer. This data shows more conclusively that the normalized shear stress distribution appears to be dependent on dp/dx rather than δ_k which, for this ramp, decreases by a factor of almost two in the streamwise direction. Sturek's⁷ results indicate a relaxation effect on the shear stress profile since the maximum τ/τ_w at his forward survey station (which was located near the mid-point of his ramp) was one-half the peak τ/τ_w observed at his downstream stations. However, in his case, dp/dx varied continuously from 0 to a finite value at the forward survey station where it remained constant over the remainder of the ramp. This contrasts the present experiment where a constant dp/dx was imposed at the ramp leading edge and may account for his observations. It should also be noted that the peak τ/τ_w increased quickly downstream of his first survey station.

The effect of pressure gradient on the turbulent shear stress distribution across the boundary layer is illustrated in Figure 58 where stress profiles τ/τ_w versus y for $dp/dx = 0$ and representative stations of Ramp 1 ($dp/dx = 1.2$ mmHg/cm) and Ramp 3 ($dp/dx = 5$ mmHg/cm) are shown. It is apparent that the stress distribution is extremely sensitive to dp/dx with the peak value of τ/τ_w rising from 60 to 300% above the wall value for the weak to moderate pressure gradients used in the present tests. It should be emphasized that while τ/τ_w versus y is invariant with x location, the absolute magnitude of τ is increasing since τ_w increases with x . This is demonstrated in Figure 59 where τ versus y has been plotted for selected x stations along Ramp 3. Note that the maximum shear stress τ at the downstream position on this ramp is 5-6 times greater than τ_w in the $dp/dx = 0$ flow ahead of the ramp.

Since δ_k is a decreasing function of x for a constant pressure gradient flow, it cannot be used to correlate the shear stress τ/τ_w which appears to be insensitive to x . However, the parameter δ_{ko} , where δ_k^* and τ_w are evaluated in the zero pressure gradient flow just upstream of the curved surface, is a characteristic of the flow field and remains constant for constant dp/dx . A plot of the peak value of τ/τ_w versus δ_{ko} , including data from Sturek's⁷ experiment and the present tests, is shown in Figure 60. The dashed line representing a linear variation of $(\tau/\tau_{wall})_{max}$ with δ_{ko} was drawn through the

most representative values of $(\tau/\tau_{\text{wall}})_{\text{max}}$ obtained from the present tests. Although the data do not follow a linear variation, they indicate a consistent trend and demonstrate a reasonable agreement between the results of the two experiments.

6. TURBULENT TRANSPORT COEFFICIENTS

With the turbulent shear stress distribution determined, it is possible to calculate the mixing length ℓ , and the eddy viscosity ϵ , using the following expressions:

$$\frac{\ell}{\delta} = \left[\frac{\tau/\rho_e u_e^2}{(\rho/\rho_e) \left[\partial(u/u_e)/\partial(y/\delta) \right]^2} \right]^{\frac{1}{2}} \quad 34$$

and

$$\frac{\epsilon}{u_e \delta_k^*} = \frac{\tau/\rho_e u_e^2}{(\rho/\rho_e) \left[\partial(u/u_e)/\partial(y/\delta) \right] (\delta_k^*/\delta)} \quad 35$$

In the above expressions, τ is the turbulent shear stress and is obtained by subtracting from the stresses computed in the previous section the laminar contribution $\mu \partial u / \partial y$. Because of the very high density of data points, $\partial u / \partial y$ was determined directly from the measured velocity profile using a simple differencing scheme and no attempt was made to smooth either the velocity profile or the variation of $\partial u / \partial y$. As a result, the results for ℓ/δ and $\epsilon/u_e \delta_k^*$ reflect the scatter in the velocity gradient term. A typical plot of $\partial(u/u_e)/\partial(y/\delta)$ is shown in Figure 61.

Near the outer edge of the boundary layer, both τ and $\partial u / \partial y$ tend toward zero. As a consequence, large errors are introduced in the calculation of $\epsilon/u_e \delta_k^*$ and, particularly, in ℓ/δ . For this reason, when $y/\delta > 0.8$ these quantities are considered unreliable and are not included in the results.

A plot of ℓ/δ versus y/δ for the zero pressure gradient boundary layer upstream of Ramp 3 is shown in Figure 62. The scatter in the data, while not small, does not detract from a well-defined trend. Both the slope of the data in the wall region ($\ell/\delta = 0.4 y/\delta$) and the magnitude of ℓ/δ in the plateau region are in good agreement with the conventionally accepted results of Maise and McDonald.²⁰ The influence of the adverse pressure gradient on ℓ/δ is shown in Figures 63 and 64 for Ramp 3 and Ramp 1, respectively. Because of the scatter in the results, the variation of ℓ/δ with y/δ has been represented by a curve drawn through the mean of the data points and the maximum range of the scatter is denoted by a vertical bar on each mean curve. While τ/τ_w was shown to be insensitive to x , the mixing length is not normalized by a wall parameter and, therefore, ℓ/δ is dependent on the x station and increases in the downstream direction. From Equations 34 and 35, it can be shown that

$$\ell/\delta \propto (\tau/\rho)^{1/2} / (\partial u/\partial y)$$

$$\frac{\epsilon}{u_e \delta_k^*} \propto (\tau/\rho) / (\partial u/\partial y)$$

A close examination of the data reveals that while τ and ρ both increase with x , the ratio τ/ρ also increases and $\partial u/\partial y$ actually decreases. As a consequence, for a given y/δ in the plateau region, both ℓ/δ and $\epsilon/u_e \delta_k^*$ increase in the downstream as shown in Figures 63 through 67. Two points of particular interest are apparent in Figures 63 and 64. First, in the adverse pressure gradient region, the slope k ($\ell/\delta = k y/\delta$) in the wall region is 0.65 and is independent of x and dp/dx . This finding is identical to Sturek's observation,² and its implication on the "wall-wake" velocity correlations described in Section IV-2 is pursued further in Appendix B. Second, the magnitude of ℓ/δ is similar to the values found by Sturek,² although Sturek's value of δ_{ko} and those for Ramps 1 and 3 differ by as much as a factor of 9.

A plot of the normalized eddy viscosity $\epsilon/u_e \delta_k^*$ versus y/δ for the same $dp/dx = 0$ station shown in Figure 62 is presented in Figure 65 where it is found to be

in excellent agreement with the universally accepted results of Maise and McDonald²⁰ for a similar M_∞ and Re_δ . The effect of adverse pressure gradient on the eddy viscosity is shown in Figures 66 and 67 where, similar to the mixing length, the data points have been replaced by continuous curves faired through the points and the maximum scatter in the data is represented by vertical bars. These figures reflect the same behavior observed for the mixing length and show that the eddy viscosity increases with x , with somewhat larger increases apparent for the larger value of dp/dx . In fact, the maximum value of $\epsilon/u_e \delta_k^*$ is even larger than that found by Sturek² although Sturek's value of ϵ_{k0} is twice as large as that for Ramp 3. However, for the zero pressure gradient case, Sturek found $\epsilon/u_e \delta_k^*$ to be only half as large as that predicted by Maise and McDonald²⁰ and this discrepancy may also be reflected in his adverse pressure gradient results.

SECTION V

SUMMARY AND CONCLUSIONS

Measurements have been made of mean flow profiles at several streamwise locations in the supersonic turbulent boundary layer over a curved ramp surface. Two ramp models, designed to produce a constant adverse pressure gradient flow, were used with $\delta_{k0} \equiv (dp/dx)(\delta_k^*/\tau_w)_0$ (with $(\delta_k^*/\tau_w)_0$ evaluated upstream of the ramp where $dp/dx = 0$) equal to 0.41 and 1.85. Analysis of the profile data indicated that:

- 1) With an appropriate compressibility transformation, the data correlates with the well-defined Coles "wall-wake" incompressible velocity profile.
- 2) Correlation of the wake parameter $\tilde{\pi}$ and the Clauser shape factor G with the local pressure gradient parameter δ_k is in agreement with the low speed data.
- 3) In agreement with the earlier findings of Lewis, et al,⁶ the boundary layer appears to be in a state of local equilibrium and is not dependent on upstream history.
- 4) The total temperature profile, in the form $(T_o - T_w)/(T_{oe} - T_w)$ versus u/u_e is insensitive to the pressure gradient and is similar to the variation for a zero pressure gradient boundary layer.
- 5) The skin friction coefficient c_f was found to be essentially the same as for $dp/dx = 0$, implying that the observed increases in wall shear are a consequence of the increased external stream dynamic pressure introduced by the pressure gradient.

Using the "indirect method," the flow field measurements were further analyzed to extract the turbulent transport terms from the mean flow data. Results show that:

- 1) The distribution of τ/τ_w , z/δ and $\epsilon/u_e \delta_k^*$ across the boundary layer for the

zero pressure gradient data of the present experiment are in good agreement with the earlier findings of Sandborn¹⁸ and Maise and McDonald.²⁰

2) The variation of the turbulent shear stress τ with distance from the surface is significantly distorted by even modest values of dp/dx . In contrast to the zero pressure gradient distribution, when $dp/dx > 0$, τ increases above its wall value, reaching a maximum at y/δ about 0.3 to 0.4.

3) The normalized shear stress distribution τ/τ_w versus y/δ is independent of the local ε_k , although the peak value of τ/τ_w appears to correlate with ε_{ko} .

4) The maximum values of ℓ/δ and $\varepsilon/u_e \delta_k^*$ for the adverse pressure gradient flows reflect the increases observed in the maximum values of τ .

5) In the region of the wall, the slope constant k in the expression $\ell/\delta = k(y/\delta)$ is 0.65 for the adverse pressure gradient case in contrast to the zero pressure gradient value of 0.4. The value of k is independent of ε_k and x and is identical to the result obtained by Sturek² for $\varepsilon_{ko} \approx 3.45$.

TABLE 1
TYPICAL OUTPUT FROM PROGRAM BLSURV2

BOUNDARY LAYER SURVEYS, X(CM) = 4.445

	PITOT SURVEY	STATIC SURVEY	TEMP SURVEY
P0(MMHG)	729	730.5	730
T0(DEG K)	316.6667	316.6667	317.2222
PW(MMHG)	43.41195	43.50127	43.4715

WHAT ARE FILES PTXXXX,PSXXXX,TXXXX,PTXXXX,PLORXXXX
33PT1750,3PS1750,3T1750,3PT1750,3MFL1750

PITOT PRESSURE PROFILE

Y(MM)	PT(MM)	Y(CM)	PT(MMHG)	PT/P0
-4791	545	.0076196	52.84865	.0724947
-4789	560	.008034	54.3032	.07449
-4782	584	.0094842	56.63048	.0776824
-4777	615	.0105201	58.63855	.081806
-4769	642	.0121776	62.25474	.0853974
-4762	669	.0136278	64.87293	.0889886
-4759	679	.0142494	65.84863	.0903191
-4752	713	.0156996	68.13961	.0948417
-4744	749	.0173571	70.63053	.0998304
-4736	777	.0180145	72.34566	.1033549
-4726	802	.0210863	75.6664	.1066863
-4723	810	.0217079	76.5457	.1077444
-4720	822	.0223294	78.70934	.1099407
-4711	841	.024194	81.55177	.111868
-4698	866	.0268874	83.97602	.1151924
-4686	883	.0293735	85.62451	.1174547
-4674	905	.0318597	87.75785	.1203811
-4664	925	.0333315	89.69723	.1230415
-4652	948	.0364176	91.92756	.1261009
-4640	958	.0389038	93.89726	.1274311
-4623	973	.0424259	94.34573	.1296924
-4615	982	.0440833	95.82454	.1306623
-4589	1007	.04947	97.64876	.1329449
-4566	1037	.0542351	100.5579	.1379995
-4541	1057	.0594146	102.4973	.1405668
-4518	1073	.0641798	104.0488	.1427281

-4496	1097	.0699808	106.3761	.1459206
-4488	1116	.0745388	108.2185	.1484479
-4444	1139	.0795111	110.4488	.1515073
-4417	1161	.0851049	112.5822	.1544337
-4379	1186	.0929778	115.0064	.1577591
-4348	1208	.0994004	117.1398	.1606835
-4314	1241	.1064443	120.3398	.1650751
-4274	1265	.1147317	122.6671	.1688676
-4238	1287	.1221902	124.8004	.1711939
-4210	1302	.1261366	126.2549	.1731892
-4194	1342	.1385574	130.1837	.1785099
-4098	1380	.1511954	133.8186	.1835646
-4036	1429	.1640405	138.5701	.1900825
-3978	1474	.176057	142.9338	.1960683
-3916	1513	.1889621	146.9095	.201522
-3853	1562	.2019545	151.4671	.2077739
-3790	1612	.2145824	156.3156	.2144247
-3727	1660	.2274375	160.9702	.2208096
-3665	1711	.2406828	165.9157	.2275693
-3602	1764	.2539713	171.0551	.2346493
-3543	1809	.2675759	175.4187	.2406993
-3486	1868	.2817989	181.14	.2484773
-3426	1916	.2964203	185.7945	.2548862
-3365	1968	.3030583	190.8337	.2617791
-3303	2028	.3159035	196.6552	.2669760
-3243	2083	.3283343	201.9983	.2770761
-3183	2137	.3407651	207.2249	.2842591
-3123	2187	.3531959	212.0734	.29091
-3064	2239	.3653419	217.1158	.2978269
-3002	2298	.3782646	222.8971	.305673
-2943	2334	.3864883	228.2674	.313124
-2888	2409	.4031268	233.6007	.32044
-2831	2461	.4161786	238.6432	.3273569
-2773	2511	.4290237	243.4917	.3340078
-2716	2566	.4416617	248.825	.3413238
-2653	2618	.4545069	253.8673	.3482407
-2592	2668	.4673552	258.716	.3548916
-2531	2718	.479999	263.5645	.3615425
-2470	2768	.4926688	268.413	.3681934
-2408	2815	.5053875	272.9706	.3744432
-2346	2864	.5183183	277.7221	.3809631
-2285	2912	.5307491	282.9766	.3873479
-2223	2953	.5431799	288.4942	.3935368
-2162	2996	.5558179	290.1342	.3979694
-2099	3027	.5682487	293.5282	.402645
-2035	3066	.5806795	297.31	.4078327
-1969	3093	.5935247	300.1222	.4116902
-1902	3127	.6061626	303.2252	.4159468
-1840	3150	.6190078	305.4553	.4190062
-1778	3172	.631853	307.5888	.4219326
-1718	3184	.6442838	308.7525	.4233628
-1656	3204	.6571289	310.6919	.4261891
-1595	3208	.6699769	311.0798	.4266761
-1533	3213	.6826121	311.5646	.4273869
-1471	3214	.6954572	311.6616	.4275319
-1406	3216	.7089236	311.8355	.4277263
-1345	3214	.7213547	311.6616	.4275319

-1285	3206	.7339927	310.8858	.4264552
-1224	3198	.7466307	310.1101	.425391
-1160	3188	.7598902	309.1404	.4240608
-1098	3174	.7727354	307.7828	.4221986
-1039	3160	.784959	306.4252	.4203363
-980	3145	.7971826	304.9706	.4183411
-918	3133	.8100278	303.807	.4167449
-857	3119	.8226657	302.4494	.4148826
-796	3108	.8353037	301.3828	.4134194
-736	3099	.8477345	300.51	.4122223
-674	3089	.8605797	299.5403	.4108921
-614	3076	.8730105	298.2797	.4091629
-552	3070	.8858556	297.6979	.4083647
-490	3064	.8987008	297.1161	.4075666
-430	3060	.9111316	296.7282	.4070346
-367	3057	.9241839	296.4373	.4066355
-305	3054	.9370291	296.1464	.4062363
-243	3051	.9498743	295.8555	.4058374
-180	3049	.9629266	295.6615	.4055714
-119	3046	.9755646	295.3706	.4051723
-57	3041	.9884097	294.8858	.4045072
4	3035	1.001048	294.3039	.4037091
67	3032	1.0141	294.013	.4033101
126	3027	1.026324	293.5282	.4028645
187	3021	1.038962	293.2464	.4018469
248	3015	1.0516	292.3645	.4010488
308	3007	1.06403	291.5888	.3999846
370	3000	1.076876	290.91	.3990535
431	2992	1.089514	290.1342	.3979894
491	2982	1.101944	289.1645	.3966592
551	2972	1.114375	288.1948	.3953329
612	2961	1.127013	287.1282	.3938858
673	2947	1.139651	285.7706	.3920035
734	2932	1.152289	284.316	.3900083
796	2916	1.165134	282.7645	.38788
857	2902	1.177772	281.4069	.3860178
919	2888	1.190617	280.0494	.3841555
981	2874	1.203463	278.6918	.3822933
1042	2866	1.216101	277.916	.3812291
1103	2857	1.228739	277.0433	.3800319
1164	2843	1.241377	275.6857	.3781697
1225	2833	1.254014	274.716	.3768395
1285	2822	1.266645	273.6493	.37533763
1346	2811	1.279083	272.5827	.37391131
1407	2801	1.291721	271.613	.3725829
1468	2788	1.304359	270.3524	.3708537
1528	2775	1.31679	269.0917	.3691245
1588	2755	1.329221	267.1522	.3664841
1647	2741	1.341444	265.7948	.3646019
1707	2712	1.353875	262.9826	.3607444
1768	2653	1.366513	257.4553	.3531623
1814	2509	1.376044	243.2977	.3337417
1841	2455	1.381637	238.0613	.3265588

STATIC PRESSURE PROFILE

V (MM)	P0 (MMV)	Y (CM)	P1 (MMHG)	P1/P0
-3704	1013	.3080803	41.66469	.0570359
-3643	1006	.3207183	41.37678	.0566417
-3580	1001	.3337706	41.17113	.0563602
-3518	995	.3466158	40.92436	.0560224
-3456	992	.3594609	40.80096	.0558535
-3394	995	.3723061	40.92436	.0560224
-3332	992	.3851512	40.80096	.0558535
-3271	996	.3977892	40.33418	.0555156
-3209	979	.4106344	40.26627	.0551215
-3149	972	.4230652	39.97836	.0547274
-3088	970	.4357032	39.8961	.0546148
-3029	967	.4479268	39.77271	.0544459
-2966	962	.4603576	39.56706	.0541644
-2903	958	.4729936	39.40254	.0539391
-2843	953	.4854264	39.19689	.0536576
-2786	946	.4982713	38.90898	.0532635
-2724	940	.5111167	38.6622	.0528257
-2663	939	.5237547	38.62107	.0528694
-2600	933	.5368007	38.37429	.0525315
-2538	927	.5496582	38.12751	.0521937
-2478	924	.5622083	38.00412	.0520248
-2416	920	.5749281	37.8396	.0517996
-2354	916	.5877733	37.67508	.0515744
-2291	912	.6008256	37.51056	.0513492
-2228	906	.613878	37.26378	.0510113
-2166	902	.6267231	37.09926	.0507861
-2104	901	.6395683	37.05813	.0507298
-2043	896	.6522063	36.81135	.050382
-1981	890	.6650514	36.6057	.0501105
-1920	884	.6776894	36.35892	.0497726
-1860	878	.6901202	36.11214	.0494348
-1797	873	.7031725	35.90649	.0491533
-1737	867	.7158033	35.65971	.0488155
-1676	863	.7282413	35.49519	.0485903
-1615	855	.7408793	35.16615	.0481398
-1554	848	.7535173	34.87824	.0477457
-1491	842	.7665696	34.63146	.0474079
-1431	836	.7790004	34.38468	.0470701
-1369	827	.7918456	34.01451	.0465633
-1307	821	.8046907	33.76773	.0462255
-1246	815	.8173287	33.52095	.0458877
-1184	808	.8301739	33.28304	.0454936
-1122	801	.843019	32.94513	.0450994
-1061	794	.855657	32.65722	.0447053
-999	788	.8685022	32.41044	.0443675
-939	781	.880933	32.12253	.0439733
-877	777	.8937781	31.95801	.0437481
-816	775	.9064161	31.87575	.0436355
-755	768	.9190541	31.58784	.0432414
-694	763	.9316921	31.38219	.0429599
-634	758	.9441229	31.17654	.0426784
-574	756	.9565537	31.09428	.0425637
-512	753	.9693988	30.97089	.0423968
-450	748	.982244	30.76524	.0421153
-389	747	.994882	30.72411	.042059
-329	746	1.007313	30.68298	.0420027

-268	745	1.019951	30.64185	.0419464
-207	743	1.032589	30.55959	.0418938
-146	736	1.045227	30.27168	.0414397
-82	734	1.058486	30.18942	.0413271
-21	731	1.071124	30.06603	.0411582
41	729	1.083969	29.98377	.0410455
101	725	1.0964	29.81925	.040820
163	722	1.109245	29.69586	.0406514
225	720	1.122091	29.6136	.0405388
287	715	1.134936	29.40795	.0402573
348	712	1.147574	29.28456	.0400984
409	709	1.160212	29.16117	.0399195
470	703	1.17285	28.91439	.0395816
529	695	1.185073	28.58535	.0391312
590	689	1.197711	28.33857	.0387934
650	684	1.210142	28.13292	.0385119
710	679	1.222573	27.92727	.0382303
772	675	1.235418	27.76275	.0380051
832	671	1.247849	27.59823	.0377799
892	664	1.26028	27.31032	.0373858
954	656	1.273125	26.98128	.0369354
1014	651	1.285336	26.77563	.0366538
1076	645	1.298401	26.52885	.036316
1138	639	1.311246	26.28207	.0359782
1199	631	1.323884	25.95303	.0355278
1261	622	1.336729	25.58286	.035021
1324	615	1.349781	25.28495	.0346269
1386	607	1.362626	24.96591	.0341765
1447	600	1.375264	24.678	.0337823
1509	591	1.38811	24.30783	.0332756
1572	580	1.401162	23.8554	.0326563
1633	564	1.4138	23.19732	.0317554
1694	552	1.426438	22.70376	.0310798
1757	537	1.43949	22.08681	.0302352
1818	522	1.452128	21.46986	.0293906
1879	508	1.464766	20.89404	.0286024
1940	494	1.477404	20.31822	.0278141
2001	479	1.490042	19.70127	.0269696
2063	465	1.502887	19.12545	.0261813

RECOVERY TEMPERATURE PROFILE

Y (MM)	TT (MM)	Y (CM)	TT (DEG F)	TT/T0
-4873	109	.0152399	300.5442	.9474249
-4841	108	.0218696	300.2986	.9466305
-4778	107	.034922	300.0529	.9458761
-4716	106	.0477671	299.8073	.9451017
-4654	107	.0606123	300.0529	.9458761
-4593	107	.0732503	300.0529	.9458761
-4530	107	.0863026	300.0529	.9458761
-4471	108	.0985262	300.2986	.9466505
-4412	108	.1107498	300.2986	.9466505
-4351	108	.1233878	300.2986	.9466505
-4288	110	.1364402	300.7899	.9481993
-4228	110	.148871	300.7899	.9481993
-4167	112	.1615089	301.2812	.9497481
-4108	112	.1737326	301.2812	.9497481
-4048	113	.1861634	301.5269	.9505223
-3992	113	.1977654	301.5269	.9505223
-3932	115	.2101962	302.0182	.9520713
-3870	115	.2230414	302.0182	.9520713
-3808	116	.2358866	302.2638	.9528457
-3747	117	.2485245	302.5095	.9536201
-3685	118	.2613697	302.7551	.9543945
-3624	119	.2740077	303.0008	.9551688
-3562	120	.2868528	303.2464	.9559432
-3501	120	.2994908	303.2464	.9559432
-3439	121	.312336	303.4921	.9567176
-3377	122	.3251811	303.7378	.957492
-3316	124	.3378191	304.2291	.9590408
-3257	123	.3500427	303.9834	.9582664
-3196	125	.3626807	304.4747	.9598152
-3137	125	.3749043	304.4747	.9598152
-3077	126	.3873351	304.7204	.9605896
-3016	127	.3999731	304.966	.961364
-2956	128	.4124039	305.2117	.9621384
-2895	128	.4250419	305.2117	.9621384
-2833	129	.4378871	305.4573	.9629128
-2771	129	.4507322	305.4573	.9629128
-2711	129	.463163	305.4573	.9629128
-2649	129	.4760082	305.4573	.9629128
-2587	129	.4888533	305.4573	.9629128
-2524	129	.5019057	305.4573	.9629128
-2462	128	.5147508	305.2117	.9621384
-2399	128	.5278032	305.2117	.9621384
-2338	129	.5404412	305.4573	.9629128
-2276	128	.5532863	305.2117	.9621384
-2215	127	.5659243	304.966	.961364
-2152	126	.5789766	304.7204	.9605896
-2091	126	.5916146	304.7204	.9605896
-2030	125	.6042526	304.4747	.9598152
-1969	125	.6168906	304.4747	.9598152
-1906	124	.6299429	304.2291	.9590408
-1846	123	.6423737	303.9834	.9582664

.0156996	.0948417	.0594219	.9473712
.0173571	.0996304	.0594084	.9471776
.0190145	.1033549	.0593948	.946984
.0210863	.1066803	.0593779	.946742
.0217079	.1077444	.0593728	.9466694
.0223294	.1093407	.0593678	.9466232
.024194	.111868	.0593526	.9465126
.0268874	.1151934	.0593306	.9463528
.0293735	.1174547	.0593103	.9462053
.0318597	.1203811	.05929	.9460578
.0339315	.1230415	.0592731	.9459349
.0364176	.1261009	.0592528	.9457859
.0389038	.1274311	.0592325	.945636
.0424259	.1296924	.0592038	.9454237
.0440833	.1306235	.0591902	.9453238
.04447	.133949	.0591463	.9452044
.0542351	.1379395	.0591074	.9454916
.0594146	.1405998	.0590651	.9458039
.0641798	.1427281	.0590262	.9458761
.0699808	.1458206	.0589789	.9458761
.0745388	.1484479	.0589417	.9458761
.0795111	.1515073	.0589011	.9458761
.0851049	.1544337	.0588555	.9458761
.0929778	.1577591	.0587912	.946299
.0994004	.1606855	.0587388	.9466505
.1064445	.1650751	.0586813	.9466505
.1147317	.1682676	.0586137	.9466505
.1221902	.1711939	.0585528	.9466505
.1261266	.1731892	.0585207	.9469755
.1385574	.1785099	.0584193	.9481993
.1511954	.1835646	.0583161	.9484841
.1640405	.1900825	.0582113	.9497481
.176057	.1960683	.0581133	.9498929
.1889021	.201522	.0580084	.9505225
.2019545	.2077739	.0579019	.9510444
.2145924	.2144247	.0577988	.9520713
.2274376	.2208096	.057694	.9523363
.2402828	.2275935	.0575891	.953115
.2527136	.2346435	.0574877	.9538726
.2657659	.2406293	.0573812	.9546638
.2779895	.2484773	.0572814	.9554089
.2904203	.2548622	.05718	.9559432
.3030583	.2617791	.0570768	.9561583
.3159035	.2697602	.0569719	.9569327
.3283343	.2770761	.0564775	.9578785
.3407651	.2842591	.0561763	.9588542
.3531959	.29091	.0559359	.9586528
.3654195	.2978269	.0559318	.9598152
.3782646	.305675	.055944	.9600246
.3904883	.313124	.0557108	.9607828
.4031262	.32044	.0553519	.9615605
.4161786	.3273569	.0549457	.9621384
.4290237	.3340078	.0546743	.9623785
.4416617	.3413238	.0545324	.9629128
.4545069	.3482407	.0542969	.9629128
.467352	.3548916	.0540397	.9629128
.47999	.3615425	.0537807	.9629128

.492628	.3681934	.0534366	.9629128
.5058873	.3744452	.0530632	.9626727
.5183183	.3809631	.0528936	.9621384
.5307491	.3873479	.0526883	.9623189
.5431799	.3935938	.0523639	.9627477
.5558179	.3979694	.0521099	.9619833
.5682487	.4026445	.0519167	.9612261
.5806795	.4078327	.0516987	.9605896
.5935247	.4116902	.0514751	.9604726
.6061626	.4159468	.051211	.9598150
.6190078	.4190062	.0509214	.9596896
.631853	.4219326	.0507636	.9589218
.6442838	.4235288	.0506038	.9581474
.6571289	.4261891	.0502841	.957492
.6697669	.4267212	.0499844	.957371
.6826121	.4273863	.0496389	.9565599
.6954572	.4275193	.0493187	.9559438
.7089239	.4277853	.0489997	.9557246
.7213547	.4275193	.048713	.9551688
.7339927	.4264552	.0483853	.9549787
.7466307	.425391	.0479605	.9543395
.7598902	.4240608	.0475808	.9543395
.7727354	.4221986	.0472403	.9542012
.784959	.4203363	.046835	.9536201
.7971826	.4183411	.046423	.9536201
.8100278	.4167449	.0460828	.9536201
.8226657	.4148826	.0457239	.9536201
.8353037	.4134194	.0453362	.9536201
.8477345	.4122223	.0449524	.9536201
.8605797	.4108921	.0445758	.9534776
.8730105	.4091629	.0442245	.9527115
.8858556	.4083647	.043887	.9520713
.8987008	.4075666	.0437043	.9524323
.91111316	.4070346	.0434885	.9534494
.9241839	.4066355	.0431271	.9528457
.9370291	.4062365	.042839	.9528457
.9498743	.4058374	.0426263	.9528457
.9629266	.4055714	.0424819	.9528457
.9755646	.4051723	.0422617	.9528457
.9884097	.4045072	.0420878	.9528457
1.001048	.4037091	.0420311	.9528457
1.0141	.4033101	.0419725	.9528457
1.026324	.402645	.0418896	.9526196
1.038962	.4018469	.0416351	.9521
1.0516	.4010488	.0413855	.9521912
1.06403	.3999846	.041253	.9522809
1.076876	.3990535	.0411077	.9523736
1.089514	.3979894	.0409451	.9524648
1.101944	.3966592	.0407474	.9525545
1.114375	.395329	.0406064	.9526442
1.127013	.3938658	.0404309	.9527354
1.139651	.3920035	.0401943	.9528266
1.152289	.3900083	.0400254	.9529177
1.165134	.38788	.0397879	.9530104
1.177772	.3860178	.0394002	.9531016

[illegible]

P0.N/M2	=	97309
T0.DEG K	=	316.6667
TW.DEG K	=	300
PS.MMHG	=	43.4715
X.CM	=	4.445

48

.0121776	.7383105 272.6355	244.324 302.3584	.0741315 43.39895	1055012 18.11211
.0136278	.7817124 269.7145	257.2972 302.6776	.0749195 43.39031	1132431 19.27657
.0142494	.7968992 268.6717	261.7883 302.7956	.0752038 43.38661	1160121 19.68748
.0156996	.8453348 265.2215	275.911 303.1265	.0761669 43.37797	1251120 21.01529
.0173571	.8921666 261.7135	289.2644 303.3763	.0771703 43.3681	1343103 22.32261
.0190145	.9259801 259.1104	298.7308 303.5447	.0779278 43.35822	1411890 23.27943
.0210863	.9545485 256.8574	306.6048 303.6649	.0785889 43.34588	1471646 24.09574
.0217079	.9633748 256.1561	309.0178 303.7033	.0787973 43.34218	1490422 24.34978
.0223294	.9763181 255.1397	312.5477 303.7794	.0791044 43.33848	1518154 24.72391
.024194	.9963088 253.5492	317.9516 303.8854	.0795802 43.32737	1561513 25.30266
.0268874	1.021786 251.5004	324.7619 304.016	.0801988 43.31132	1617882 26.0455
.0293735	1.038516 250.1343	329.1818 304.0891	.0806092 43.29651	1655544 26.53507
.0318597	1.05946 248.4244	334.6706 304.1934	.0811362 43.2817	1703561 27.15391
.0339315	1.077933 246.9098	339.4665 304.2887	.0816106 43.26936	1746692 27.70406
.0364176	1.098615 245.2029	344.7816 304.3926	.0821505 43.25455	1795841 28.324
.0389038	1.107591 244.4375	347.0556 304.4105	.0823796 43.23974	1817327 28.59029
.0424259	1.122542 243.1692	350.8267 304.4527	.082769 43.21876	1853571 29.03757
.0440833	1.128642 242.6474	352.3546 304.4658	.082928 43.20888	1868481 29.22007
.04947	1.150016 240.8735	357.7126 304.5863	.0834766 43.17679	1920877 29.86064

.0542351	1.174798 238.9162	363.9334 304.8643	.0841051 43.1484	1982141 30.60866
.0594146	1.191177 237.6481	368.0268 305.088	.0844934 43.11755	2022462 31.09583
.0641798	1.204154 236.5967	371.2123 305.2091	.084813 43.08916	2055124 31.48361
.0699808	1.223158 235.0272	375.8181 305.3528	.0853108 43.0546	2104278 32.06134
.0745388	1.237954 233.803	379.3721 305.4649	.0857034 43.02745	2143115 32.51346
.0795111	1.25553 232.3464	383.5578 305.5985	.0861812 42.99783	2190059 33.05546
.0851049	1.272177 230.965	387.4864 305.7253	.0866294 42.9645	2234940 33.56771
.0929778	1.290982 229.5052	391.9695 306.0055	.0870851 42.9176	2284602 34.13472
.0994004	1.307233 228.2381	395.8065 306.2434	.0874905 42.87934	2328322 34.62929
.1064445	1.330912 226.2665	401.2319 306.425	.0881663 42.83738	2395603 35.37515
.1147317	1.348231 224.8241	405.1554 306.5579	.0886297 42.78801	2444666 35.90879
.1221902	1.3639 223.5191	408.6729 306.6782	.0890544 42.74358	2489714 36.39414
.1261266	1.374346 222.7257	411.0713 306.8638	.0893226 42.72012	2519302 36.71795
.1385574	1.402057 220.7034	417.4517 307.4736	.0899847 42.64607	2597020 37.56424
.1511954	1.428011 218.6082	423.1561 307.766	.0906866 42.57078	2674252 38.37457
.1640405	1.460422 216.2016	430.3718 308.426	.0915309 42.49426	2770735 39.39234
.176057	1.488727 213.8946	436.3559 308.6914	.0923664 42.42267	2860664 40.30464
.1889021	1.515343 211.8215	442.0097 309.1011	.0930976 42.34615	2944597 41.15005
.2019545	1.545117 209.4788	448.1954 309.5001	.0939657 42.26839	3042073 42.11498

.2145924	1.576052 207.1584	454.6295 310.0721	.0948487 42.19311	3144256 43.12101
.2274376	1.605316 204.8182	460.4482 310.3831	.0957581 42.11658	3246203 44.09165
.2402828	1.635773 202.5013	466.5228 310.87	.0966774 42.04006	3352940 45.10221
.2527136	1.667032 200.1259	472.6411 311.3557	.0976522 41.96601	3465935 46.15446
.2657659	1.692225 198.2581	477.5398 311.8055	.0983893 41.88825	3556756 46.98482
.2779895	1.726182 195.688	483.9547 312.3066	.0995078 41.81543	3686624 48.15726
.2904203	1.753108 193.6514	488.9394 312.6846	.1003759 41.74138	3791133 49.07772
.3030583	1.78176 191.4271	494.0681 312.9706	.1013586 41.66609	3907247 50.07806
.3159035	1.817309 188.7893	500.4416 313.4888	.1022612 41.43807	4041258 51.17576
.3283343	1.850525 186.3886	506.338 314.044	.1030044 41.22854	4164744 52.15503
.3407651	1.882734 184.0912	511.9663 314.6003	.1037332 41.00866	4287041 53.10788
.3531959	1.911613 181.8443	516.6372 314.7456	.104565 40.83317	4408048 54.02217
.3654195	1.936702 180.1609	520.9896 315.311	.105534 40.83023	4523208 54.98209
.3782646	1.964441 178.1136	525.4403 315.5827	.1067697 40.83914	4662003 56.1011
.3904883	1.995178 175.9615	530.4278 316.0526	.1076244 40.66889	4795210 57.08698
.4031262	2.027737 173.699	535.6069 316.5392	.1083232 40.40688	4929759 58.01866
.4161786	2.060909 171.3801	540.7232 316.9623	.1089826 40.11039	5067433 59.92942
.4290237	2.089327 169.3702	544.9553 317.2401	.1097305 39.91224	5196635 59.79823
.4416617	2.117138 167.476	549.1125 317.6106	.110683 39.80868	5335239 60.77741

.4545069	2.145396 165.4789	553.1108 317.8059	.1115355 39.6367	5474262 61.69147
.467352	2.173108 163.5376	556.9625 317.9954	.112323 39.44899	5610646 62.55968
.47999	2.200765 161.6231	560.7396 318.183	.1131081 39.25994	5749107 63.42419
.492628	2.23025 159.6049	564.693 318.3802	.1138048 39.00875	5892126 64.26478
.5058875	2.259098 157.6141	568.4188 318.4815	.1144361 38.73613	6032466 65.04761
.5183183	2.284095 155.8571	571.4962 318.4812	.1153554 38.61231	6176792 65.9252
.5307491	2.309392 154.2136	574.771 318.7068	.1161316 38.46248	6315027 66.7491
.5431799	2.33703 152.4734	578.3588 319.0266	.1167331 38.22567	6454316 67.51362
.5558179	2.357081 151.0549	580.601 318.902	.1172571 38.04025	6564722 68.07961
.5682487	2.376508 149.691	582.7377 318.7757	.1178861 37.89919	6678959 68.69669
.5806795	2.398207 148.2145	585.1511 318.7027	.1185599 37.74009	6808170 69.37547
.5935247	2.415876 147.0841	587.2099 318.7741	.1189538 37.57685	6903706 69.85085
.6061626	2.435842 145.7379	589.3473 318.68	.119436 37.38405	7016684 70.3893
.6190078	2.452779 144.6702	591.2674 318.741	.1196365 37.17262	7099865 70.73716
.631853	2.465962 143.7454	592.5421 318.5676	.1200327 37.05745	7181620 71.12444
.6442838	2.475078 143.0728	593.3395 318.3658	.1202169 36.94075	7233985 71.32945
.6571289	2.491728 141.9642	595.0125 318.2472	.1203898 36.7074	7317948 71.63344
.6697669	2.501323 141.3662	596.0443 318.261	.1201784 36.48863	7346810 71.63165
.6826121	2.512647 140.566	597.0457 318.0558	.1200267 36.23637	7389164 71.66142

.6954572	2.521694 139.9343	597.8474 317.901	.1197932 36.00339	7416053 71.61864
.7089239	2.530374 139.3849	598.7265 317.8754	.1194784 35.76781	7434938 71.53486
.7213547	2.537414 138.886	599.3167 317.7285	.1192124 35.56048	7450845 71.44598
.7339927	2.543202 138.5148	599.8805 317.694	.1187277 35.32126	7446314 71.22246
.7466307	2.551817 137.9214	600.622 317.5438	.1181916 35.01115	7452007 70.9885
.7598902	2.558403 137.5331	601.324 317.5756	.117587 34.73396	7442354 70.70786
.7727354	2.562212 137.2803	601.6653 317.5272	.1169607 34.48544	7419823 70.37122
.784959	2.567972 136.8585	602.0908 317.3606	.1163146 34.18955	7405589 70.03198
.7971826	2.573582 136.5295	602.6806 317.3853	.1155693 33.88876	7382153 69.65137
.8100278	2.57845 136.2449	603.1907 317.407	.1149623 33.64047	7364142 69.34418
.8226657	2.583063 135.9754	603.672 317.4267	.1142931 33.37846	7340888 68.99554
.8353037	2.589961 135.5748	604.392 317.4593	.1136587 33.09539	7329333 68.69439
.8477345	2.597737 135.1254	605.2008 317.4969	.1130714 32.81523	7324278 68.43089
.8605797	2.604948 134.6897	605.9017 317.484	.1124869 32.54036	7317281 68.15603
.8730105	2.610104 134.2851	606.1884 317.2524	.1119368 32.28391	7305816 67.85477
.8858556	2.617196 133.7897	606.7134 317.074	.1114938 32.03754	7308875 67.64477
.8987008	2.620415 133.6563	607.1566 317.2085	.1111404 31.90412	7297962 67.47961
.9111316	2.625716 133.4967	608.0213 317.5721	.1107239 31.74658	7289264 67.32247
.9241839	2.635667 132.8486	608.8424 317.4215	.1103394 31.4828	7307599 67.17933

.9370291	2.645108 132.3163	609.7985 317.4696	.1100429 31.27248	7327425 67.10401
.9498743	2.651722 131.9451	610.4647 317.5029	.1098046 31.11717	7339233 67.03183
.9629266	2.654753 131.7748	610.7679 317.517	.1095743 31.01182	7336526 66.92444
.9755646	2.660973 131.4268	611.3901 317.5477	.1092948 30.85105	7343822 66.82176
.9884097	2.664642 131.2216	611.7549 317.5647	.1090154 30.72413	7340385 66.69069
1.001048	2.663716 131.2724	611.6607 317.558	.1088263 30.68269	7323814 66.56478
1.0141	2.664318 131.2385	611.7198 317.5601	.1087027 30.6399	7318011 66.49558
1.026324	2.664799 131.18	611.694 317.4859	.1085365 30.57942	7309639 66.39115
1.038962	2.669875 130.8255	612.0304 317.3364	.1081693 30.39359	7307822 66.20288
1.0516	2.675632 130.5179	612.6287 317.3936	.1077745 30.21145	7304727 66.02573
1.06403	2.676423 130.4853	612.7332 317.4248	.1074561 30.11466	7286139 65.84194
1.076876	2.678138 130.4021	612.9303 317.4619	.1071462 30.00864	7271907 65.67316
1.089514	2.679994 130.3108	613.1405 317.4988	.1067972 29.88992	7255572 65.48165
1.101944	2.682136 130.2033	613.3774 317.5361	.1063694 29.74562	7235024 65.24456
1.114375	2.682289 130.2058	613.4182 317.5634	.1059995 29.6427	7210217 65.02202
1.127013	2.683186 130.1672	613.5324 317.5947	.1055727 29.51457	7184560 64.77225
1.139651	2.684812 130.0881	613.7174 317.6285	.1050187 29.34181	7153193 64.45183
1.152289	2.68353 130.1692	613.6158 317.6476	.1045124 29.21851	7113266 64.13045
1.165134	2.684218 130.1418	613.7084 317.6767	.1039144 29.04515	7075067 63.77314

1.177772	2.691383 129.7575	614.4374 317.7382	.1032069 28.76218	7055237 63.41417
1.190617	2.699772 129.3076	615.2832 317.8062	.1024693 28.4576	7037898 63.04765
1.203463	2.704665 129.0505	615.785 317.8567	.1018311 28.22409	7013170 62.70607
1.216101	2.7114 128.694	616.4654 317.9177	.1013573 28.01516	7006865 62.48325
1.228739	2.716509 128.427	616.9858 317.9703	.100894 27.82924	6994695 62.25017
1.241377	2.717978 128.3576	617.1526 318.0034	.1003527 27.66494	6982673 61.93295
1.254014	2.724923 127.9851	617.8314 318.0483	.0998143 27.43663	6952359 61.66838
1.266445	2.734363 127.4669	618.7151 318.0742	.0991139 27.13379	6940548 61.32328
1.279083	2.743164 126.9854	619.5331 318.097	.0985017 26.8643	6932063 61.02505
1.291721	2.750225 126.5991	620.1825 318.1116	.0979734 26.63893	6922446 60.76136
1.304359	2.756775 126.2411	620.7798 318.1227	.0973564 26.39629	6904351 60.43688
1.31679	2.765322 125.7782	621.5618 318.1435	.0966914 26.11983	6890272 60.09967
1.329221	2.773818 125.3191	622.3325 318.1617	.095789 25.78157	6858671 59.61259
1.341444	2.784693 124.7375	623.321 318.1932	.0950406 25.46141	6846694 59.24078
1.353875	2.785815 124.6686	623.3999 318.1734	.0940156 25.17284	6777344 58.60933
1.366513	2.772958 125.3333	622.1749 318.0783	.0923567 24.86034	6610515 57.46205
1.376044	2.70472 128.9804	615.6306 317.692	.0889468 24.63867	6127481 54.75836
1.381637	2.682792 130.1757	613.4624 317.5604	.0875545 24.47758	5957311 53.71138

TABLE 2
TYPICAL OUTPUT FROM PROGRAM VCOLES

CORRELATION OF VELOCITY PROFILE, $\% \text{ STR} = 4.445$

Y	Y/D W	Y+	U+CALC	U+MEAS
.0531353	.0801155 .1146733	49.80966	14.57864	14.79432
.0582098	.0877667 .0993218	54.56656	14.81653	14.97616
.0628783	.0948057 .0810152	58.94287	15.02022	15.11615
.0685617	.1033749 .0769021	64.27055	15.25188	15.31576
.0730273	.110108 .0773659	68.45666	15.42326	15.47029
.0778987	.1174529 .0871261	73.02317	15.60111	15.65252
.0833791	.125716 .0906379	78.16056	15.79141	15.82684
.0910923	.1373457 .0855661	85.39101	16.04444	16.02869
.0973847	.1468332 .0875906	91.28958	16.24012	16.19625
.104286	.1572387 .1144229	97.75894	16.44546	16.43221
.1124051	.1694804 .1139447	105.3699	16.6766	16.61315
.1197124	.1804981 .1162526	112.2198	16.87654	16.77219
.1235689	.1863128 .1265411	115.835	16.97939	16.87591
.1357477	.2046755 .1499877	127.2515	17.294	17.16513
.1481294	.2233442 .1688905	138.8583	17.60081	17.42626

.160714	.2423188 .2167247	150.6552	17.90218	17.74845
.1724868	.3600694 .2558528	161.6812	18.17658	18.0217
.1850714	.279044 .2910561	173.4881	18.46348	18.28412
.1978591	.2983249 .3366755	185.4755	18.74952	18.56477
.2102408	.3169936 .3827732	197.0822	19.02215	18.85774
.2228255	.3359683 .4443797	208.8793	19.29556	19.13284
.2354102	.3549431 .5007945	220.6763	19.56576	19.41264
.2475889	.3733057 .5623822	232.0928	19.82447	19.69462
.2603765	.3925864 .6090759	244.08	20.09338	19.93838
.2723523	.4106431 .6787914	255.3063	20.34275	20.22844
.284531	.4290057 .7333837	266.7227	20.5939	20.47631
.2969127	.4476744 .78842	278.3295	20.84662	20.72254
.3094974	.4666491 .8620567	290.1266	21.10065	21.01437
.3216761	.4850117 .9342685	301.543	21.34357	21.29542
.3338549	.5033745 1.003763	312.9596	21.58341	21.56593
.3460336	.5217371 1.060022	324.376	21.81993	21.79889
.3580093	.5397936 1.111551	335.6022	22.049	22.01519
.3705939	.5587682 1.163589	347.3991	22.28565	22.23409
.3825697	.5768249 1.224856	358.6254	22.50669	22.47025

.3949514	.5954936 1.291039	370.2321	22.73062	22.71928
.4077391	.6147744 1.355325	382.2195	22.95661	22.96342
.4203237	.633749 1.408696	394.0164	23.17341	23.17569
.4327054	.6524177 1.460601	405.6232	23.38092	23.38083
.4452901	.6713925 1.509123	417.4202	23.58558	23.57633
.4578748	.6903672 1.556225	429.2173	23.78358	23.7662
.4702565	.7090359 1.603102	440.824	23.97153	23.9526
.4826382	.7277046 1.653876	452.4308	24.15235	24.14742
.4956288	.7472914 1.701692	464.6083	24.33406	24.33595
.5078075	.765654 1.741689	476.0248	24.49665	24.49867
.5199862	.7840166 1.781859	487.4413	24.65146	24.66042
.532165	.8023793 1.827006	498.8578	24.79821	24.83376
.5445467	.821048 1.85451	510.4646	24.93891	24.96097
.5567254	.8394106 1.877499	521.881	25.06872	25.07433
.5689041	.8577733 1.903132	533.2975	25.18982	25.19339
.5814889	.8767482 1.927032	545.0946	25.30561	25.30854
.5938705	.8954167 1.9464	556.7013	25.4101	25.40996
.6064552	.9143915 1.968009	568.4983	25.50657	25.51695

M	=	12
H	=	3
DEL*CM	=	.6632337
TAUM*POF	=	.9254465
UTAU*MC	=	25.72302
U-ID*MC	=	597.4773
FI	=	1.067166
RMS	=	.6774918

.0074651	.0112556	6.997874	9.729444	7.240673
.0078711	.0118678	7.378463	9.858316	7.707232
.0092919	.01401	8.710338	10.26227	8.40309
.0103068	.0155402	9.661717	10.51475	9.155495
.0119307	.0179887	11.18398	10.87133	9.756812
.0133514	.0201308	12.51576	11.14577	10.28938
.0138604	.021049	13.08665	11.25464	10.47628
.0153812	.0231912	14.41852	11.49137	11.05221
.0170051	.0256397	15.94078	11.73679	11.60948
.0186289	.028088	17.46295	11.96009	12.00858
.0206587	.0311484	19.36571	12.21372	12.34238
.0212677	.0320667	19.9366	12.28506	12.4432
.0218766	.0329848	20.50739	12.35442	12.58612
.0237034	.0357391	22.21985	12.55172	12.822
.0263422	.0397178	24.69349	12.81205	13.11116
.0287778	.0433901	26.97665	13.03083	13.30135
.0312136	.0470627	29.26	13.23251	13.53383
.0332434	.0501232	31.16276	13.38939	13.73708
.0356791	.0537957	33.44601	13.56608	13.9646
.0381149	.0574683	35.72936	13.73176	14.0688
.0415656	.0626711	38.96409	13.95031	14.23103
.0431894	.0651194	40.48626	14.04741	14.28779
.0484668	.0730765	45.43336	14.34151	14.52833
.6190399	.9333662	580.2954	25.59311	25.59337
.6312186	.9517288	591.7118	25.66733	25.64959
.6438033	.9707036	603.5089	25.73412	25.73119
.656185	.9893723	615.1156	25.78997	25.78834

INTERGAL PROPERTIES OF BOUNDARY LAYER

DELTA STAR K	(CM)=	.111976
DEL	(CM)=	3.405397
G	=	8.672578

VELOCITY DEFICIT CORRELATION

Y/DEL	U+DEF CAL	U+DEF MERC
.0021921	16.10727	18.59953
.0023114	15.9784	18.13298
.0027286	15.57444	17.43712
.0030266	15.32197	16.68471
.0035035	14.96538	16.0834
.0038207	14.69095	15.55083
.0040995	14.58208	15.36392
.0045167	14.34535	14.788
.0049936	14.09992	14.23073
.0054704	13.87653	13.83163
.0060665	13.62299	13.49783
.0062453	13.55165	13.39701
.0064241	13.4823	13.25409
.0069605	13.28499	13.01821
.0077354	13.02466	12.72905
.0084506	12.80588	12.53886
.0091659	12.6042	12.30637
.009762	12.44732	12.10313
.0104772	12.27063	11.87561
.0111925	12.10495	11.77141
.0122058	11.8864	11.60918
.0126826	11.7893	11.54242
.0142324	11.4952	11.31188
.0156033	11.25807	11.04589
.0170934	11.02018	10.86405
.0184643	10.81649	10.72406
.0201332	10.58484	10.52445
.0214446	10.41346	10.36991
.0228751	10.2356	10.18768
.0244844	10.0453	10.01336
.0267494	9.792267	9.811521
.0285972	9.596591	9.643957
.0306237	9.391252	9.407998
.0330079	9.160112	9.227056
.0351537	8.960176	9.068022
.0362862	8.857322	8.964295
.0398625	8.542717	8.675075
.0434984	8.235907	8.413945
.0471939	7.934536	8.091758
.050651	7.660135	7.818504
.0543465	7.37323	7.556091
.0581016	7.087188	7.275434
.0617375	6.814563	6.982463
.0654331	6.541148	6.707367
.0691286	6.270956	6.427566
.0727049	6.012245	6.145286
.07646	5.743333	5.901827
.0799767	5.493959	5.611768
.083553	5.242812	5.363897

.0871889	4.990091	5.117667
.0908844	4.738066	4.825839
.0944807	4.493144	4.544791
.098037	4.253299	4.274875
.1016133	4.016782	4.041319
.10513	3.787716	3.825016
.1088253	3.551106	3.606119
.1123428	3.330021	3.369957
.1159781	3.106093	3.120929
.1197339	2.88801	2.876791
.1234887	2.663304	2.664562
.1270646	2.455795	2.459373
.1307601	2.251133	2.263881
.1344556	2.053136	2.074012
.1380916	1.865183	1.887609
.1417375	1.684358	1.69279
.1453422	1.502651	1.504253
.1489185	1.340059	1.341542
.1526948	1.185256	1.179783
.1562711	1.038501	1.006449
.159907	.8977995	.8792348
.1634833	.767988	.7558727
.1670596	.6468909	.6468148
.1707551	.5311	.5316694
.174391	.4266121	.4302449
.1780865	.3301415	.3232527
.181782	.243597	.2468398
.1853583	.1693785	.1906152
.1890538	.1023949	.1090171
.1926897	.0467463	.0518658

READY

♦

TABLE 3
TYPICAL OUTPUT FROM PROGRAM TBLJNDIM

MEAN FLOW PROFILES
RAMP NO 3
% STATION CM= 4.445

WHAT ARE FILES NEWFLOWX, MEANXXXX, NEWFLOW3, 3MEAN175

VE CM = .7077287
TOE DEG K = 317.6915
TE DEG K = 138.1242
PE N/M2 = 4640.834
UE M/S = 600.477
PHOE KG/M3 = .1172954
REE M-1 = 7399242
ME = 2.549552

Y RE/REE	Y/D T/TE	M T0/TOE	U/UE P/PE	PHO/PHOE H
.0074651 .098391	.0112562 2.054554	.5381613 .945009	.3025571 1.24337	.6039412 .0125087
.0078711 .1060298	.0118684 2.046567	.573789 .9483852	.3219595 1.246962	.6097513 .0731369
.0092919 .1178002	.0140107 2.023841	.6285808 .9494479	.3507402 1.246659	.616443 .0922196
.0103068 .1312419	.015541 1.997098	.6885507 .9506188	.3816558 1.24644	.6245968 .1132467
.0119307 .142529	.0179896 1.97443	.7370736 .9517054	.4062262 1.246094	.6315842 .1327589
.0133514 .1530084	.0201318 1.953266	.7805458 .9527092	.4278733 1.24579	.638264 .1507844
.0139604 .1568004	.0210501 1.945616	.7959385 .9530835	.435456 1.245659	.6407005 .1575051

.0153812	.0231924	.843735	.4586752	.6487614
.1689363	1.920994	.9541131	1.245356	.1759944
.0170051	.025641	.8907117	.4809963	.6572809
.1813973	1.895557	.9549088	1.245008	.1902838
.0186289	.0280894	.9248149	.4969041	.6637432
.1907659	1.876564	.9554439	1.244659	.1998928
.0206587	.03115	.9536656	.5101528	.6693777
.198912	1.860099	.9558267	1.244223	.2067663
.0212677	.0320683	.9624432	.5141493	.6711263
.201432	1.855051	.955946	1.244092	.2089085
.0218766	.0329864	.9748909	.5198039	.6736319
.2050355	1.847969	.9561717	1.243963	.2129613
.0237034	.035741	.9955495	.529108	.6777777
.2110812	1.836076	.956517	1.243571	.219162
.0263422	.0397198	1.021067	.5404702	.6829912
.2186971	1.821222	.9569278	1.243003	.2265385
.0287778	.0433923	1.038005	.5479242	.6864747
.2238361	1.811213	.9571616	1.24248	.2307382
.0312136	.0470651	1.058814	.5570072	.6908756
.2302686	1.798912	.9574862	1.241957	.2365659
.0332434	.0501258	1.077124	.5649251	.6948289
.2360321	1.788042	.9577811	1.241519	.2418622
.0356791	.0537984	1.097761	.5737597	.6993576
.242642	1.775711	.9581063	1.240995	.2477011
.0381149	.0574712	1.107329	.5778002	.7013824
.2457194	1.769822	.9581755	1.240469	.2489448
.0415656	.0626743	1.12227	.584076	.7046161
.250589	1.760645	.9583071	1.239728	.2513074
.0431894	.0651227	1.128456	.5866563	.7059495
.252619	1.756815	.9583496	1.239376	.2520705
.0484668	.0730802	1.149738	.595538	.7104791
.2596301	1.74401	.9587169	1.238238	.2586668
.0531353	.0801196	1.174173	.6057484	.7156455
.267756	1.730008	.9595621	1.237229	.2738437
.0582098	.0877711	1.190918	.6127126	.7189168
.2732882	1.720591	.960264	1.23613	.2864486

.0628783	.0948105	1.264004	.6180645	.7215392
.2776928	1.712929	.9606559	1.235119	.2934859
.0685617	.1033801	1.222851	.6256741	.7255811
.2842167	1.701677	.9611136	1.233884	.3017046
.0730273	.1101135	1.237544	.6315524	.7287705
.2893766	1.692876	.9614643	1.232907	.3080015
.0778987	.1174588	1.254975	.6384658	.7326829
.2956167	1.682414	.9618785	1.231857	.31544
.0833791	.1257224	1.271758	.6450623	.7363787
.3016664	1.672331	.9622805	1.230661	.3226582
.0910923	.1373527	1.290975	.652681	.7401682
.3084316	1.661476	.9631492	1.228978	.3382588
.0973847	.1468406	1.307026	.6589919	.7433917
.3142057	1.652417	.9638896	1.227603	.3515535
.104286	.1572467	1.330198	.6678469	.7487779
.3229856	1.638951	.9644842	1.226091	.362231
.1124051	.169489	1.348146	.6746197	.7526572
.329757	1.62769	.9649189	1.224314	.370037
.1197124	.1805072	1.364033	.6805588	.7561092
.335827	1.618114	.9653048	1.222708	.3769669
.1235689	.1863222	1.374185	.6844271	.7582431
.3396742	1.61247	.9656355	1.221873	.3864968
.1357477	.2046859	1.402273	.6951747	.7636312
.350163	1.597534	.9677225	1.219183	.4203831
.1481294	.2233555	1.428638	.7048428	.7692674
.3605403	1.582224	.9687166	1.216436	.4382335
.160714	.2423311	1.460757	.7167194	.7760443
.3732817	1.56484	.9707012	1.213669	.4738722
.1724868	.2600826	1.489193	.7267491	.7827283
.3852317	1.548084	.9715992	1.21104	.4899986
.1850714	.2790582	1.51635	.7363443	.7887038
.3965929	1.532818	.972897	1.208257	.5133036
.1978591	.29834	1.545856	.7465628	.7954748
.4093255	1.51608	.9741848	1.205359	.5364277
.2102408	.3170097	1.576603	.7571822	.8026029
.4228384	1.499283	.9759078	1.202699	.5673693

.2228255	.3359854	1.606531	.767108	.810009
.4366005	1.482049	.9769667	1.199873	.586384
.2354102	.3549611	1.636888	.7771575	.8174509
.4307441	1.465236	.9784288	1.197176	.6126396
.2475889	.3733246	1.667866	.7872476	.8253089
.4656165	1.448198	.9799432	1.19464	.6388334
.2603765	.3926063	1.694745	.7959173	.8315811
.478433	1.433689	.981393	1.191703	.6658686
.2723523	.4106639	1.72742	.8061936	.8401338
.4948997	1.415828	.9829332	1.188967	.693526
.284531	.4290274	1.755797	.8149368	.8475467
.5094979	1.400319	.9842017	1.186354	.7163053
.2969127	.4476971	1.784722	.8235823	.8553714
.5248858	1.384205	.9852024	1.18355	.7342743
.3094974	.4666728	1.819109	.8337838	.8629301
.5424235	1.36358	.9866616	1.177951	.760479
.3216761	.4850363	1.852369	.8435739	.8690421
.5589201	1.34809	.9883391	1.171122	.790601
.3338549	.5034	1.884748	.8529652	.8749434
.5752379	1.331324	.9900552	1.164432	.8214181
.3460336	.5217636	1.914393	.8610223	.8815455
.5914548	1.314904	.9907222	1.158702	.8333955
.3580093	.539821	1.940522	.8684704	.889377
.6071275	1.301968	.9923788	1.157541	.8631445
.3705939	.5587966	1.968438	.8759671	.8990654
.625282	1.287241	.9933675	1.156933	.8808987
.3825697	.5768542	1.998498	.8840227	.9063104
.6429091	1.271883	.9947037	1.152354	.9048932
.3949514	.5955238	2.030687	.8924885	.9124632
.6609961	1.255587	.9961196	1.145319	.9303178
.4077391	.6148056	2.062892	.9007629	.9180124
.679007	1.239355	.9974492	1.13736	.9541938
.4203237	.6337812	2.091862	.9079335	.9240741
.6963817	1.224531	.9983346	1.131197	.9700941
.4327054	.6524508	2.119844	.9148355	.9316208
.714693	1.210614	.9993951	1.127495	.9891371

.4452901	.6714266	2.147639	.921388	.9386458
.7329638	1.196439	1.000032	1.122694	1.000583
.4578748	.6904023	2.175303	.9277303	.9450749
.7510706	1.182311	1.000519	1.117051	1.009316
.4702565	.7090719	2.202491	.9339362	.9513701
.7691	1.168783	1.001168	1.111618	1.020966
.4826382	.7277416	2.231254	.9404036	.9568963
.7875628	1.154671	1.001884	1.104561	1.033825
.4956288	.7473293	2.260153	.9466454	.9620901
.8062262	1.14032	1.002302	1.096753	1.041332
.5078075	.7656929	2.286077	.952014	.9686555
.8249545	1.127282	1.002395	1.091649	1.043005
.5199862	.7840564	2.311239	.9573334	.9751153
.8433644	1.115229	1.002895	1.087194	1.051992
.532165	.8024201	2.337808	.9630194	.9799552
.8612612	1.103011	1.003755	1.080813	1.067429
.5445467	.8210897	2.359463	.9671846	.983686
.8761653	1.092245	1.003618	1.074178	1.06497
.5567254	.8394533	2.379325	.9708877	.9882591
.8910884	1.082326	1.003362	1.069387	1.060375
.5689041	.8578168	2.400388	.9747667	.993376
.9073376	1.071929	1.003108	1.064601	1.055808
.5814889	.8767927	2.41985	.9785126	.9964154
.9208531	1.062878	1.003308	1.058898	1.058408
.5938705	.8954621	2.438683	.9818055	1.00044
.9352999	1.053581	1.002915	1.053867	1.052343
.6064552	.9144379	2.457305	.9852767	1.001807
.9470659	1.045023	1.003054	1.046792	1.054835
.6190399	.9334136	2.472172	.9877528	1.004324
.9581119	1.037688	1.002626	1.042103	1.047148
.6312186	.9517771	2.483938	.9895731	1.005973
.9667078	1.031673	1.002045	1.037833	1.036719
.6438033	.9707529	2.499681	.9922135	1.007098
.977042	1.024162	1.001737	1.031429	1.031197
.656185	.9894225	2.510499	.9940637	1.006175
.9824889	1.019145	1.001633	1.025445	1.029326

.6687697	1.008398	2.521717	.9957434	1.005475
.9886037	1.013514	1.001074	1.019059	1.019287
.6813543	1.027374	2.531821	.9972306	1.00414
.9934442	1.008448	1.000546	1.012622	1.008802
.6945479	1.047268	2.541044	.9987583	1.002064
.9968397	1.004209	1.000427	1.006275	1.007672
.7067266	1.065631	2.549043	.9999191	1.000244
.9999391	1.000237	1.000012	1.000482	1.00021
.7191094	1.084301	2.555342	1.000919	.997227
1.000693	.9973035	.9998669	.9945228	.9976102
.7314901	1.102971	2.563734	1.002188	.993509
1.002032	.9932995	.9995629	.9868161	.99215
.7444807	1.122558	2.570508	1.003352	.9894168
1.001863	.9903666	.9996069	.9798231	.9929413
.7570654	1.141534	2.574195	1.003855	.9855735
1.000237	.9885224	.9993759	.9741698	.9887923
.7690411	1.159592	2.579053	1.004467	.9811548
.9987717	.9960032	.9999755	.9673006	.9816026
.7810169	1.177649	2.583387	1.005272	.9761333
.9964669	.983905	.9999774	.9602749	.9816364
.7936016	1.196625	2.588606	1.006092	.9717435
.9947101	.9919091	.9990422	.9537986	.9828008
.8059832	1.215294	2.59297	1.006765	.9672616
.9926981	.9799151	.9989405	.9476562	.9809751
.8183649	1.233964	2.598068	1.007619	.9627627
.9910176	.9777313	.9989642	.9411251	.981399
.8305436	1.252328	2.603778	1.008598	.958662
.9900567	.9753402	.9990403	.9348039	.9827669
.8431284	1.271303	2.609944	1.009607	.9543532
.9891587	.9726799	.9990343	.9280514	.9826596
.8553071	1.289667	2.614356	1.010105	.9503027
.9876926	.9703553	.9985918	.921892	.9747121
.8678917	1.308642	2.619002	1.010638	.9467971
.9869103	.9679379	.9981502	.9161889	.9667819
.8804764	1.327618	2.62224	1.011259	.9437492
.9855041	.9667359	.9983374	.9121022	.970145

.8926551	1.345982	2.627291	1.012455	.9399835
.9841239	.9653021	.9990822	.9071207	.9835186
.9054428	1.365264	2.634613	1.013574	.9362442
.9844395	.9620662	.9989563	.9004764	.9812578
.9180275	1.384239	2.641738	1.014733	.9332927
.9853844	.9590735	.998984	.8948335	.981755

DELTA.CM	=	.6632
DEL+K.CM	=	.1209007
DEL+K.CM	=	.2354091
THETA.CM	=	.0559061
RE THETA	=	4136.624

READY

+

TABLE 4

SUMMARY OF BOUNDARY LAYER PARAMETERS - RAMP NO. 1

$$P_o = 97301 \text{ N/M}^2$$

$$dp/dk = 1.2 \text{ mmHg/cm}$$

$$T_o = 317 \text{ }^\circ\text{K}$$

$$\beta_{ko} = 0.41$$

$$Re_\infty = 6.62 \times 10^6 \text{ M}^{-1}$$

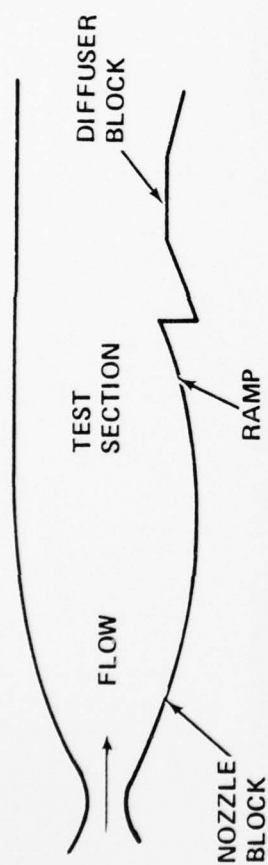
X (cm)	u_e m/sec	ρ_e KG/M ³	M_e	Re_η	β_k	δ (1) cm	δ_k^* (1) cm	δ^* cm	θ cm	τ_w (1) N/M ²	C_f (1)	η	G	Δ
-1.27	642	.0776	3.01	2734	0	.645	.089	.233	.043	34.7	.00207	.481	7.21	2.46
2.74	625	.088	2.81	2972	.38	.624	.092	.230	.046	38.4	.00217	.615	7.56	2.57
4.01	623	.093	2.80	3450	.393	.683	.097	.242	.051	39.3	.00215	.607	7.34	2.75
5.28	621	.097	2.77	3644	.369	.718	.095	.246	.052	41.2	.00211	.499	6.80	2.67
6.44	625	.096	2.81	3667	.377	.749	.099	.244	.052	42.2	.00216	.483	6.82	2.78
7.71	620	.101	2.76	3934	.378	.781	.103	.249	.055	43.6	.00218	.492	6.82	2.95
8.98	617	.107	2.75	4255	.368	.798	.104	.252	.056	45.1	.00215	.472	6.70	2.93
10.25	607	.112	2.62	4378	.336	.778	.099	.255	.059	46.9	.00218	.429	6.57	2.77
11.52	603	.116	2.58	4511	.318	.810	.098	.256	.060	49.3	.00218	.346	6.34	2.72
12.79	603	.118	2.58	4521	.306	.816	.098	.250	.060	51.1	.00224	.343	6.23	2.72

(1) From velocity correlation

TABLE 4
SUMMARY OF BOUNDARY LAYER PARAMETERS - RAMP NO. 3
 $P_O = 97301 \text{ N/M}^2$
 $dp/dx = 5 \text{ mmHg/cm}$
 $T_O = 317 \text{ }^\circ\text{K}$
 $Re_{co} = 6.62 \times 10^6 \text{ M}^{-1}$
 $\beta_{ko} = 1.85$

X (cm)	u_e M/sec	ρ_e Kg/M ³	Re_θ	β_k	$\delta^{(1)}$ cm	$\delta_k^{(1)}$ cm	δ^* cm	θ cm	τ N/M ²	$C_f^{(1)}$	π	G	Δ
-3.18	630	.0803	2.85	0	.660	.093	.250	.048	35.1		.567	7.19	2.59
-1.91	634	.0811	2.90	0	.683	.097	.248	.048	36.2		.573	7.14	2.73
-.63	635	.0821	2.91	0	.711	.097	.256	.049	36.0		.513	6.96	2.72
0	630	.0812	2.85	0	.704	.098	.264	.051	35.8	.00221	.505	7.08	2.70
.63	627	.079	2.83	1.86	.684	.101	.261	.051	37.8	.00231	.57	7.55	2.77
1.91	619	.084	2.74	1.84	.657	.105	.249	.052	33.6	.00233	.85	8.03	3.03
3.18	610	.103	2.64	1.86	.677	.094	.247	.054	41.8	.00175	.58	7.37	2.71
3.81	605	.109	2.59	1.77	.663	.112	.242	.055	44.5	.00209	1.03	8.61	3.36
4.45	601	.117	2.55	1.67	.663	.112	.235	.056	47.3	.00210	1.06	8.67	3.41
5.08	596	.127	2.51	1.60	.684	.114	.231	.057	51.3	.00209	1.06	8.64	3.50
5.72	588	.141	2.43	1.38	.690	.107	.225	.058	53.6	.00210	.87	7.96	3.20
6.35	581	.147	2.38	1.26	.684	.102	.224	.058	58.0	.00216	.77	7.68	2.99
6.99	580	.151	2.37	1.19	.711	.105	.220	.060	60.7	.00229	.73	7.47	3.05
7.62	573	.161	2.30	1.13	.740	.103	.220	.061	64.7	.00230	.64	7.16	3.01

(1) From velocity correlation



SCHEMATIC OF WIND TUNNEL
SHOWING RAMP INSTALLATION

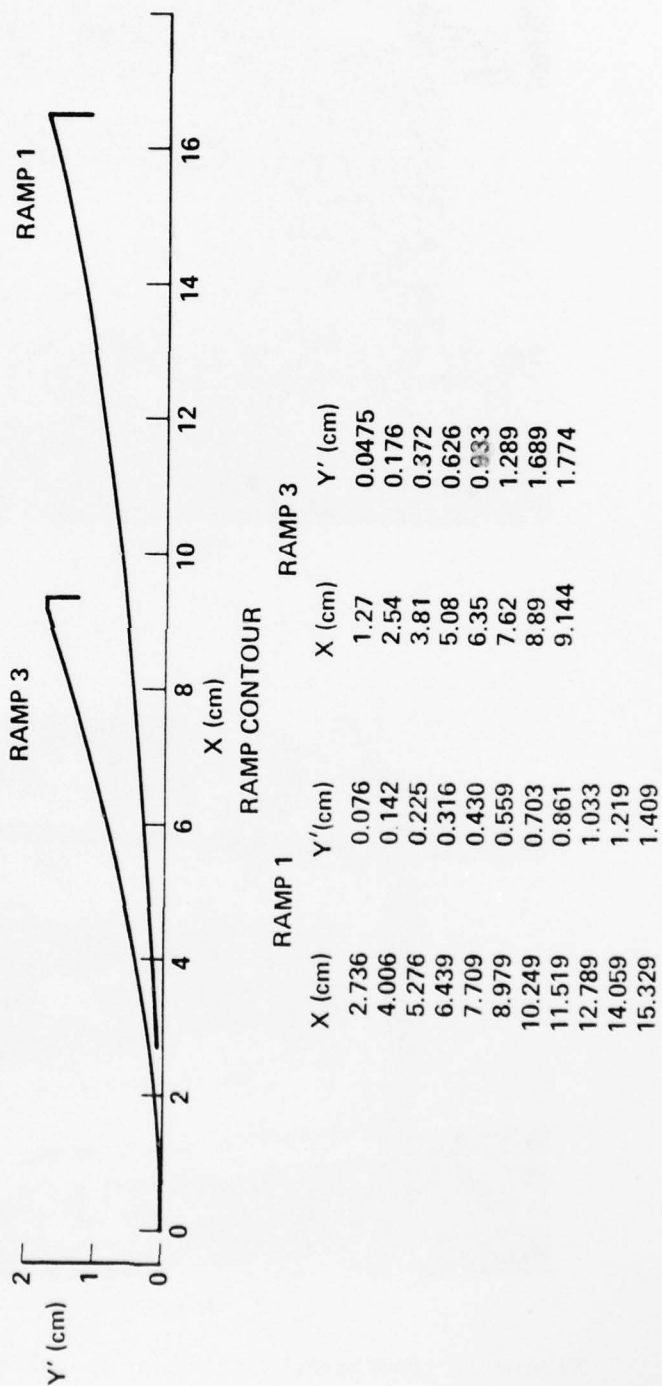
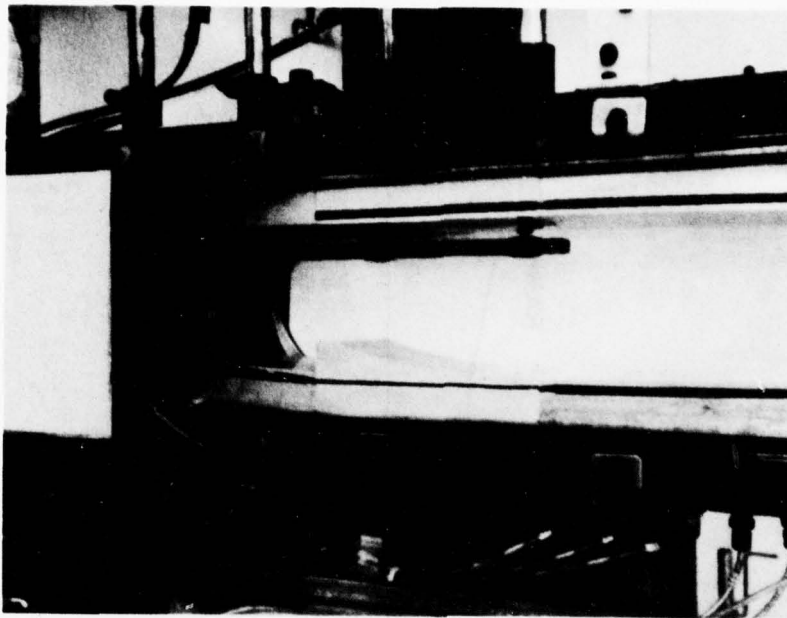
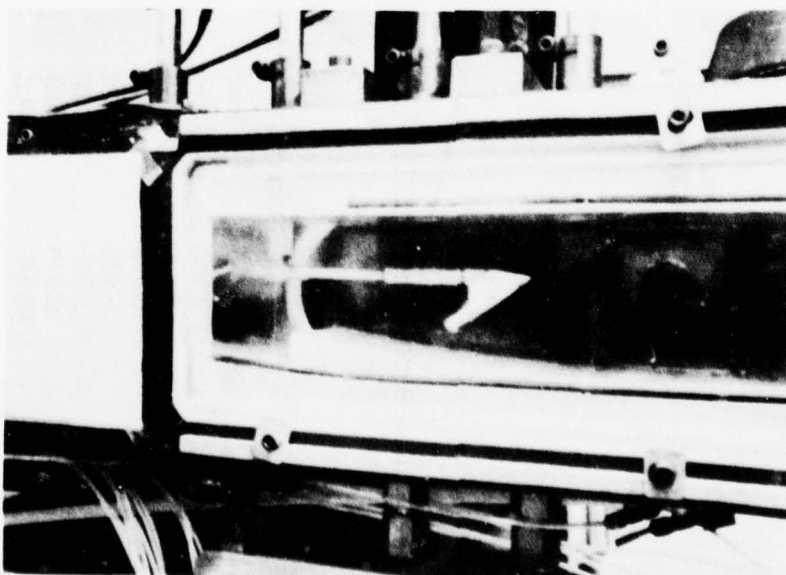


Figure 1. Schematic of Ramp Contours and Wind Tunnel Installation

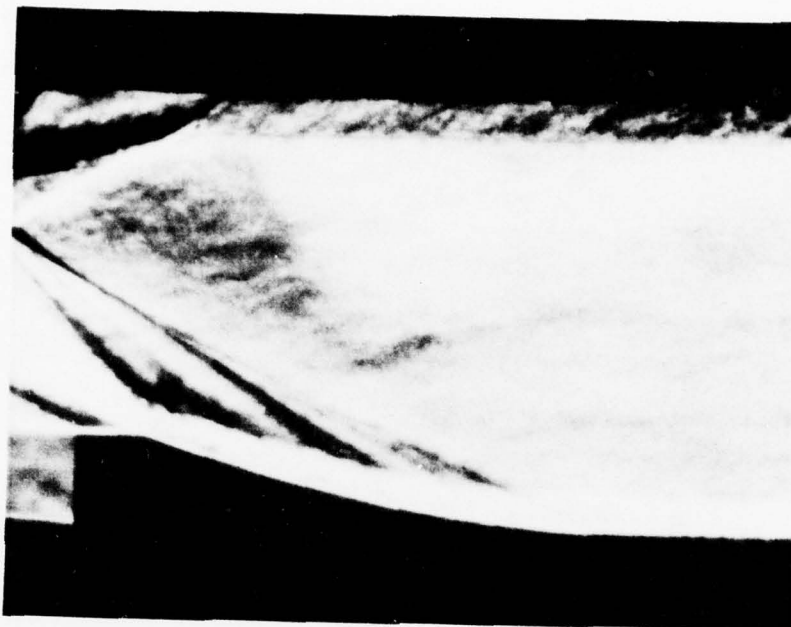


RAMP 3



RAMP 1

Figure 2. Photographs of Ramps Installed in the Wind Tunnel



RAMP 3



RAMP 1

Figure 3. Schlieren Photograph of Ramp Flow Field

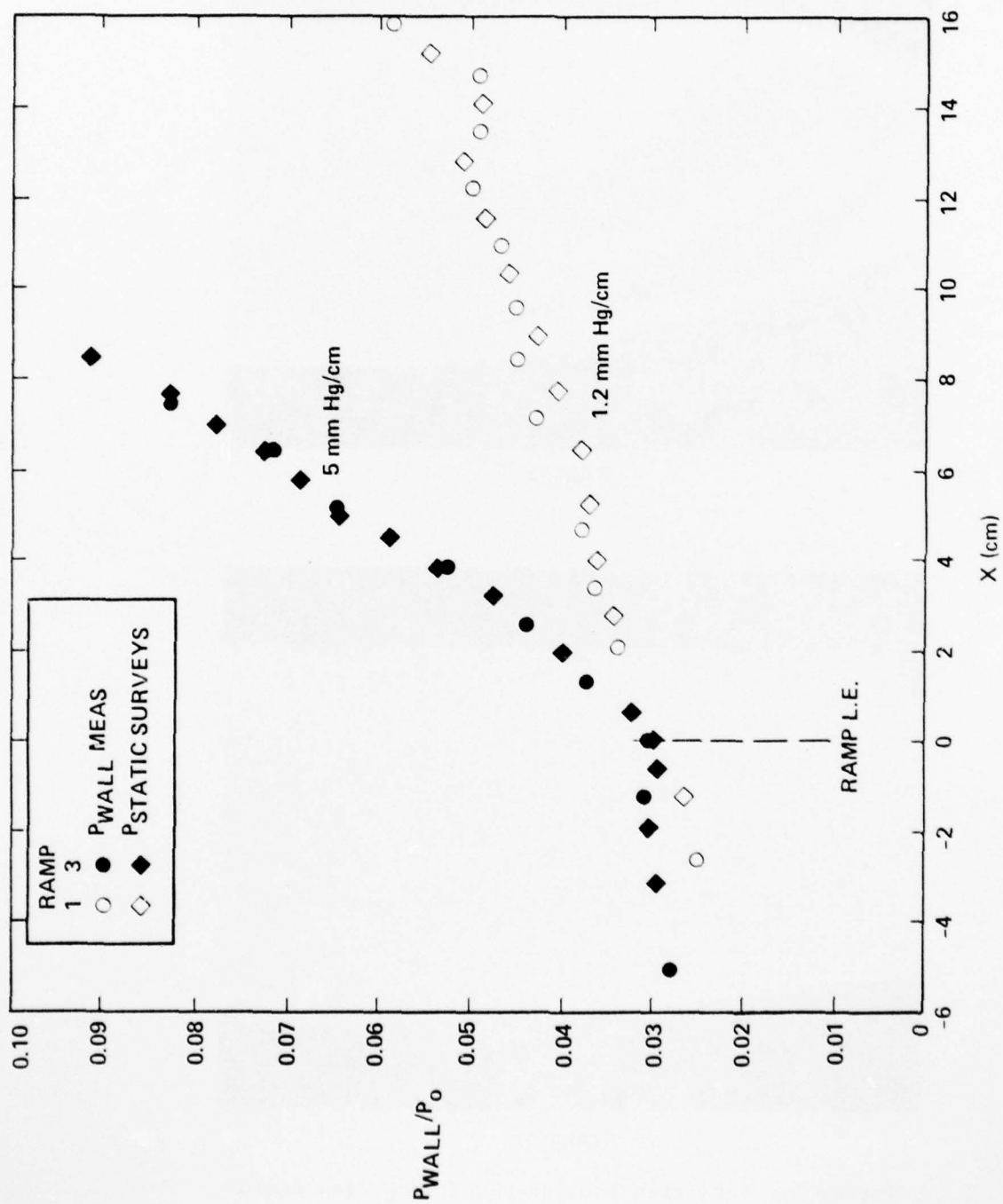


Figure 4. Surface Pressure Distributions

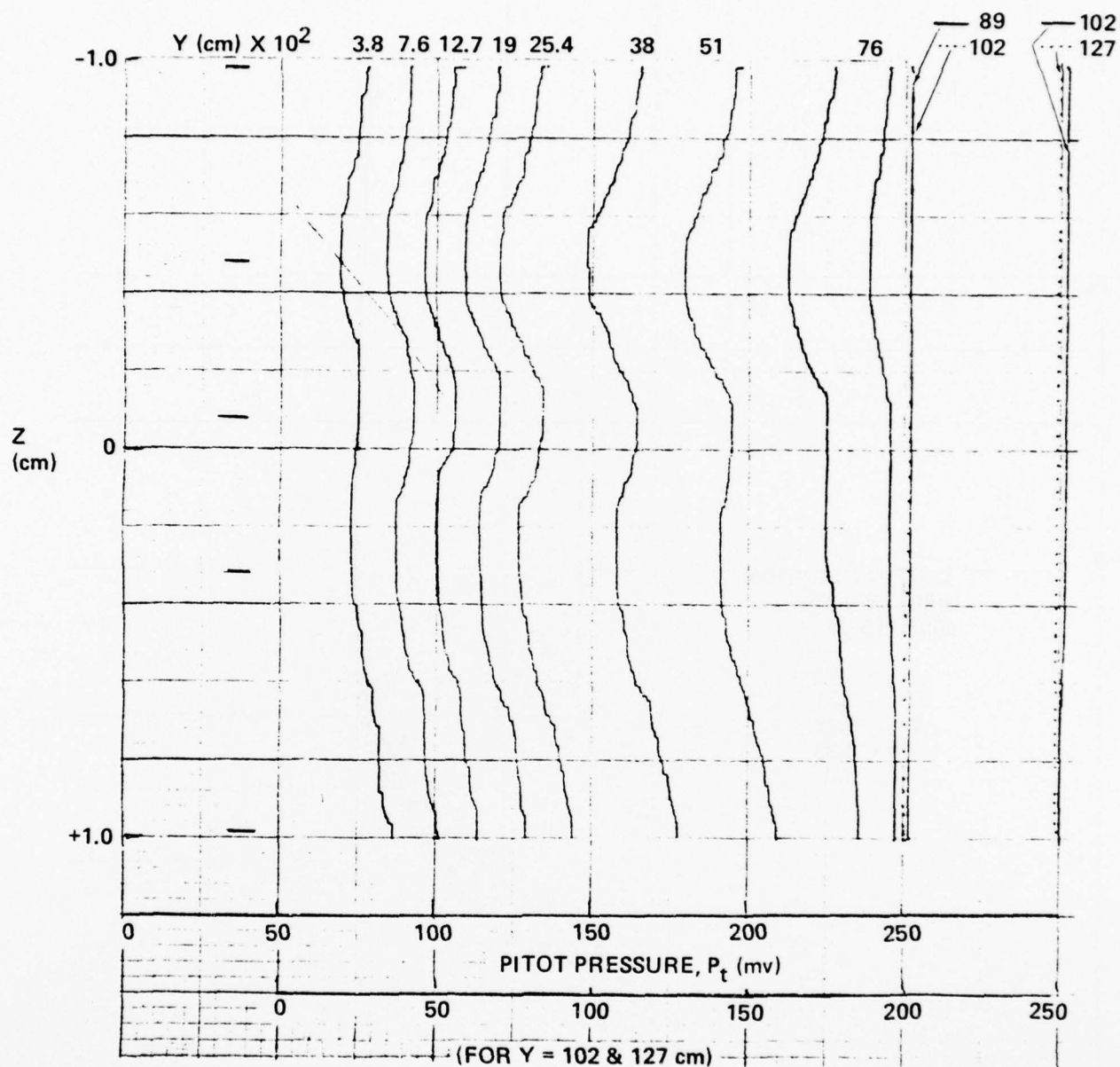


Figure 5. Lateral Pitot Pressure Surveys at Selected y' Locations Above Surface for Ramp 1. X Station is 5 cm Upstream of Ramp T.E. (- Denotes Location of p_t vs y Profiles in Figure 6)

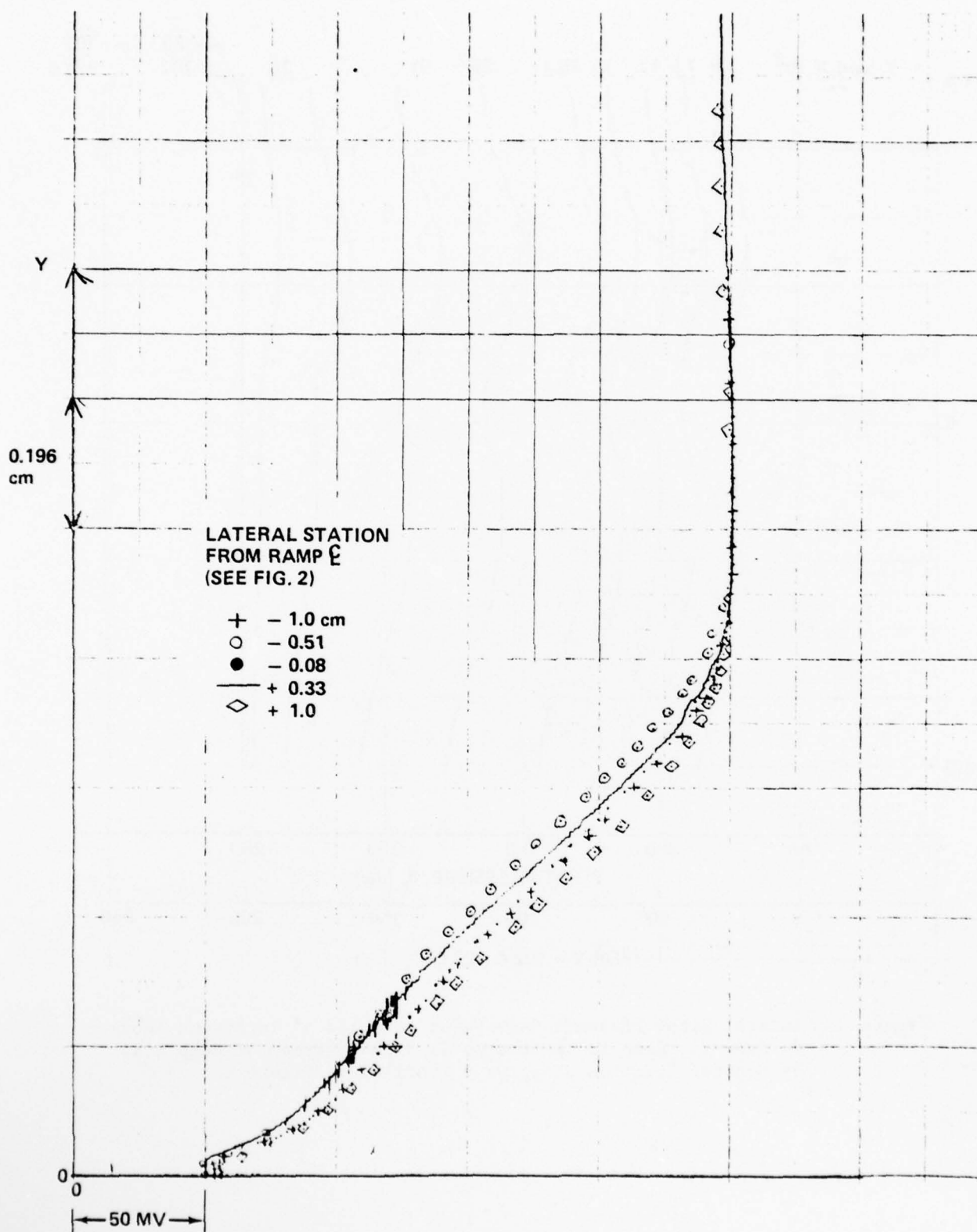


Figure 6. Vertical Pitot Pressure Profiles for Ramp 1 at x Station 12.7 cm Upstream of Ramp T.E.

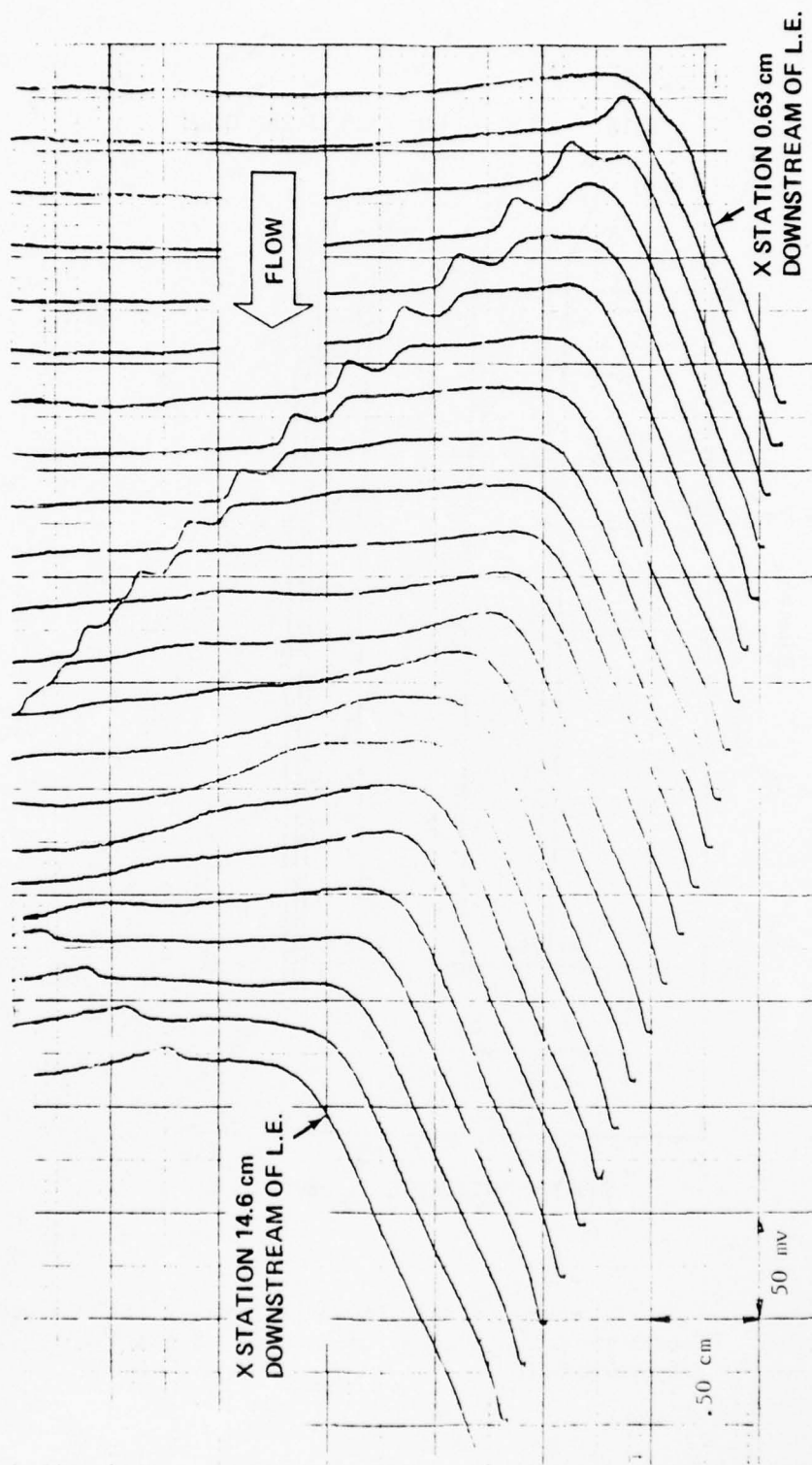


Figure 7. Pitot Pressure Surveys P_t vs y' at .635 cm Intervals along Centerline of Ramp I

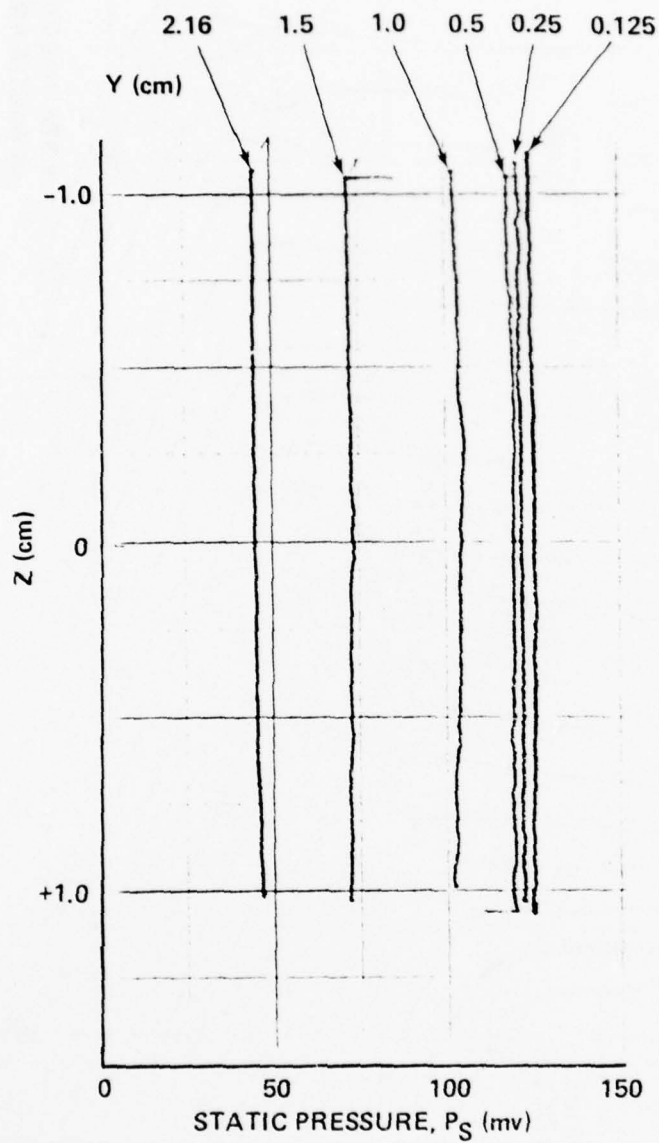


Figure 8. Typical Lateral Static Pressure Surveys at Selected y' Locations Above Surface of Ramp 3. X Station is 5.7 cm from Ramp L.E.

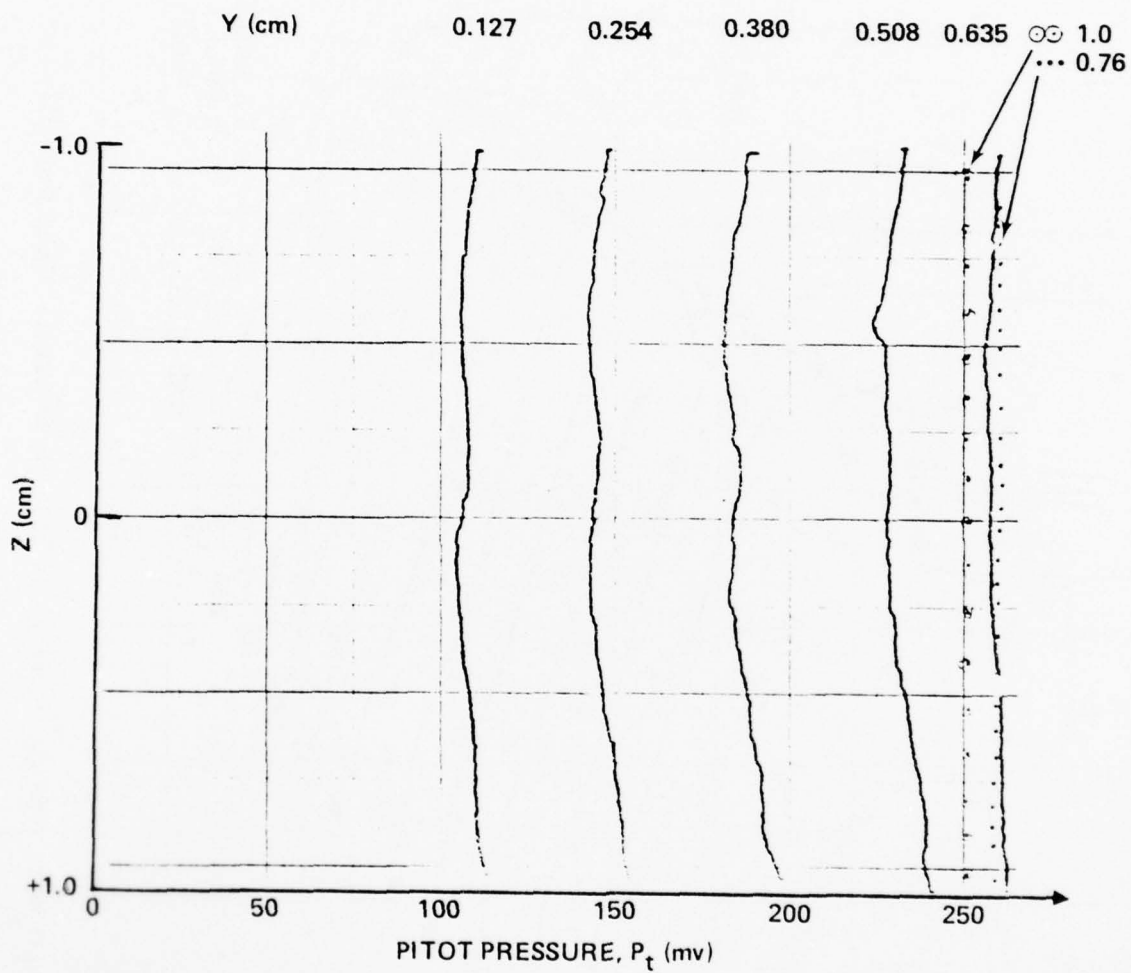


Figure 9. Typical Lateral Pitot Pressure Surveys at Selected y' Locations Above Surface of Ramp 3. X Station is 4.4 cm from Ramp L.E.

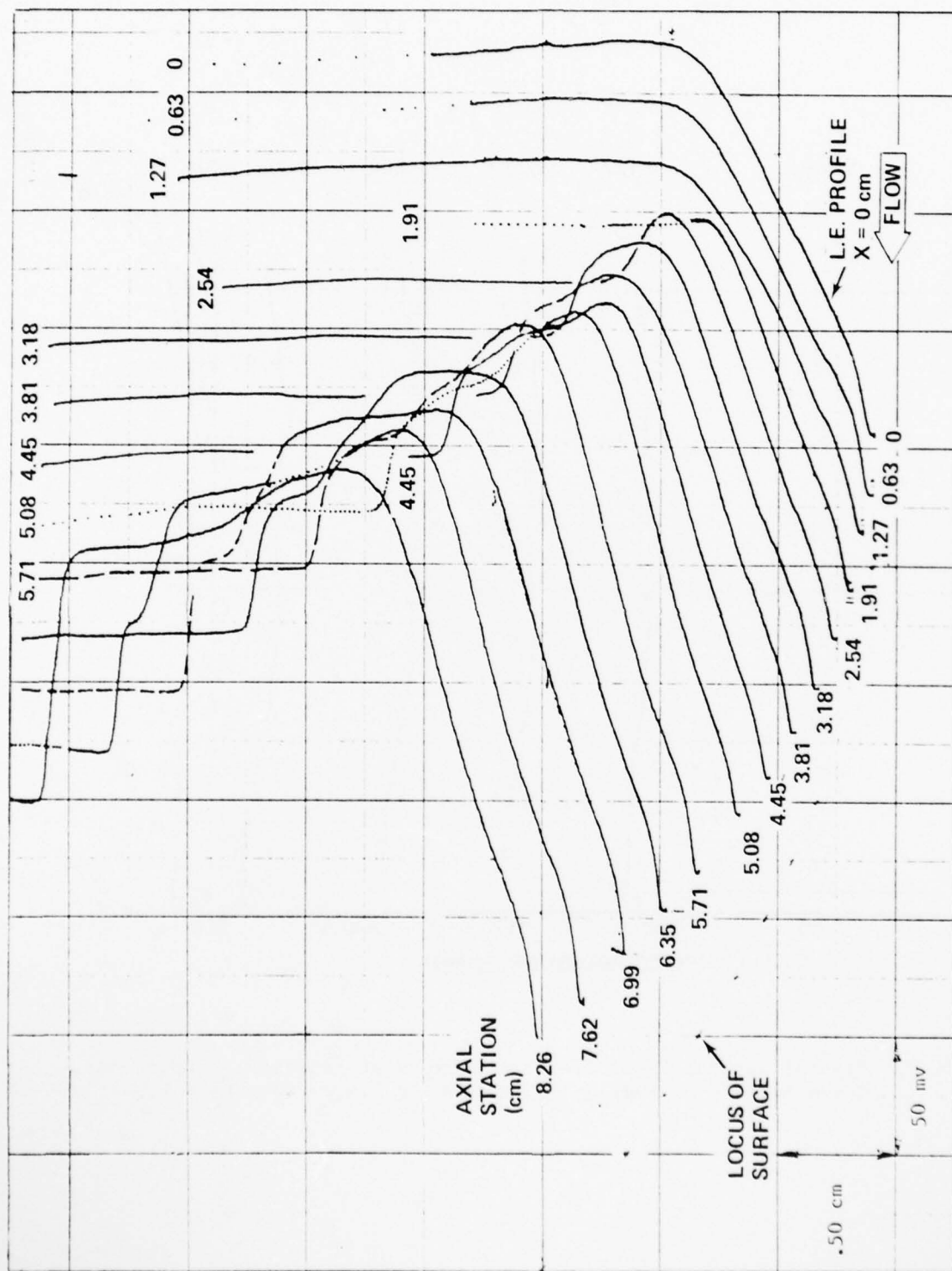
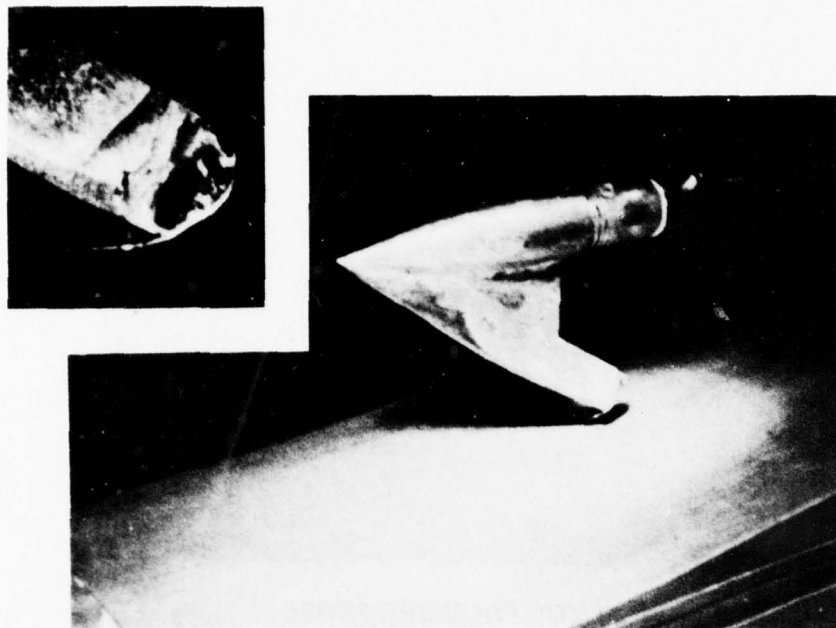
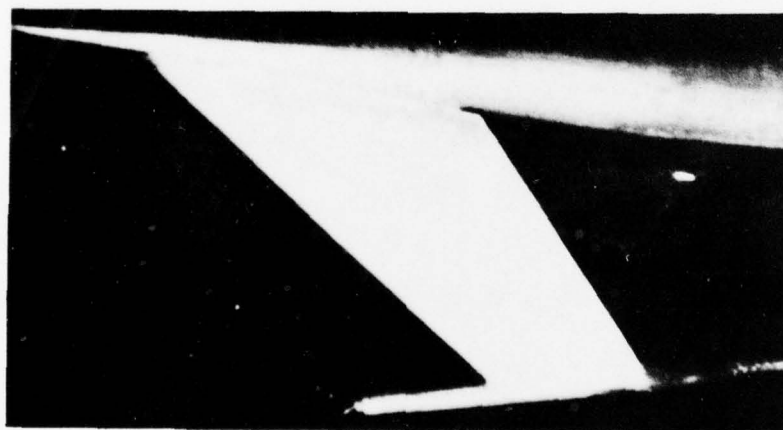


Figure 10. Pitot Pressure Surveys P_L vs y' at .635 cm Intervals Along Centerline of Ramp 3



A) PITOT PRESSURE PROBE



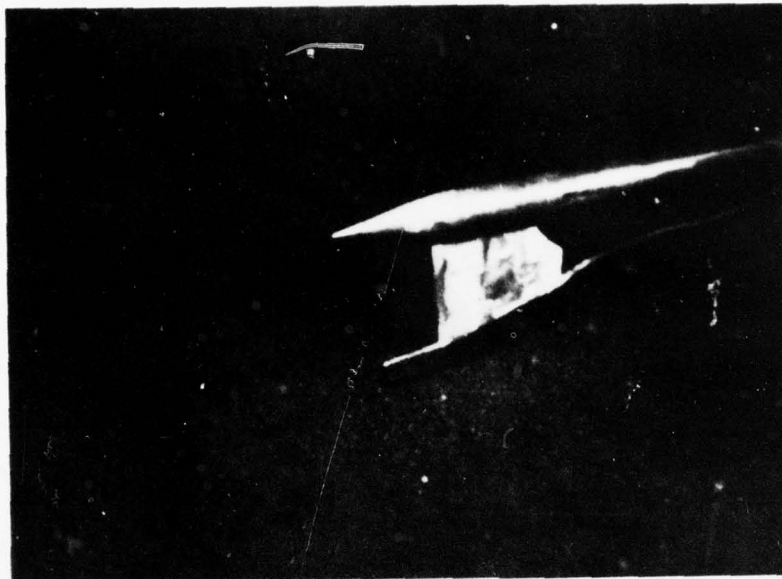
SIDE
VIEW



BOTTOM
VIEW

B) TOTAL TEMPERATURE PROBE

Figure 11. Photographs of the Pitot Pressure and Total Temperature Probes



A) STATIC PRESSURE PROBE



B) PRESTON TUBE

Figure 12. Photographs of the Static Pressure and Preston Tube Probes

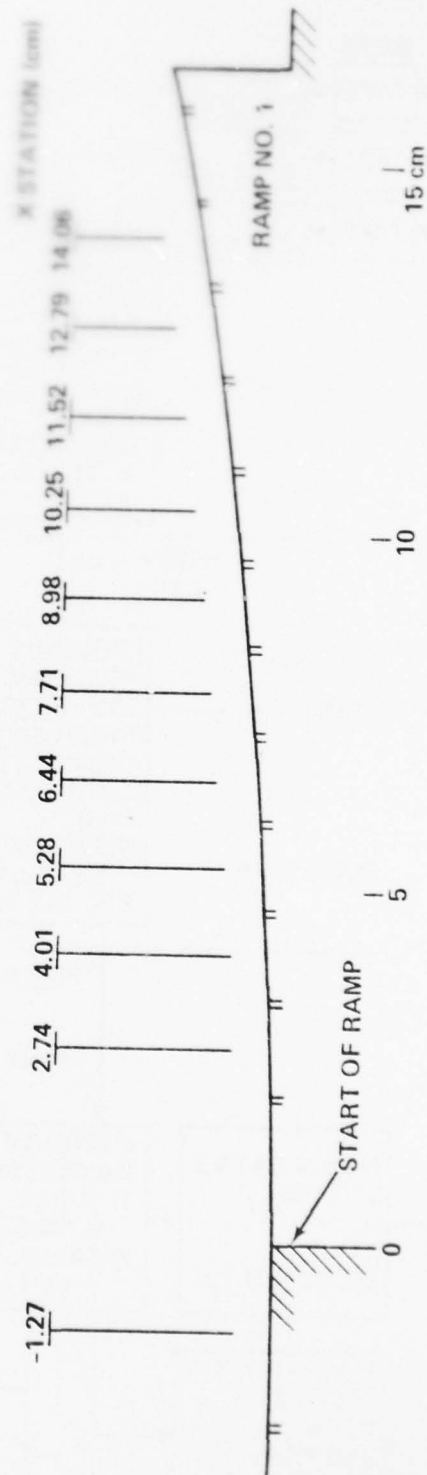
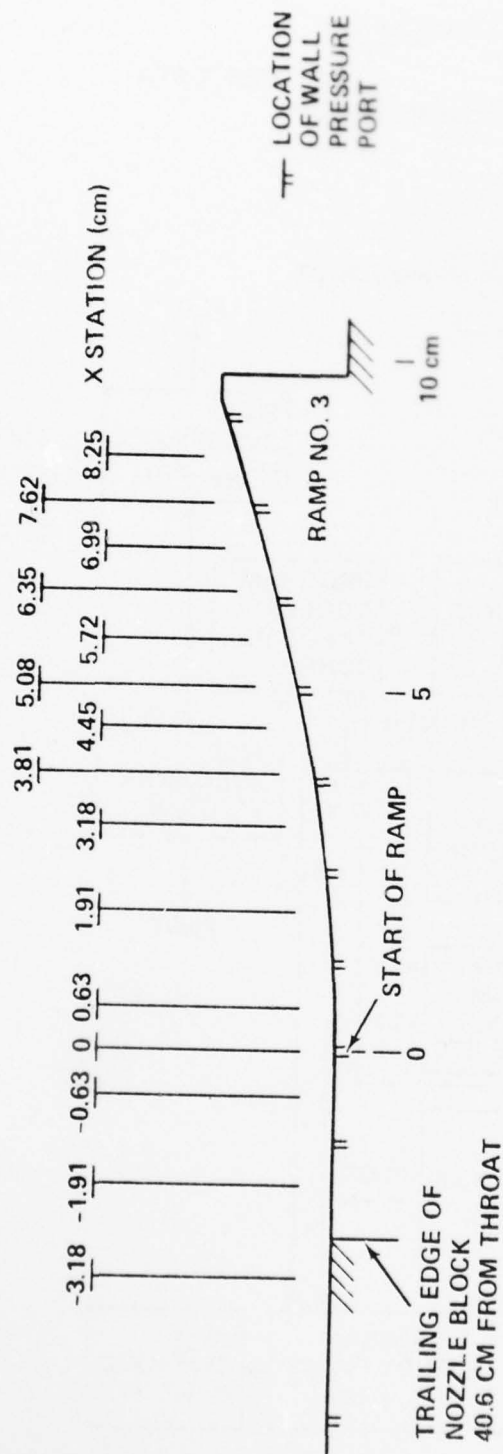


Figure 13. Schematic of Adverse Pressure Gradient Ramps Indicating Location of Survey Stations

AD-A070 254

FORD AEROSPACE AND COMMUNICATIONS CORP NEWPORT BEACH --ETC F/G 20/4
PRESSURE GRADIENT EFFECTS ON SUPERSONIC BOUNDARY LAYER TURBULEN--ETC(U)
FEB 79 A J LADERMAN F33615-77-C-3016

UNCLASSIFIED

U-6467

AFFDL-TR-79-3005

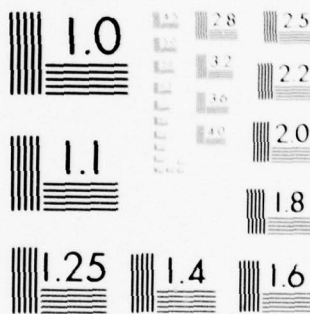
NL

2 OF 2

AD
A070254



END
DATE
FILMED
7-79
DDC



MICROCOPY RESOLUTION TEST CHART
NATIONAL BUREAU OF STANDARDS-1963-A

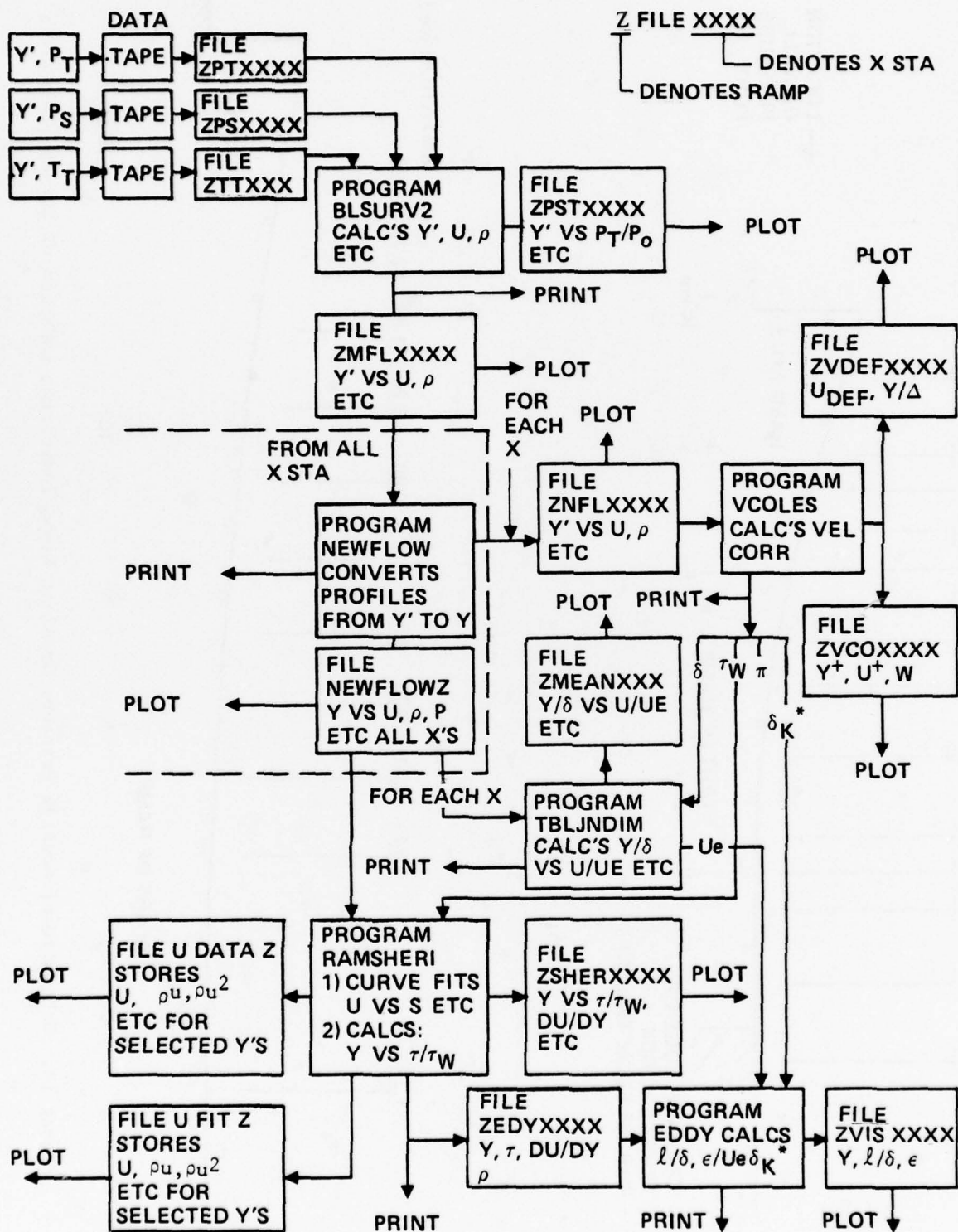


Figure 14. Schematic of Data Reduction Routine

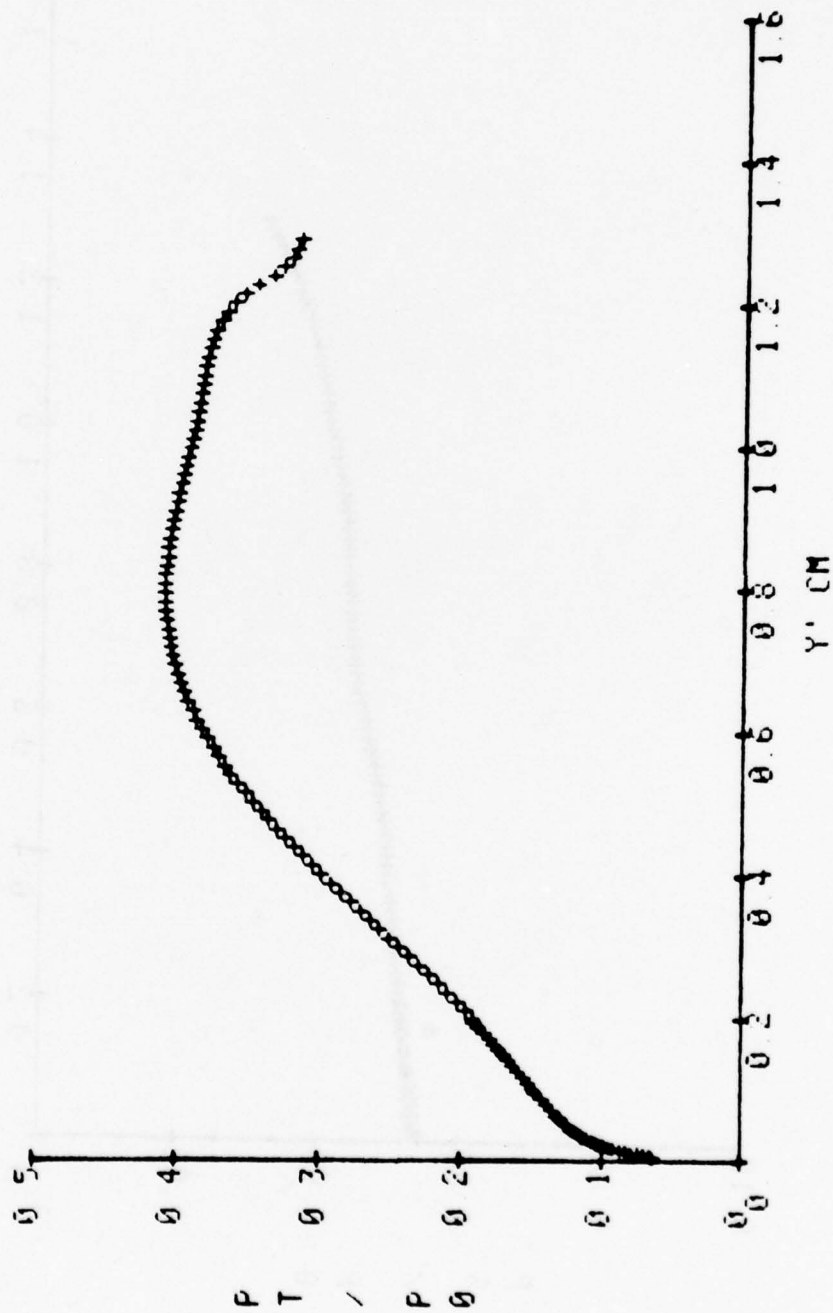


Figure 15. Typical Plot of p_T/p_0 versus y' (Ramp 3, $x = 3.81$ cm)

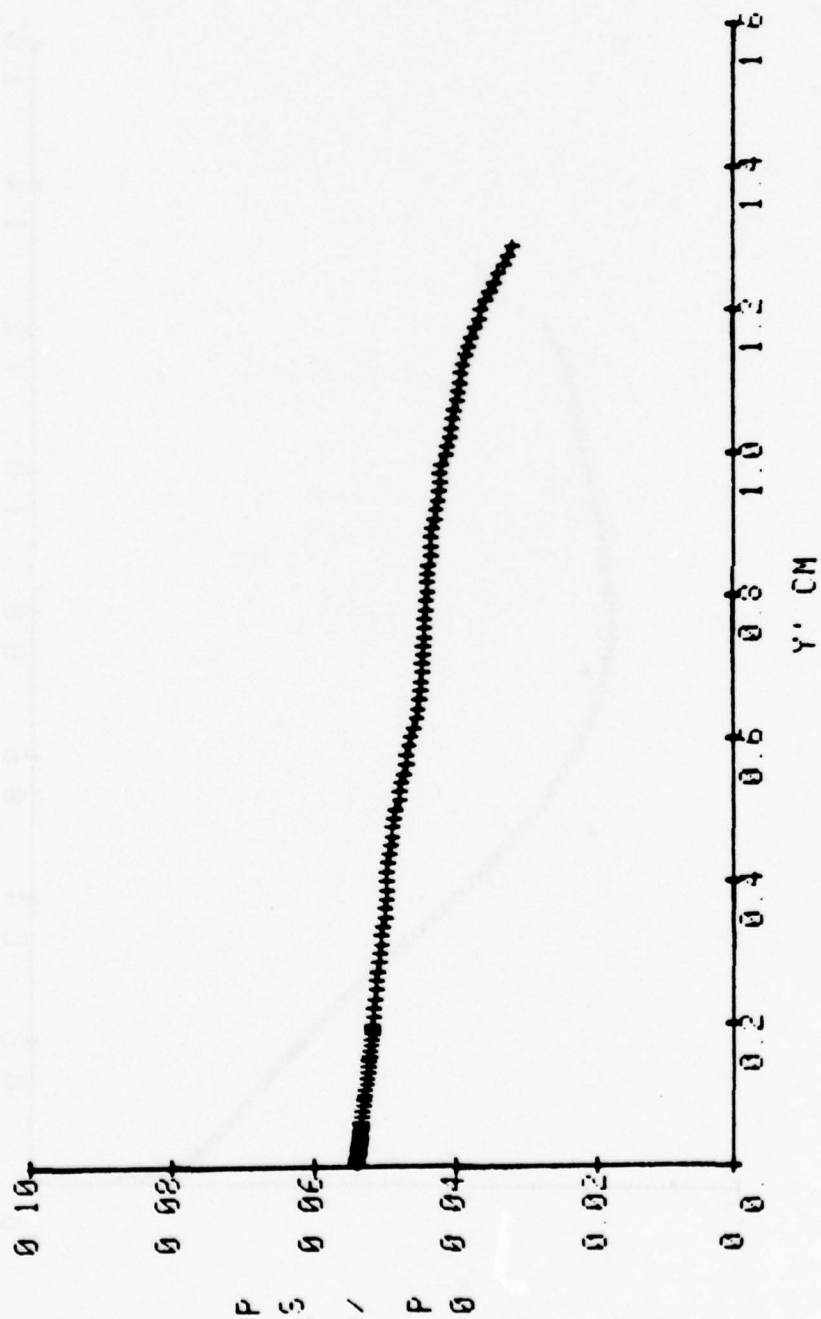


Figure 16. Typical Plot of P_S/P_0 versus y' (Ramp 3, $x = 3.81$ cm)

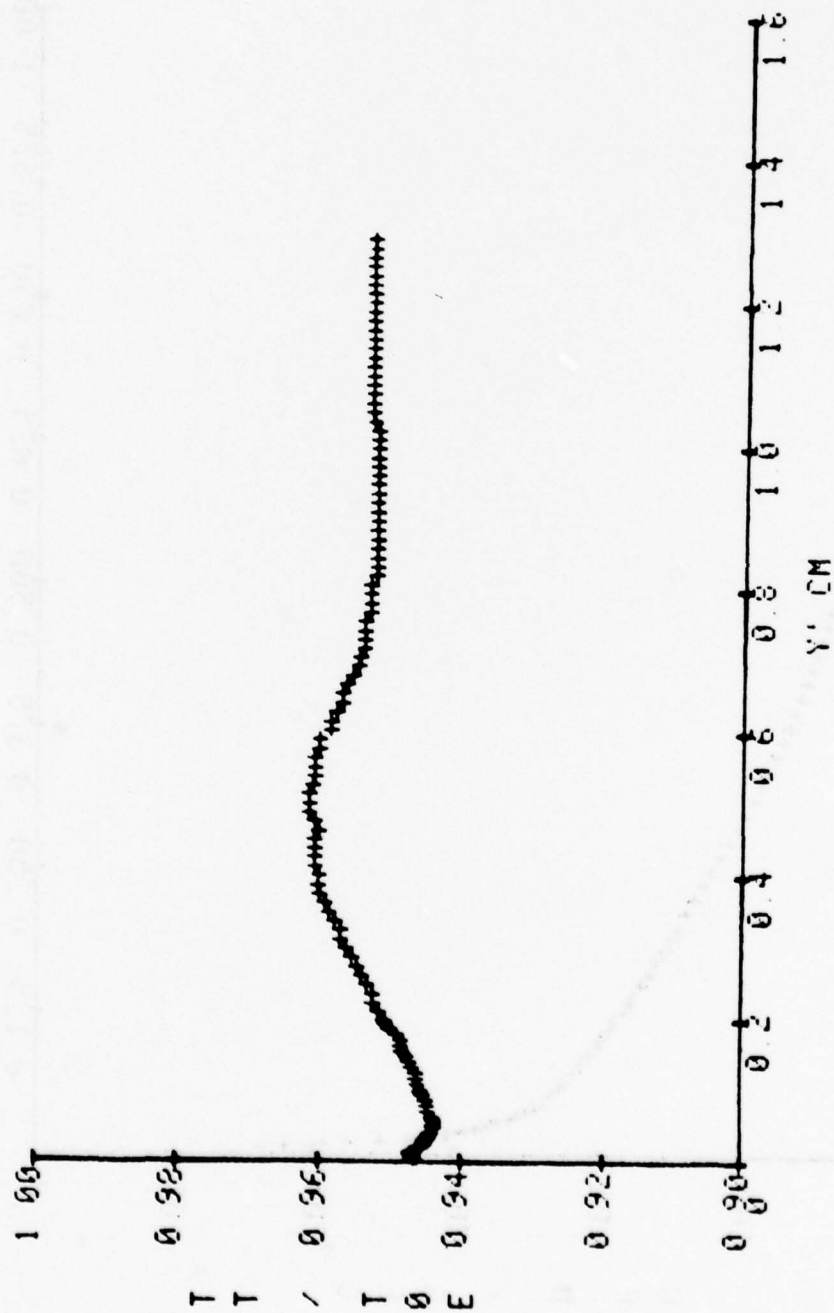


Figure 17. Typical Plot of T_t/T_{oe} versus y' (Ramp 3, $x = 3.81$ cm)

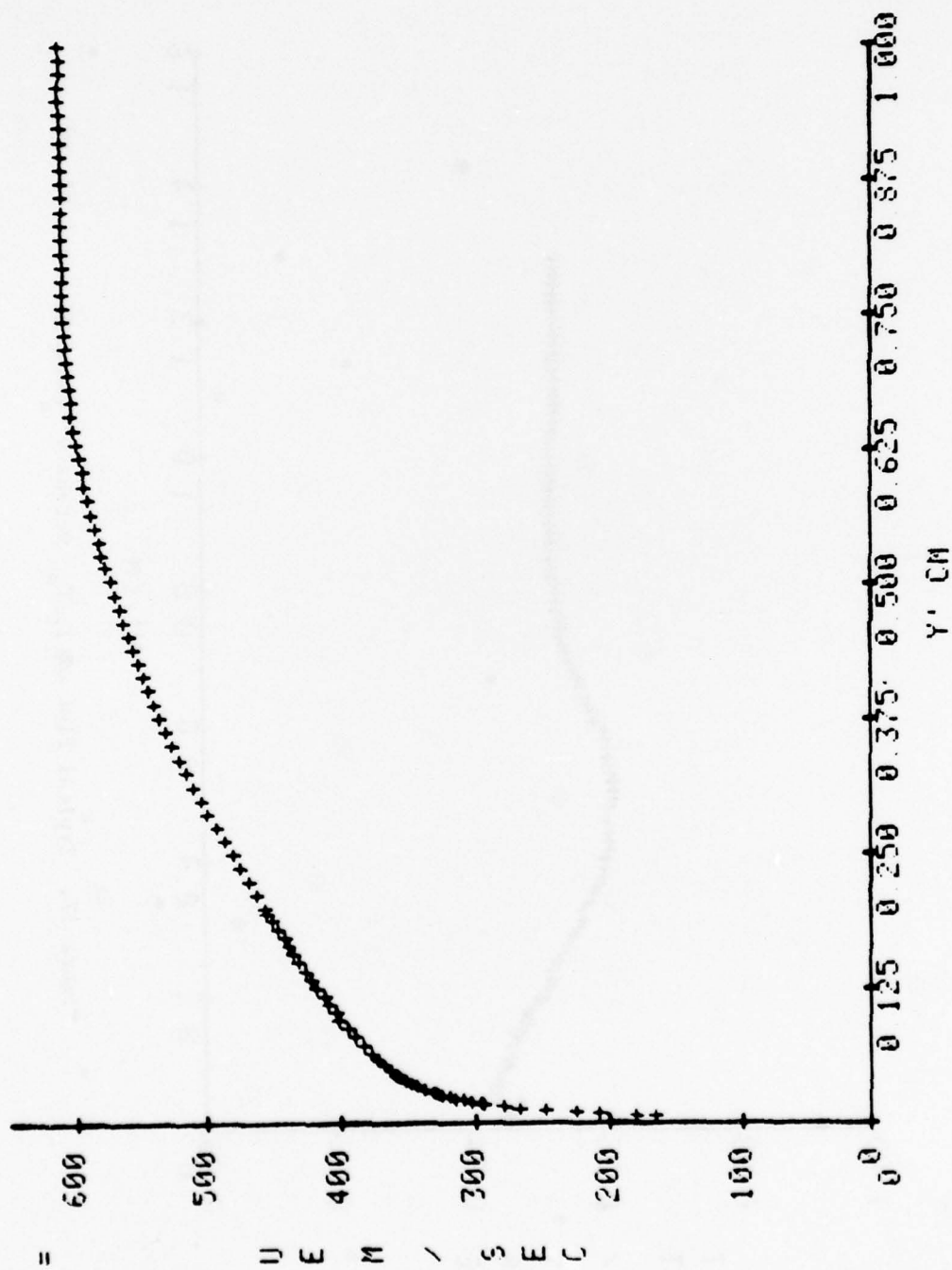


Figure 18. Typical Plot of U_{meas} versus y' (Ramp 3, $x = 3.81$ cm)

=

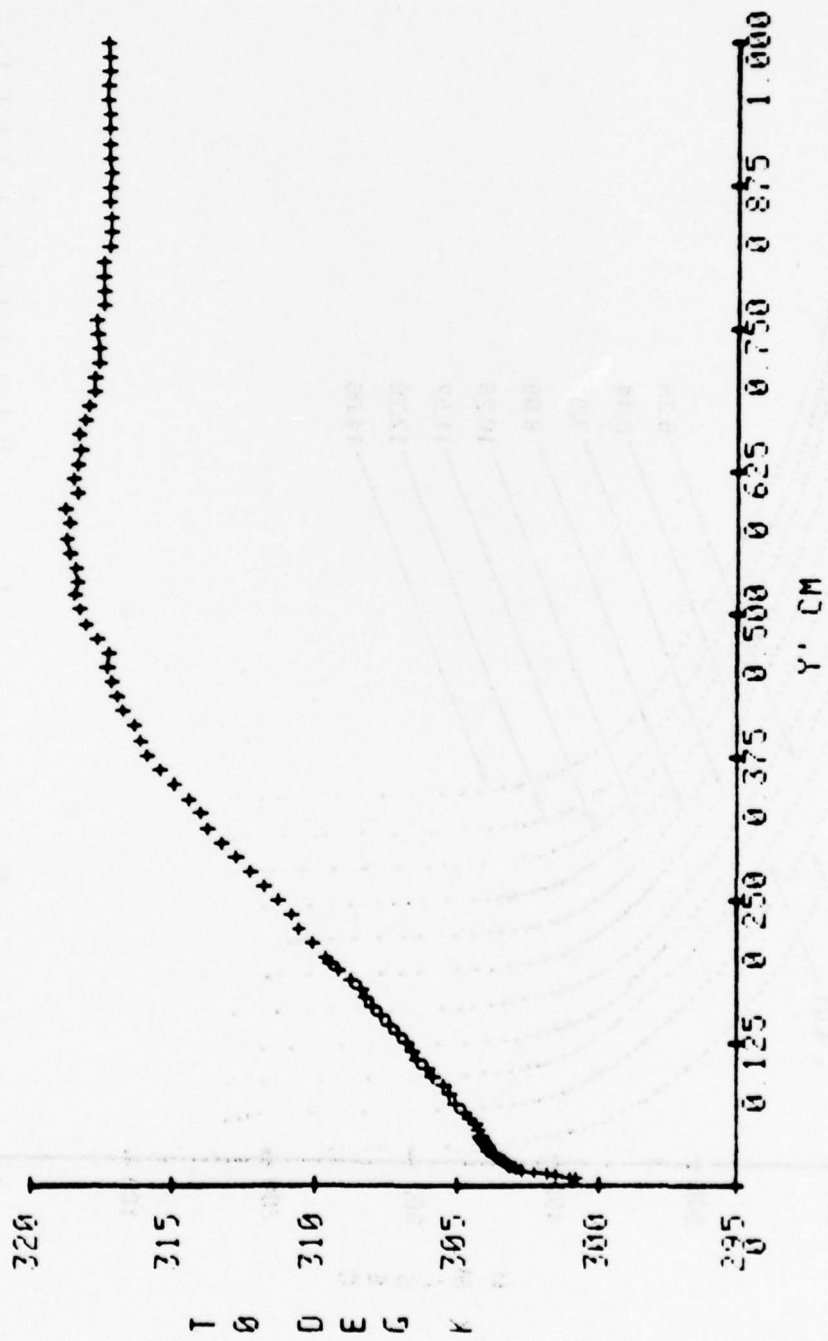


Figure 19. Typical Plot of $T_{o_{meas}}$ versus y' (Ramp 3, $x = 3.81$ cm)

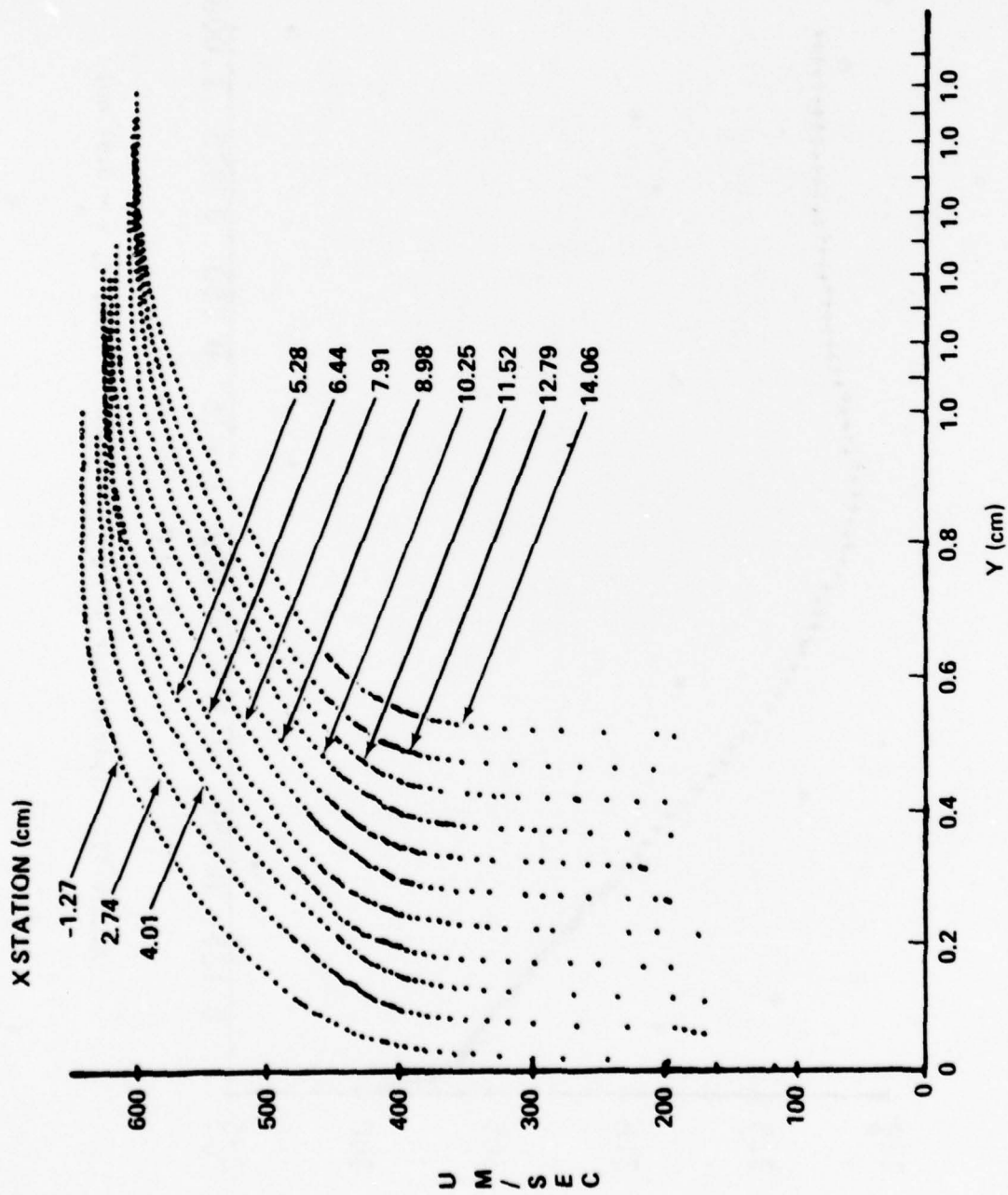


Figure 20. Profiles of u versus Distance y Normal to the Surface for Ramp 1

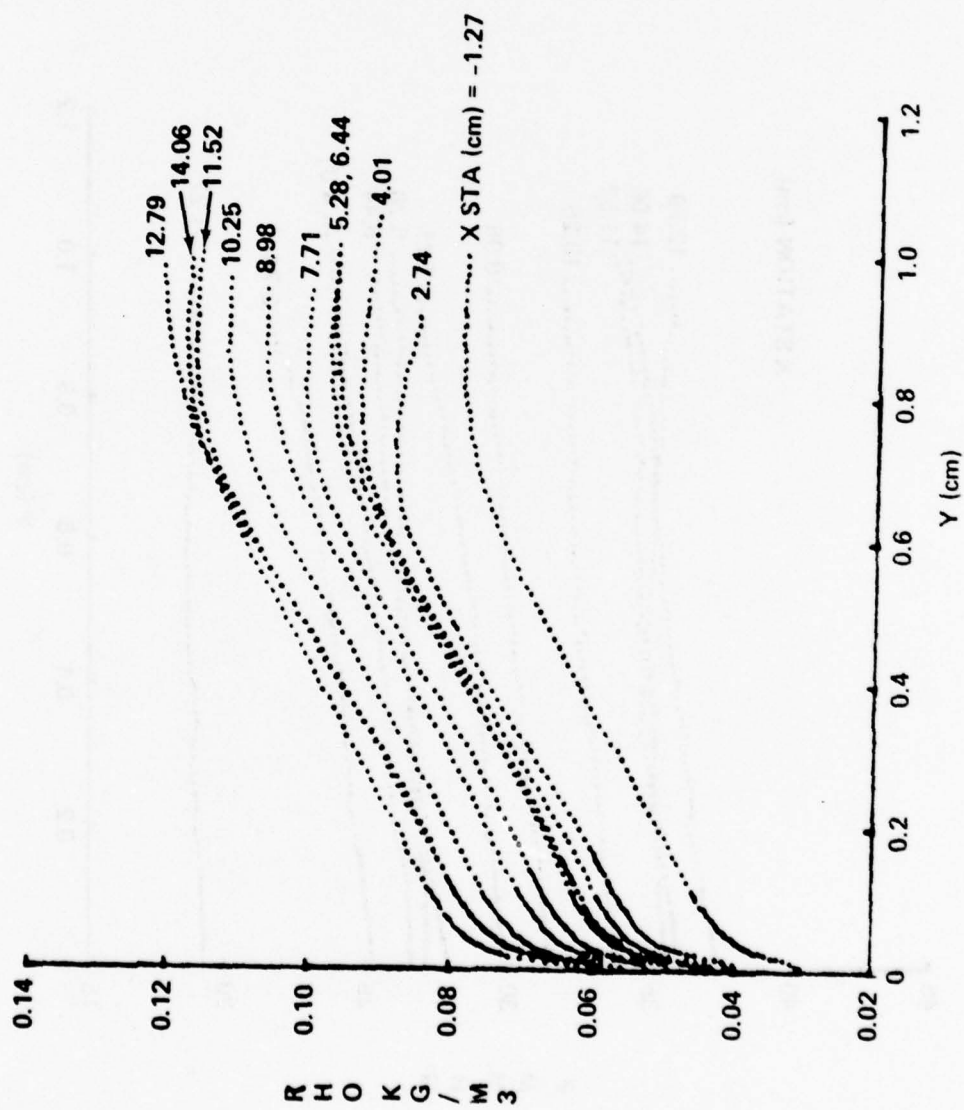


Figure 21. Profiles of ρ versus Distance y Normal to the Surface for Ramp 1

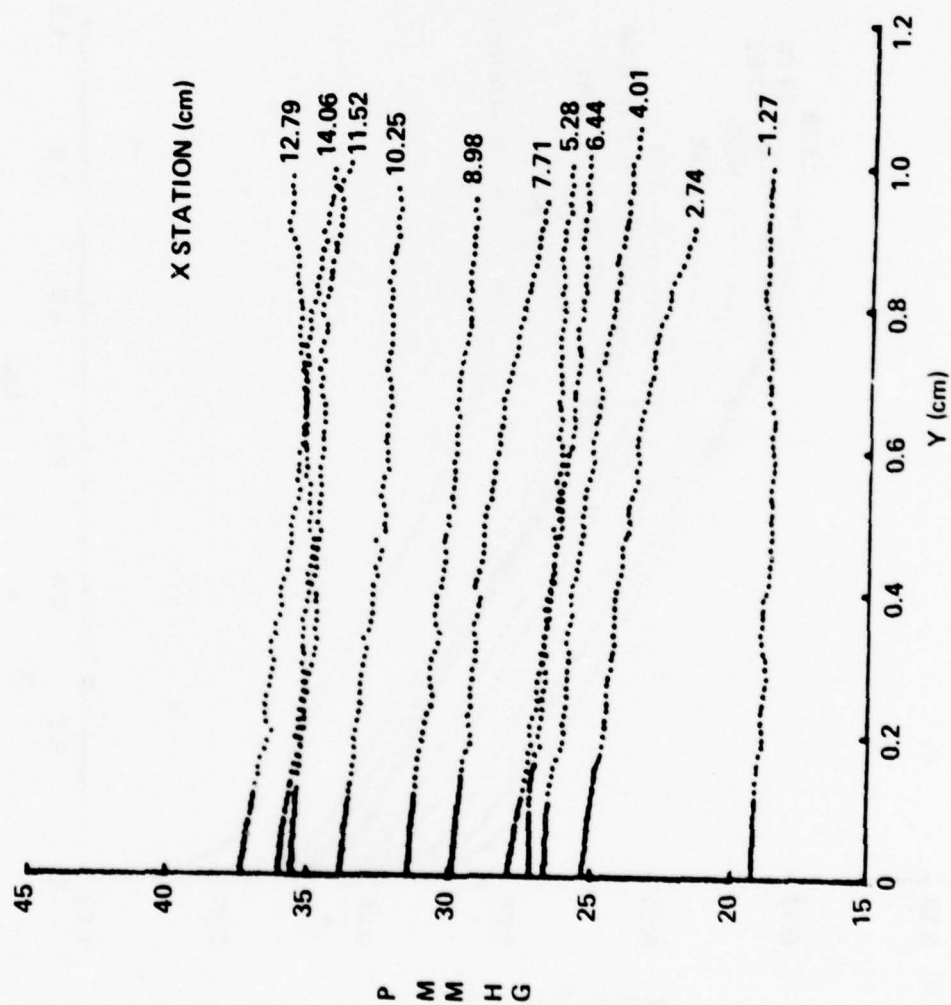


Figure 22. Profiles of p versus Distance y Normal to the Surface for Ramp 1

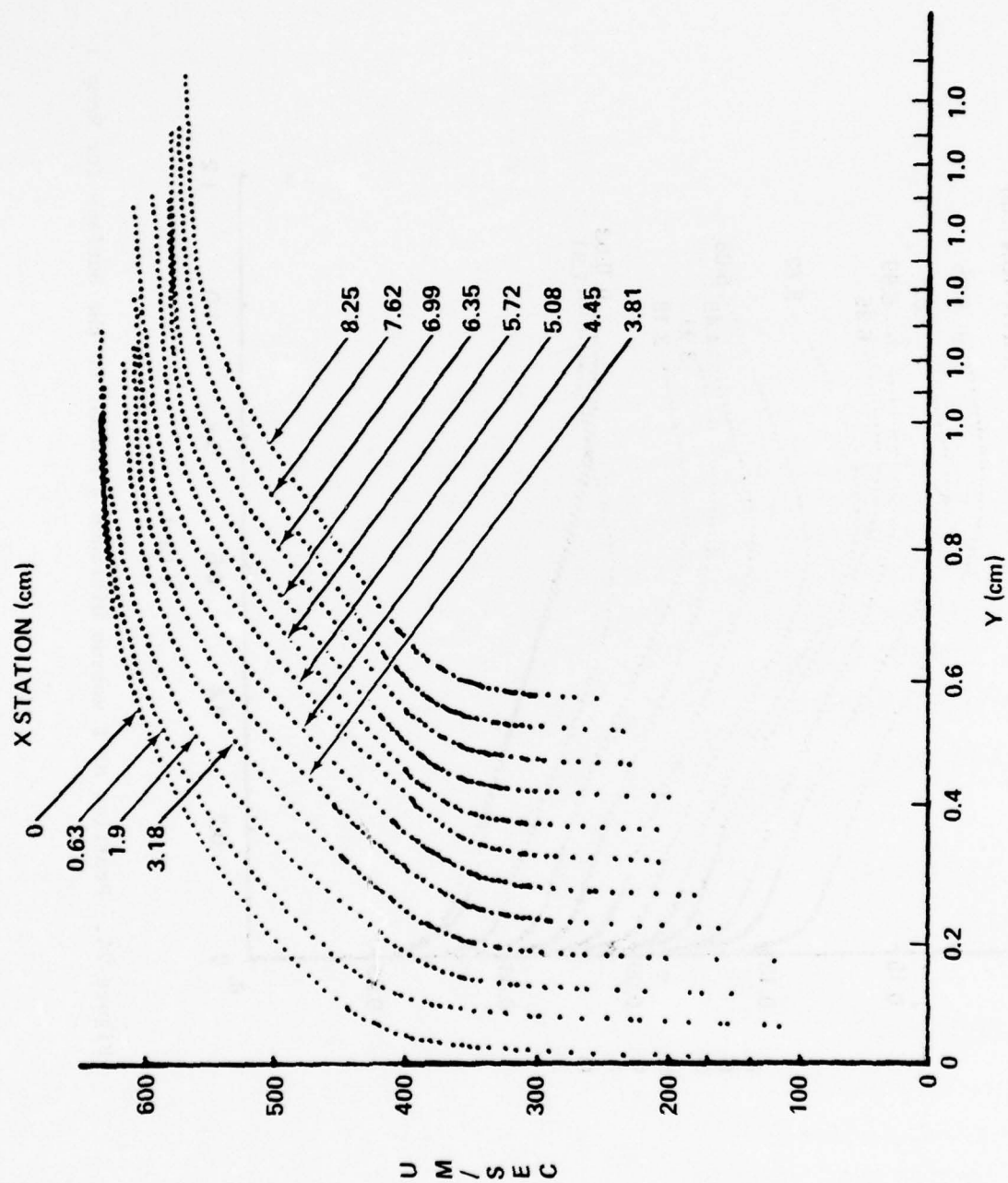


Figure 23. Profiles of u versus Distance y Normal to the Surface for Ramp 3

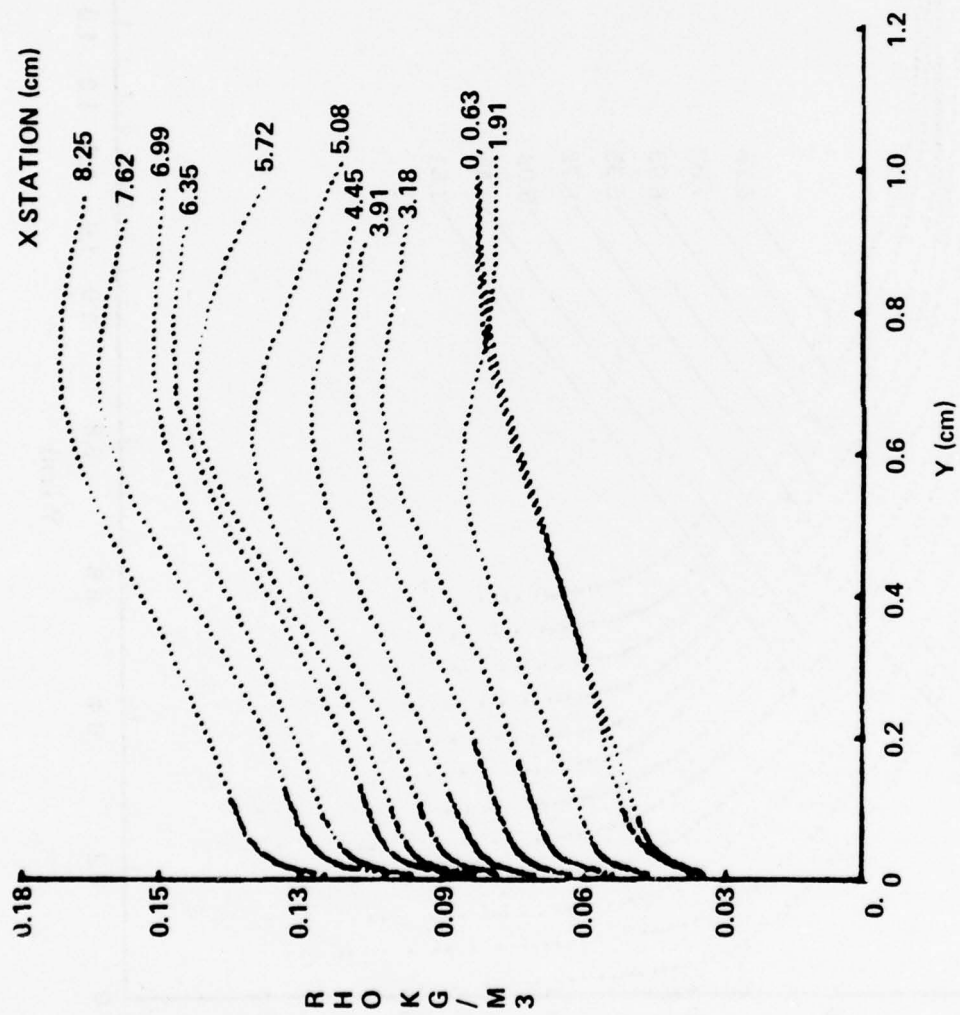


Figure 24. Profiles of ρ versus Distance y Normal to the Surface for Ramp 3

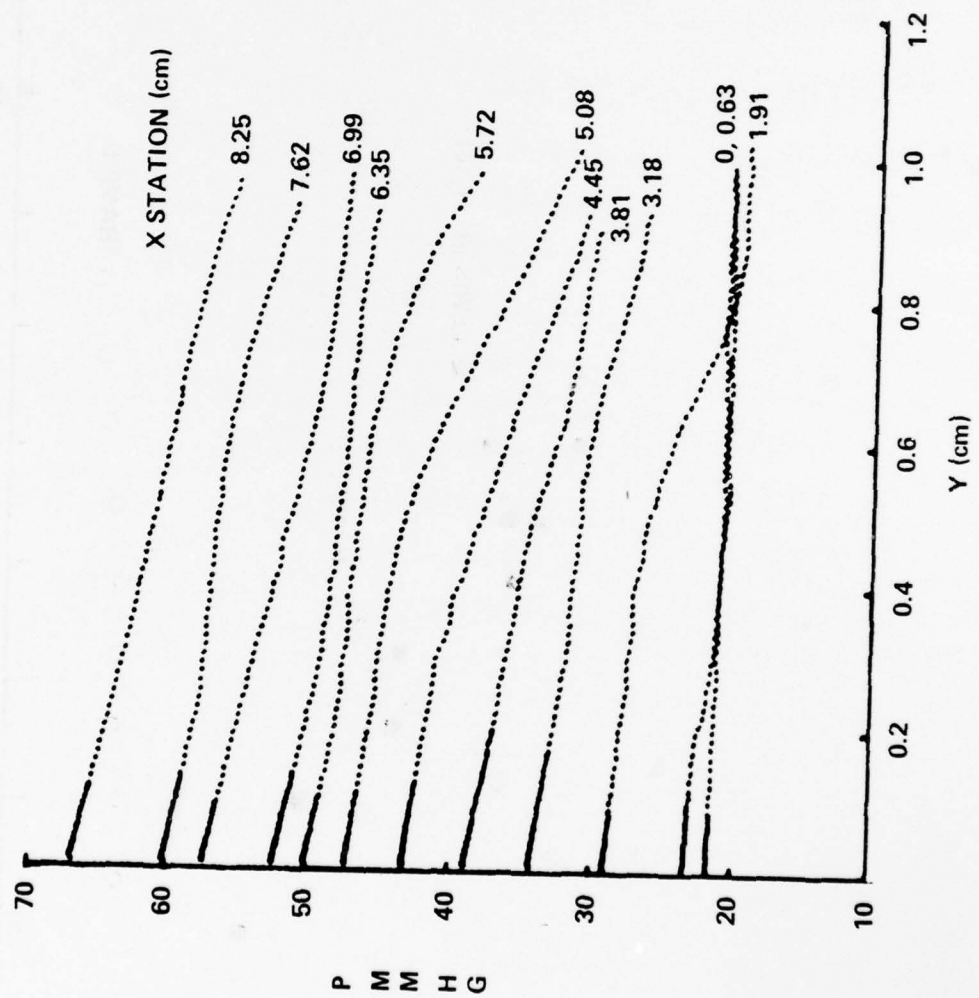


Figure 25. Profiles of p versus Distance y Normal to the Surface for Ramp 3

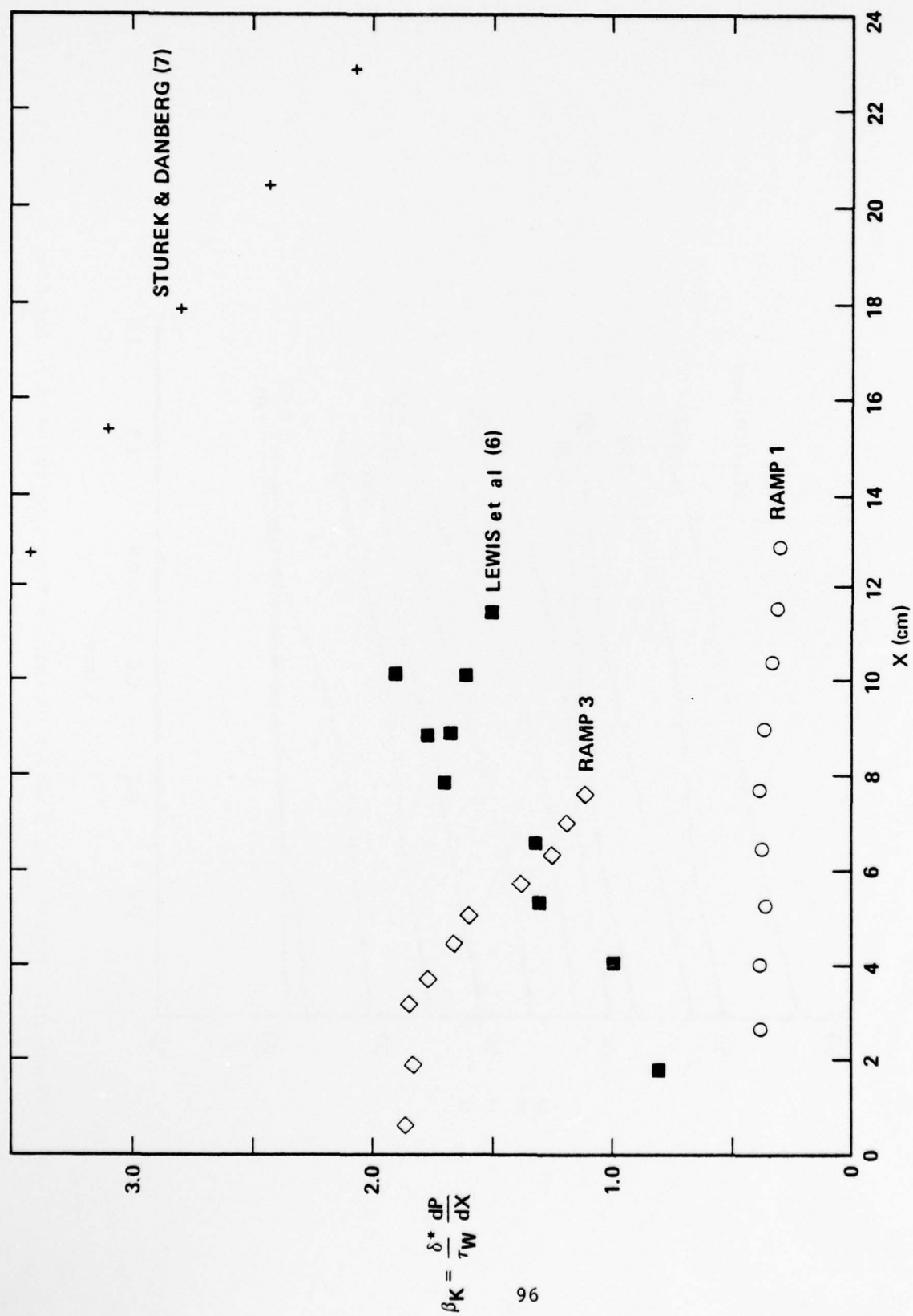


Figure 26. Streamwise Variation of Pressure Gradient Parameter β_K

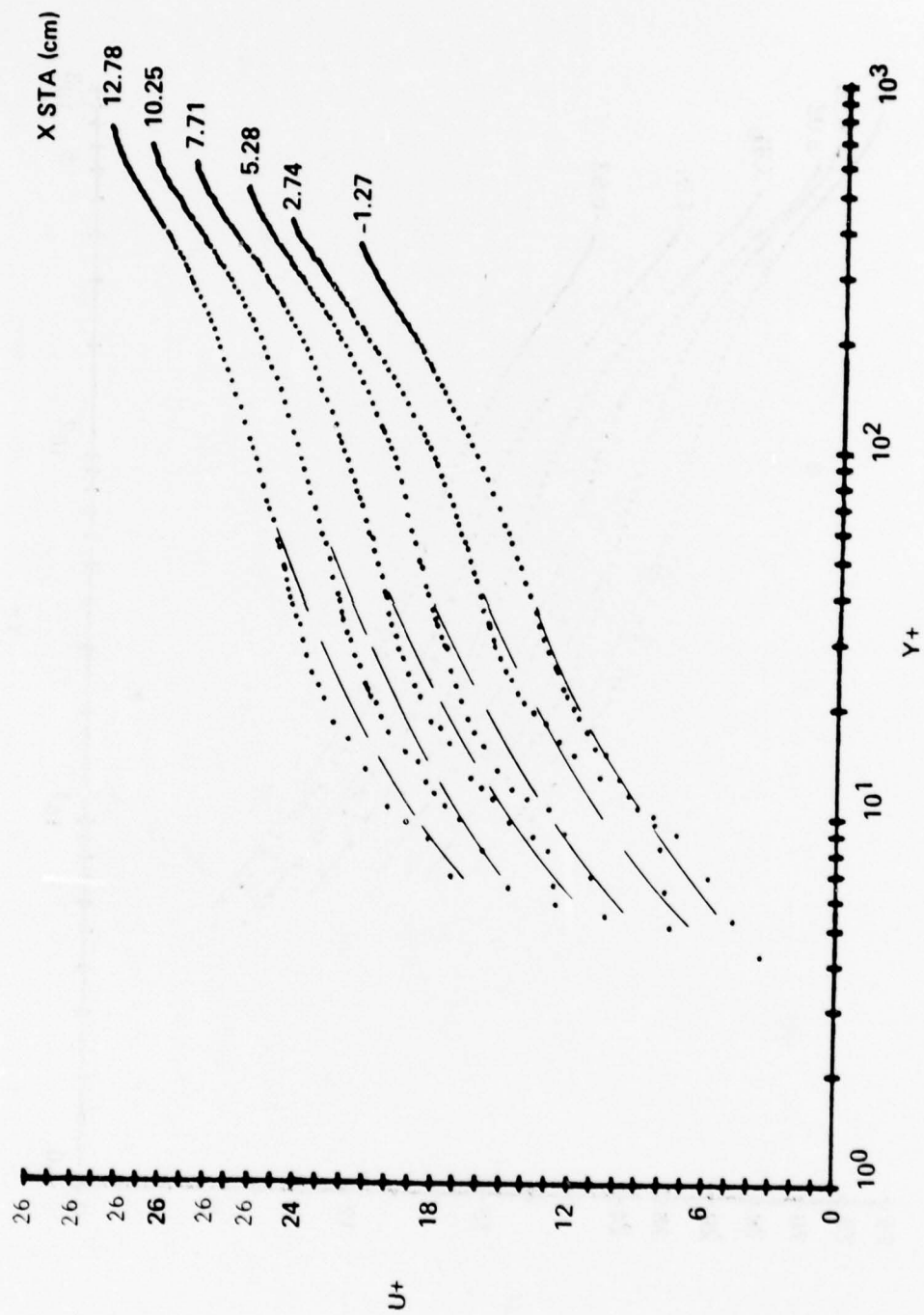


Figure 27. Typical Law-of-the-Wake Velocity Correlations, Ramp 1

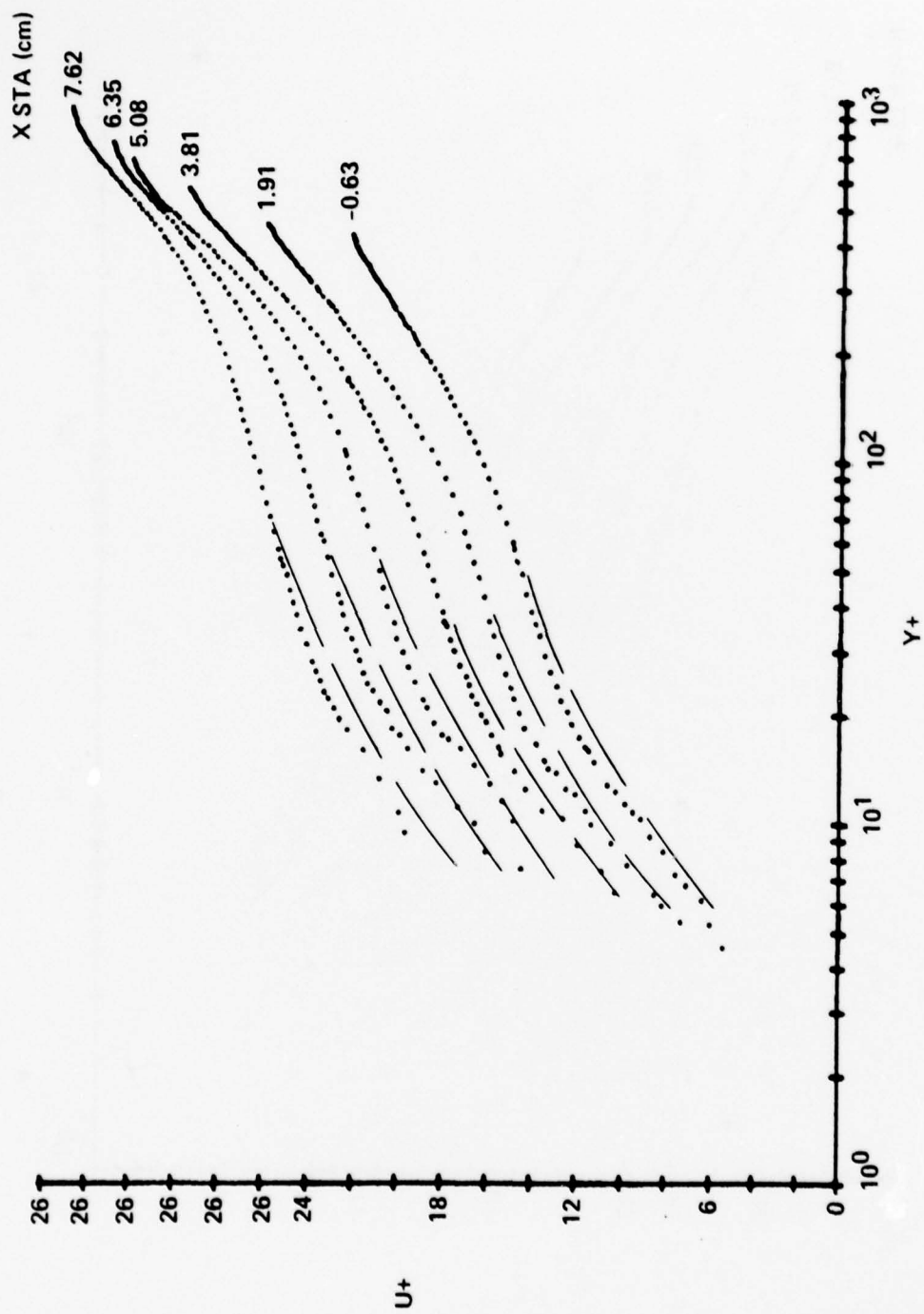


Figure 28. Typical Law-of-the-Wake Velocity Correlations, Ramp 3

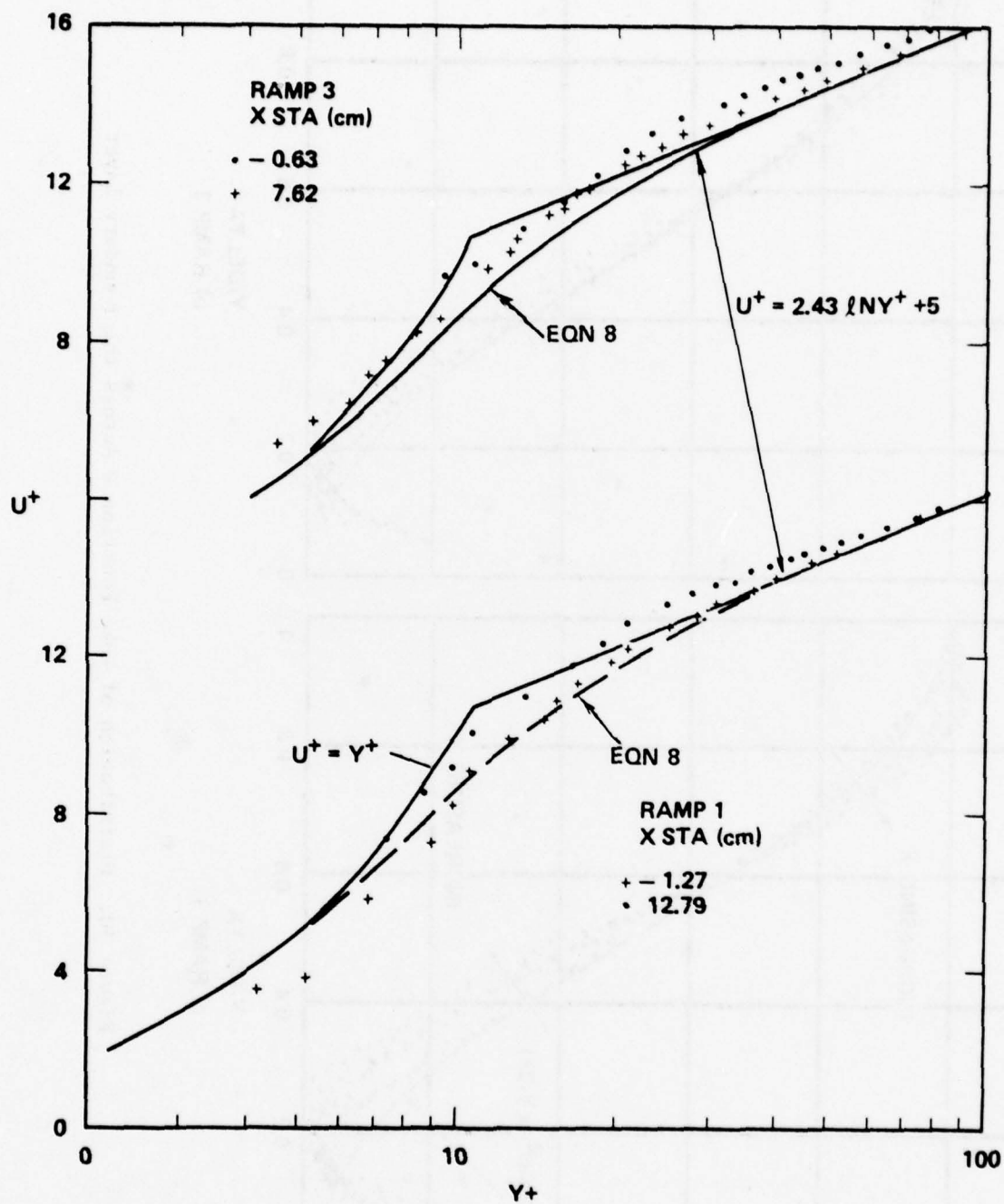


Figure 29. Velocity Correlations in the Vicinity of $y^+ = 10$

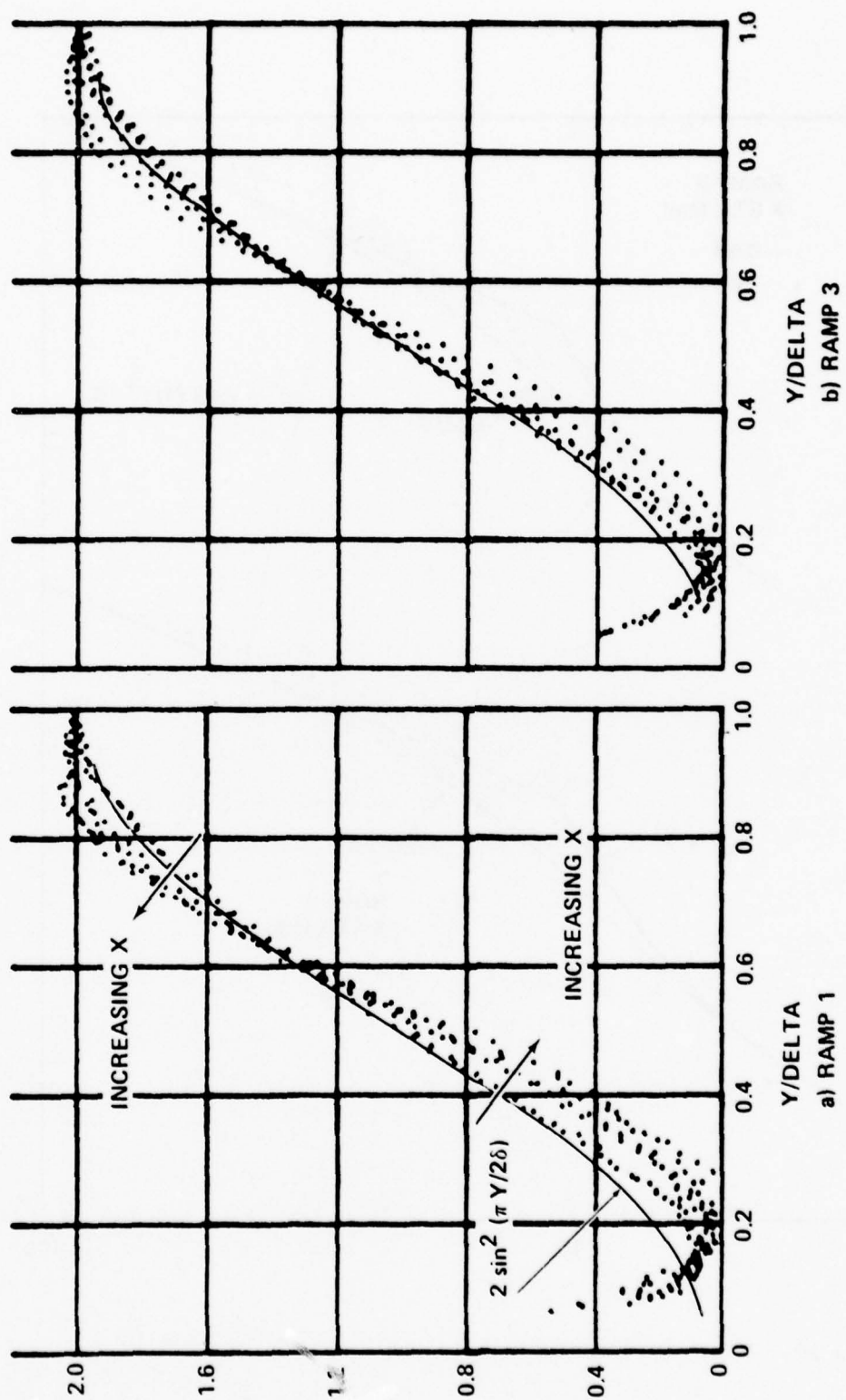


Figure 30. Distribution of Wake Function W Across the Boundary Layer

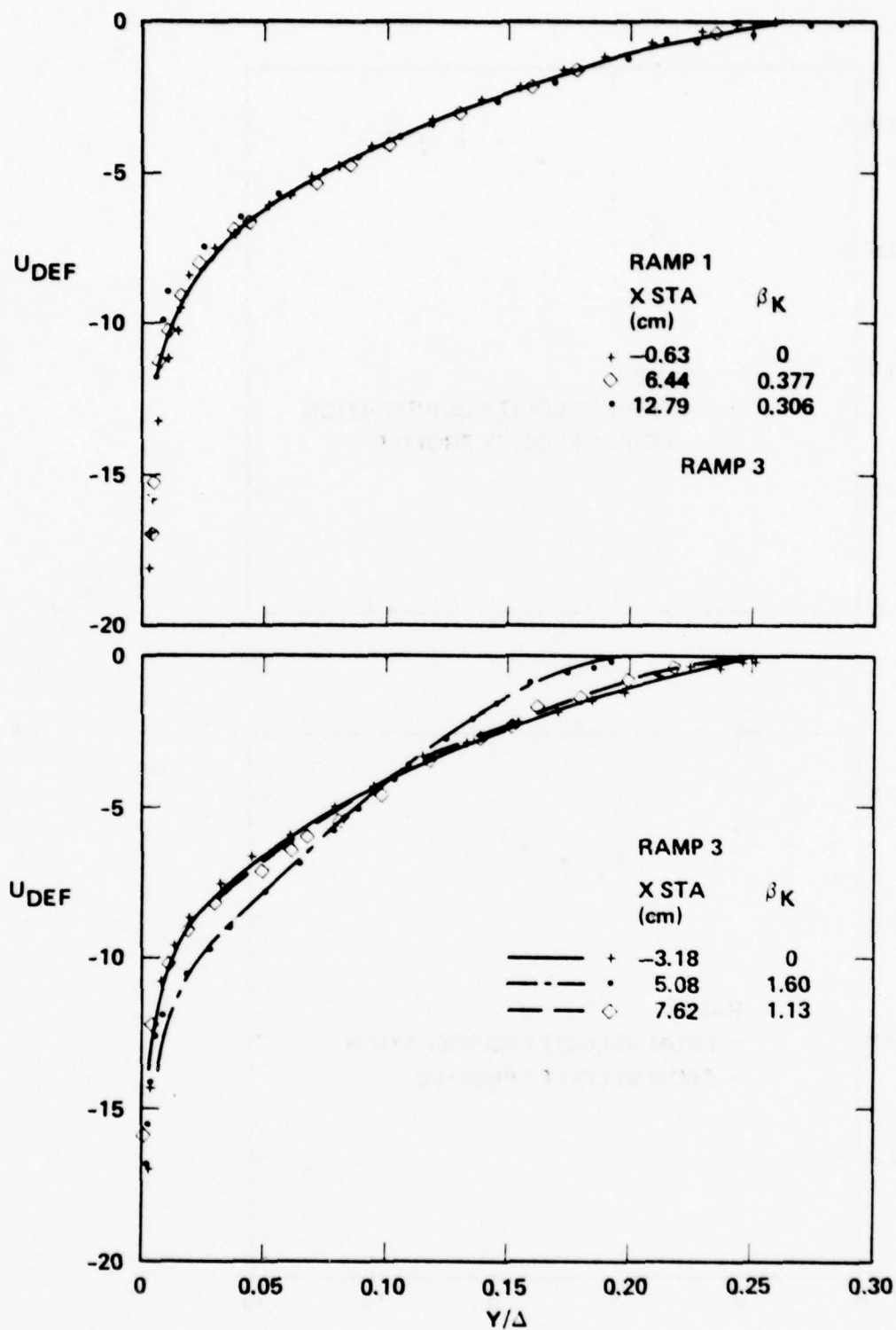


Figure 31. Velocity Deficit Form of the Velocity Profiles

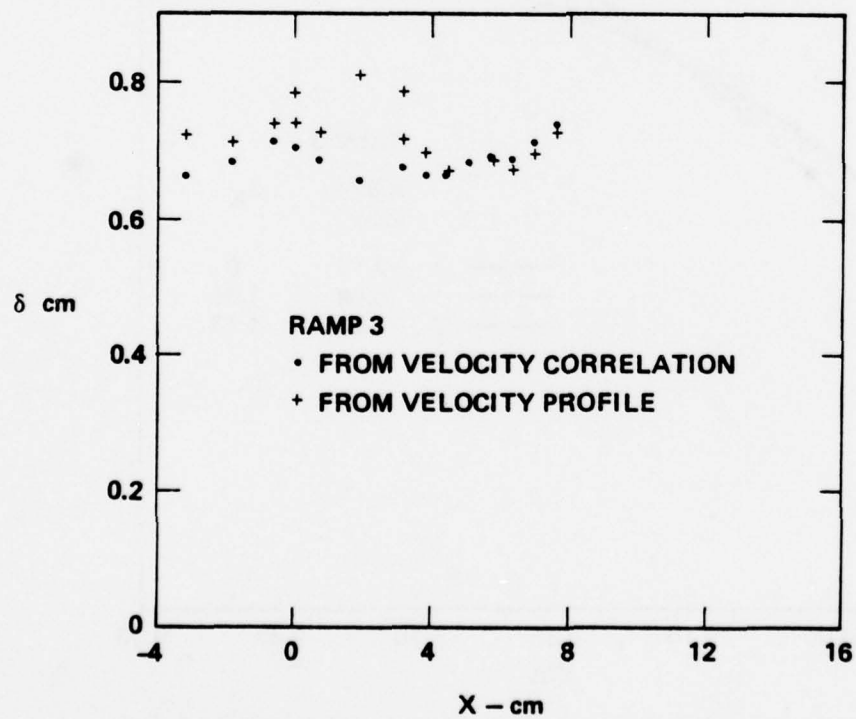
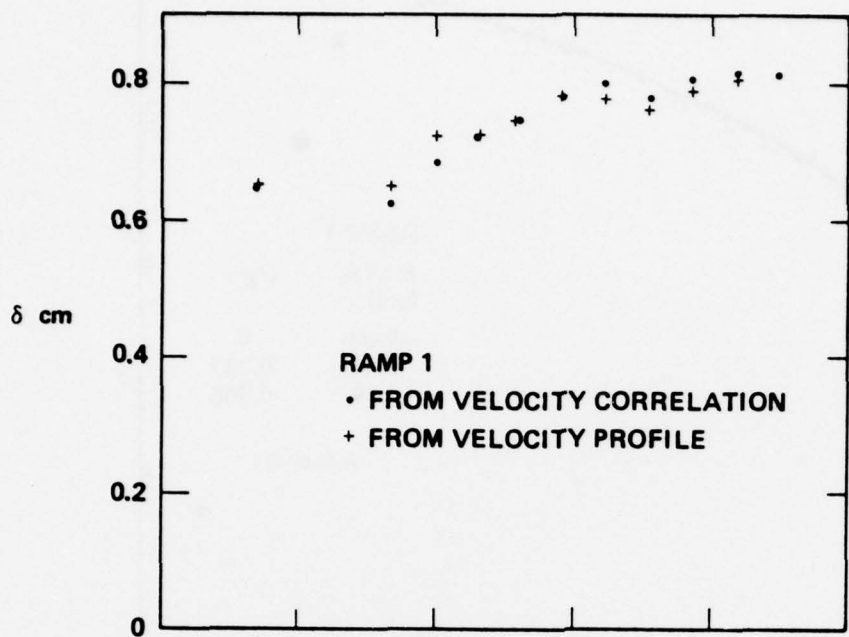


Figure 32. Streamwise Variation of the Boundary Layer Thickness

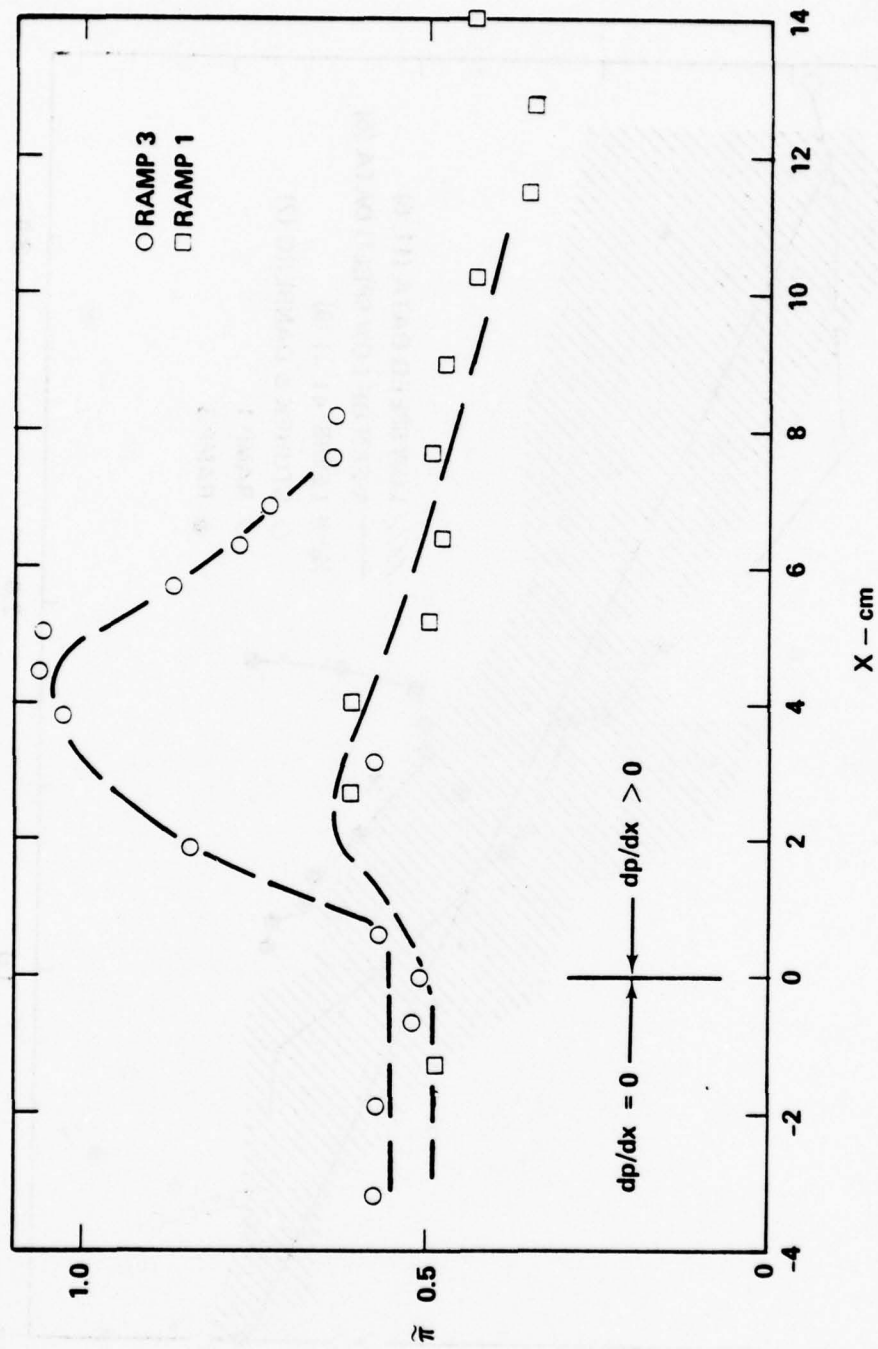


Figure 33. Streamwise Variation of the "Wake Strength Parameter" $\tilde{\pi}$

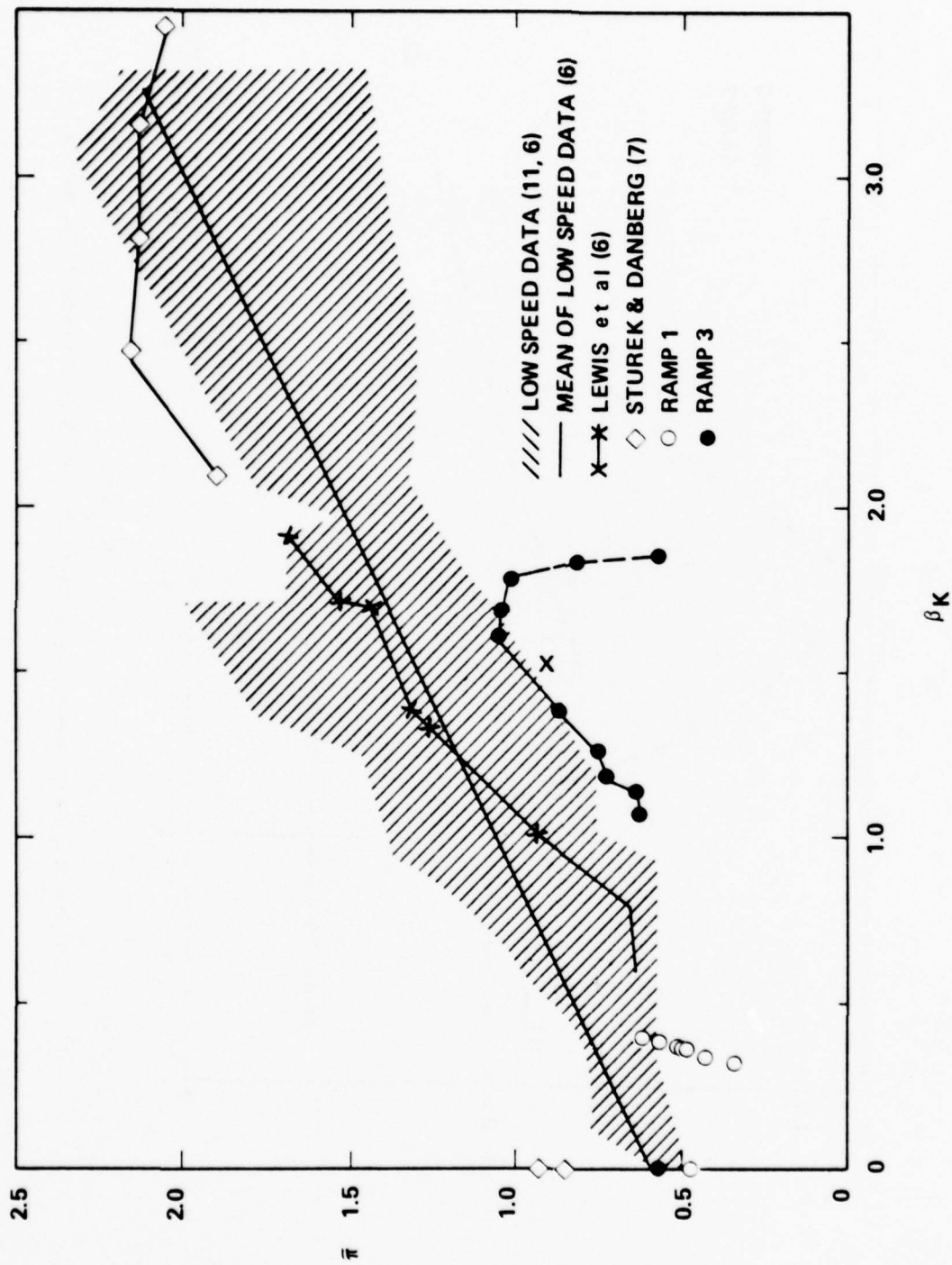


Figure 34. Correlation of Wake Parameter $\tilde{\pi}$ with Pressure Gradient Parameter β_K

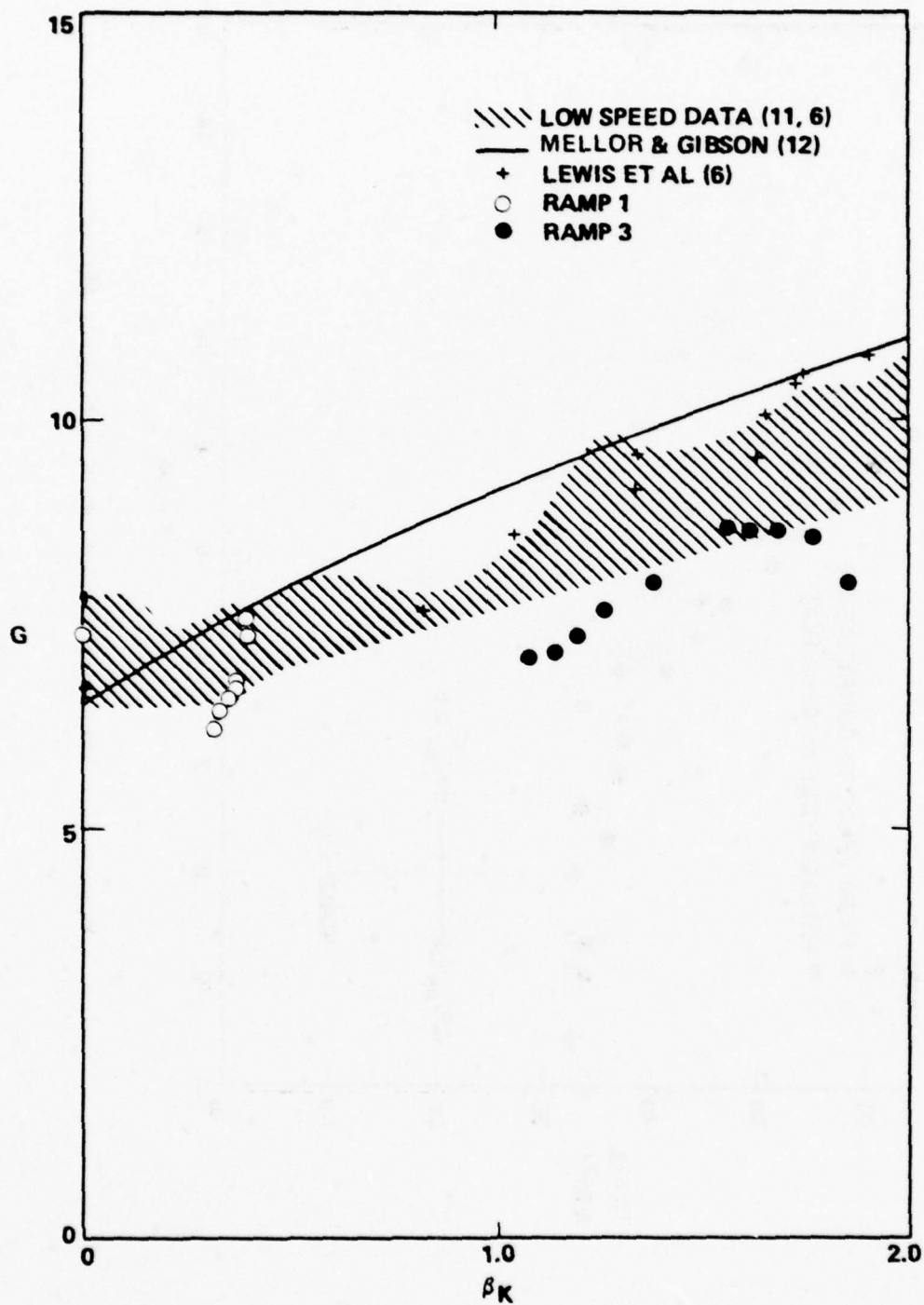


Figure 35. Correlation of Clauser Shape Factor G with Pressure Gradient Parameter $\beta\kappa$

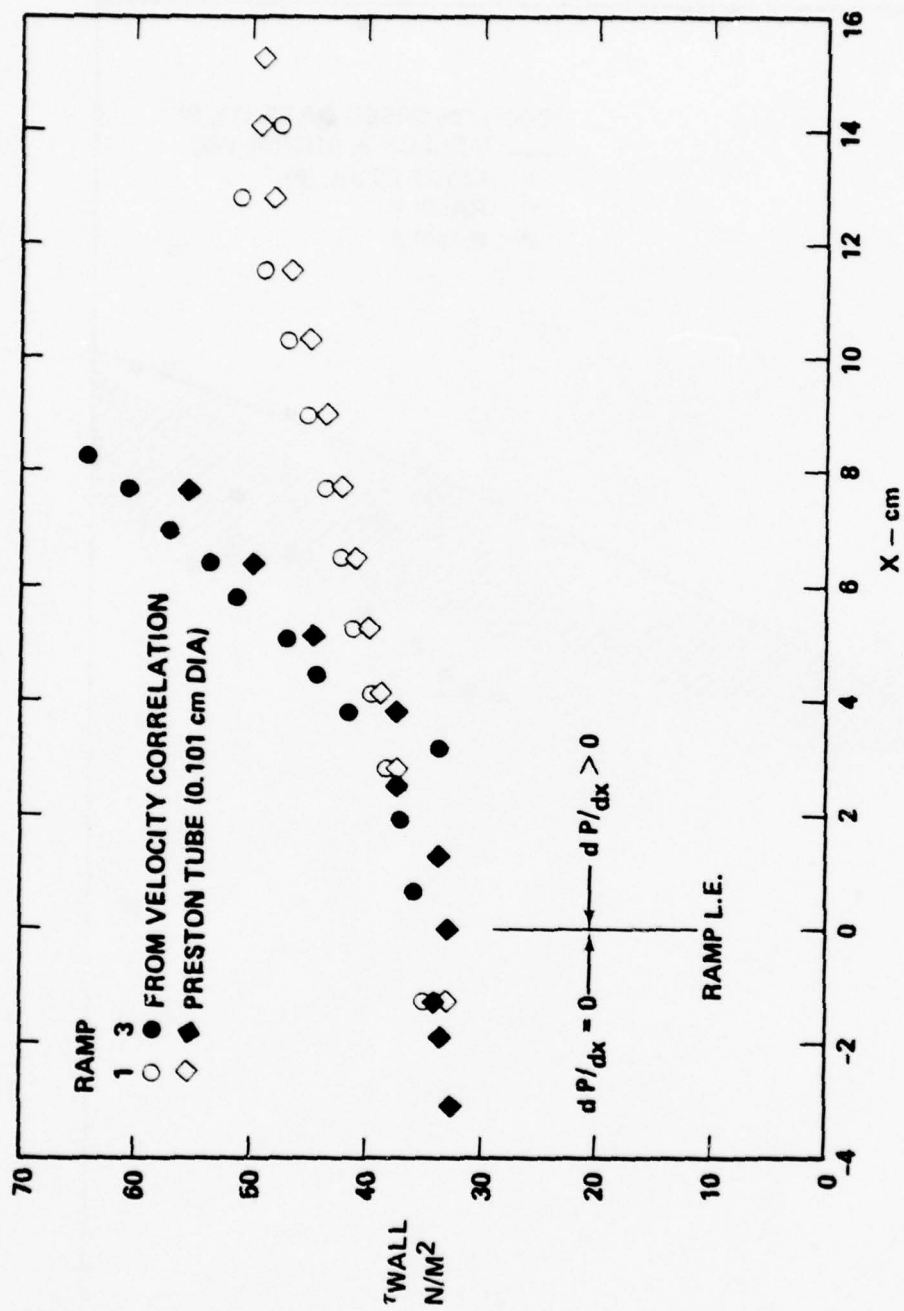


Figure 36. Streamwise Variation of Wall Shear Stress

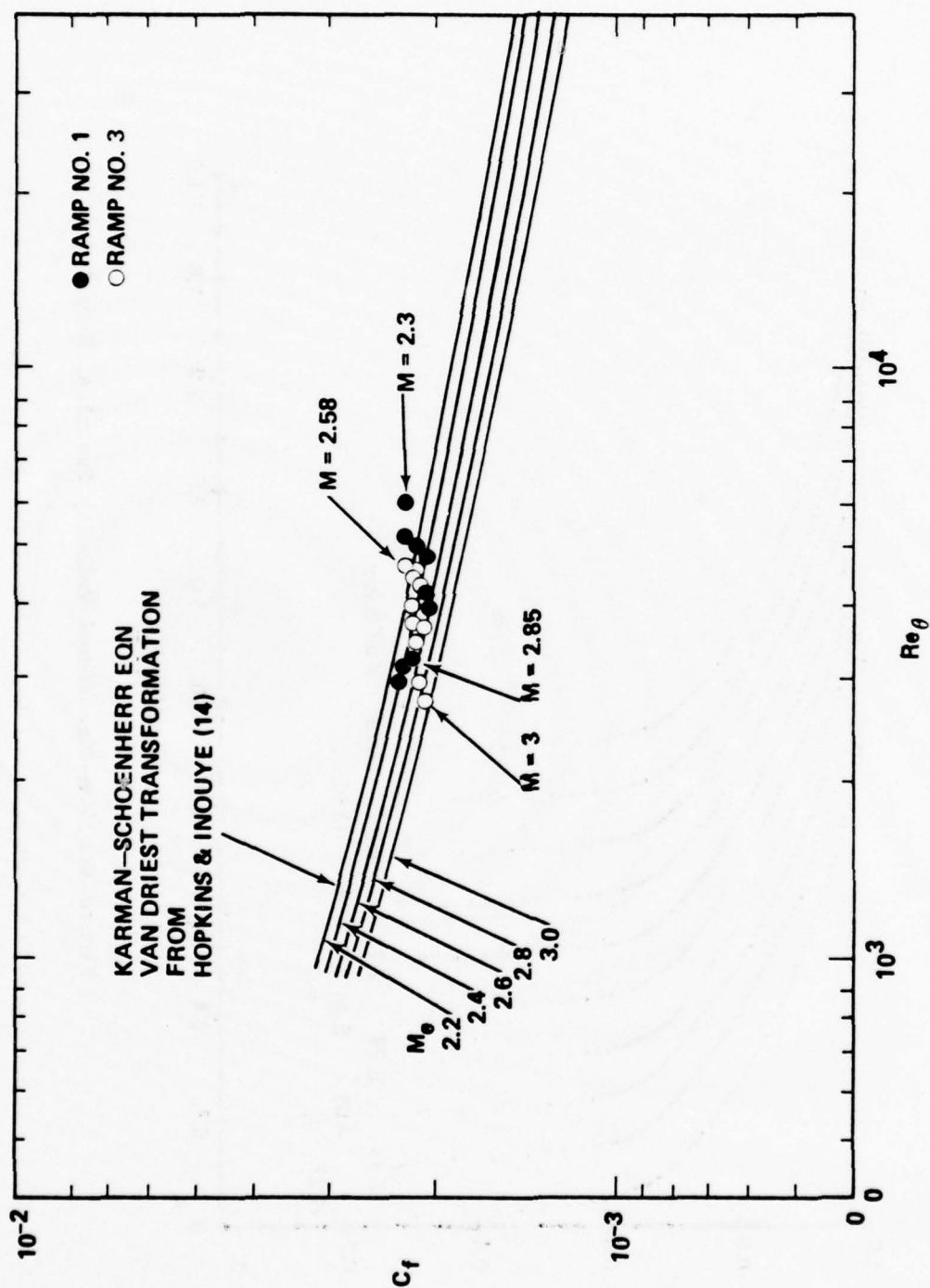


Figure 37. Comparison of Skin Friction Coefficient to Zero Pressure Gradient Results

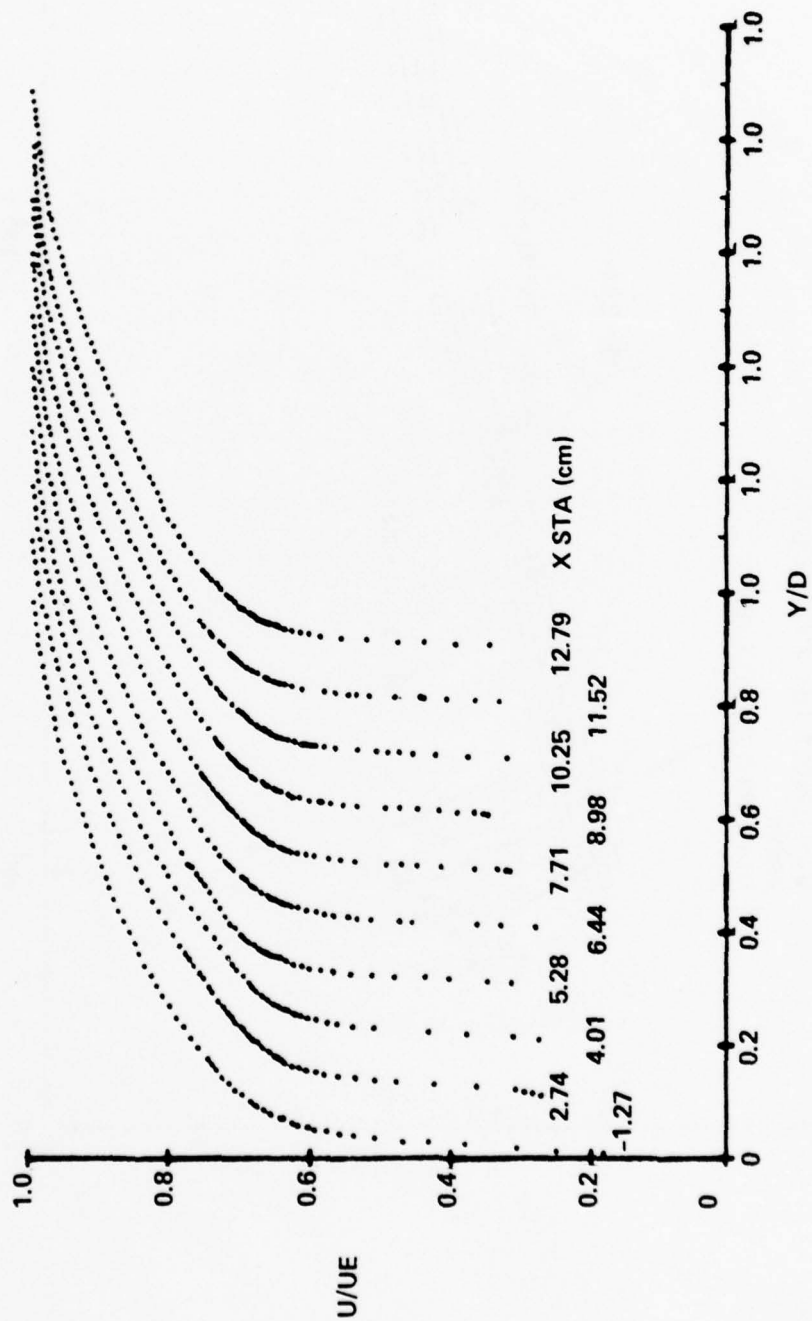


Figure 38. Non-dimensional Velocity Profiles, Ramp 1

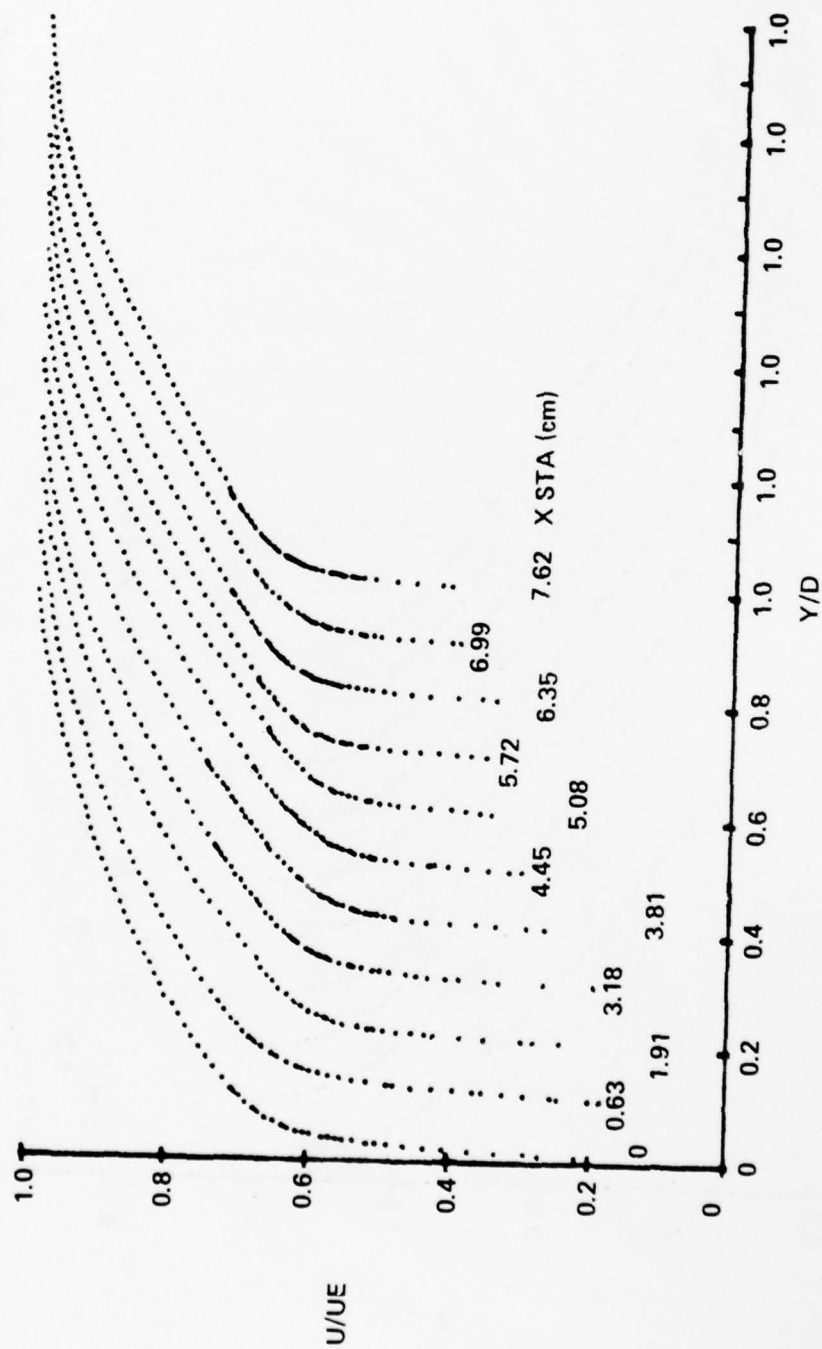


Figure 39. Non-dimensional Velocity Profiles, Ramp 3

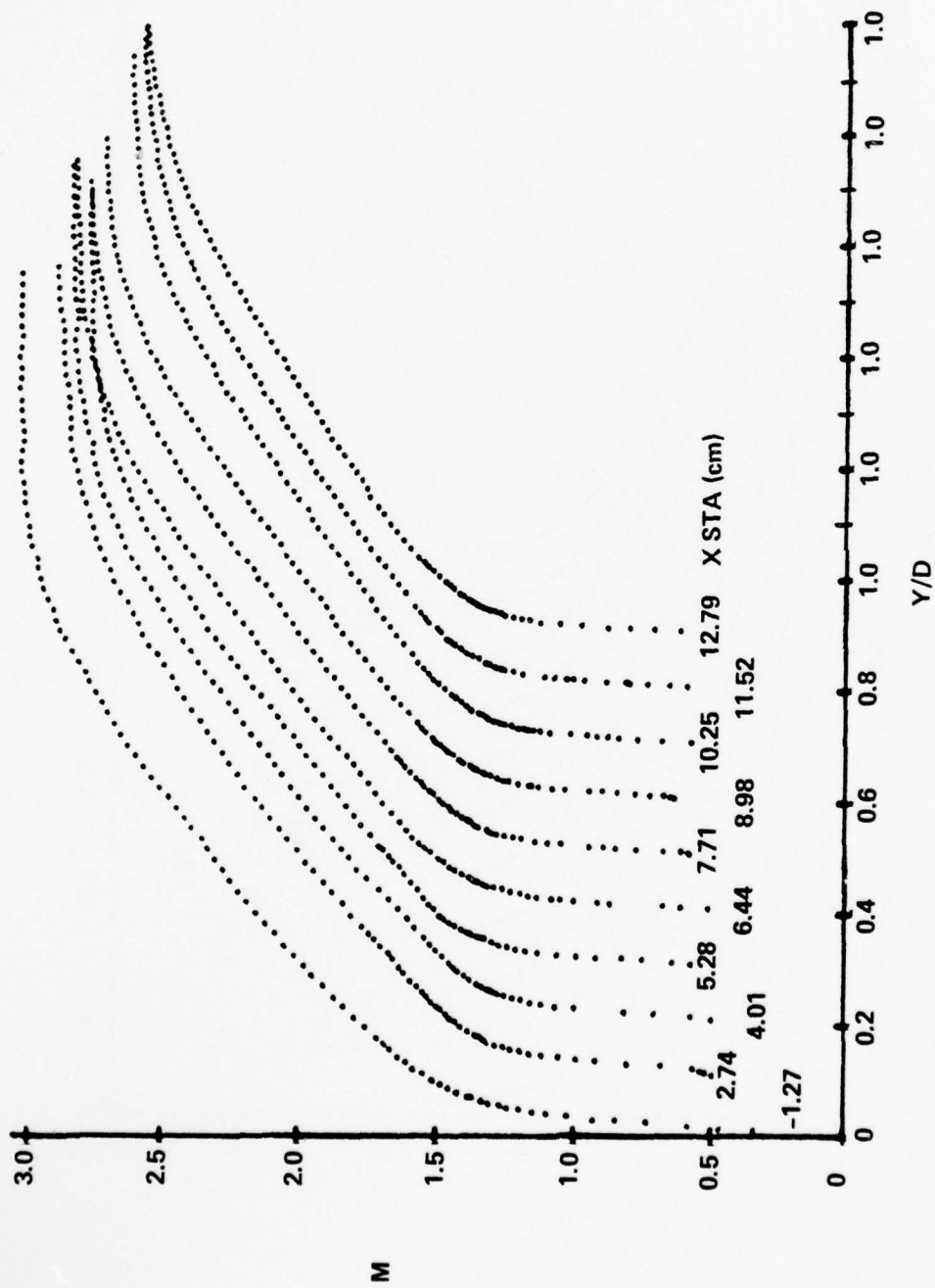


Figure 40. Mach Number Profiles, Ramp 1

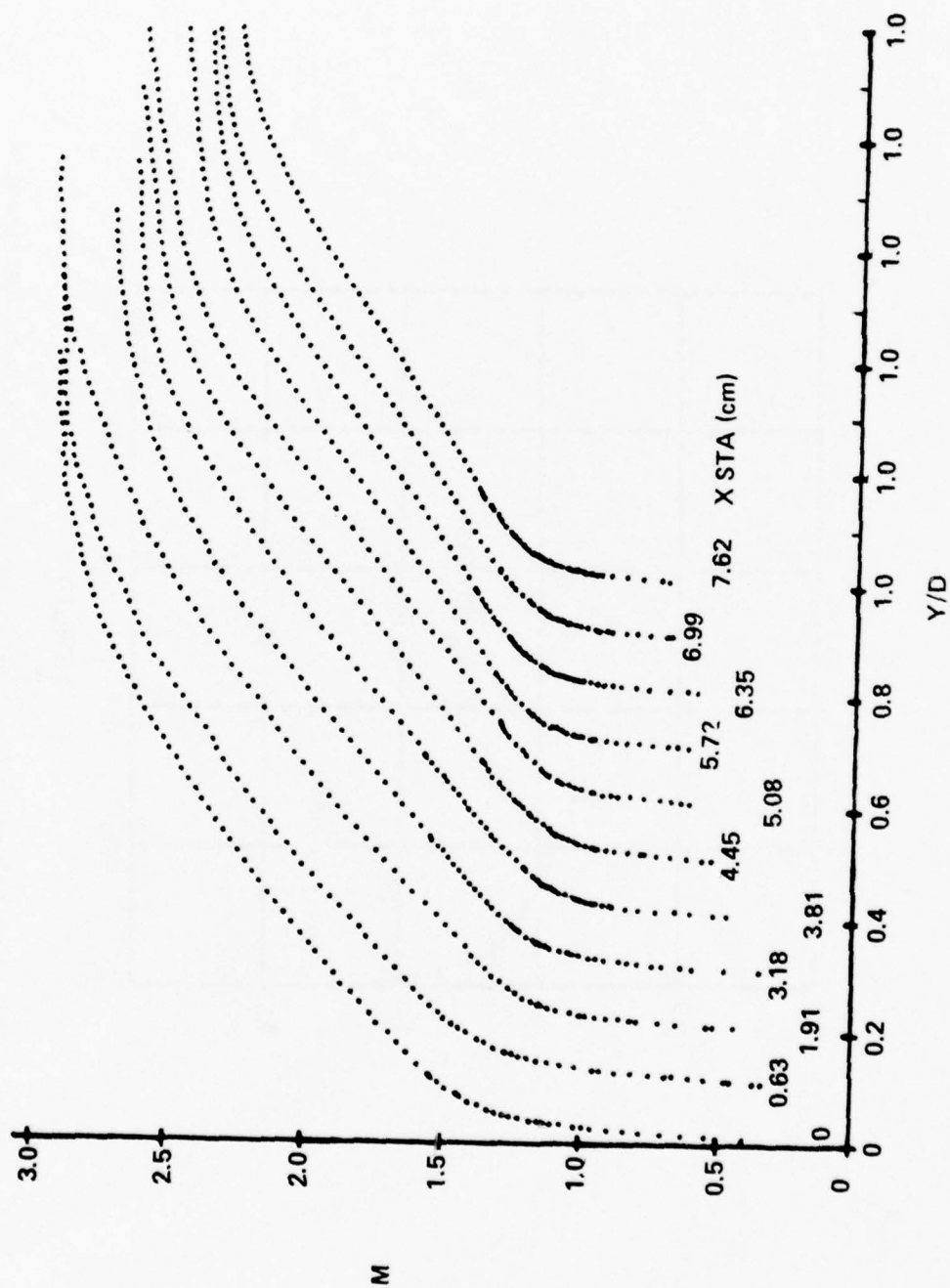


Figure 41. Mach Number Profiles, Ramp 3

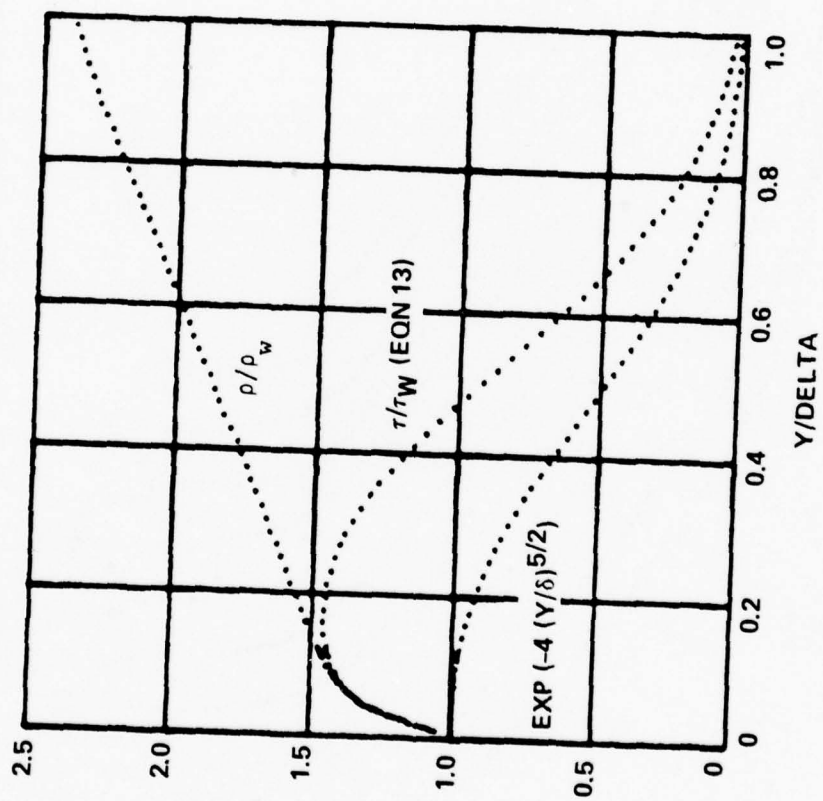


Figure 42. Whitfield-High Model of Turbulent Shear Stress Distribution Across the Boundary Layer

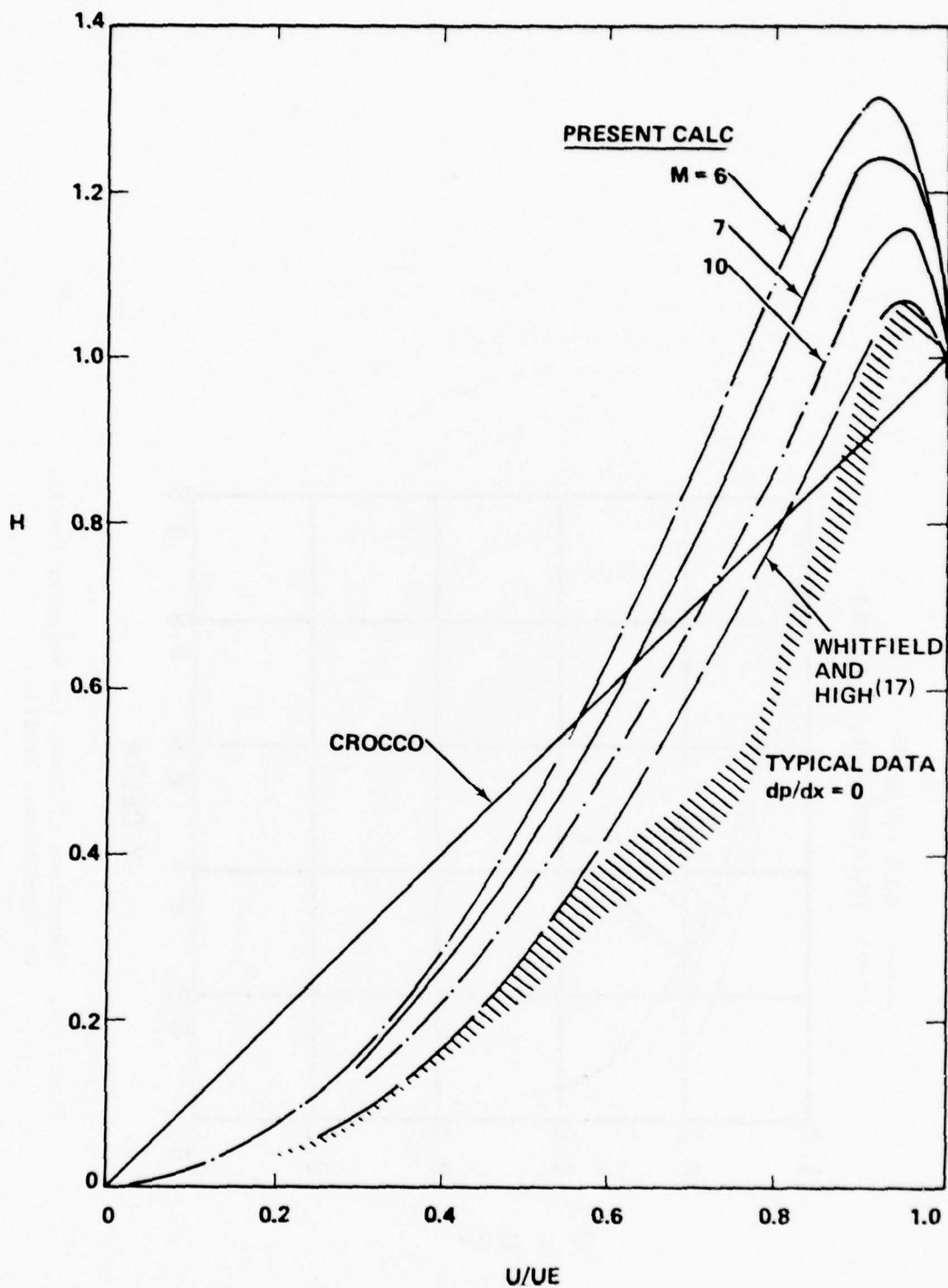


Figure 43. Non-dimensional Total Temperature-Velocity Profiles for Non-unity Prandtl Number, Zero Pressure Gradient Flow with Adiabatic Walls Showing Effect of Exponent in Velocity Power Law.

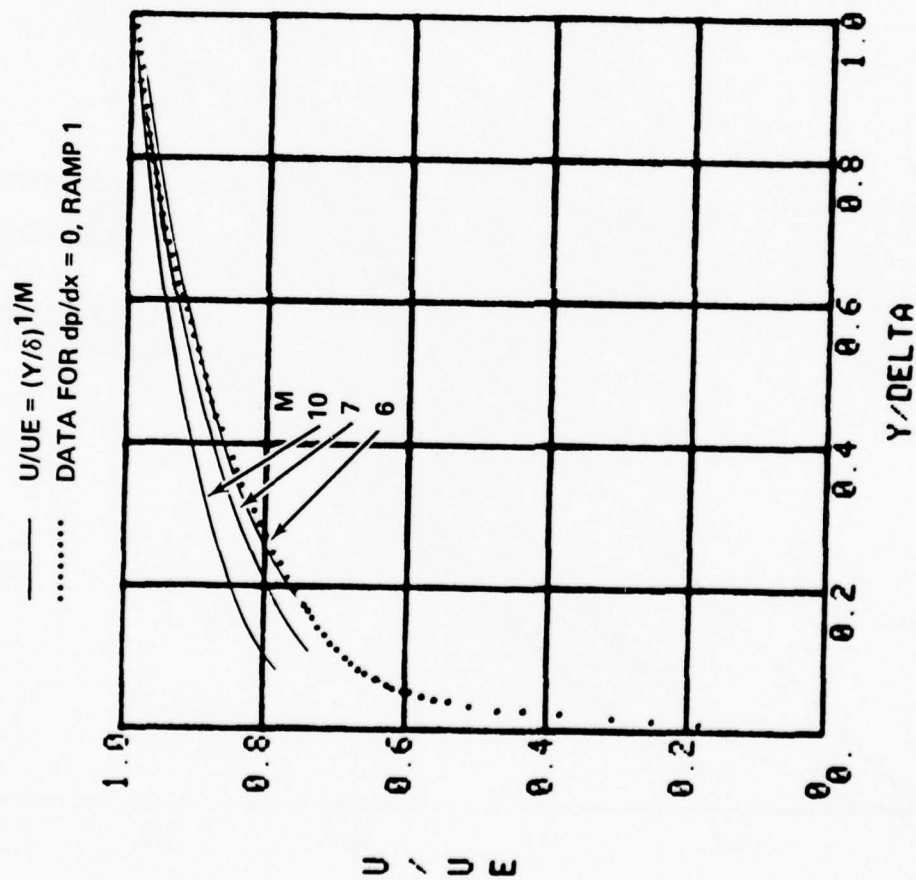


Figure 44. Comparison of Power Law Velocity Profile to Experimental Profile

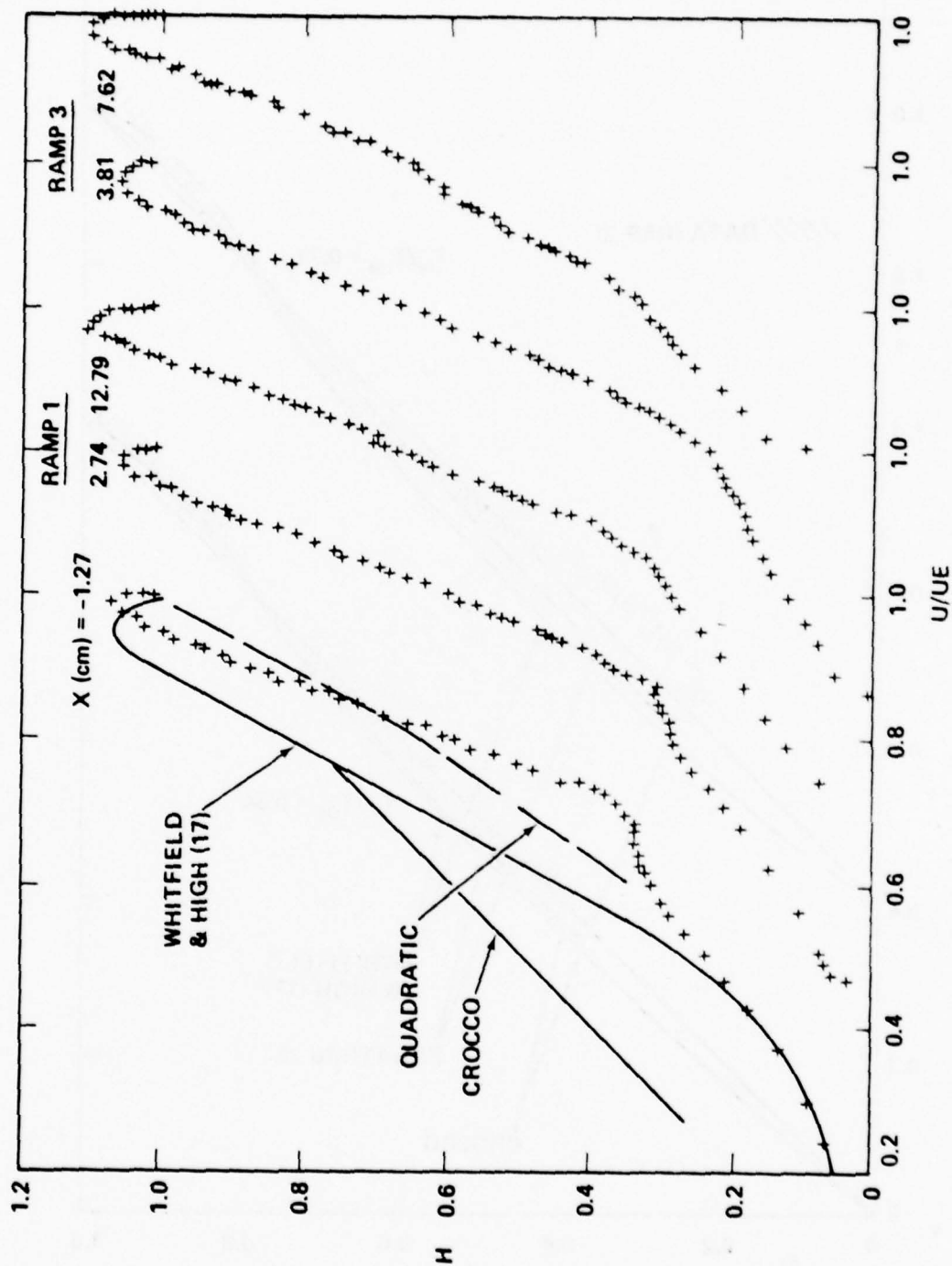


Figure 45. Experimental Non-dimensional Profiles of Total Temperature versus Velocity Showing Influence of Pressure Gradient

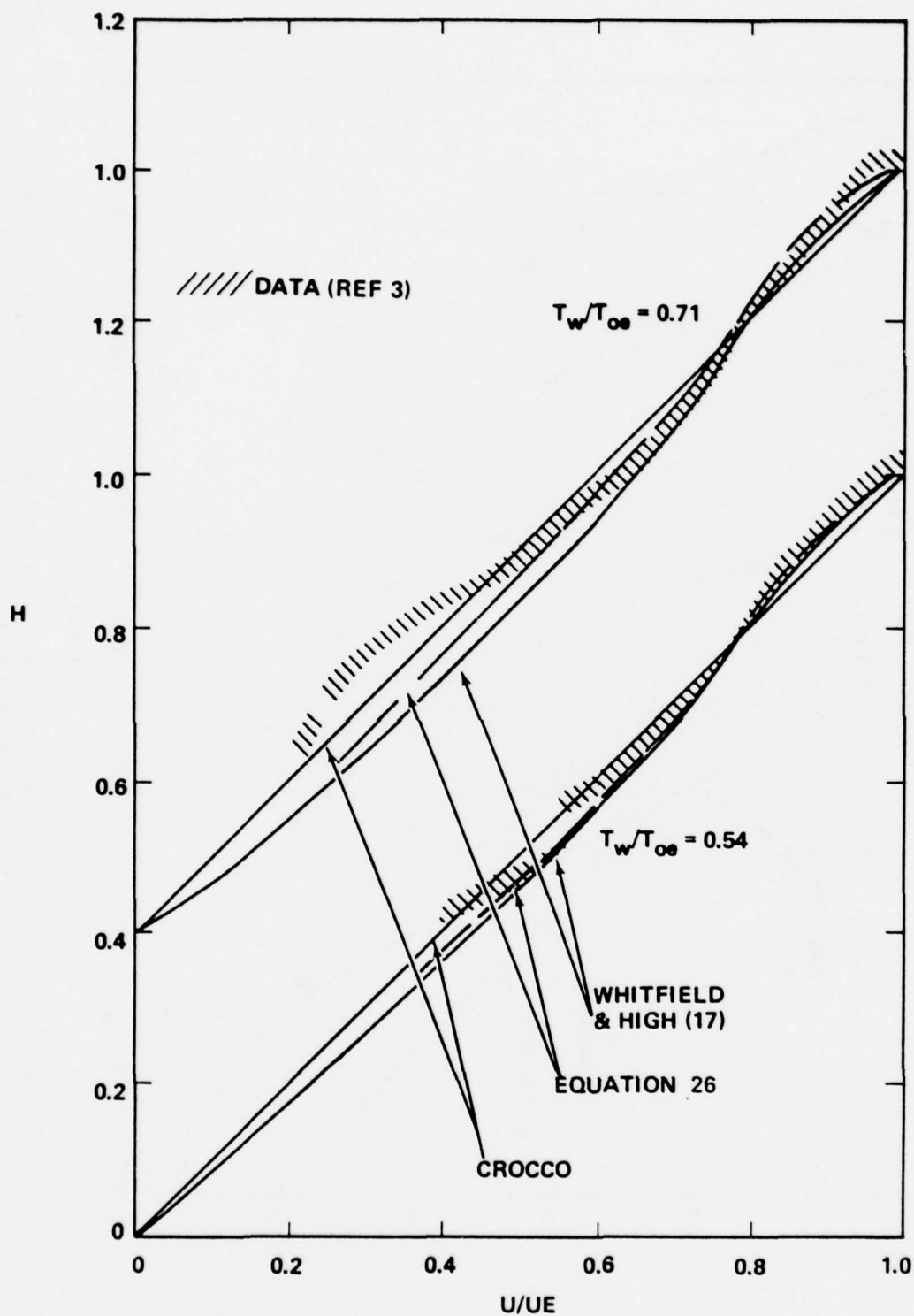


Figure 46. Effect of Heat Transfer on Total Temperature-Velocity Profiles for Non-unity Prandtl Number, Zero Pressure Gradient Boundary Layer

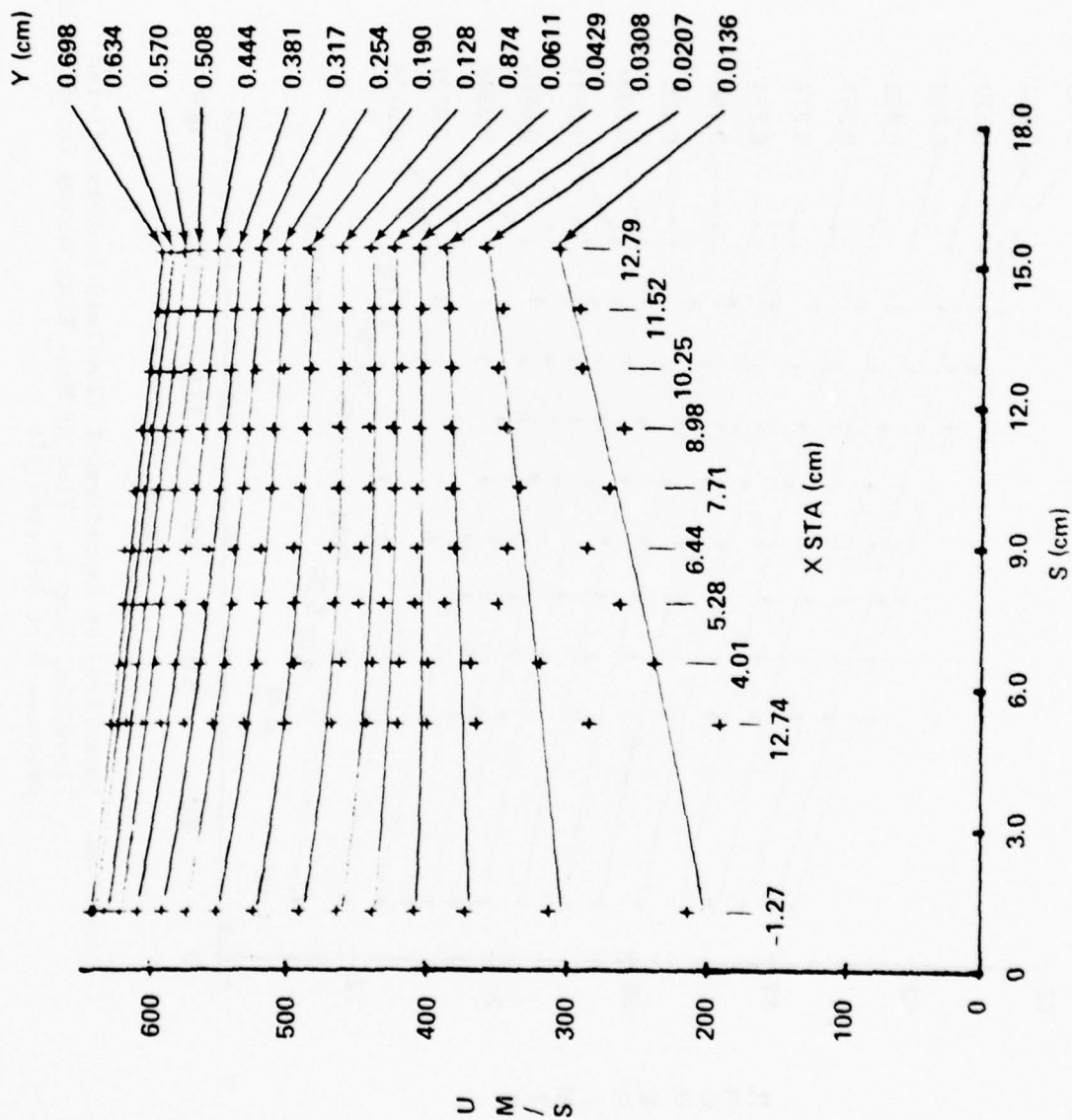


Figure 47. Comparison of Experimental Flowfield to Curve-fitted Flowfield, Ramp 1. Plot of Velocity versus Curvilinear Distance S at Selected y's

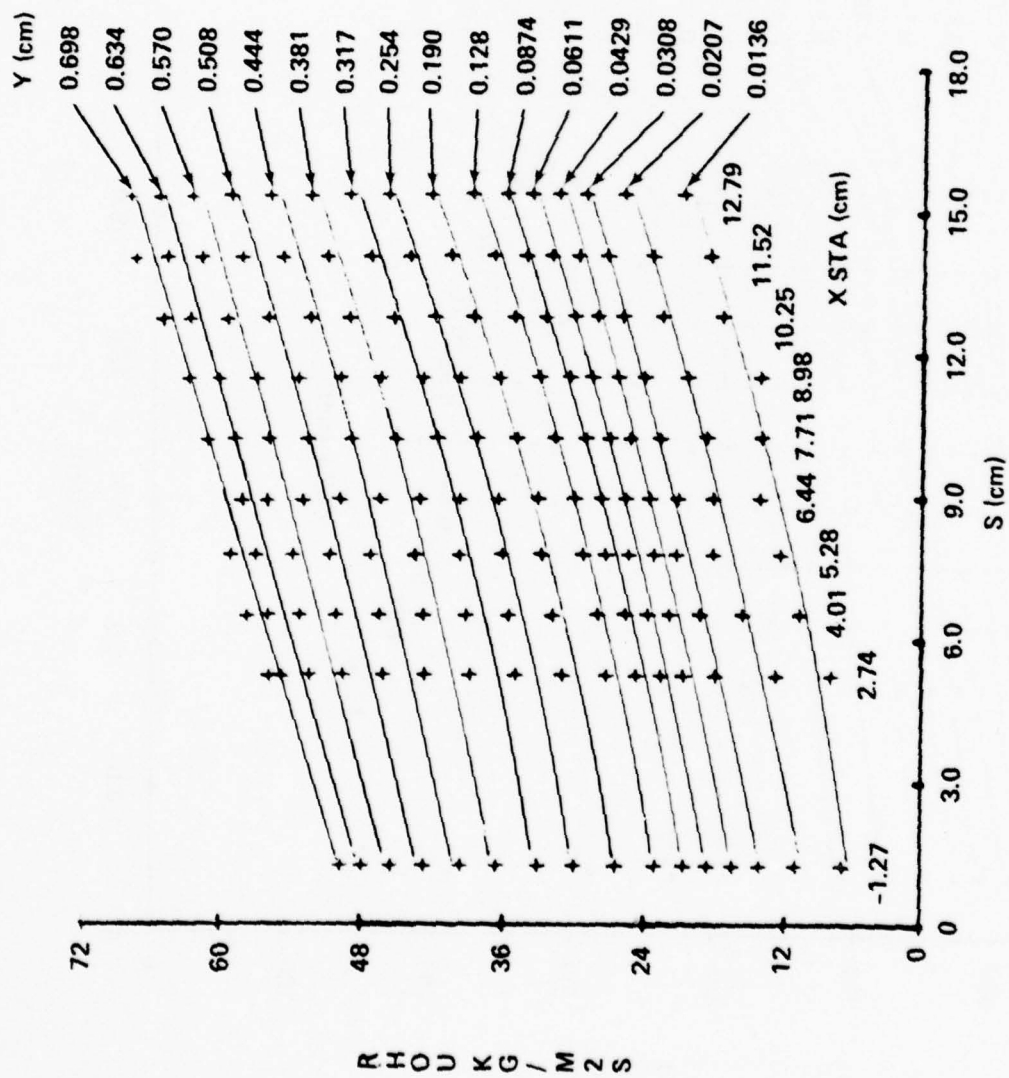


Figure 48. Comparison of Experimental Flowfield to Curve-fitted Flowfield, Ramp 1. Plot of Mass Flux versus Curvilinear Distance S at Selected y 's

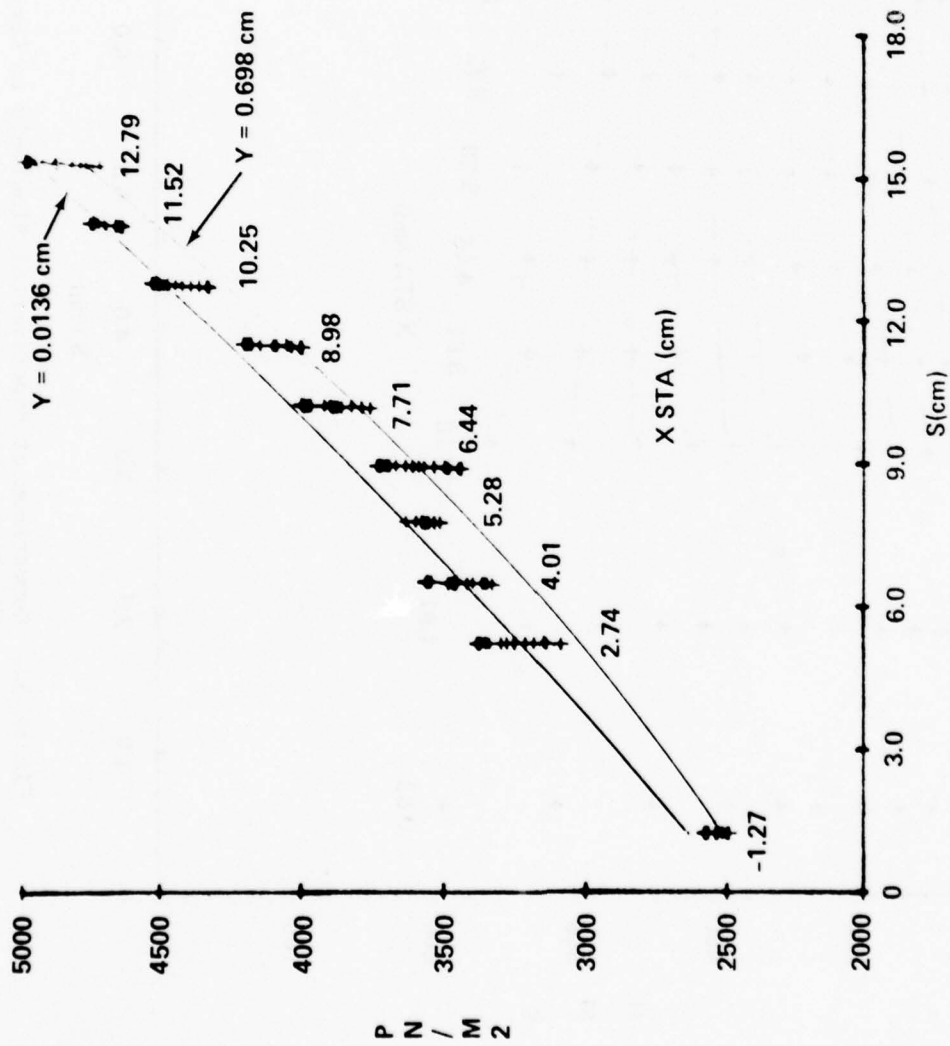


Figure 49. Comparison of Experimental Flowfield to Curve-fitted Flowfield, Ramp 1. Plot of Static Pressure versus Curvilinear Distance S at Selected y 's

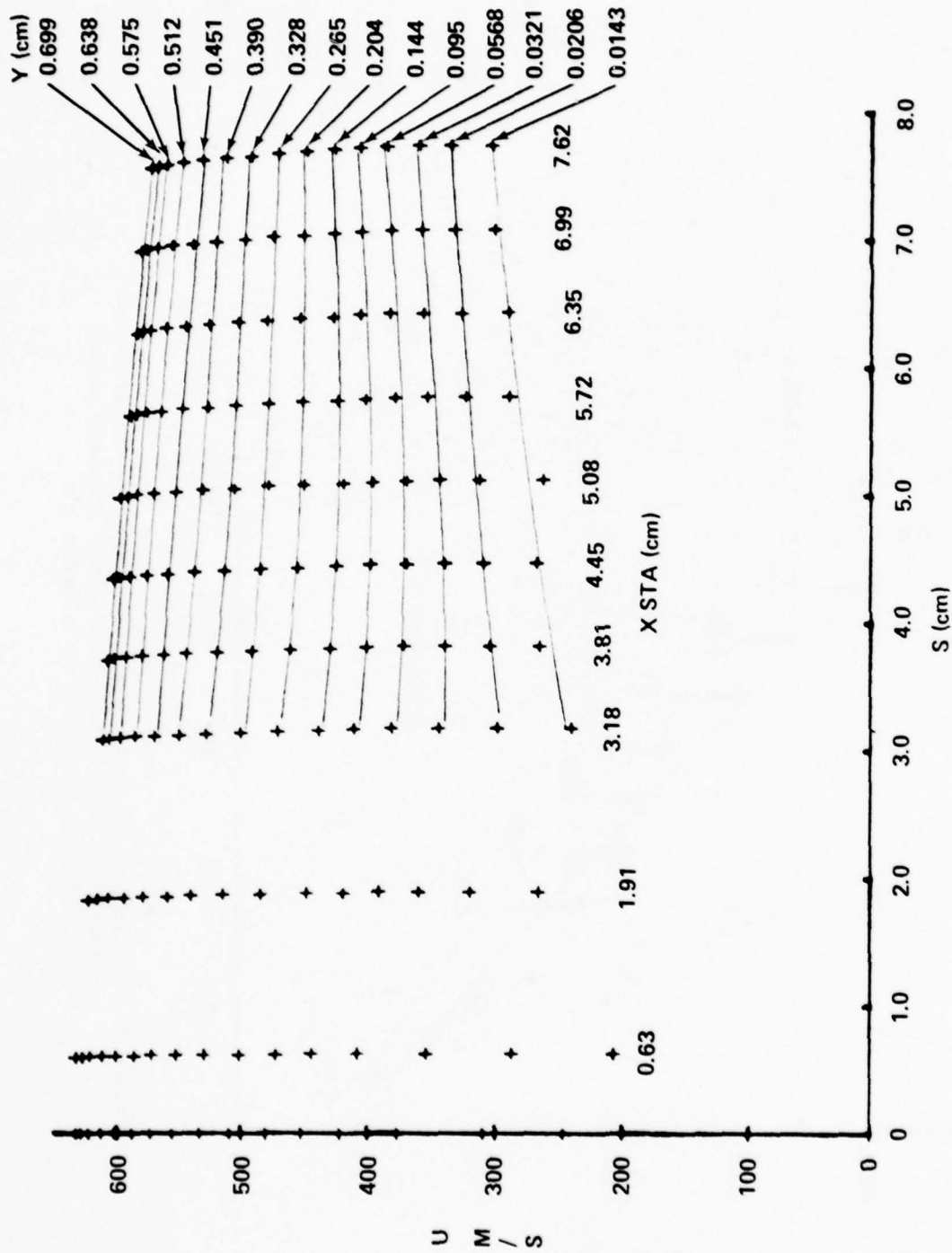


Figure 50. Comparison of Experimental Flowfield to Curve-fitted Flowfield, Ramp 3. Plot of Velocity versus Curvilinear Distance S at Selected y's

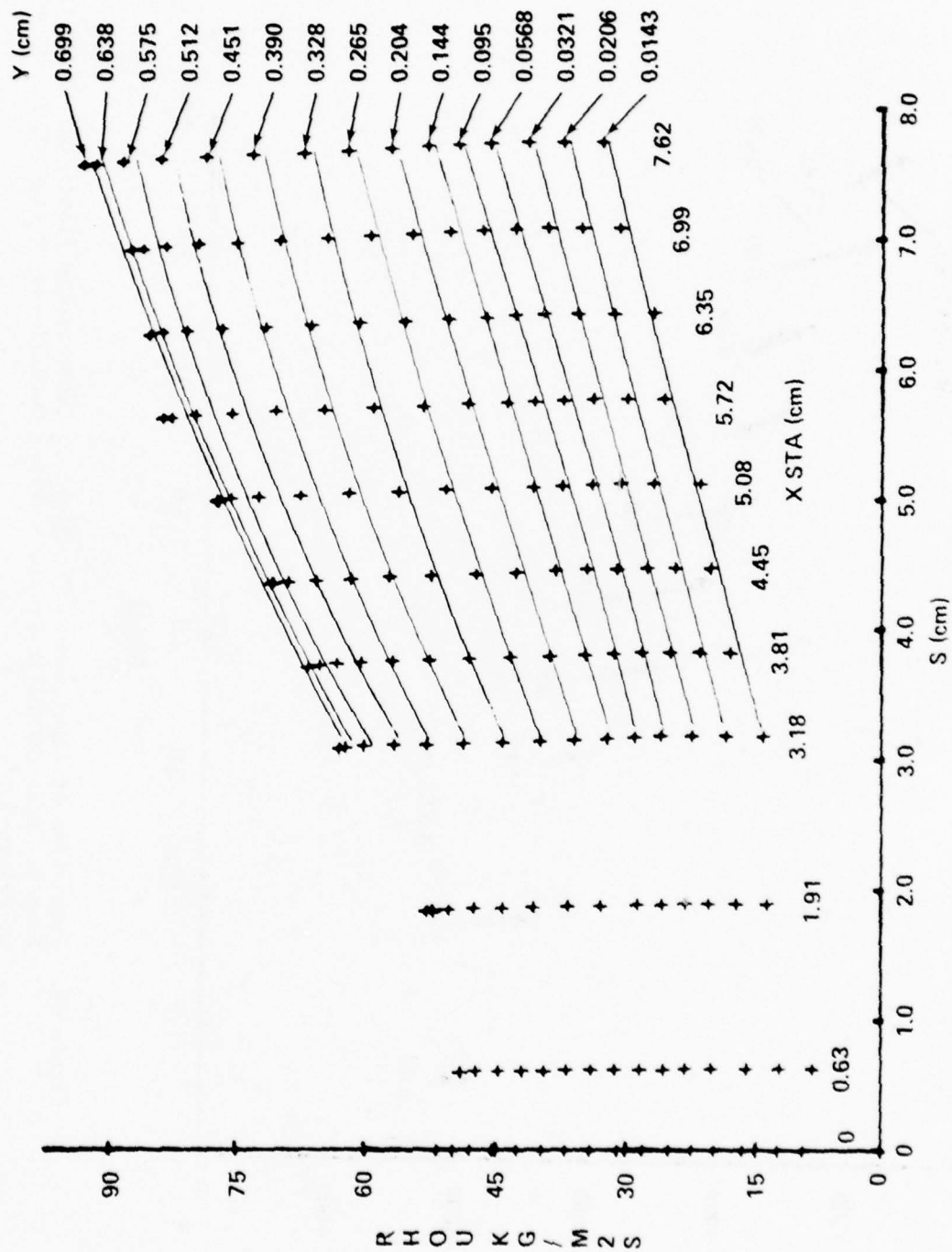


Figure 51. Comparison of Experimental Flowfield to Curve-fitted Flowfield, Ramp 3. Plot of Mass Flux versus Curvilinear Distance S at Selected y 's

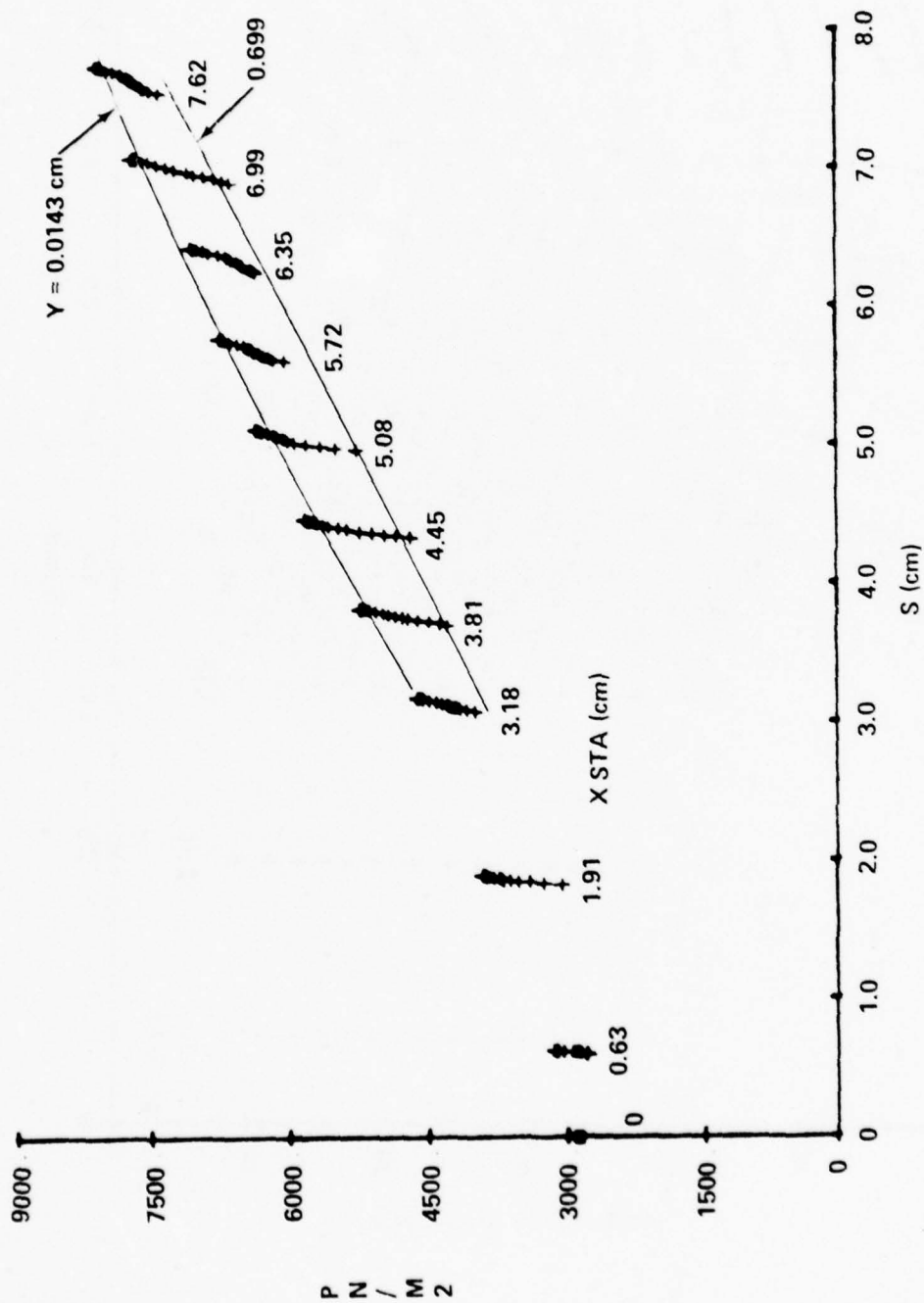


Figure 52. Comparison of Experimental Flowfield to Curve-fitted Flowfield, Ramp 3. Plot of Static Pressure versus Curvilinear Distance S at Selected y's

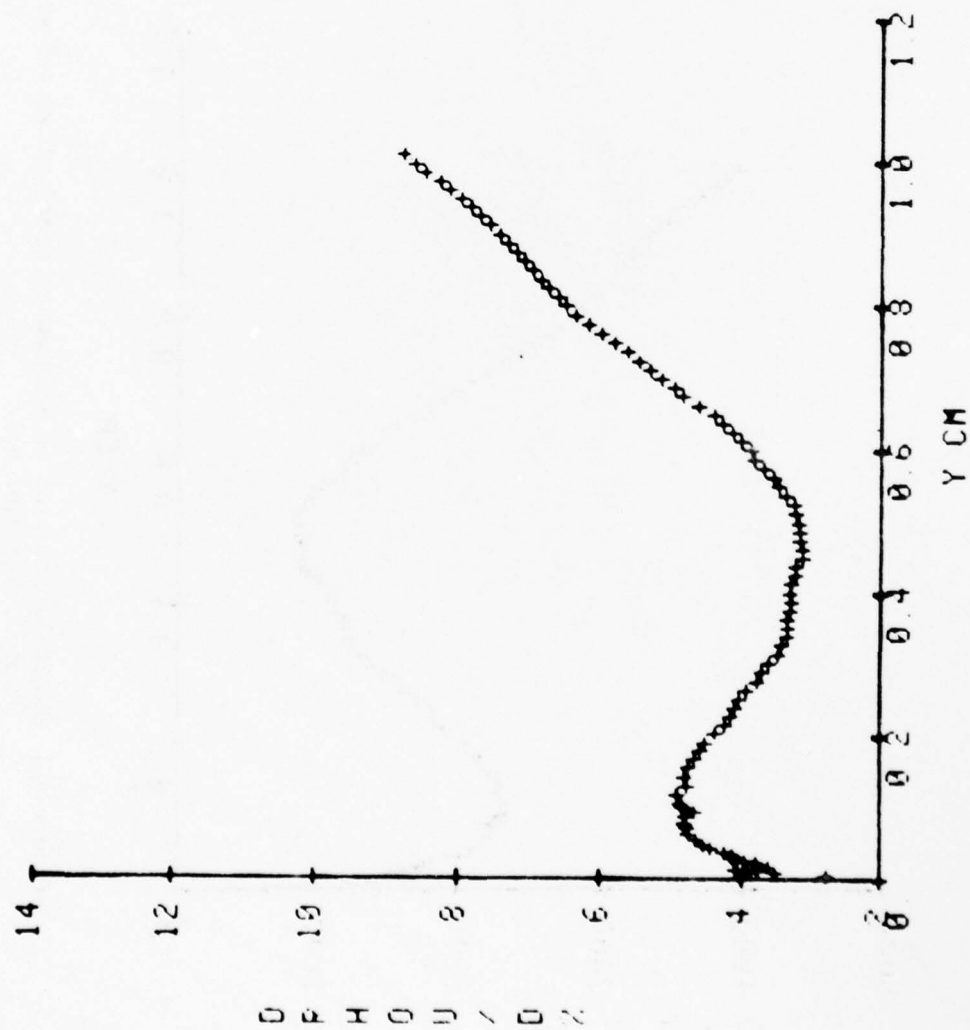


Figure 53. Typical Variation of Streamwise Gradient of u with y ,
(Ramp 3, $x = 7.62$ cm)

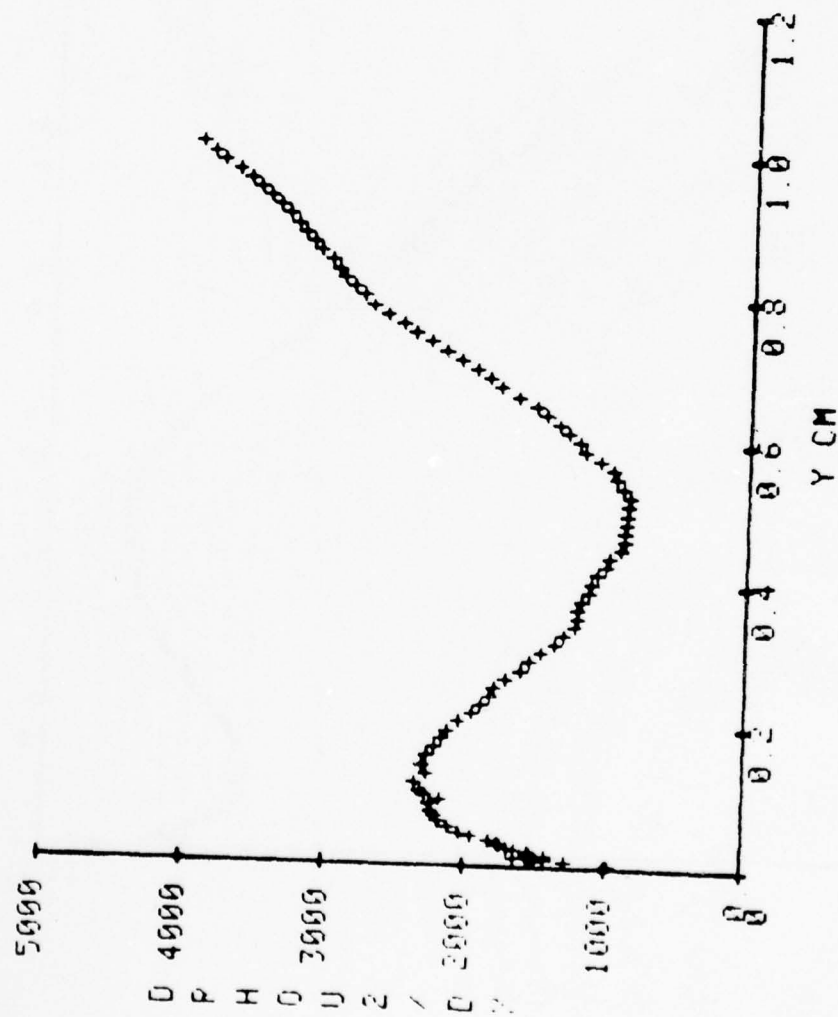


Figure 54. Typical Variation of Streamwise Gradient of pu^2 with y ,
(Ramp 3, $x = 7.62$ cm)

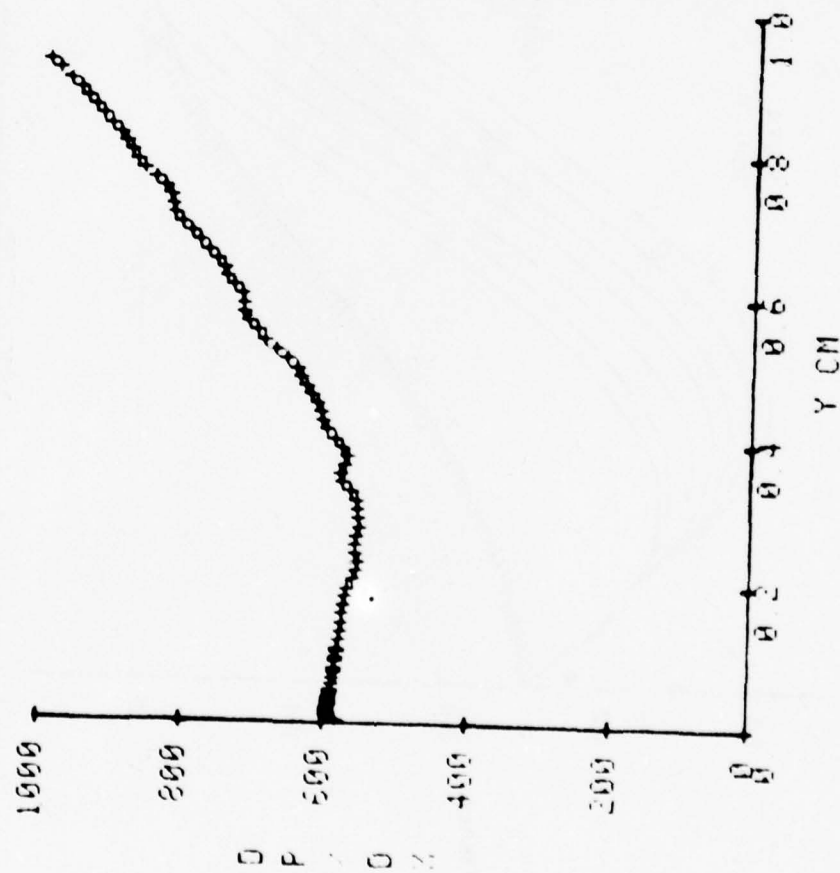


Figure 55. Typical Variation of Streamwise Gradient of p with y ,
(Ramp 3, $x = 7.62$ cm)

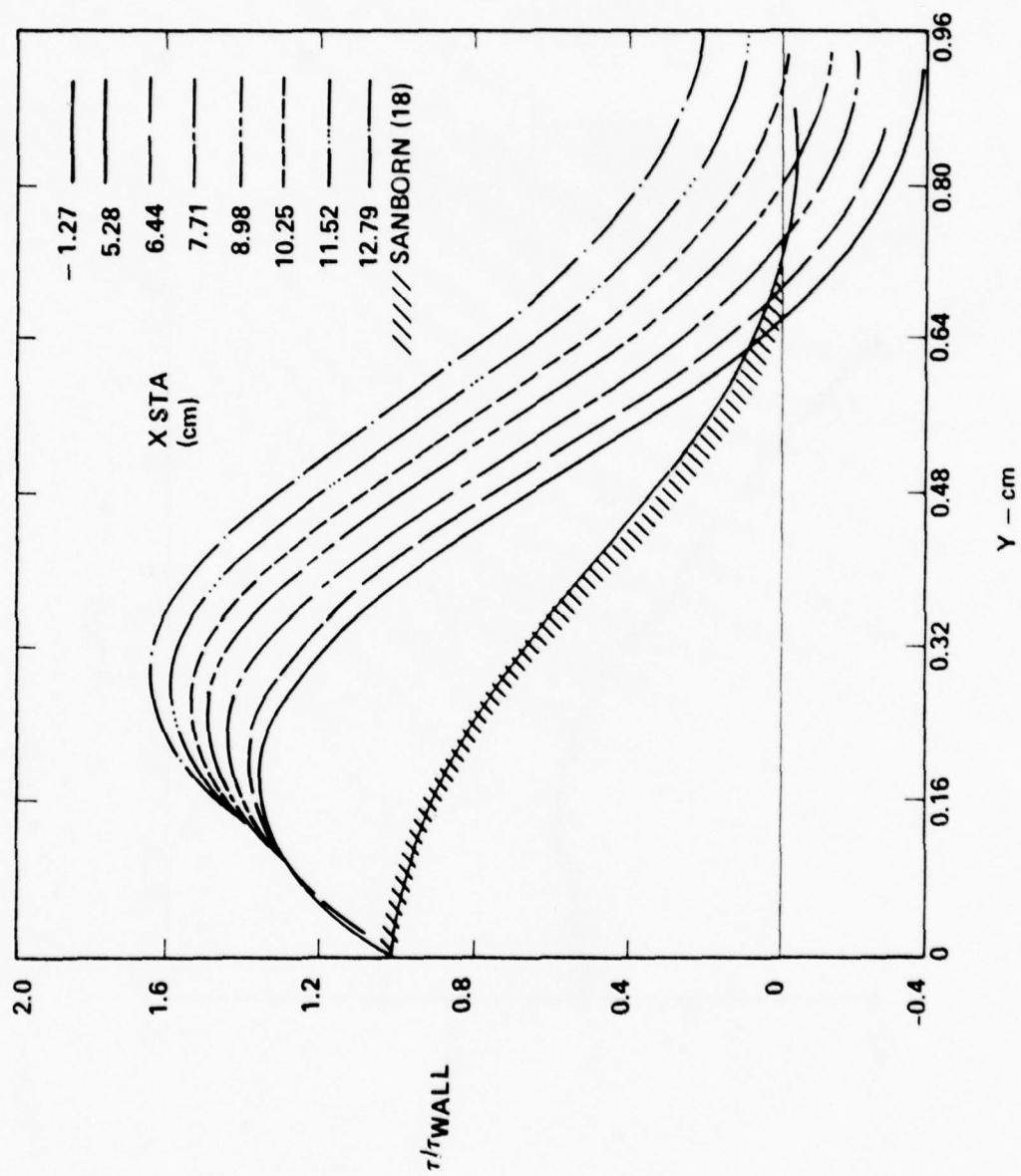


Figure 56. Normalized Turbulent Shear Stress Distributions for Ramp 1

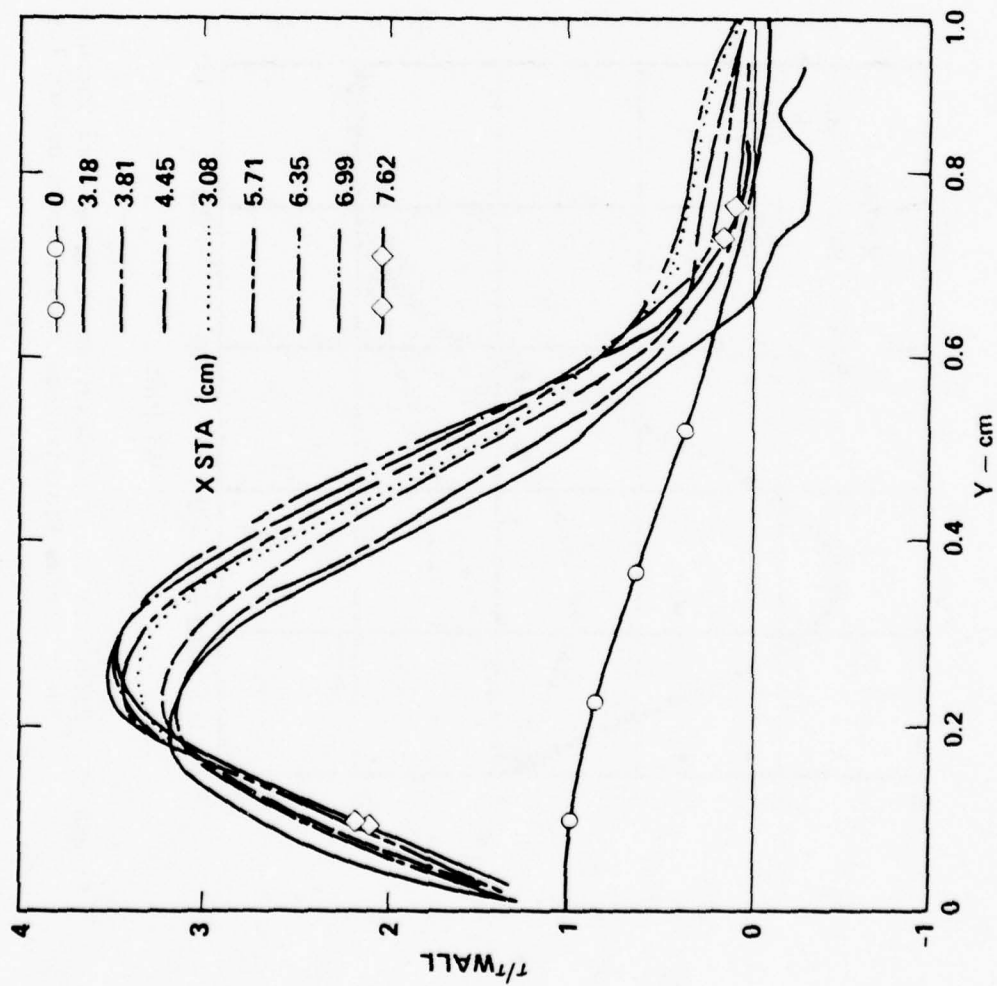


Figure 57. Normalized Turbulent Shear Stress Distributions for Ramp 3

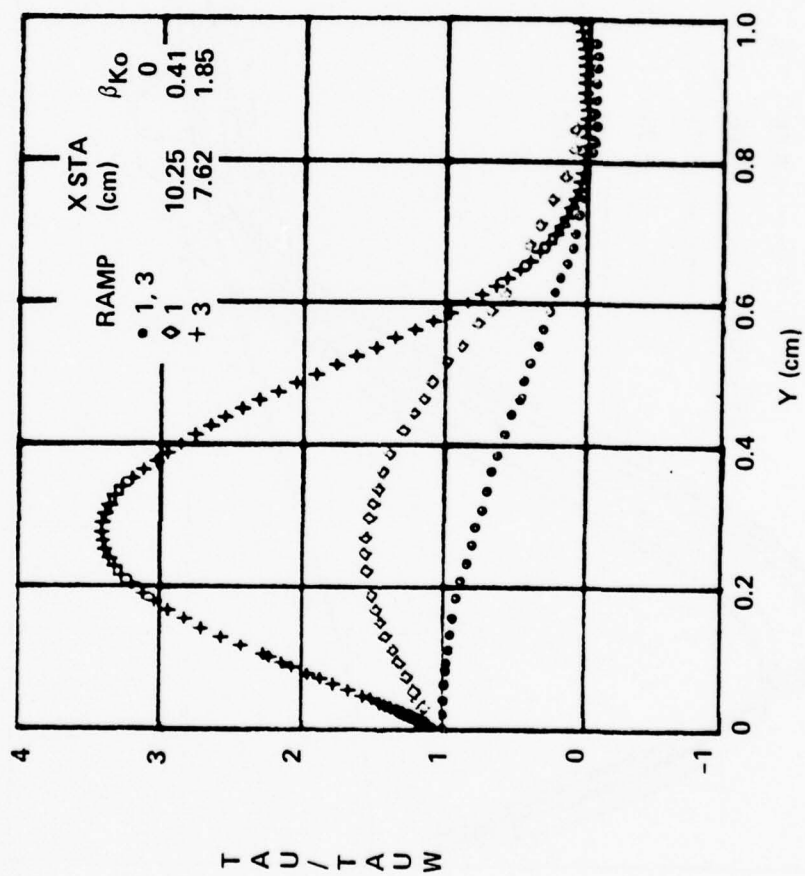


Figure 58. Effect of Pressure Gradient on Normalized Turbulent Shear Stress Distribution Across the Boundary Layer.

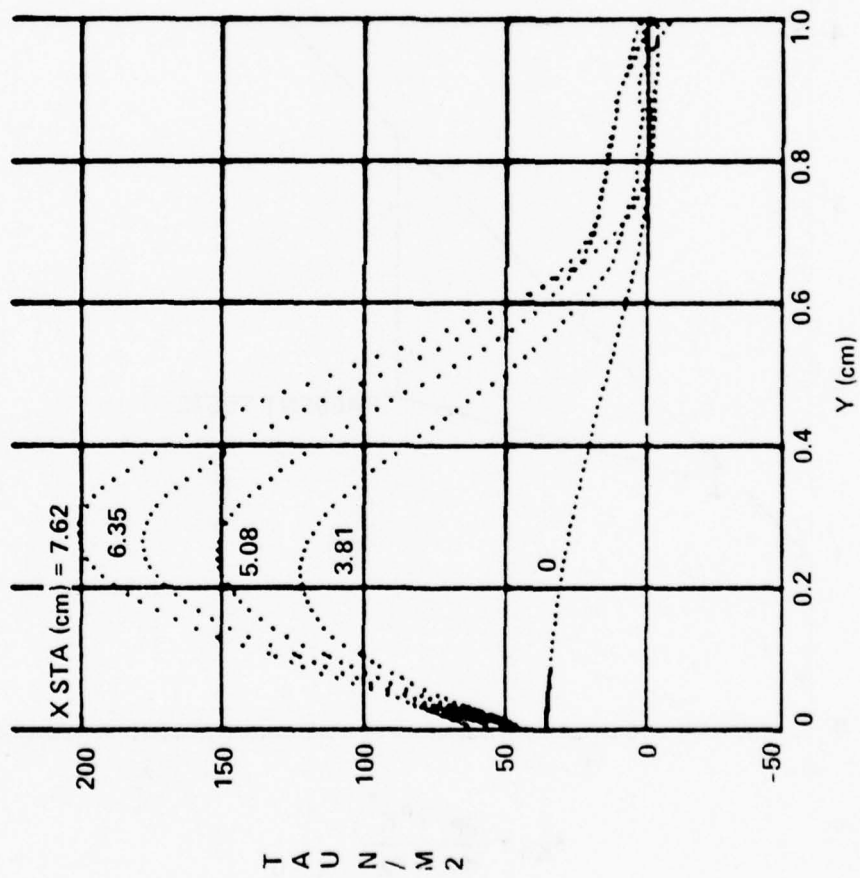


Figure 59. Streamwise Variation of Turbulent Shear Stress τ for Ramp 3

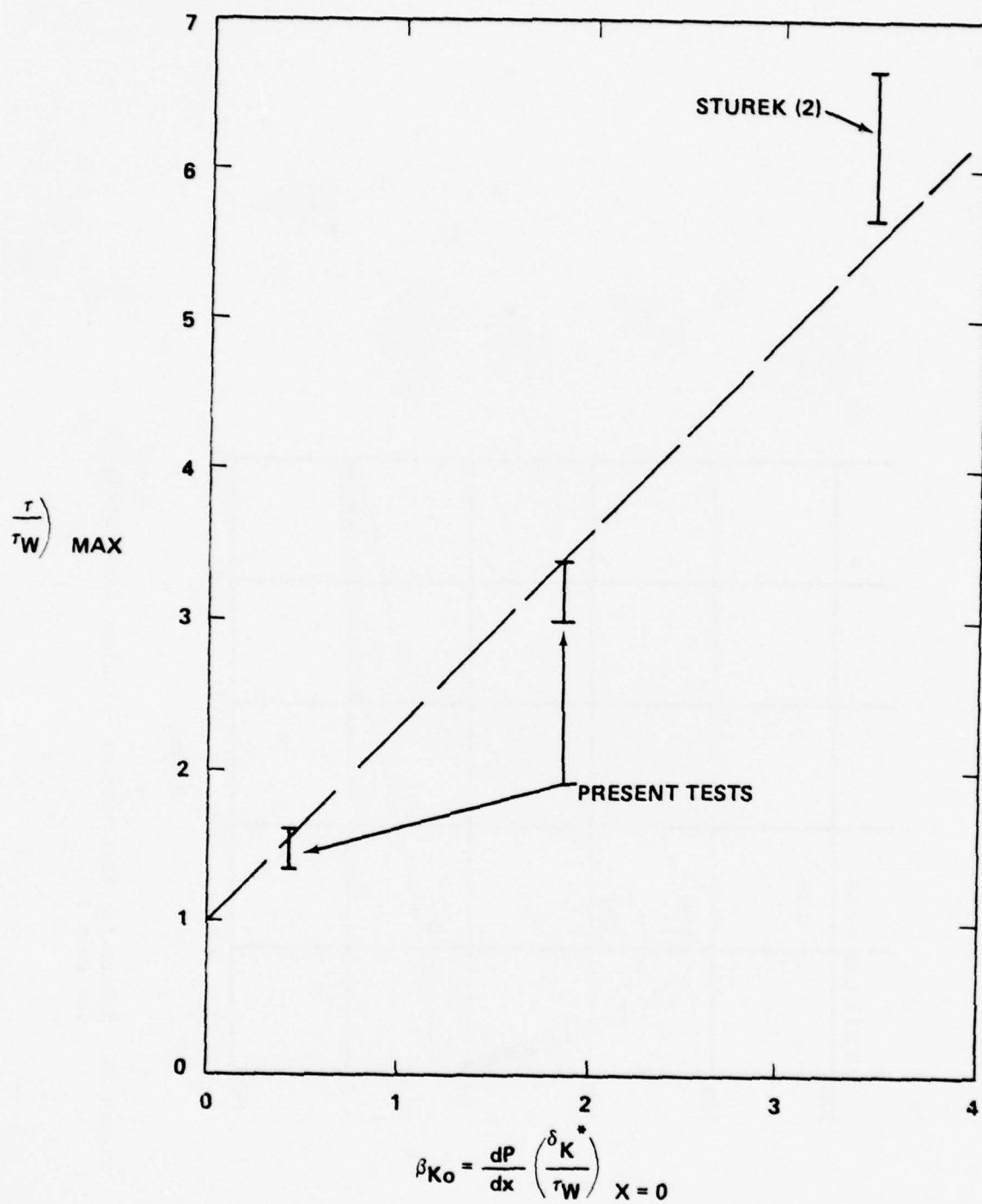


Figure 60. Variation of Peak Shear Stress τ/τ_w with Pressure Gradient Parameter β_{ko}

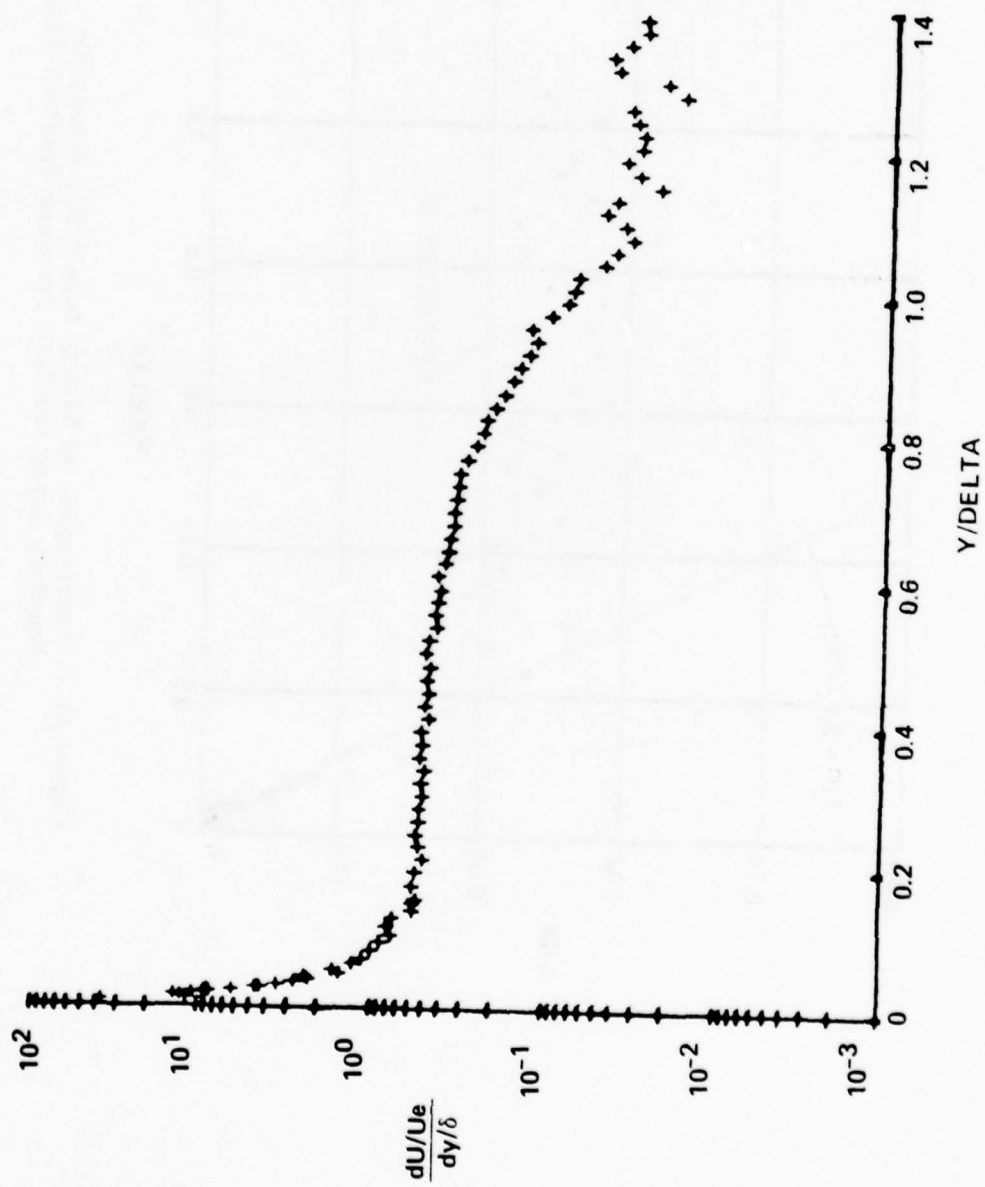


Figure 61. Typical Profile of du/dy versus y

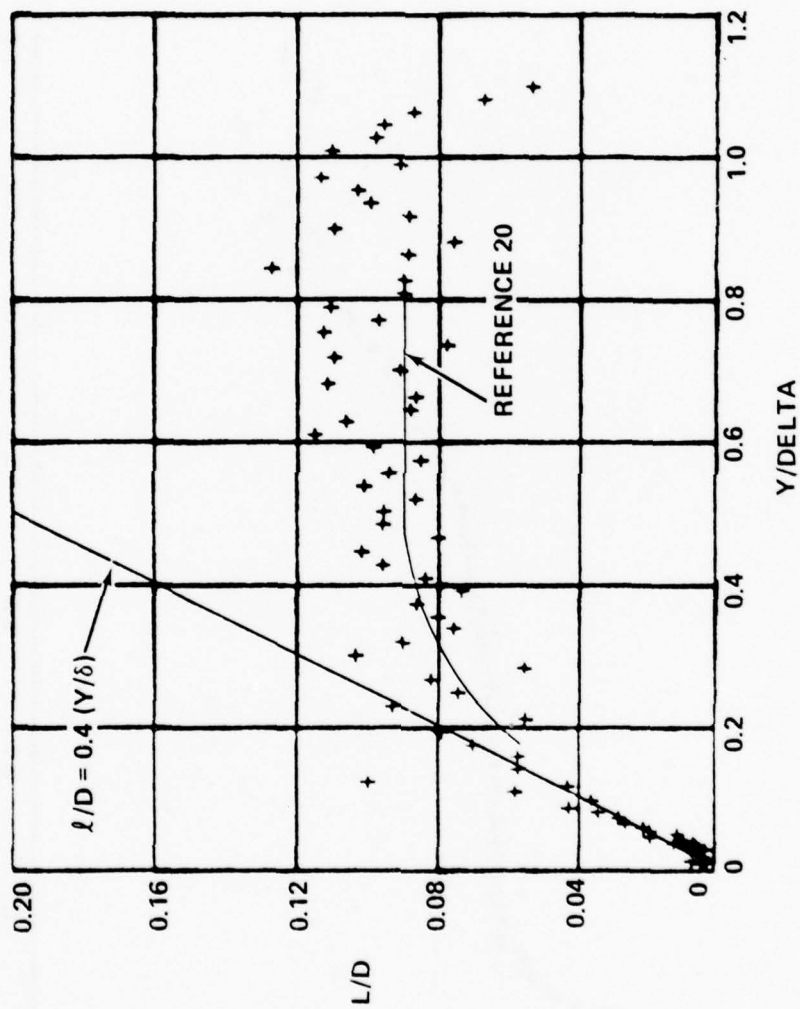


Figure 62. Distribution of Mixing Length l/δ Across the Boundary Layer for Zero Pressure Gradient Flow

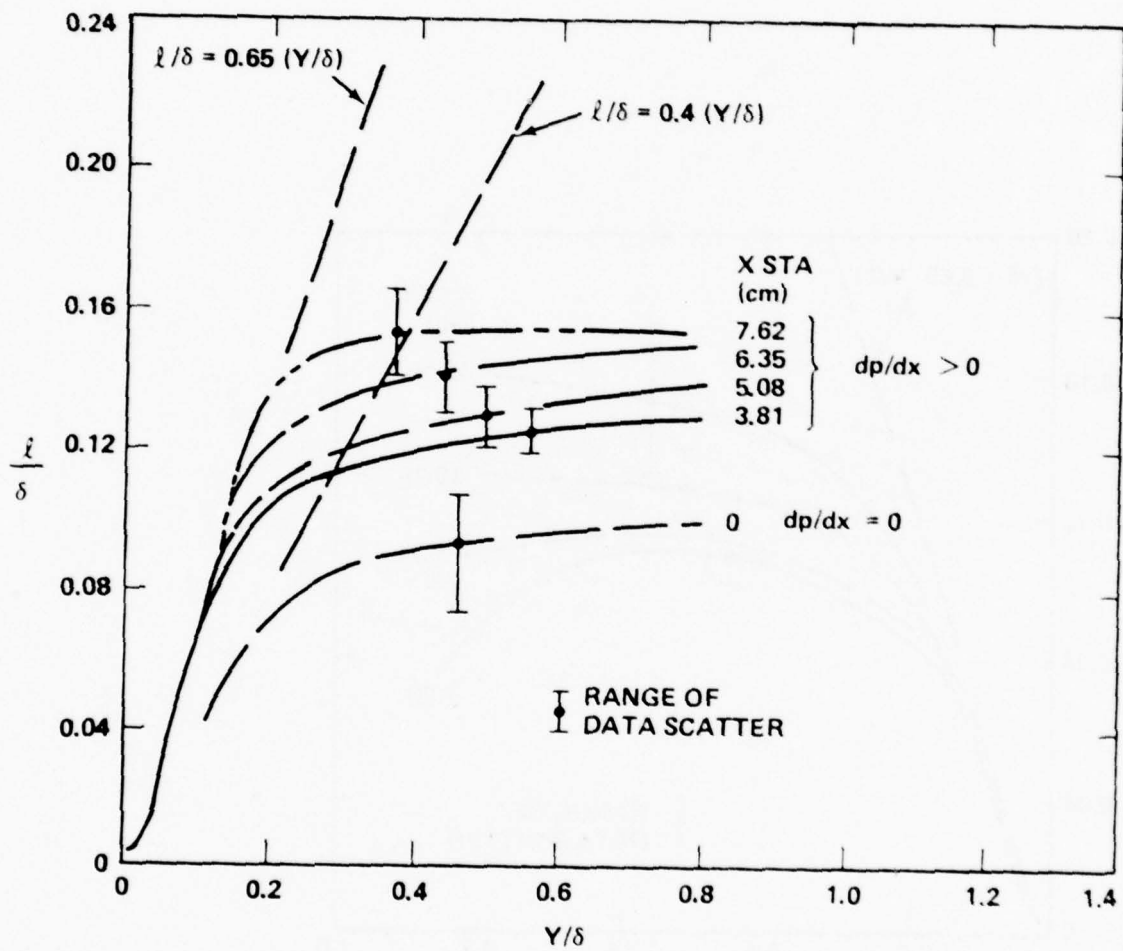


Figure 63. Effect of Adverse Pressure Gradient on Mixing Length, Ramp 3

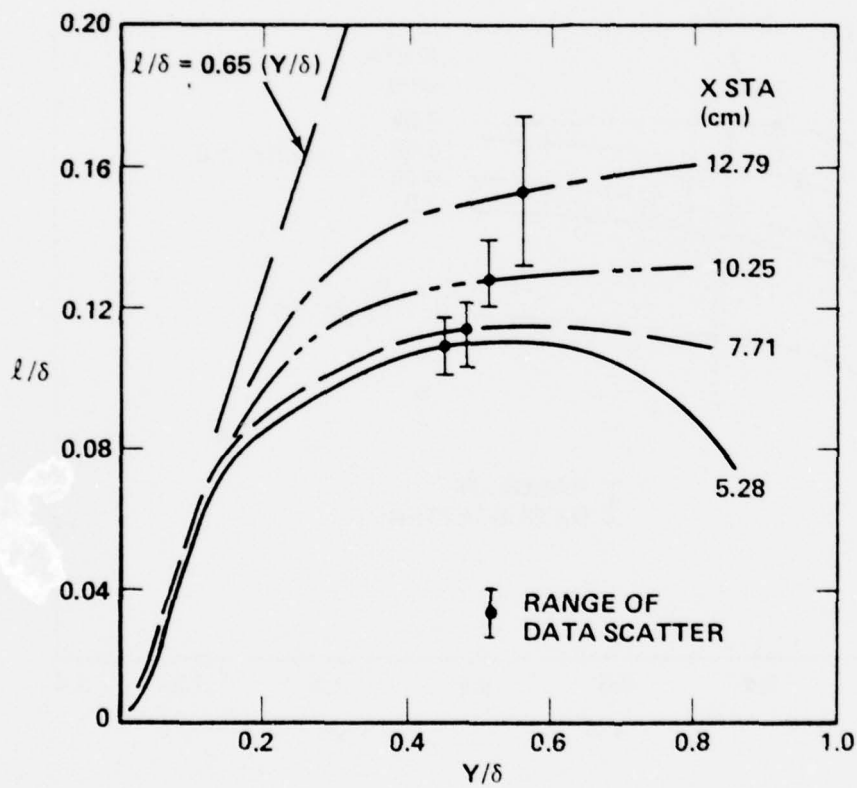


Figure 64. Effect of Adverse Pressure Gradient on Mixing Length, Ramp 1

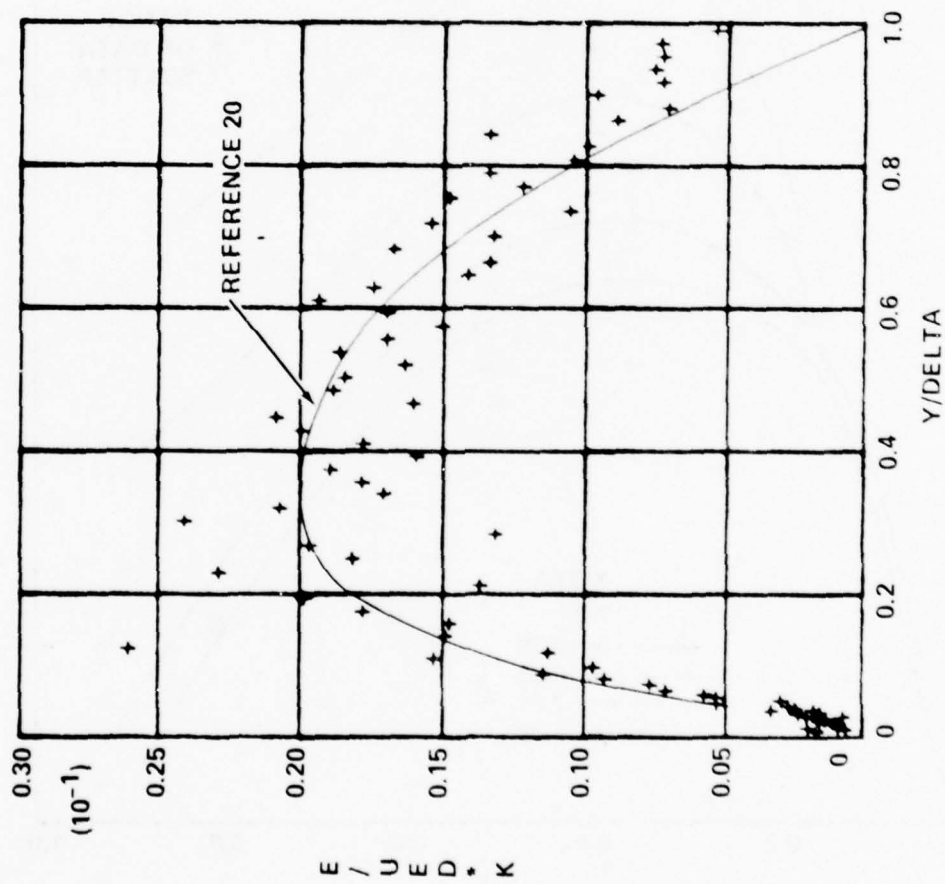


Figure 65. Variation of Normalized Eddy Viscosity with y/δ for Zero Pressure Gradient Flow

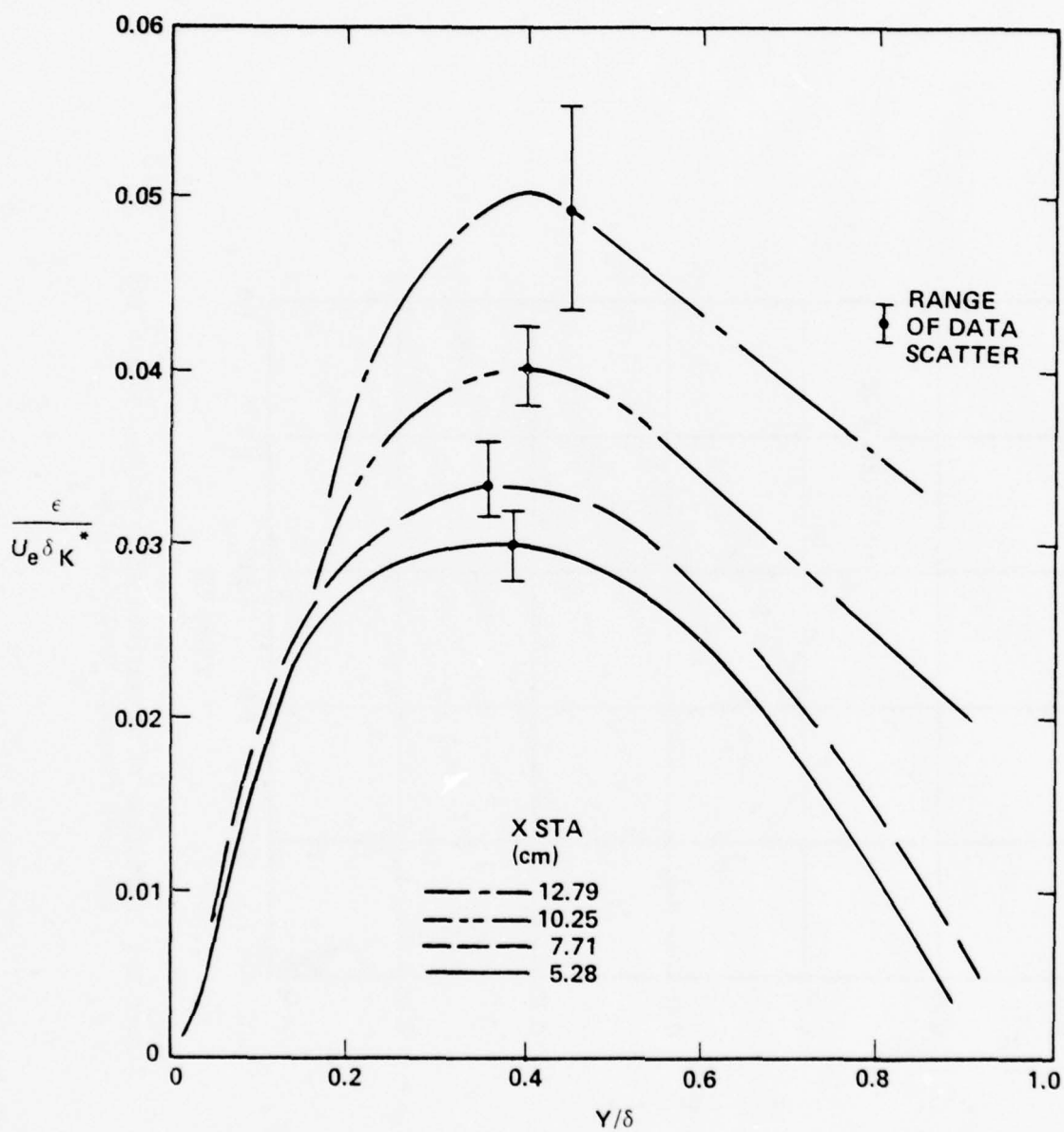


Figure 66. Effect of Adverse Pressure Gradient on Eddy Viscosity, Ramp 1

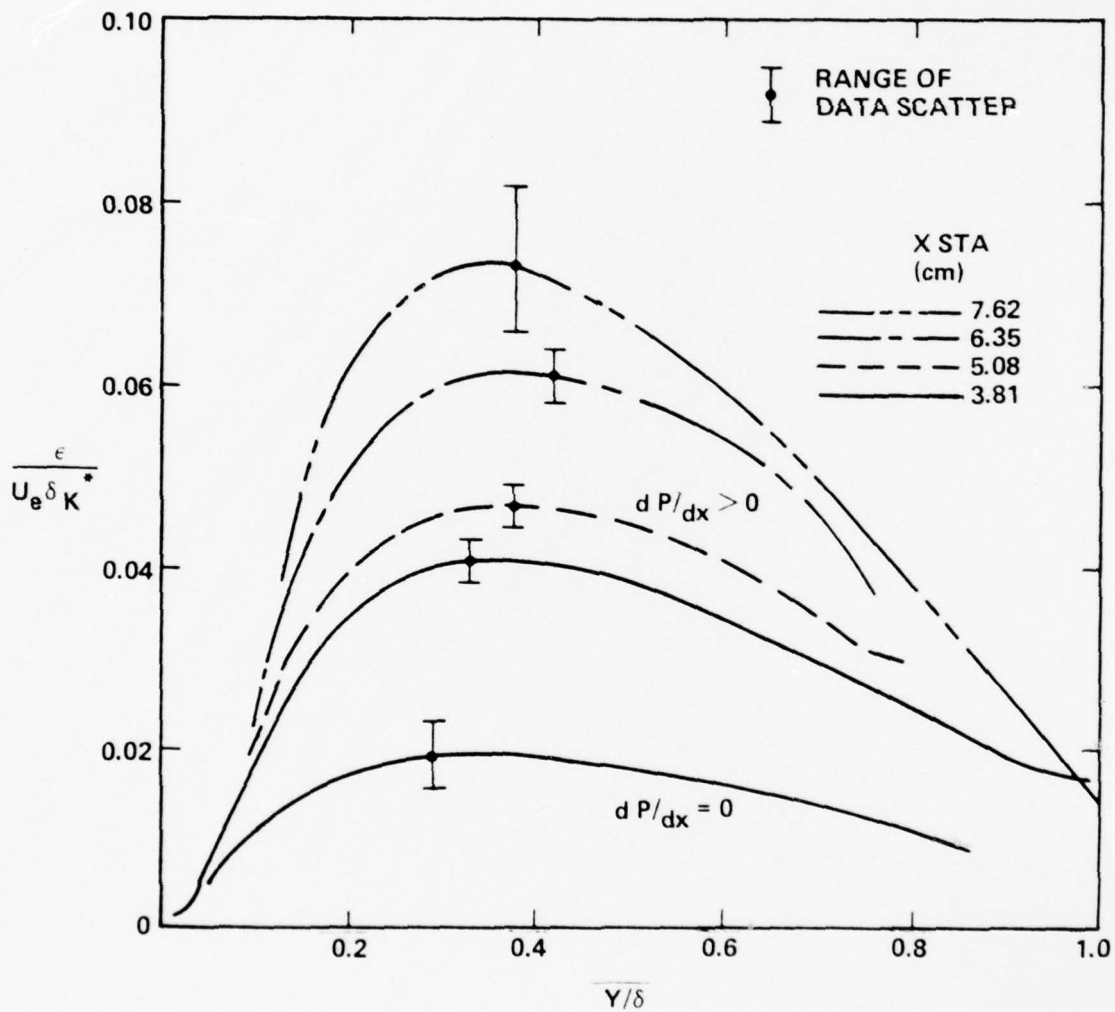


Figure 67. Effect of Adverse Pressure Gradient on Eddy Viscosity, Ramp 3

APPENDIX A
DATA REDUCTION PROGRAMS

This section contains Program Listings for the various computer codes used in the data reduction. Each listing contains REMARK statements providing an explanation of the data inputs required for program execution and in some instances, typical input is illustrated in DATA statements. Figure 14 of the text indicates the sequence in which the programs are used during the overall data reduction process.

PROGRAM BLSURV2

```

10 REM BL-SURVEY-2
11 REM R IS THE RAMP NO, Q1 IS 730 MMHG, Q2 IS 570 DEG R, W IS THE WALL
12 REM TEMP 540 DEG R, S5 IS THE T0 PROBE DIA=.005 IN, AND N4 IS THE
13 REM NUMBER OF X PROFILES. X IS THE PROFILE STA(IN), P0, A0, B0 ARE THE
14 REM P0'S(MMHG) FOR THE PT, PS, TT SURVEYS; C0, D0, T0 ARE THE T0'S FOR
15 REM T0SURVEYS; N1, N2, N3 ARE THE NUMBER OF POINTS IN THE PT, PS, TT SURVEYS
16 REM C1, C2 ARE COEFF IN  $Y(CM) = C1 * Y(MV) + C2$ , C3 IS  $P(MM) / P(MV)$  FOR
17 REM PT SURVEY; C4, C5, C6 ARE SAME FOR PS SURVEY; C7, C8 ARE Y CONVERSION
18 REM FOR TT SURVEY AND C9, D1 ARE FOR  $T(DEG F) = C9 * T(MV) + D1$ . X1(N) AND
19 REM S2(N) ARE X(IN) AND PW/P0(X).
20 FILES F1;F2;F3;F4;F5
21 DIM Y(200), P(200), Z(200), S(200), W(200), T(200)
25 DIM X1(15), S2(15)
30 DIM U(200), P1(200), Q3(200), T1(200)
35 READ X, P0, A0, B0, C0, D0, T0, N1, N2, N3
40 READ R, Q1, Q2, W, S5, N4
45 READ C1, C2, C3, C4, C5, C6, C7, C8, C9, D1
50 FOR N=1 TO N4
55 READ X1(N), S2(N)
60 IF X=X1(N) GO TO 70
65 NEXT N
70 LET S(0)=S2(N)*A0
75 LET Z(0)=0
76 LET T(0)=W
77 LET W(0)=0
80 PRINT "      BOUNDARY LAYER SURVEYS, X(CM) = "X*2.54
85 PRINT
90 PRINT
95 PRINT
100 PRINT TAB(15), "PITOT SURVEY", "STATIC SURVEY", "TEMP SURVEY"
105 PRINT
110 PRINT " P0(MMHG) ", P0, A0, B0
115 PRINT " T0(DEG K) ", (C0+460)/1.8, (D0+460)/1.8, (T0+460)/1.8
120 PRINT " PW(MMHG) ", S2(N)*P0, S2(N)*A0, S2(N)*B0
125 PRINT
130 PRINT
135 PRINT
140 PRINT "      WHAT ARE FILES PTXXXX, PSXXXX, TXXXX, PSTXXXX, PLORXXXX"
145 INPUT F1$, F2$, F3$, F4$, F5$
150 FILE #1, F1$
155 FILE #2, F2$
160 FILE #3, F3$
165 FILE #4, F4$
170 FILE #5, F5$
175 PRINT
180 PRINT
185 PRINT
190 PRINT
195 PRINT

```

```

200 PRINT "
205 PRINT
210 PRINT
215 PRINT
220 PRINT
225 PRINT "      PITOT PRESSURE PROFILE"
230 PRINT
235 PRINT
240 PRINT "Y(MV) ", "PT(MV) ", "Y(CM) ", "PT(MMHG) ", "PT/P0"
245 PRINT
250 FOR L=1 TO N1
255 READ #1, Y(L), P(L)
260 PRINT Y(L), P(L),
265 LET Y(L)=C1*Y(L)+C2
270 LET P(L)=C3*P(L)
275 PRINT Y(L), P(L), P(L)/P0
280 NEXT L
285 PRINT
290 PRINT
295 PRINT
300 PRINT
305 PRINT
310 PRINT "
315 PRINT
320 PRINT
325 PRINT
330 PRINT
335 PRINT "      STATIC PRESSURE PROFILE"
340 PRINT
345 PRINT
350 PRINT "Y(MV) ", "PS(MV) ", "Y(CM) ", "PS(MMHG) ", "PS/P0"
355 PRINT
360 FOR L=1 TO N2
365 READ #2, Z(L), S(L)
370 PRINT Z(L), S(L),
375 LET Z(L)=C4*Z(L)+C5
380 LET S(L)=C6*S(L)
385 PRINT Z(L), S(L), S(L)/A0
390 NEXT L
395 PRINT
400 PRINT
405 PRINT
410 PRINT
415 PRINT
420 PRINT "
425 PRINT
430 PRINT
435 PRINT
440 PRINT
445 PRINT "      RECOVERY TEMPERATURE PROFILE"
450 PRINT
455 PRINT
460 LET T0=T0+460
465 PRINT "Y(MV) ", "TT(MV) ", "Y(CM) ", "TT(DEG K) ", "TT/T0"

```

```

470 FOR L=1 TO N3
475 READ #3,W(L),T(L)
480 PRINT W(L),T(L),
485 LET W(L)=C7*W(L)+C8
490 LET T(L)=(C9*T(L)+D1)+460
495 PRINT W(L),T(L)/1.8,T(L)/T0
500 NEXT L
505 PRINT
510 PRINT
515 PRINT
520 PRINT
525 PRINT
530 PRINT "
535 PRINT
540 PRINT
545 PRINT
550 PRINT
555 PRINT "          SUMMARY OF PROFILE DATA, X="X*2.54
560 PRINT
565 PRINT "Y(CM)", "PT/P0", "PS/P0", "TT/T0"
570 PRINT
575 SCRATCH #4
580 FOR J=1 TO N1
585 FOR K=1 TO N2
590 IF Z(K)>Y(J) GO TO 600
595 NEXT K
600 LET Q3(J)=S(K-1)+(S(K)-S(K-1))*(Y(J)-Z(K-1))/(Z(K)-Z(K-1))
605 FOR L=1 TO N3
610 IF W(L)>Y(J) GO TO 620
615 NEXT L
620 LET T1(J)=T(L-1)+(T(L)-T(L-1))*(Y(J)-W(L-1))/(W(L)-W(L-1))
625 PRINT Y(J),P(J)/P0,Q3(J)/A0,T1(J)/T0
630 WRITE #4,Y(J),P(J)/P0,Q3(J)/A0,T1(J)/T0
635 NEXT J
640 PRINT
645 PRINT
650 PRINT
655 PRINT
660 PRINT
665 PRINT "
670 PRINT
675 PRINT
680 PRINT
685 PRINT
690 PRINT
695 PRINT "          MEAN FLOW PROFILES (TBL-J), RAMP NO"R
700 PRINT
705 PRINT
710 PRINT
715 PRINT
720 PRINT
725 PRINT "          P0,N/M2          ="Q1*133.3
730 PRINT "          T0,DEG K          ="Q2/1.8
735 PRINT "          TW,DEG K          ="W/1.8
740 PRINT "          PS,MMHG          ="S2(N)*Q1

```

```

745 PRINT "                                X,CM                                ="X*2.54
750 PRINT
755 PRINT
760 PRINT
765 PRINT
770 PRINT "Y(CM)", "M", "U(M/SEC)", "RHO(KG/M3)", "RE(M-1)"
775 PRINT TAB(15), "T(DEG K)", "T0(DEG K)", "PS(MMHG)", "RHOU(KG/M2SEC)"
780 PRINT
785 SCRATCH #5
790 FOR N=1 TO N1
795 LET P2=(P(N)+P0)/(Q3(N)+P0)
800 IF P2>1.89286 GO TO 820
805 IF P2<1 GO TO 965
810 LET M1=SQR(5+(((P2)^(1/3.5))-1))
815 GO TO 860
820 LET M1=(.5+P2)^(1/1.6)
825 LET F1=(1.2+M1+M1)^3.5
830 LET F2=(6/(7+M1+M1)-1)^2.5
835 LET P1=F1+F2
840 LET Z1=(P2-P1)/P2
845 IF ABS(Z1)<=.001 GO TO 860
850 LET M1=M1+Z1
855 GO TO 825
860 LET T3=T1(N)+Q2/T0
865 LET F=1+(.2+M1+M1)
870 LET S1=.001623+Q3(N)+F+Q1/(T3+P0)
875 LET S2=49.01+M1+SQR(T3/F)
880 LET S3=.0000000227*(T3^1.5)/(T3+199)
885 LET S4=S1+S2+S3/(12+S3)
890 LET S6=.915094+.0004799+SQR(S4)-.0000230237+S4
895 LET S6=(S6+(1-(1/F)))+(1/F)
900 LET T4=(T1(N)+Q2)/(T0+S6)
905 IF ABS(T3-T4)<=.5 GO TO 920
910 LET T3=T4
915 GO TO 865
920 LET P1(N)=S1+S2+.16.04
925 LET T5=T4/F
930 LET U(N)=M1+49.01+SQR(T5)+.3048
935 LET V1=.0000000227*(T5^1.5)/(T5+199)
940 LET S7=((P1(N)+U(N))/(12+V1+157.426))+100/2.54
945 PRINT Y(N), M1, U(N), P1(N), S7
950 PRINT TAB(15), T5/1.8, T4/1.8, Q3(N)+Q1/P0, U(N)+P1(N)
955 PRINT
960 WRITE #5, Y(N), U(N), P1(N), U(N)+P1(N), T4/1.8
965 NEXT N
970 PRINT
975 PRINT
980 STOP
1000 DATA 3.25,730,730.5,730.5,110,109,110,146,132,123
1010 DATA 3,730,570,540,.005,15
1020 DATA .00020718,1.026531,.09697,.00020718,1.09449,.04113,.00020718
1030 DATA 1.027314,.44218,32.782
1040 DATA -1.25,.02986,-.75,.03071,-.25,.02975,0,.02986,.25,.03212
1050 DATA .75,.04,1.25,.04732,1.5,.05361,1.75,.05955,2,.06504
1060 DATA 2.25,.06899,2.5,.07207,2.75,.07882,3,.08277,3.25,.09206
9999 END

```


PROGRAM NEWFLOW

```

10 REM NEWFLOW
11 REM Q1 IS THE NUMBER OF THE FIRST X STATION
12 REM Q2 IS THE NUMBER OF THE LAST X STATION MINUS ONE
13 REM B IS THE RAMP NUMBER
14 REM X(N) IS THE LOCATION OF THE X STATION (INCHES)
15 REM D(N) IS THE HEIGHT OF THE RAMP (CM) AT X
16 REM A(N) IS THE SLOPE OF THE RAMP (RAD) AT X
17 REM ENTER Q1,Q2,B AT LINE 1000
18 REM ENTER 1ST 5 INPUT FILES AT 202
19 REM ENTER REMAINING INPUT FILES AT 204
20 REM A TOTAL OF 10 FILE NAMES,REAL OR FICTICIOUS,MUST BE INPUT
100 FILES F1:F2:F3
110 DIM Y1(118),U1(118),R1(118),P1(118),T1(118)
120 DIM Y2(118),U2(118),R2(118),P2(118),T2(118)
125 DIM A(15),D(15),X(15)
130 READ Q1,Q2,B
132 FOR N=1 TO Q2+1
140 READ X(N),D(N),A(N)
142 NEXT N
150 PRINT "                INTERPOLATED RAMP FLOW FIELD"
160 PRINT "                RAMP NO" B
170 PRINT
180 PRINT
190 PRINT
200 PRINT "        WHAT ARE PROFILE INPUT FILES"
202 INPUT F1$,F2$,F3$,F4$,F5$
204 INPUT F6$,F7$,F8$,F9$,F0$
212 PRINT
214 PRINT
216 PRINT
218 SCRATCH #3
220 FOR Q=Q1 TO Q2
222 ON Q GO TO 270,224,230,236,242,248,254,260,266
224 LET F1$=F2$
226 LET F2$=F3$
228 GO TO 270
230 LET F1$=F3$
232 LET F2$=F4$
234 GO TO 270
236 LET F1$=F4$
238 LET F2$=F5$
240 GO TO 270
242 LET F1$=F5$
244 LET F2$=F6$
246 GO TO 270
248 LET F1$=F6$
250 LET F2$=F7$
252 GO TO 270
254 LET F1$=F7$
256 LET F2$=F8$

```

```

258 GO TO 270
260 LET F1$=F8$
262 LET F2$=F9$
264 GO TO 270
266 LET F1$=F9$
268 LET F2$=F0$
270 FILE #1,F1$
280 FILE #2,F2$
372 PRINT "      X(CM)="X(Q+1)*2.54
374 PRINT
376 PRINT
378 PRINT "Y(CM)", "U(M/SEC)", "PHI(KG/M3)", "P(MMHG)", "T0(DEG K)"
382 PRINT
384 FOR N=1 TO 118
390 READ #1,Y1(N),U1(N),P1(N),P1(N),T1(N)
400 READ #2,Y2(N),U2(N),R2(N),P2(N),T2(N)
410 NEXT N
412 LET Y1(0)=0
414 LET Y2(0)=0
420 FOR N=1 TO 100
430 LET Y=Y2(N)*COS(A(Q+1))
435 LET S=(X(Q+1)-X(Q))*2.54-Y*SIN(A(Q+1))
437 LET S1=(X(Q+1)-X(Q))*2.54
440 LET Z=Y*COS(A(Q+1))+D(Q+1)
470 LET M=N
480 FOR L=1 TO 100
490 IF Y1(L)*COS(A(Q))=>Y GO TO 510
500 NEXT L
510 LET Z1=Y2(M)+D(Q+1)
520 LET Z2=Y2(M-1)+D(Q+1)
530 LET Z3=Y1(L)+D(Q)
540 LET Z4=Y1(L-1)+D(Q)
550 LET Z5=Z3+(Z1-Z3)*S/S1
552 LET Z6=Z4+(Z2-Z4)*S/S1
554 IF Z6>Z GO TO 560
556 IF Z5<Z GO TO 564
558 GO TO 570
560 LET L=L-1
562 GO TO 530
564 LET L=L+1
566 GO TO 530
570 LET V1=U1(L-1)+(U2(M-1)-U1(L-1))*S/S1
580 LET V2=U1(L)+(U2(M)-U1(L))*S/S1
590 LET U=V1+(V2-V1)*(Z-Z6)/(Z5-Z6)
600 LET V1=P1(L-1)+(P2(M-1)-P1(L-1))*S/S1
610 LET V2=P1(L)+(P2(M)-P1(L))*S/S1
620 LET R=V1+(V2-V1)*(Z-Z6)/(Z5-Z6)
630 LET V1=P1(L-1)+(P2(M-1)-P1(L-1))*S/S1
640 LET V2=P1(L)+(P2(M)-P1(L))*S/S1
650 LET P=V1+(V2-V1)*(Z-Z6)/(Z5-Z6)
660 LET V1=T1(L-1)+(T2(M-1)-T1(L-1))*S/S1
670 LET V2=T1(L)+(T2(M)-T1(L))*S/S1

```

```

680 LET T=V1+(Y2-Y1)♦(Z-Z6)/(Z5-Z6)
690 PRINT Y,U,R,P,T
700 WRITE #3,Y,U,R,P,T
705 NEXT N
710 PRINT
720 PRINT
730 PRINT
740 NEXT Q
750 STOP
1000 DATA 1,1,1
1010 DATA 1.077,.07601,.044472,1.577,.14171,.058744
1020 DATA 2.077,.22501,.07211,2.535,.31587,.083673
1030 DATA 3.035,.43013,.095679,3.535,.55943,.10717
1040 DATA 4.035,.70324,.11828,4.535,.86118,.12915
1050 DATA 5.035,1.03308,.1399,5.535,1.21889,.15066
9999 END

```

READY

♦

PROGRAM VCOLES

```

10 REM VCOLES
11 REM F1$ IS NFLOXXX( FROM NEWFLOW), F2$ IS VDEXXX, F3$ IS VCOXXXX, X IS
12 REM X STA(IN), P IS PW(MMHG), T IS WALL TEMP=540 DEG R, D IS FIRST
13 REM GUESS FOR DELTA(CM), C7 IS FIRST GUESS FOR TAUW(PSE), N1 IS 1ST
14 REM GUESS FOR NO OF Y POINT WHERE Y+ =50, N2 IS FIRST GUESS FOR
15 REM NO OF Y POINT WHERE Y/DELTA=.9, N3 IS NO OF POINTS IN NFLOXXXX,
16 REM S1 AND B1 ARE CONVERGENCE CRITERIA FOR TAUW AND DELTA.
100 FILES F1:F2:F3
110 DIM U(200),Y(200),Z(1000),R1(200),Q1(200),T0(200)
115 DIM G(100),B(100)
116 DIM U3(200)
117 DIM U5(100),U6(100)
120 READ F1$,F2$,F3$,X,P,T,D,C7,N1,N2,N3
122 READ S1,B1
123 LET K8=N2+1
124 LET K9=N1
130 PRINT "          CORRELATION OF VELOCITY PROFILE, X STA ="X*2.54
132 PRINT "          COLES V/D GENERALIZED CORRELATION"
140 PRINT
150 PRINT
152 LET R2 =.00162*P/T
165 LET D7=0
170 FILE #1,F1$
175 FILE #2,F2$
180 FILE #3,F3$
181 LET U(0)=0
182 FOR N=1 TO N3
184 READ #1,Y(N),U(N),R1(N),Q1(N),T0(N)
186 LET Y(N)=Y(N)/2.54
188 LET U(N)=U(N)*3.2808
189 LET R1(N)=R1(N)/516.488
190 LET Q8=(SQR(R1(N)/R2))*U(N)-U(N-1)
192 LET D7=D7+Q8
193 LET U3(N)=D7
195 NEXT N
200 PRINT
210 PRINT
250 LET V=.0000000227*(T^1.5)/((T+199)*R2)
281 LET H=1
282 LET B(H)=D/2.54
285 LET V5=0
286 LET V6=0
290 LET M=1
300 LET S=C7
310 LET F=SQR(S/R2)
320 GOSUB 700
350 LET M=M+1
360 LET S=S+S1*S
370 LET F=SQR(S/R2)
380 GOSUB 700
400 IF Z(M)>Z(M-1) GO TO 420

```

```

410 GO TO 350
420 LET M=M+1
430 LET S=S-S1+S
440 LET F=SQR(S/R2)
450 GOSUB 700
470 IF Z(M)>Z(M-1) GO TO 500
480 GO TO 420
490 PRINT "Y", "Y/D", "Y+", "U+CALC", "U+MEAS"
491 PRINT TAB(15); "W"
495 PRINT
500 LET S=S+S1+S
505 LET F=SQR(S/R2)
508 SCRATCH #3
510 GOSUB 700
512 IF V5=0 GO TO 560
514 PRINT
516 PRINT
520 PRINT
522 PRINT "      M      ="M
524 PRINT "      H      ="H
525 PRINT "      DEL,CM    ="B(H)*2.54
530 PRINT "      TAUW,PSF     ="S
535 PRINT "      UTAU,M/S     ="F*.3048
536 PRINT "      U(D),M/S     ="U9/3.2808
540 PRINT "      PI           ="(1/4.86)*((U4/F)-2.43*LOG(R3)-5)
550 PRINT "      RMS          ="Z(M)
551 LET N2=N1-1
552 LET N1=1
553 PRINT
554 PRINT
555 PRINT
556 GOSUB 700
557 GO TO 600
560 LET G(H)=Z(M)
562 IF H=>2 GO TO 570
564 LET H=H+1
566 LET B(H)=B(H-1)+B1*B(H-1)
568 GO TO 285
570 IF G(H)>G(H-1) GO TO 576
572 IF B(H)>B(H-1) GO TO 586
574 GO TO 580
576 IF H=2 GO TO 580
578 GO TO 592
580 LET H=H+1
582 LET B(H)=B(H-1)-B1*B(H-1)
584 GO TO 285
586 LET H=H+1
588 LET B(H)=B(H-1)+B1*B(H-1)
590 GO TO 285
592 LET B(H)=B(H-1)
593 LET V5=1

```



```

594 GO TO 490
600 LET N1=K8
610 LET N2=N3
611 PRINT
612 LET V6=1
620 GOSUB 700
624 LET A2=U5(N)
626 LET U7=U6(N)
630 FOR N=1 TO N3
632 LET D4=D4+(1-((U(N)+U(N+1))*0.5/U9))*((Y(N)-Y(N-1))*2.54
634 LET D5=A2-((U5(N)+U5(N-1))*0.5)
636 LET D6=D6+D5*((Y(N)-Y(N-1))*2.54
638 LET D8=D8+D5*D5*((Y(N)-Y(N-1))*2.54
640 IF B(H)<=Y(N) GO TO 644
642 NEXT N
644 PRINT
646 PRINT
647 PRINT
648 PRINT "      INTERGAL PROPERTIES OF BOUNDARY LAYER"
649 PRINT
650 PRINT "      DELTA STAR K (CM)=""D4
652 PRINT "      DEL      (CM)=""D6
654 PRINT "      G      ""D8/D6
656 PRINT
658 PRINT
660 PRINT
661 SCRATCH #2
662 PRINT "      VELOCITY DEFICIT CORRELATION"
664 PRINT
666 PRINT "Y/DEL","U*DEF CAL","U*DEF MEAS"
668 PRINT
670 FOR N=1 TO N3
672 IF B(H)<=Y(N) GO TO 676
674 PRINT Y(N)*2.54/D6,U7-U6(N),A2-U5(N)
675 WRITE #2,Y(N)*2.54/D6,U7-U6(N),A2-U5(N)
676 NEXT N
678 STOP
700 LET T8=0
705 FOR N=1 TO N3
710 IF B(H)>Y(N) GO TO 740
720 LET U4=U3(N-1)+(U3(N)-U3(N-1))*((B(H)-Y(N-1))/(Y(N)-Y(N-1)))
722 LET U9=U(N-1)+(U(N)-U(N-1))*((B(H)-Y(N-1))/(Y(N)-Y(N-1)))
730 GO TO 750
740 NEXT N
750 LET A3=B(H)*F/(12*Y)
760 FOR N=N1 TO N2
770 LET W=2*((SIN((1.5707*Y(N))/(B(H))))^2)
780 LET L=.5*((U4/F)-(2.43*LOG(A3))-5)
790 LET L1=2.43*LOG(Y(N)*F/(12*Y))
800 LET U1=L1+5+L*W
810 LET U2=U3(N)/F
851 LET W1=(U2-L1-5)/L

```

```

852 LET U5(N)=U2
853 LET U6(N)=U1
860 LET T8=(U1-U2)^2+T8
870 IF V5=0 GO TO 893
872 IF B(H)<=Y(N) GO TO 910
880 PRINT Y(N)*2.54,Y(N)/B(H),Y(N)*F/(12*V),U1,U2
881 IF V6=1 GO TO 885
882 IF N1=1 GO TO 885
883 PRINT TAB(15);W1
884 PRINT
885 IF N=>K9 GO TO 892
886 LET W1=3
887 IF (Y(N)*F/(12*V))>= 10 GO TO 892
888 LET U1=(Y(N)*F/(12*V))
892 WRITE #3,Y(N)*F/(12*V),U1,U2,Y(N)/B(H),W1
893 NEXT N
900 LET Z(M)=SQR(T8)
910 RETURN
1000 DATA "3MFL-125","3VDE-125","3VCO-125"
1010 DATA -1.25,21.8,540,.68,.75,24,69,100,.01,.01
9999 END

```

READY

PROGRAM TBLJNDIM

```

010 REM TBLJNDIM
11 REM P9 IS RAMP NO,Z IS NO OF X STA, X(L) IS XSTA(IN),D(L) IS
12 REM DELTA(CM)FROM YCOLES, P5(L) IS PWALL (PW/P0)
100 FILES F1:F2
110 DIM Y(100),U(100),R(100),P(100),T0(100)
120 DIM R1(2),U1(2)
130 DIM X(11),D(11),P5(11)
140 READ P9,Z
150 FOR L=1 TO 11
160 READ X(L),D(L),P5(L)
170 LET P5(L)=P5(L)*97309
180 NEXT L
190 PRINT "
200 PRINT "
210 PRINT "
220 PRINT "
230 PRINT "
240 PRINT "
250 PRINT "
260 INPUT F1$,F2$
262 PRINT "
264 PRINT "
266 PRINT "
270 FILE #1,F1$
280 FILE #2,F2$
290 SCRATCH #2
300 FOR L=1 TO Z
310 FOR M=1 TO 100
320 IF L=Z GO TO 350
330 READ #1,Q1,Q2,Q3,Q4,Q5
340 GO TO 360
350 READ #1,Y(M),U(M),R(M),P(M),T0(M)
352 LET P(M)=P(M)*133.3
360 NEXT M
370 NEXT L
400 PRINT "
410 PRINT "
420 LET R(0)=.00349*P5(Z)/300
430 LET M4=SQR(5*((97309/P5(Z))^(.2857)-1))
440 LET T4=317/(1+.2*M4*M4)
450 LET P4=.00349*P5(Z)/T4
460 LET U4=M4*20.04*SQR(T4)
470 LET R1(1)=P4
480 LET U1(1)=U4
490 FOR N=1 TO 100
500 IF Y(N)>D(Z) GO TO 520
510 NEXT N
520 LET U2=U(N-1)+(U(N)-U(N-1))*((D(Z)-Y(N-1))/(Y(N)-Y(N-1)))
530 LET U2=U2/.995
540 FOR N=1 TO 100
550 IF U(N)>U2 GO TO 570
560 NEXT N

```

MEAN FLOW PROFILES"

RAMP NO="P9

X STATION,CM="X(Z)*2.54

WHAT ARE FILES NEWFLOWX,MEANXXXX":

```

570 LET Y2=Y(N-1)+(Y(N)-Y(N-1))*((U2-U(N-1))/(U(N)-U(N-1)))
580 LET Y3=(Y2-Y(N-1))/(Y(N)-Y(N-1))
590 LET R2=R(N-1)+(R(N)-R(N-1))*Y3
600 LET P2=P(N-1)+(P(N)-P(N-1))*Y3
610 LET T3=T0(N-1)+(T0(N)-T0(N-1))*Y3
620 LET A3=20.04*SQR(T3)
630 LET T2=T3*(1-.2*(U2*U2/(A3*A3)))
640 LET M2=SQR(5*((T3/T2)-1))
650 LET V2=.0000010869*((T2*1.8)^1.5)/((T2*1.8)+199)
652 LET S2=U2*R2/V2
654 PRINT "      YE,CM      ="Y2
656 PRINT "      T0E,DEG K      ="T3
658 PRINT "      TE,DEG K      ="T2
660 PRINT "      PE,M/M2      ="P2
662 PRINT "      UE,M/S      ="U2
664 PRINT "      RHOE,KG/M3      ="R2
666 PRINT "      REE,M-1      ="S2
668 PRINT "      ME      ="M2
670 PRINT
671 PRINT
672 PRINT
673 PRINT "Y","Y/D","M","U/UE","RHO/RHOE"
674 PRINT "RE/REE","T/TE","T0/T0E","P/PE","H"
675 PRINT
676 PRINT
677 PRINT
678 FOR N=1 TO 100
680 LET A=20.04*SQR(T0(N))
690 LET T=T0(N)*(1-.2*U(N)*U(N)/(A*A))
700 LET M=SQR(5*((T0(N)/T)-1))
710 LET V=.0000010869*((T*1.8)^1.5)/((T*1.8)+199)
720 LET S=R(N)*U(N)/V
730 LET H=(T0(N)-300)/(T3-300)
740 PRINT Y(N),Y(N)/D(Z),M,U(N)/U2,R(N)/R2
750 PRINT S/S2,T/T2,T0(N)/T3,P(N)/P2,H
760 PRINT
770 WRITE #2,Y(N)/D(Z),M,U(N)/U2,R(N)/R2,H
780 IF Y(N)>Y2 GO TO 930
790 LET W=Y(N)-Y(N-1)
800 LET M1=SQR(5*((97309/P(N))^1.2857)-1))
810 LET T1=317/(1+.2*M1*M1)
820 LET R1(2)=.00349*(P(N)/T1)
830 LET U1(2)=M1*20.04*SQR(T1)
840 LET C1=C1+((U1(2)+U1(1))/2-(U(N)+U(N-1))/2)*W
850 LET V=(R(N)*U(N)+R(N-1)*U(N-1))/2
860 LET V1=(R1(2)*U1(2)+R1(1)*U1(1))/2
870 LET C2=C2+(V1-V)*W
880 LET V=(R(N)*U(N)+R(N-1)*U(N-1)+U(N-1)*U(N-1))/2
890 LET V1=(R(N)*U(N)+R1(2)*U1(2)+R(N-1)*U(N-1)+U1(1))/2
900 LET C3=C3+(V1-V)*W
910 LET R1(1)=R1(2)
920 LET U1(1)=U1(2)
930 NEXT N
940 PRINT

```

```

942 PRINT
944 PRINT
946 PRINT
948 PRINT ~
950 PRINT ~
952 PRINT ~
954 PRINT ~
956 PRINT ~
970 STOP
1000 DATA 3.2
1010 DATA 0.,.7042,.02986
1020 DATA .25,.6835,.03212
1030 DATA .75,.6566,.04
1040 DATA 1.25,.6767,.04732
1050 DATA 1.5,.6632,.05361
1060 DATA 1.75,.6632,.05955
1070 DATA 2.,.6835,.06504
1080 DATA 2.25,.6903,.06899
1090 DATA 2.5,.6835,.07207
1100 DATA 2.75,.7112,.07882
1110 DATA 3,.7401,.08277

```

```

DELTA.CM      = "D(Z)
DEL+.CM      = "C1/U4
DEL+.CM      = "C2/(U4+P4)
THETA.CM      = "C3/(U4+U4+P4)
RE THETA      = "S2+C3/(100+U4+U4+P4)

```

READY

◆

PROGRAM RAMSHER

```

10 REM RAMSHER1
11 REM H IS RAMP NO, N1 IS NO OF FIRST X STA USED IN CURVE FIT, N2 IS
12 REM THE NO OF THE LAST X STA IN CURVE FIT, Z IS THE X STA FOR TAU CALC
13 REM (MUST BE<N2),W IS REFERENCE X STA WHICH DETERMINES Y VALUES,
14 REM K1 IS NO OF TIMES 1ST X STA INCLUDED IN CURVE FIT (USUALLY=1).
15 REM F(N) IS TAUW(MMHG),R5(N) IS RAD OF CURVATURE(CM), X(N) IS X STA(IN),
16 REM A1(N) IS SURFACE SLOPE (RAD), D6(N) IS LOCAL HEIGHT, Y(CM), OF
17 REM SURFACE WITH RESPECT TO RAMP L.E.
100 FILES F1:F2:F3
110 DIM Y(11,100),U(11,100),R(11,100),P(11,100)
120 DIM C1(11),C2(11),C3(11),C4(11),C5(11),S(11)
130 DIM A(3,3),B(3,1),D1(2),D2(2),D3(2),D4(2),X1(1,3)
140 DIM R5(11),F(11),X(11),A1(11),D6(11),W1(3,3),Z6(3,1)
142 DIM C6(11)
230 READ H,N1,N2,Z,W,K1
240 FOR N=1 TO N2
250 READ F(N),R5(N),X(N),A1(N),D6(N)
252 LET X(N)=X(N)*2.54
254 LET F(N)=F(N)*133.29
260 NEXT N
270 PRINT "          TURBULENT SHEAR STRESS DISTRIBUTION"
280 PRINT "          RAMP NO" H
290 PRINT "          X STATION(CM)="X(Z)
292 PRINT
294 PRINT
296 PRINT
300 PRINT "          WHAT ARE FILES NEWFLOWX,SHERXXXX,EDYXXXX"
310 INPUT F1$,F2$,F3$
312 PRINT
314 PRINT
316 PRINT
320 FILE #1,F1$
322 FILE #2,F2$
323 FILE #3,F3$
324 SCRATCH #2
325 SCRATCH #3
330 FOR N=N1 TO N2
340 FOR M=1 TO 100
350 READ #1,Y(N,M),U(N,M),R(N,M),P(N,M),Q9
352 LET P(N,M)=P(N,M)*133.29
360 NEXT M
370 NEXT N
380 PRINT "Y(CM)", "TAU/TAUW", "I1", "I2", "I3"
382 PRINT TAB(15), "I4"
384 PRINT
385 PRINT
386 LET D1(1)=0
387 LET D2(1)=0
388 LET D3(1)=0
389 LET D4(1)=0
390 FOR M=1 TO 100

```

```

400 LET Y=Y(W,M)
410 LET S(1)=.00001
420 FOR L=1 TO N2
430 LET Z2=Y*COS(A1(L))+D6(L)
440 LET Z1=Y*COS(A1(L-1))+D6(L-1)
450 LET L2=X(L)-Y*SIN(A1(L))
460 LET L1=X(L-1)-Y*SIN(A1(L-1))
470 LET Z3=Z2-Z1
472 LET L3=L2-L1
474 LET S(L)=SQRT((L3*L3)+(Z3*Z3))+S(L-1)
476 NEXT L
478 MAT A=ZER
480 LET K=0
482 FOR L=N1 TO N2
483 LET K=K+1
484 LET A(1,1)=A(1,1)+1
486 LET A(1,2)=A(1,2)+S(L)*S(L)
488 LET A(1,3)=A(1,3)+S(L)
490 LET A(2,2)=A(2,2)+S(L)*S(L)*S(L)*S(L)
492 LET A(2,3)=A(2,3)+S(L)*S(L)*S(L)
494 LET A(3,3)=A(3,3)+S(L)*S(L)
495 IF L>1 GO TO 497
496 IF K<K1 GO TO 483
497 NEXT L
498 LET A(2,1)=A(1,2)
500 LET A(3,1)=A(1,3)
502 LET A(3,2)=A(2,3)
505 FOR L=N1 TO N2
510 FOR N=1 TO 100
515 IF Y(L,N)=Y GO TO 525
520 NEXT N
525 LET Y1=(Y-Y(L,N-1))/(Y(L,N)-Y(L,N-1))
530 LET C1(L)=U(L,N-1)+(U(L,N)-U(L,N-1))*Y1
535 LET B1=U(L,N-1)*R(L,N-1)
540 LET B2=U(L,N)*R(L,N)
545 LET C2(L)=B1+(B2-B1)*Y1
550 LET B1=U(L,N-1)*U(L,N-1)*R(L,N-1)
555 LET B2=U(L,N)*U(L,N)*R(L,N)
560 LET C3(L)=B1+(B2-B1)*Y1
565 LET C4(L)=P(L,N-1)+(P(L,N)-P(L,N-1))*Y1
567 LET C6(L)=R(L,N-1)+(R(L,N)-R(L,N-1))*Y1
570 NEXT L
578 LET K=0
580 FOR L=N1 TO N2
581 LET K=K+1
585 LET C5(L)=C1(L)
586 IF L>1 GO TO 590
587 IF K<K1 GO TO 581
590 NEXT L
595 GOSUB 800
600 LET D1(2)=X1(1,1)+X1(1,3)*S(Z)+X1(1,2)*S(Z)*S(Z)
602 LET K=0
605 FOR L=N1 TO N2

```

```

606 LET K=K+1
610 LET C5(L)=C2(L)
611 IF L>1 GO TO 615
612 IF K<K1 GO TO 606
615 NEXT L
620 GOSUB 800
625 LET D2(2)=X1(1,3)+2*X1(1,2)*S(Z)
629 LET K=0
630 FOR L=N1 TO N2
631 LET K=K+1
635 LET C5(L)=C3(L)
636 IF L>1 GO TO 640
637 IF K<K1 GO TO 631
640 NEXT L
645 GOSUB 800
650 LET D3(2)=X1(1,3)+2*X1(1,2)*S(Z)
654 LET K=0
655 FOR L=N1 TO N2
656 LET K=K+1
660 LET C5(L)=C4(L)
661 IF L>1 GO TO 665
662 IF K<K1 GO TO 656
665 NEXT L
670 GOSUB 800
672 LET D4(2)=X1(1,3)+2*X1(1,2)*S(Z)
673 FOR L=N1 TO N2
674 LET C5(L)=C6(L)
675 NEXT L
676 GOSUB 800
677 LET D5=X1(1,1)+X1(1,3)*S(Z)+X1(1,2)*S(Z)*S(Z)
678 LET K=1/R5(Z)
680 LET T=Y(W,M)-Y(W,M-1)
685 LET B1=1/(1+K*((Y(W,M)+Y(W,M-1))/2))
690 LET D=(D3(2)+D3(1))/2
695 LET I1=I1+B1*D*T
700 LET D=(D2(2)+D2(1))/2
705 LET V=(D1(2)+D1(1))/2
707 LET G1=(D1(2)-D1(1))/T
710 LET G=G+D*T
715 LET I2=V*B1*G
720 LET I3=I3+2*I2*B1*K*T
725 LET D=(D4(2)+D4(1))/2
730 LET I4=I4+B1*D*T
735 LET T1=1+(1/F(Z))*((I1-I2-I3+I4)
740 PRINT Y,T1,I1/F(Z),I2/F(Z),I3/F(Z)
745 PRINT TAB(15),I4/F(Z)
747 PRINT
748 WRITE #2,Y,T1,D2(2),D3(2),D4(2)
749 WRITE #3,Y,T1*F(Z),G1,D5
750 LET D1(1)=D1(2)
752 LET D2(1)=D2(2)

```

```

754 LET D3(1)=D3(2)
756 LET D4(1)=D4(2)
760 NEXT M
765 STOP
800 MAT B=ZER
805 FOR L=N1 TO N2
810 LET B(1,1)=B(1,1)+C5(L)
815 LET B(2,1)=B(2,1)+S(L)*S(L)*C5(L)
820 LET B(3,1)=B(3,1)+S(L)*C5(L)
825 NEXT L
830 MAT W1=CON(3,3)
835 MAT W1=INV(A)
840 MAT X1=CON(1,3)
845 MAT Z6=CON(3,1)
850 MAT Z6=W1*B
855 MAT X1=TRN(Z6)
860 RETURN
1000 DATA 3,4,11,6,7,1
1010 DATA .26,-1000000,0,0,0
1020 DATA .263,-18.14,.25,.03748,.01264
1030 DATA .276,-22.5,.75,.1005,.1026
1040 DATA .246,-26.75,1.25,.1527,.2659
1050 DATA .307,-28.84,1.5,.1759,.3716
1060 DATA .326,-30.91,1.75,.1976,.4919
1070 DATA .347,-32.97,2,.2179,.6261
1080 DATA .376,-35.02,2.25,.2371,.7734
1090 DATA .393,-37.07,2.5,.2553,.9333
1100 DATA .426,-39.11,2.75,.2726,1.1052
1110 DATA .446,-41.55,3,.2891,1.2886
9999 END

```

READY

♦

PROGRAM EDDY

```

10 REM EDDY
11 REM R8 IS THE RAMP NO,Z IS THE NO OF THE X STA,X(L) IS X STA(IN),
12 REM D(L) IS DELTA (CM),D1(L) IS DELTA STAR SUB K (D*) IN CENTI-
13 REM METERS FROM VCOLES OR TBLJNDIM, U(L) IS UE(M/SEC) FROM
14 REM TBLJNDIM
100 FILES F1:F2
110 DIM X(11),D(11),D1(11),U(11)
190 READ R8,Z
200 FOR L=1 TO Z
210 READ X(L),D(L),D1(L),U(L)
220 NEXT L
230 PRINT "          EDDY VISCOSITY CALCULATION"
232 PRINT "          RAMP NO"R8
234 PRINT "          X STATION="X(Z)+2.54
236 PRINT
238 PRINT
240 PRINT
250 PRINT "          WHAT ARE FILES EDDYXXXX,VISCXXXX",
260 INPUT F1$,F2$
270 FILE #1,F1$
280 FILE #2,F2$
282 PRINT
284 PRINT
286 PRINT
290 SCRATCH #2
295 PRINT "          Y","          Y/D","          L/D","          E/UED*K";"          D(U/UE)/D(Y/D)"
296 PRINT
300 FOR N=1 TO 100
310 READ #1,Y,T,G,R
312 IF T<0 GO TO 354
320 LET L=SQR(T/R)/(D(Z)+6)
330 LET V=T/(U(Z)+D1(Z)+R+6)
340 PRINT Y,Y/D(Z),L,V,6+D(Z)/U(Z)
350 WRITE #2,Y,Y/D(Z),L,V,6+D(Z)/U(Z)
352 GO TO 360
354 PRINT Y,Y/D(Z),TAB(61);6+D(Z)/U(Z)
356 WRITE #2,Y,Y/D(Z),9999,9999,6+D(Z)/U(Z)
360 NEXT N
400 STOP
1000 DATA 3,4
1007 DATA 0,1,1,1
1008 DATA .25,1,1,1
1009 DATA 1,1,1,1
1010 DATA 1.25,.6767,.0944,610.2
1020 DATA 1.5,.6632,.119,605
1030 DATA 1.75,.6632,.112,600.5
1040 DATA 2,.6835,.1138,596.4
1050 DATA 2.25,.6903,.1069,587.6
1060 DATA 2.5,.6835,.1021,581.4
1070 DATA 2.75,.7112,.1045,580
1080 DATA 3,.7401,.1033,573
9999 END

```

READY

APPENDIX B

COMMENTS ON THE MIXING LENGTH CONSTANT

In Section 4.6, it was shown that in the region of adverse pressure gradient (APG), the constant κ in the mixing length relation $\ell = \kappa y$ was 0.65 in contrast to 0.4 for the zero pressure gradient (ZPG) flow. This implies, therefore, an inconsistency of the APG data with the Law-of-the-Wall correlation, since the latter is based on the value $\kappa = 0.41$, and raises the question whether the increase in κ is real or possibly due to experimental error. Recall that the derivation of the wall-wake velocity correlation

$$u^+ = \frac{1}{\kappa} \ln y^+ + C + \frac{\tilde{\pi}}{\kappa} W(y/\delta) \quad \text{B.1}$$

includes the assumption $\ell = \kappa y$. References 8 and 11 document the basis for selecting the currently accepted values of the constants $\kappa = 0.41$ and $C = 5.0$. These values are concluded to be independent of pressure gradient, whose effects are reflected instead in the magnitude of the wake strength parameter $\tilde{\pi}$. It should be noted that the values of κ and C are based on data for which $100 < y^+ < 300$, since it was felt that closer to the wall experimental errors may cause the measured velocity to be too high, while farther away the effects of the wake-like outer flow become large.

In the present study, the curve-fit described in Section 4.2 was restricted to data for $y^+ > 50$. A plot of the velocity profiles in $u^+ - y^+$ coordinates, shown in Figure 28 for Ramp 3, is reproduced in Figure B.1 which includes, now, lines of constant y/δ . Notice that for the ZPG case, $y/\delta = 0.05$ corresponds to $y^+ \sim 20$. Moving downstream in the APG region the y^+ value corresponding to $y/\delta = 0.05$ increases (the increase in Reynolds number shifts the velocity profile to the right, i.e., to larger y^+ values) so that at the rear of the ramp y^+ at $y/\delta = 0.05$ is about 50.

A plot of ℓ/δ versus y/δ to an enlarged scale is shown in Figure B.2 which indicates clearly that the slope κ shifts rapidly from 0.4 to 0.65 along the

ramp and that the linear portion of the ℓ versus y variation extends from $y/\delta = 0.05$ to almost 0.2 (see also Figures 63 and 64 to define the upper limit). A value of $y/\delta = 0.05$ corresponds to about 0.035 cm which is near the outer edge of the viscous sublayer while y/δ of 0.2 corresponds to y^+ ranging from 80 to 200 for the profiles in Figure B.1. Therefore, most of the data points (particularly for the APG region) shown in Figure B.2 are included in the curve-fit to the Law-of-the-Wake, Equation 4.5. However, these points are small in number compared to those in the outer portion of the boundary layer, where contributions from the wake function are large, and although they deviate from Equation 4.5 (i.e., they reflect $\kappa = 0.65$ instead of 0.4) the rms error of the curve-fit is still small.

For both ramps, the $u^+ - y^+$ profiles for representative stations located upstream of the leading edge (ZPG), at its mid-point, and at the rear station have been plotted in Figure B.3 together with the sub-layer relation $u^+ = y^+$, Equation 4.8, and the Law-of-the-Wall, Equation 4.4. It is observed that

- 1) For the ZPG case, the data for $y^+ < 50$ fall on or parallel to Equation 4.4 until $y^+ \sim 20$ ($y/\delta = 0.05$) where they then merge with the sublayer profile.
- 2) For the APG region, the data below $y^+ = 100$ deviate from Equation 4.4, showing a smaller slope (i.e., a larger value of κ) than the Law-of-the-Wall until $y^+ \sim 25$ where again, they approach the sublayer profile. The trend of the APG data is clear and consistent. In fact, since $\kappa = 0.65$ is determined directly from the mixing length calculations, this guarantees that the APG data will not fit the classic Law-of-the-Wall (with $\kappa = 0.41$).

In view of this discussion, the possibility of experimental error causing the observed increase in κ in the APG region is considered unlikely since:

1. The effect is not observed in the ZPG case although the techniques and instrumentation were the same at all x stations.

2. The data for all stations were collected from the same region of the boundary layer, that is, for y/δ up to 0.2 and this is sufficiently far from the wall for probe errors to be negligible.

3. Sturek obtained the same value of κ for much larger values of Re_δ and S_k . Thus, two experiments conducted in different facilities, under different operating conditions, with different instrumentation and data reduction, yield the same result.

It appears, then, that the observed mixing length constant $\kappa = 0.65$ in the APG flow is not due to experimental error although the cause for the shift from the ZPG value is not known and it appears to conflict with low speed results. It is suggested that the change in κ may be an effect of pressure gradient or longitudinal curvature introduced by compressibility. Clearly, there is a need for more information to resolve the issue.

It is instructive here to apply Spalding's formulation of the Law-of-the-Wall in the buffer region to the APG data in order to determine the $u^+ - y^+$ velocity profile associated with $\kappa = 0.65$. This is done by applying Equation 4.8 to the point $y^+ = 100$, $u^+ = 16.2$ where the data from both the ZPG and APG profiles agree and are identical to the conventional Law-of-the-Wall, Equation 4.4. At this point, we assume $\kappa = 0.65$ and use Equation 4.8 to calculate K_2 . With both κ and K_2 known, we can then use Equation 4.8 to calculate u^+ versus y^+ . The results are plotted in Figure B.3 where they seem to coincide with the APG data throughout the entire y^+ range near the wall.

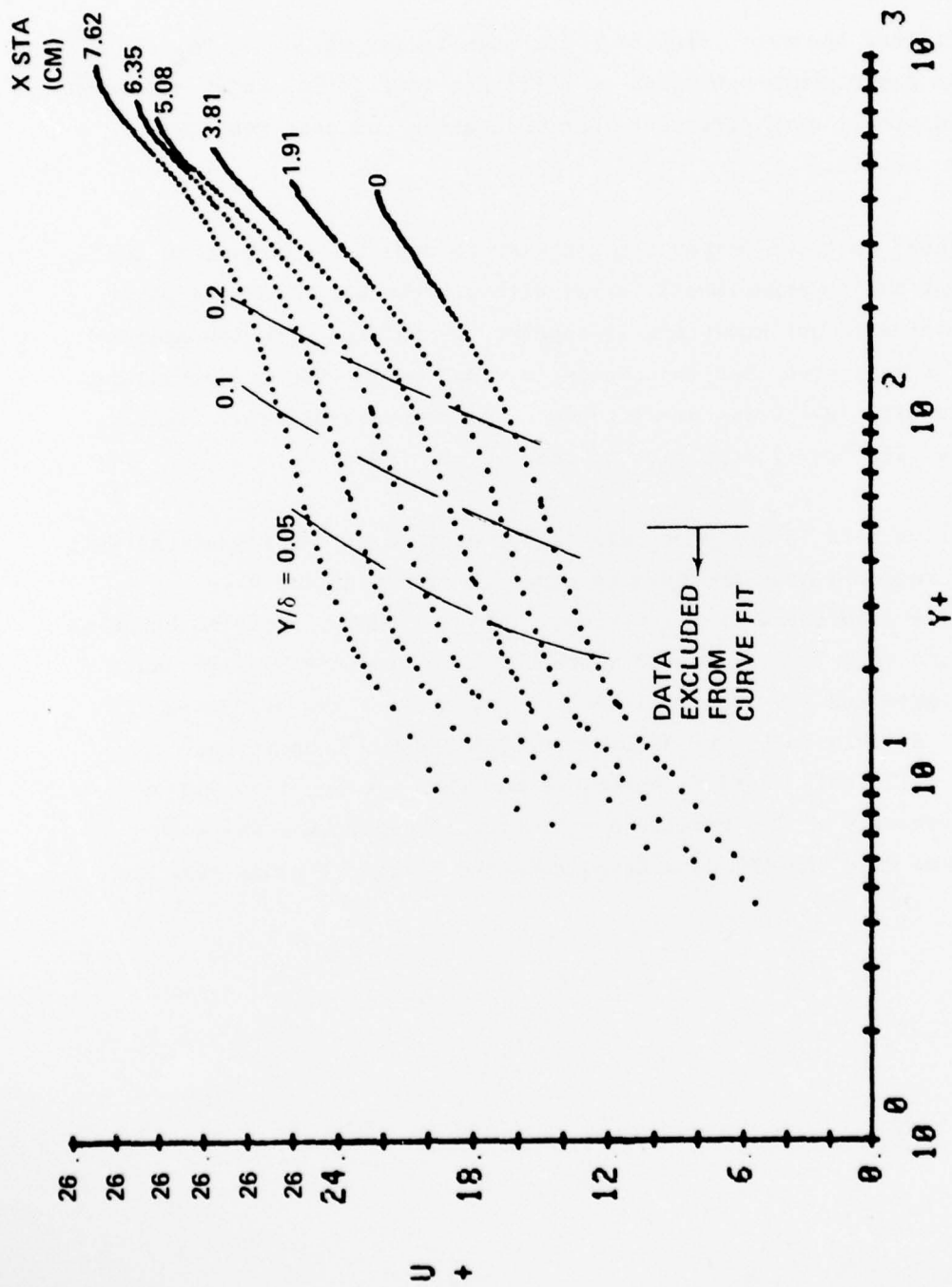


Figure B.1 Velocity Profiles in $u^+ - y^+$ Coordinates Showing Lines of Constant y/δ

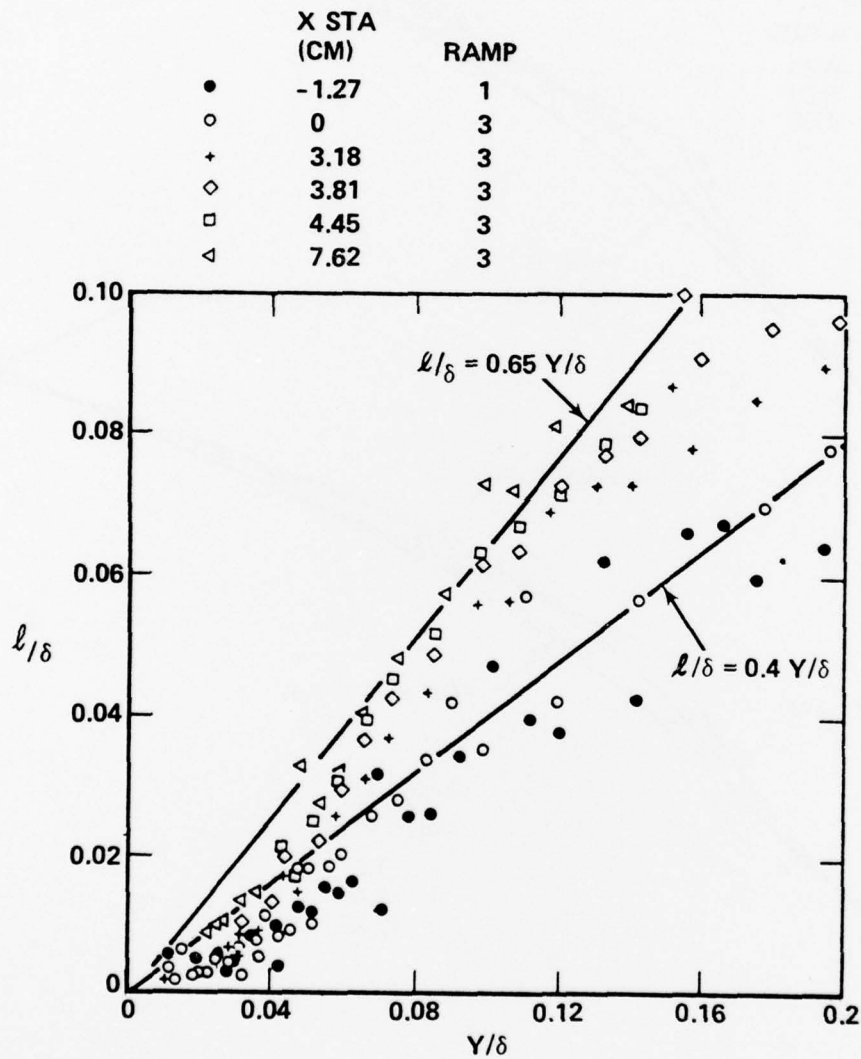


Figure B.2 Variation of Mixing Length l/δ with Position y/δ in the Wall Region

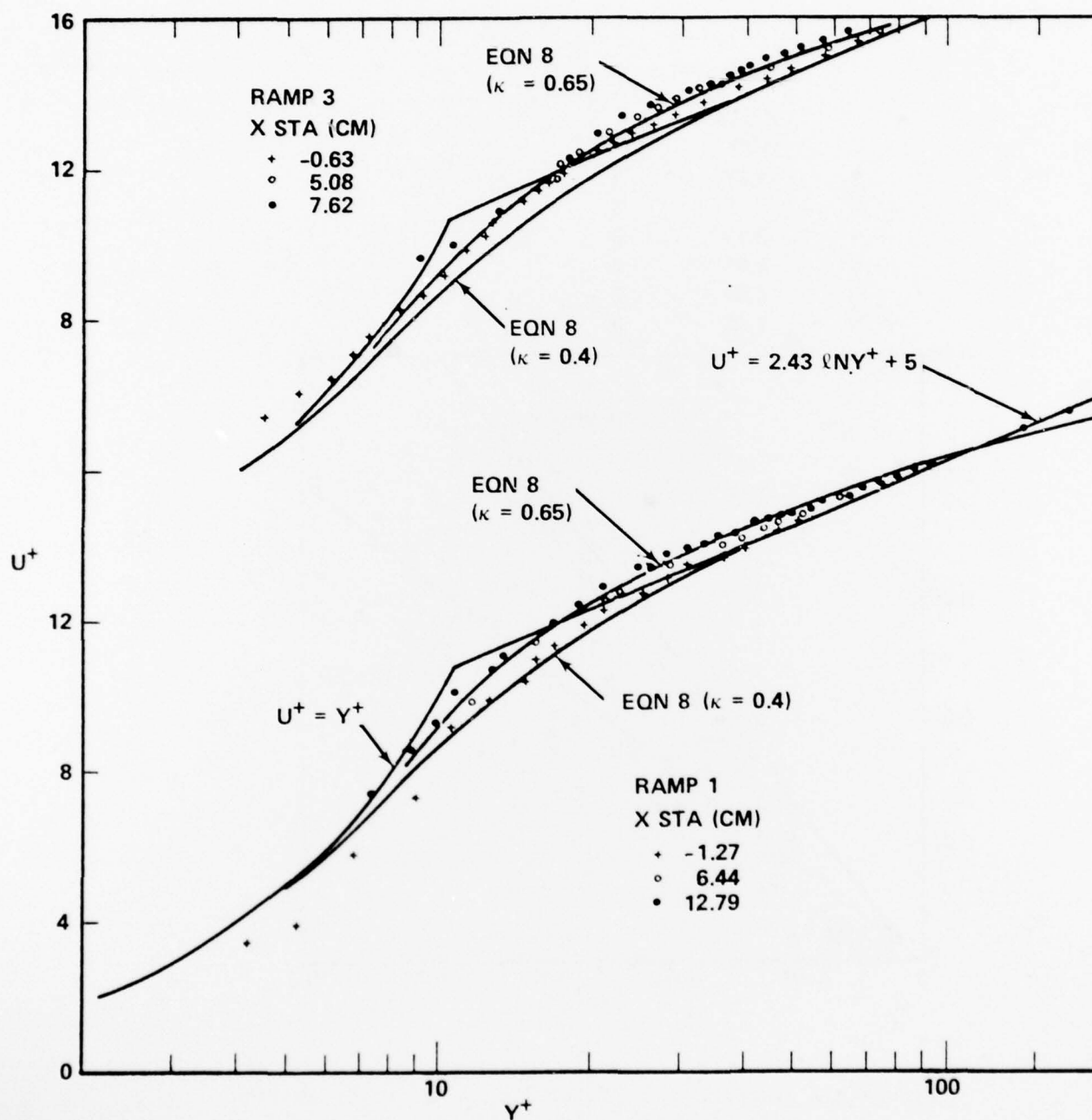


Figure B.3 Velocity Profiles in $y^+ - y^+$ Coordinates in the Wall Region

REFERENCES

1. Fernholz, H.H. and Finley, P.J., "A Critical Compilation of Compression Turbulent Boundary Layer Data," AGARDograph No. 223, June 1977
2. Sturek, W.B., "Turbulent Boundary Layer Shear Stress Distributions for Compressible Adverse Pressure Gradient Flow," AIAA Journal, Vol. 12, No. 3, pp 375-376, March 1974. See also AIAA Paper 73-166, 1973
3. Laderman, A.J., "Effect of Wall Temperature on a Supersonic Turbulent Boundary Layer," AIAA Journal, Vol. 16, No. 7, pp 723-729, July 1978
4. Clauser, F.H., "The Turbulent Boundary Layer," Advances in Applied Mechanics, Vol. 4, pp 1-51, 1956
5. Alber, I.E. and Coats, D.E., "Analytical Investigation of Equilibrium and Non-Equilibrium Compressible Turbulent Boundary Layers," AIAA Paper 69-689, 1969
6. Lewis, J.E., Gran, R.L. and Kubota, T., "An Experiment on the Adiabatic Compressible Turbulent Boundary Layer in Adverse and Favourable Pressure Gradients," J. Fluid Mech., Vol. 51, part 4, pp657-672, 1972
7. Sturek, W.B., and Danberg, J.E., "Supersonic Turbulent Boundary Layer in Adverse Pressure Gradient; Part II: Data Analysis", AIAA Journal, Vol. 10, No. 5, May 1972, pp 630-635. See also "Supersonic Turbulent Boundary Layer in Adverse Pressure Gradient," AIAA Journal, Vol. 10, No. 4, April 1972, pp 475-480 and "Supersonic Turbulent Boundary Layer in Adverse Pressure Gradient Data Tabulation," Technical Report No. 141, University of Delaware, Dept of Mechanical and Aerospace Engineering, revised 1973
8. Coles, P.E., "The Young Person's Guide to the Data," Proc 1968 AFOSR-IFFP - Stanford Conference on Computation of Turbulent Boundary Layers,

REFERENCES (continued)

Vol. 2, (D. Coles & E. Hirst, eds), Stanford University, pp 1-45, 1969

9. Spalding, D.B., "A Single Formula for the Law-of-the-Wall." Trans. ASME, 28E, (J. Appl. Mech), pp 455-457, 1961
10. Kleinstein, G., "Generalized Law-of-the-Wall and Eddy Viscosity Model for Wall Boundary Layers," AIAA Journal, Vol. 5, pp 1402-1407, August 1967
11. Coles, D.E. and Hirst, E.A., Proceedings of 1968 AFOSR-1FP-Stanford Conference on Computation of Turbulent Boundary Layers, Vol. 2, Stanford University 1969
12. Mellor, G.L. and Gibson, D.M., "Equilibrium Turbulent Boundary Layers," J. Fluid Mech., Vol. 24, pp 225-253, 1966
13. Bradshaw, P. and Unsworth, K., "Comment on 'Evaluation of Preston Tube Calibration Equations in Supersonic Flow' ", AIAA Journal, Vol. 12, pp 1294-4, September 1974
14. Hopkins, E.J. and Inouye, M., "An Evaluation of Theories for Predicting Turbulent Skin Friction and Heat Transfer on Flat Plates at Supersonic and Hypersonic Mach Numbers," AIAA Journal, Vol. 9, pp 993-1003, January 1971
15. McLafferty, G.H. and Barber, R.E., "The Effect of Adverse Pressure Gradient on the Characteristics of Turbulent Boundary Layers in Supersonic Streams", J. of Aerospace Sciences, Vol. 29, No. 1, pp 1-10, January 1962
16. Whitfield, D.L. and High, M.D., "Velocity-Temperature Relations in Turbulent Boundary Layers with Non-unity Prandtl Numbers, AIAA J., Vol. 15, pp 431-434, March 1977

REFERENCES (continued)

17. Whitfield, D.L., "Analytical, Numerical and Experimental Results in Turbulent Boundary Layers," AEDC TR-76-62, 1976
18. Sandborn, V.A., "A Review of Turbulence Measurements in Compressible Flow," NASA TMX-62337, March 1974
19. Walz, A., "Compressible Turbulent Boundary Layers," Mechanique de La Turbulence, Centre National de La Rescherche Scientifique, Paris, pp 300-350, 1962
20. Maise, G., and McDonald, H., "Mixing Length and Kinematic Eddy Viscosity in a Compressible Boundary Layer," AIAA Journal, Vol. 6, pp 73-79, January 1968.